Biomarkers of Coronary Atherosclerotic Plaque Rupture

Regent Lee

RDM Cardiovascular Medicine

&

Trinity College



A thesis submitted for the degree of

Doctor of Philosophy in Cardiovascular Medicine

University of Oxford
Michaelmas Term 2014

Biomarkers of Coronary Atherosclerotic Plaque Rupture

Regent Lee

Trinity College, University of Oxford

A thesis submitted for the degree of Doctor of Philosophy in Cardiovascular Medicine
Michaelmas Term 2014

Coronary atherosclerotic plaque rupture is a critical event during atherosclerosis disease progression. Clinical consequences of atherosclerotic plaque rupture vary from asymptomatic to acute arterial thrombosis, yet the mechanisms underpinning such divergent biological response remain poorly understood. Novel biological signatures of plaque rupture will confer further insights into the dynamic responses triggered by plaque rupture event(s), and may provide alternative strategies for modulation of this prevalent disease. This thesis aims to investigate the events that accompany coronary plaque rupture and their relations to subsequent, downstream systemic effects.

In a prospective clinical study of patients undergoing non-emergency percutaneous coronary intervention (PCI), stenting induced plaque disruption was used as a model of plaque rupture *in vivo*. Optical coherence tomography (OCT) imaging of the plaque lesion was performed prior to stenting, followed by serial blood sampling from targeted anatomical sites in reference to the plaque disruption event. Coronary plaque debris were also retrieved in a controlled manner.

Analysis of candidate markers demonstrated a role of matrix metalloproteinase 9 (MMP9) in the systemic response to plaque disruption. Local and systemic elevations of MMP9 were observed promptly after plaque disruption. The systemic release of MMP9 was independent to the myocardial injury and systemic inflammation as a result of PCI. OCT analysis further suggested that plaque morphology may be a determining factor in the subsequent MMP9 release, as the disruption of lipid rich plaque(s) resulted in more acute elevation of MMP9 when compared to disruption of non-lipid lesions.

Changes of systemic MMP9 served as an index of response to the stent induced plaque disruption. Subjects with divergent MMP9 responses to the plaque disruption event were put forward for further comprehensive investigation during the *discovery phase*, using mass spectrometry techniques to investigate the lipidomic, metabolomics, and proteomic signatures of plaque disruption.

Coronary atherosclerotic plaque disruption was associated with immediate changes in the plasma lipidomics and metabolomics profiles, which had distinct relations to the subsequent systemic MMP9 release. Coronary plaque debris provided a “catalogue” of proteins which could be acutely liberated into systemic circulation. Several such novel proteins were detected in circulation after plaque disruption, which triggered disparate responses in known canonical pathways. Evidence from this thesis implicates the role of liver X receptor / retinoic acid receptor pathway (LXR/RXR) as a key mediator to the divergent systemic responses after plaque disruption, and pinpoints a direction for future investigations.

Table of Contents

LIST OF FIGURES.....V

LIST OF TABLES.....VIII

LIST OF ABBREVIATIONS.....IV

CHAPTER 1: Introduction 0

1.1 Atherosclerosis and clinical implications 1

1.2 A brief overview of Atherosclerosis 1

1.3 Plaque rupture or erosion as the culprit event 2

1.4 Mechanisms of plaque rupture and erosion.....3

1.5 Dynamic nature of plaque progression.....5

1.6 Variable consequences of plaque rupture 8

1.7 Novel biomarkers of plaque rupture and clinical implications.....10

1.8 Discovery of novel biomarkers using "-omics" platforms 11

1.9 Hypothesis and Aims.....15

1.9.1 Hypothesis.....15

1.9.2 Aims 15

CHAPTER 2: General Methods and Pre-analytic Considerations.....16

2.1 Ethics and regulatory approval.....17

2.3 Study design 17

2.4 Blood sample collection.....18

2.4.1. Use of aspiration catheter for arterial sampling 19

2.4.2 Coronary artery plaque debris retrieval by filter wire.....19

2.4.3 Use of distal protection device 19

2.5 Overall strategy for the discovery workflow.....20

2.6 Pre-analytic considerations for plasma sample preparation.....23

2.6.1 Parameters for plasma preparation 23

2.6.2 Choice of anti-coagulant for plasma preparation.....32

2.6.3 *In vivo* effect of heparin administration on biomarker measurement.....36

2.7 Discussion.....38

CHAPTER 3: Candidate Markers of Coronary Atherosclerotic Plaque rupture 42

3.1 Introduction 43

3.2 Candidate markers of atherosclerotic plaque rupture 44

3.2.1 Myeloperoxidase 44
3.2.2 Matrix metalloproteinases 44
3.2.3 Tissue inhibitors of MMPs 45
3.2.4 Other candidate markers of plaque instability 45
3.3 Intra-vascular assessment of plaque morphology 46
3.3.1 Features of vulnerable plaque 46
3.3.2 Optical coherence tomography (OCT) 46
3.4 Hypotheses and Aims 48
3.5 Methods 48
3.5.1 Study design and subjects 48
3.5.2 Intravascular imaging by optical coherence tomography 49
3.5.3 Clinical diagnostic blood tests 50
3.5.4 Single analyte measurement with enzyme linked immunosorbent assay 50
3.5.5 Multi-analyte screening with Luminex® platform 52
3.5.6 List of candidate markers measured 54
3.5.7 Data analysis – general considerations 54
3.6 Results 57
3.6.1 Study population 57
3.6.2 Baseline comparisons of candidate biomarkers according to clinical status 57
3.6.3 Myeloperoxidase 57
3.6.4 Evidence of myocardial injury and systemic inflammation after PCI 62
3.6.5 Plasma levels of MMP8 and MMP9 after plaque disruption 62
3.6.6 Plasma levels of other candidate markers after plaque disruption 65
3.6.7 Candidate marker response after plaque disruption according to clinical status, using fold change values 65
3.6.8 Candidate marker response according to plaque morphology 67
3.6.9 Candidate markers response in relation to plaque volume disrupted 69
3.6.10 Candidate markers response according to stratification by AUC 69
3.6.11 Correlations of candidate markers with CRP, CKMB, and cTnI 69
3.6.12 Arterial plasma MMP9 levels at early time points after plaque disruption 72
3.6.13 Other anatomical gradients of candidate markers in the *Screening Phase* 73
3.6.14 Additional notes 75
3.6.15 Selection of a discovery subject subset 75
3.6.16 Results from the *Confirmation Phase* 77
3.7 Discussion 79
CHAPTER 4: Small Molecule Profiling of Coronary Atherosclerotic Plaque Disruption 89
4.1 Introduction 90
4.1.1 Principles of LC-MS data acquisition 90
4.1.2 Principles of MALDI-TOF-MS data acquisition 91
4.1.3 Principles of post processing for untargeted small molecules MS analysis 93
4.1.4 Conferring the identity of small molecules 93

4.1.5 Sample size considerations for -omics analysis 96
4.1.6 Pooling of plasma samples for -omics analysis 96
4.1.7 Principal component analysis – an overview 98
4.2 Hypotheses and Aims 99
4.3 Methods 101
4.3.1 Plaque debris for analysis 101
4.3.2 Plasma samples for analysis 101
4.3.3 Additional samples and controls used for MALDI-TOF-MS and LC-MS analysis 103
4.3.4 Extraction of lipid and metabolite fractions from FW and FW INC samples 103
4.3.5 Data acquisition for lipidomic fraction 104
4.3.6 Data acquisition for metabolomics fraction 106
4.4 Data analysis 106
4.4.1 Data analysis for MALDI-TOF lipidomics 107
4.4.2 Data analysis for LC-MS metabolomics 108
4.5 Results 109
4.5.1 MALDI-TOF MS lipidomic screen 109
4.5.2 LC-MS metabolomic screen 114
4.6 Discussion 117
CHAPTER 5: Proteomics Signatures of Coronary Atherosclerotic Plaque Disruption 122
5.1 Introduction 123
5.1.1 Brief overview of untargeted proteomics for biological samples 123
5.1.2 Dynamic range of human proteome and its implications for shot gun proteomics 126
5.1.3 Strategies for improving coverage for plasma proteomics analysis 128
5.1.4 Pathways and integrated -omics analysis 130
5.2 Hypotheses and Aims 132
5.3 Methods 132
5.3.1 Samples analysed 132
5.3.3 Extraction of protein fraction from plaque debris samples 132
5.3.4 Extraction of protein fraction from plasma samples 133
5.3.5 In-solution trypsin digest for protein 133
5.3.6 Desalting and purification of peptides 134
5.3.7 Data acquisition for shot gun proteomics by LC MS/MS 134
5.3.8 Data analysis 135
5.3.9 Technical validation of putative protein targets 137
5.4 Results 139
5.4.1 Proteomics profile of samples analysed - qualitative analysis 139
5.4.2 Proteomics profiles – semi quantitative analysis 142
5.4.3 Ingenuity pathway analysis 147
5.4.4 γ -Linoleate biosynthesis pathway 155

5.4.5 Technical validation of protein targets by ELISA 155
5.5 Discussion 162
5.5.1 Key findings of proteomics analysis 162
5.5.2 Spectrum of proteomics profile changes after plaque disruption 163
5.5.3 Integration of proteomics and small molecules data 165
CHAPTER 6: General Discussion 170
6.1 Original hypotheses and aims 171
6.2 Principal findings of research 171
6.3 Future directions 173
6.4 Conclusion 178
CHAPTER 7: Data Appendix 179
CHAPTER 8: Appendices 190
8.1 Timing and venue of research 191
8.2 Sources of funding 191
8.3 Attributions 192
8.4 Research Publications arising from work in this thesis 193
8.5 Other publications during DPhil study 193
8.6 Abstracts presented at scientific conferences 195
8.7 Figure legends not included in main text 196
8.8 Acknowledgements 242
REFERENCES 244

List of Figures

Figure 1	Dynamic nature of plaque progression and varied consequences after plaque events	P8
Figure 2	Summary of study procedures and blood sampling time points	P18
Figure 3	Failure to detect differences in a biological effect due to inappropriate grouping of subjects	P21
Figure 4	Flowchart of biomarker discovery workflow for this research	P22
Figure 5	Centrifugation protocol to obtain plasma with differential residual platelet counts, and the corresponding experimental design to test the effect of residual platelet count on the level of plasma candidate markers	P26
Figure 6	Level of plasma platelet counts and soluble CD40 ligand in plasma prepared using different centrifugation protocols	P29
Figure 7	Effect of temperature during centrifugation on the levels of residual plasma platelets and soluble CD40 ligand	P30
Figure 8	Comparison between protein profiles in paired plasma samples prepared using EDTA or lithium heparin as anticoagulant	P33
Figure 9	Comparison between metabolite and lipid profiles in paired plasma samples prepared using EDTA or lithium heparin as anticoagulant	P35
Figure 10	Effect of systemic administration of heparin and the level of plasma MMP9 in coronary artery disease patients	P37
Figure 11	Effect of temperature during centrifugation on the level of plasma MMP9 and VCAM	P40
Figure 12	Representative features of coronary artery obtained by OCT imaging.	P47
Figure 13	Illustration of the scoring method for the classification of plaque morphology on OCT imaging.	P51
Figure 14	Principles of multi-analyte profiling by the Luminex® platform	P53
Figure 15	Baseline comparison of candidate marker levels between CAD patients who presented with acute coronary syndrome or stable angina	P58
Figure 16	Effect of systemic administration of heparin and plasma level of myeloperoxidase in CAD patients undergoing stenting induced plaque disruption	P59
Figure 17	Evidence of myocardial injury and systemic inflammation after plaque disruption	P61
Figure 18	Plasma levels of MMP8 and MMP9 after plaque disruption	P62
Figure 19	Plasma levels (fold change) of MMP2, MMP3, MMP8, MMP9, TIMP1, TIMP 2, and TIMP4 after plaque disruption	P64
Figure 20	Comparison of MMP9 and TIMP1 after plaque disruption according to clinical status and plaque morphology	P66

Figure 21	Candidate marker response after plaque disruption, stratified by area under curve over the entire time course	P68
Figure 22	Correlation between candidate markers to CRP, CKMB, or cTnI	P69
Figure 23	Changes in arterial MMP9 at early time points after plaque disruption	P72
Figure 24	Plasma levels of NGAL and GDF15 in the discovery subject subset after plaque disruption	P76
Figure 25	Typical work flow for untargeted-omics experiments	P88
Figure 26	Schematic diagram for MALDI-TOF-MS	P90
Figure 27	Comparison of MALDI-TOF-MS spectra between different samples	P92
Figure 28	Presence of isobaric species for small molecules	P93
Figure 29	Sample size calculation for discovery –omics research	P95
Figure 30	Conceptual illustration of how a principal component analysis is performed	P98
Figure 31	Samples analysed during the *discovery phase* of this research	P100
Figure 32	Summary of the organic extraction protocol used for the extraction of lipid and metabolites from plaque debris samples	P103
Figure 33	MALDI-TOF-MS spectra showing unique features in biological samples analysed during the *discovery phase*	P109
Figure 34	Lipidomic profiles differ between the type of samples, and in plasma samples before and after plaque disruption	P110
Figure 35	Correlation matrix of the 15 most significantly changed mass features selected by the Medicwave Spectrolyzer^{TM} software in each of the discovery subject subset	P111
Figure 36	Metabolomic profiles differ between types of samples, and in plasma samples before and after plaque disruption	P113
Figure 37	Metabolite features which were differentially expressed in plaques and in plasma after plaque disruption.	P114
Figure 38	Mass features which demonstrate distinct patterns in the plasma samples analysed during the *discovery phase*	P116
Figure 39	Overview of untargeted “shotgun” proteomics workflow	P123
Figure 40	The wide dynamic range of human plasma proteome, predisposing under sampling of low abundance protein peptides by shotgun proteomics	P125
Figure 41	Two strategies utilised in this thesis for improving protein peptide coverage for shot gun proteomics analysis	P127
Figure 42	The concept of inferential pathway analysis	P128
Figure 43	The Progenesis LC-MS^{TM} analysis workflow	P136
Figure 44	Qualitative proteomics profile of the samples analysed during the *discovery phase*	P138

Figure 45	emPAI scores for individual samples highlight one limitation of qualitative proteomic analysis in a shotgun proteomics design.	P139
Figure 46	Proteomic profiles differ between plaque debris and plasma.	P141
Figure 47	Rapid changes in global proteomic profile are observed after plaque disruption	P144
Figure 48	Rapid changes of LXR/RXR pathway and acute phase response signalling pathway are observed after plaque disruption	P149
Figure 49	The LXR/RXR canonical pathway, superimposed with the proteins observed in the $CONTROL_{Dx}$ group	P150
Figure 50	The LXR/RXR canonical pathway is implicated after coronary atherosclerotic plaque disruption in the $PCI_{MMP9High}$ group	P151
Figure 51	The LXR/RXR canonical pathway is implicated after coronary atherosclerotic plaque disruption in the $PCI_{MMP9Low}$ group	P152
Figure 52	γ-Linoleate biosynthesis pathway may be implicated after coronary atherosclerotic plaque disruption	P154
Figure 53	Non-performance of the commercially available ELISA kits for CYB5R3, HADH and CD84	P157
Figure 54	Acute changes of plasma LBP and HPX after coronary atherosclerotic plaque disruption.	P158
Figure 55	Plasma LBP correlates with plasma HPX and $MMP9_{AUC}$ after coronary atherosclerotic plaque disruption	P159
Figure 56	Potential mechanisms of biological pathway activations due to acute release of LBP and CYB5R3 after plaque disruption	P164
Figure 57	Glutaryl–CoA degradation pathway may be involved after coronary atherosclerotic plaque rupture	P166
Figure 58	Tryptophan metabolism pathway may be involved after coronary atherosclerotic plaque rupture	P167

List of Tables

Table 1	Summary of studies which utilised an integrated proteomics, metabolomics, or lipidomics analysis in cardiovascular research	P13
Table 2	Summary of the plasma preparation protocols for four major studies on the prognostic value of sCD40L in coronary artery disease patients and healthy volunteers	P24
Table 3	Characteristics of study subjects in the *screening phase* of the study	P57
Table 4	Characteristics of the discovery subject subset for the *discovery phase* of the study	P74
Table 5	List of proteins which differed between the healthy volunteers and the CAD patients of the discovery subject subset	P143
Table 6	List of proteins significantly changed after plaque disruption in the $PCI_{MMP9High}$ group	P146
Table 7	List of proteins significantly changed after plaque disruption in the $PCI_{MMP9Low}$ group	P147-P148
Appendix Table	Proteins present in the plaque debris	P178 – P187

List of Abbreviations

A1BG	alpha 1B glycoprotein
ACS	acute coronary syndrome
AUC	area under curve (over the time course after plaque disruption)
AMI	acute myocardial infarction
ANOVA	analysis of variance
$ApoE^{-/-}$	apolipoprotein E deficient
BD	Beckon and Dickson (vacutainer manufacturer)
CABG	coronary artery bypass graft
CAD	coronary artery disease
CCMP	Center of Cellular and Molecular Physiology, University of Oxford
CKMB	Creatine kinase MB isoenzyme
$CONTROL_{Dx}$	discovery subject subset which was selected from the $Dx_{Lower1/2}$ of $MMP9_{AUC}$
CRP	c-reactive protein
cTnI	cardiac troponins
CYB5R3	cytochrome B5 reductase 3
DHB	dihydrobenzoic acid - matrix solution used for MALDI-TOF-MS
DTT	dithiothreitol
Dx	diagnostic (angiography)
$Dx^{upper1/2}$	upper ½ of Dx subjects according to AUC over the time course after plaque disruption
$Dx_{lower1/2}$	lower ½ of Dx subjects according to AUC over the time course after plaque disruption
ECM	extra cellular matrix
EDTA	ethylene-diamine-tetra-acetic acid
ELISA	enzyme link immunosorbent assay
FDR	false discovery rate
FW	plaque debris samples collected by the filterwire device during PCI
FW INC	filterwire incubated in whole blood at 37°C (*ex vivo*) for the duration of PCI
GDF15	growth differentiation factor 15
HADH	hydroxyacyl coenzyme A dehydrogenase
HDL	high density lipoprotein
HPX	hemopexin
HV	healthy volunteers
IPA	Ingeuity Pathway Analysis
IV	intravenous
LBP	lipopolysaccharide binding protein
LC	liquid chromatography
LDL	low density lipoprotein
LH	lithium heparin
LLOQ	lower limit of quantification

LMWH	low molecular weight heparin
$LpPLA_2$	lipoprotein associated phospholipase A_2
LXR/RXR	liver X receptor / retinoic acid receptor
MALDI-TOF-MS	matrix assisted laser desorption ionisation – time of flight
MMP	matrix metalloproteinase
MPO	myeloperoxidase
MS	mass spectrometry
MS/MS	tandom mass spectrometry
NADH	nicotinamide adenine dinucleotide
NC	negative control
NGAL	neutrophil gelatinase associated lipocalin
NSTEMI	non-ST-elevation myocardial infarction
OCT	optical coherence tomography
O.D.	optical density
JRH	John Radcliffe Hospital
OxLDL	oxidised low density lipoprotein
PAPP-A_2	pregnancy associated plasma protein A_2
PCA	principal component analysis
PCI	percutaneous coronary intervention
$PCI^{upper1/3}$	upper tertile of PCI subjects according to venous AUC of a candidate marker
$PCI_{lower1/3}$	lower tertile of PCI subjects according to venous AUC of a candidate marker
$PCI_{MMP9High}$	discovery subject subset which was selected from the $PCI^{upper1/3}$ group
$PCI_{MMP9Low}$	discovery subject subset which was selected from the $PCI_{lower1/3}$ group
PRP	platelet enriched plasma
PPP	platelet poor plasma
QC	quality control
RT	room temperature
SAP	stable angina pectoris
sCD40L	soluble CD40 ligand
SNR	signal to noise ratio
STEMI	ST-elevation myocardial infarction
SWATH-MS	sequential window acquisition of all theoretical mass spectra
TCFA	thin cap fibro-atheroma
TFA	trifluoroacetic acid
TIC	total ion current
TIMP	tissue inhibitors of metalloproteinase
cTnI/T	cardiac troponin I, troponin T
TFA	trifluroacetic acid
UAP	unstable angina pectoris
UF	unfractionated heparin

VCAM	vascular cell adhesion molecule
VH- IVUS	virtual histology - intravascular ultrasound
WB	whole blood
4°C	4 degree celcius / refrigerated condition

CHAPTER 1

INTRODUCTION

1.1 Atherosclerosis and clinical implications

Atherosclerosis is the pathology which underpins coronary artery disease (CAD) - the leading cause of morbidity and mortality in UK. Acute coronary syndromes (ACS) encompass a spectrum of clinical manifestations of the underlying CAD including unstable angina pectoris (UAP), myocardial infarction (MI) or sudden cardiac death. In the peripheral circulation, atherosclerosis leads to other acute vascular syndromes such as cerebral vascular events and limb ischaemia. The entire spectrum of cardiovascular disease poses the foremost burden on our healthcare system.

1.2 A brief overview of Atherosclerosis

The systemic process of atherosclerosis involves mainly medium and large sized arteries leading to multifocal plaque development, predominantly at sites characterised by low and oscillatory endothelial shear stress.(1) The disease begins to develop early in life as fatty streak infiltrations, which are an accumulation of lipid laden cells beneath the endothelium. Most cells in the fatty streak are macrophages, together with some T lymphocytes. As the fatty streak progresses to form an atheroma, it develops a core which contains foam cells and extracellular lipid droplets. This is surrounded by a cap of smooth muscle cells and a collagen rich matrix. T cells, macrophages and mast cells infiltrate the lesion and are particularly abundant in the shoulder region where the atheroma is vulnerable to rupture. Many of these immune cells exhibit signs of activation and produce inflammatory cytokines.

Acute vascular syndromes occur when the atherogenic process leads to sudden disruption of blood flow to the downstream tissue. The classical view of atherosclerosis was that progressive stenosis resulted in narrowing of the lumen of an atherosclerotic coronary artery to such an extent that a small platelet thrombus could occlude the vessel completely. Angiography acquired from patients presenting with ACS showed evidence of coronary

artery disease and arterial thrombosis in most cases, with the degree and location of coronary thrombosis and resultant lumen obstruction relating the severity of the event.(2) Thus an occlusive thrombus complicating a high grade stenosis could arrest flov w and cause ST elevation myocardial infarction (STEMI); whereas ACS without ST elevation would result from an incomplete or transient obstruction of flow in the culprit coronary artery at a site of critical stenosis.(3)

Findings from subsequent clinical and pathological studies have challenged such traditional views, and it became apparent that thrombotic complications do not always occur at the sites of most severe arterial narrowing by plaques.(4) Angiographic studies have provided evidence that culprit plaque lesions without significant accompanying luminal stenosis could also trigger acute thrombosis and myocardial infarction(5), and a significant majority of AMI arise from plaques with mild to moderate stenosis.(6, 7) Observations from intravascular imaging examination of the coronary arteries, performed during acute coronary syndrome, further suggested that culprit lesions often lie proximal to the site of maximal stenosis, before bifurcation points.(8)

1.3 Plaque rupture or erosion as the culprit event

The discrepancy between luminal stenosis of a culprit lesion and its propensity to cause acute coronary thrombosis can be explained by the phenomenon of plaque rupture and erosion. Plaque rupture, whereby a sudden breach of the fibrous cap results in contact of circulating blood to the necrotic core of a plaque, has been shown in autopsy series to be the most common cause of coronary artery thrombosis; both in the settings of acute myocardial infarction and sudden cardiac death.(1) Superficial erosion of the plaque with the loss of endothelium, but without disruption of the fibrous cap, accounts for the majority of the remaining cases.(9) Plaque erosion occurs more frequently in women and in persons with

certain risk factors such as hyperglycaemia. Observations made with the use of optical coherence tomography (OCT) of patients who presented with acute coronary syndrome support the findings reported by autopsy studies(9, 10) and indicate plaque rupture is also the most common cause of coronary thrombosis in patients who survived the initial event.(10)

Other causes of ACS are uncommon and include coronary artery spasm, Takosubo syndrome, coronary arteritis, arterial dissection, trauma, thromboembolism, cocaine abuse, and complication of cardiac catheterization.(11) In some of these instances of presumed non-atherosclerotic cases, more sensitive diagnostic tools such intravascular ultrasound can reveal the presence of bystander atherosclerotic disease.(12)

1.4 Mechanisms of plaque rupture and erosion

Sudden rupture or erosion of the fibrous cap may occur spontaneously, triggered by underlying pathological processes. A significant body of evidence indicate inflammatory cell activation plays a central role in the pathogenesis of plaque ruptures. Widespread coronary inflammation has been observed in patients with ACS.(13) Activated macrophages, T cells and mast cells at the site of rupture produce several types of molecules that can destabilise lesions.(14) Amongst these, matrix metalloproteinases (MMPs) are a family of proteases which has been implicated as key players in plaque destabilization.(15) Many members of this family of protease are present in the plaque and may degrade its extracellular matrix. The activities of MMPs are regulated by the tissue inhibitors of metalloproteinases (TIMPs) and inflammatory signals. Increased breakdown of collagens reduce the content of extracellular matrix molecules in plaques. Inflammatory cell activation also leads to release of excessive reactive oxygen species, and the resultant oxidative stress promotes endothelial apoptosis and plaque erosion. For example, leukocytes associated with atheroma release myeloperoxidase, an enzyme which produces hypochlorous acid. Hypochlorous acid can initiate apoptosis of

endothelial cells and contribute to their desquamation.(16) Oxidised LDL (OxLDL), a central element to the atherogenic process, may induce the expression of MMPs by human endothelial cells. This leads to activation of other members within the MMP family resulting in degradation of basement membrane collagen and desquamation of endothelial cells.(4, 17) The resultant friable cap may render plaques susceptible to rupture and thrombosis.

In the seminal work by Burke *et al*, post-mortem microscopic examinations of men with coronary artery disease who died suddenly showed the average thickness of ruptured fibrous caps to be 23±19μm.(18) This observation led to the adoption of a thickness of 65μm (based on the mean ± 2SD) as the defining point of a thin fibrous cap, and the widely accepted notion that thin cap fibro-atheromas were "vulnerable" and prone to rupture. However, weakened fibrous cap alone does not always suffice to precipitate plaque rupture, neither is a thin fibrous cap a pre-requisite for plaque rupture.(4) Computational simulations of plaque progression gives evidence that the propensity of plaque to rupture is dependent on the stage of plaque progression, and that the thickness of the necrotic core is also critical in determining the likelihood of plaque rupture.(19) Mechanistic studies of the proteinases implicated in plaque destabilisation have shown similarly complex results, indicating the presence of dynamic interactions between these proteases and the progression/remodelling of plaques.(20)

In addition to inflammatory cell activation, other mechanisms must also have a pathogenic role in plaque rupture or erosion. A proportion of patients presenting with acute coronary syndrome do not show signs of upstream inflammatory activation, as evidenced by normal level of CRP measured by high sensitivity assays.(21) Examples of alternative triggers include extreme emotional disturbance, intense physical exertion, temperature changes, and infections. The ability of external stressors to trigger acute coronary events has been

attributed to the surge in sympathetic nervous system action, which leads to an increase in heart rate, blood pressure and cardiac workload, as well as local vasoconstriction at the site of vulnerable plaques, thereby precipitating plaque destabilisation.(22, 23) Mechanical shear stress at the level of the arterial wall can also precipitate subclinical inflammation in the micro-environment of culprit stenosis, precipitating a chain of events leading to plaque instability.(24)

1.5 Dynamic nature of plaque progression

Despite the central role of plaque rupture or erosion in acute atherothrombosis, a proportion of plaque events are clinically silent.(25-29) In the absence of clinical sequelae, the ruptured plaque is organised, remodelled, and incorporated into the atherosclerotic plaque itself. The majority of plaques causing over 50% diameter stenosis have evidence of old healed plaque rupture with incorporation of thrombus into the atheroma.(26, 30) Multiple healed plaque ruptures are typically required for high-grade coronary arterial stenosis to develop.(31) Amongst patients who died suddenly of myocardial infarction, evidence of healed myocardial infarction were found in approximately half of those patients without obvious vascular thrombosis, suggesting that coronary event(s) had occurred in the past.(32) In non-selected patients without a history of heart disease who died of non-cardiac cause, post mortem studies revealed evidence of plaque rupture at around 10% of cases. In patients with known risk factors for CAD who died of non-cardiac causes, evidence of plaque rupture could be found in slightly higher proportions.(33) When extensive histological examination of coronary arterial was performed in such populations, the evidence for plaque rupture was over 30%.(34) These evidence strongly support the concept of a variable response after acute plaque destabilisation.

The dynamic nature of plaque progression is further demonstrated by the PROSPECT trial, which remains the largest prospective study of the natural history of coronary atherosclerosis. In this study, intravascular ultrasound (IVUS) was used to follow up patients with acute coronary syndrome (n=697) for 3 years in order to observe the occurrence of adverse cardiac event. Of the 595 thin cap fibro-atheromas (TCFAs) identified in 313 patients by virtual histology (VH) on IVUS, only 26 of these plaques were at the sites of subsequent plaque events during a median follow up of 3.4 years. More than 3000 non-culprit lesions were identified by IVUS at the index coronary events in this study, but only 6.4% were directly accountable for subsequent MIs and deaths at 1 year. Assessed by angiography, nearly half of the new coronary events originated from non-culprit lesions, most of which appeared to be mild at the time of initial revascularization.(35) Similarly, in the VIVA (VH-IVUS in vulnerable atherosclerosis) study, 170 CAD patients underwent 3-vessel VH-IVUS at the time of index treatment. Over a median follow up of 625 days, 68% (13 of 19) of MACEs resulted from non-culpril lesiosns at the initial examination.(36)

The dynamic nature of plaque progression is further supported other prospective studies using VH-IVUS to document plaque progression. In one study, 216 non-culprit lesions in 99 patients were examined by IVUS over a 12-months period. During this time, resolution of VH-TCFA was observed in 75% (n=15) of the lesions classified as TCFA at baseline, while 13 lesions progressed to TCFAs during this period. Six lesions which were deemed thick cap fibro-atheromas subsequently became TCFA at follow up.(37) In another study, 14 patients with 28 distinct ruptured plaques without significant luminal stenosis were followed up for a mean of 22 months with serial IVUS, while being maintained on optimal medial therapy. By the time of final follow up, half of the ruptured plaques had healed with improvement of luminal stenosis. Importantly, no clinical events related to the ruptured plaques were recorded during the period.(38) One study used IVUS to serially examine left main coronary artery of

207 patients, and observed reduction of atheroma area in up to 36% of cases. Interestingly, a change in the position of maximal plaque area was observed in 4% of cases at the time of follow up.(39)

1.6 Variable consequences of plaque rupture

These observations convey the important information that stability, or vulnerability, of each plaque lesion may change in a temporal manner; that plaque rupture or erosion is frequently asymptomatic and contributes to stepwise plaque progression of the lesion. The complexity of post-mortem and clinical observations has underpinned the challenge in existing efforts to identify a common phenotype of plaque "vulnerability". Given the dynamic nature of plaque progression which may result in morphological changes of a lesion over time, and the frequency of plaque rupture without clinically symptomatic events, other substrates must be present to catalyse significant arterial thrombosis after a plaque rupture/erosion event. Accordingly, the paradigm which implies a single type of culprit coronary plaque at the root of all plaque vulnerability cannot hold true, and it is likely that plaque destabilisation can occur in plaques of different phenotypes.

Irrespective of the underlying phenotype, a subset of plaque rupture or erosion events trigger the extremes of clinical manifestation via significant arterial thrombosis, while the rest resolve otherwise unnoticed with no symptoms and progress on the path of plaque remodelling. It is plausible that such divergent pathological cascades are the results of differential biological pathway(s) activation after the plaque rupture event. For example, plaque rupture may lead to the acute release of protein molecules that activate an enzymatic pathway, and corresponding changes of the substrates involved in the process. Alternatively, the acutely released molecules can mediate biological signals, resulting in activation of other cell types and secondary uptake or release of molecules and further downstream signalling as a para-phenomenon (Figure 1). Such complex interactions form the spectrum of biomarkers the plaque rupture event, but are challenging to characterise using conventional candidate marker based research techniques.

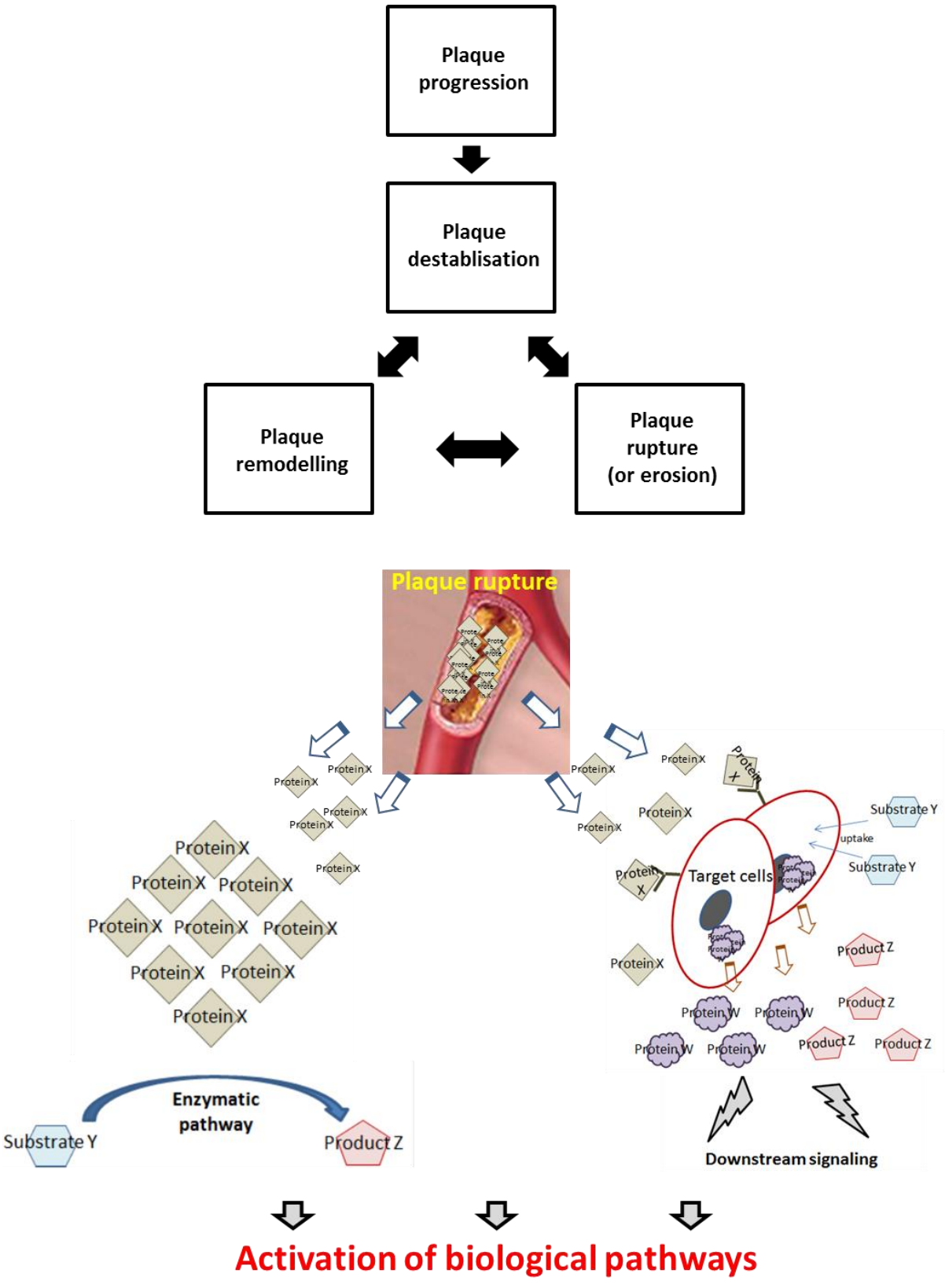


Figure 1: Dynamic nature of plaque progression and potential biological signatures of plaque rupture

1.7 Novel biomarkers of plaque rupture and clinical implications

Specific biomarkers of coronary atherosclerotic plaque rupture have remained elusive despite significant research effort in the scientific community.(40) Although several candidate markers have been proposed as potential markers of plaque rupture, based on their plausible implication in the plaque destabilisation process, none have been established as a robust biomarker of the event. Examples of these candidate markers include MMPs, TIMPs, myeloperoxidase, and oxidised low density lipoproteins. The utility of these candidate markers will be further examined in Chapter 3.

In modern clinical practice, the most widely used biomarkers in the setting of ACS are the cardiac troponins (cTnIs), which are subunits of the thin-filament-associated troponin-tropomysin complex. Since the seminal reports on the specificity of cardiac troponin as a marker of myocardial injury in the setting of acute coronary syndrome(41), elevated plasma troponin level have been shown by several large-scale studies to predict the risk of adverse outcomes in ACS. Such evidence has led to the acceptance of cardiac troponin as the gold standard of diagnostic and prognostic marker in ACS(42), and the inclusion of troponins as a key index in the "universal definition" for the criteria of diagnosis of AMI.(43)

Despite their critical importance in modern clinical practice, there are limitations to the use of leakage proteins due to myocardial cellular damage as a biomarker for ACS. One major limitation related to the lag time to diagnosis, due to the release kinetics of cTnIs, has largely been negated by newer generations of high sensitivity assays which detect clinically relevant changes within few hours of clinical presentation.(44)

Irrespective of the potential for improvement of clinical troponin assays the fundamental issue remains: biomarkers of myocardial ischemic damage do not advance our insights to the upstream pathological event of plaque rupture. Given the systemic involvement of

atherosclerosis, biomarker(s) of plaque rupture can be of value to the management of other acute vascular syndromes since end organ damage due to acute plaque events can also occur elsewhere in the vasculature. One such prime example is in the management of carotid artery stenosis in the absence of definitive symptoms, which remains a major challenge in vascular medicine.(45) More importantly, novel biomarkers of plaque rupture will confer further insights into the biological processes ensuing plaque rupture that is applicable to different vascular territories. Ultimately, it may provide alternative strategies for modulation of atherothrombotic disease.

1.8 Discovery of novel biomarkers using "-omics" platforms

Advances in mass spectrometry (MS) based analytical techniques have triggered a paradigm shift in biomarker research away from traditional approaches that focus on a limited number of candidate markers, enzymatic reactions, or single pathways.(46) Mass spectrometry based techniques have assisted target discovery in cardiovascular disease in recent years and enabled high-throughput identification or quantification of large and small molecules (proteins, metabolites, and lipids) in biological samples affected by atherosclerosis.(46-48) Amongst the different mass spectrometry platforms, liquid chromatography (LC) – tandem mass spectrometry (MS/MS) is a technique widely employed for proteomics profiling in atherosclerotic disease. For example, Bagnato *et al* demonstrated feasibility of proteomics analysis using paraformaldehyde fixed coronary arteries by LC-MS/MS.(49) Similar techniques have also been applied to examine the secretome of human atherosclerotic arteries to ascertain what may be released to the circulation *in vivo*(50) for the analysis plasma of patients presenting with acute coronary syndrome.(51, 52)

LC-MS is less established as a tool for plasma metabolite profiling in patients with coronary atherosclerosis. Nevertheless, studies have utilised this as a tool to characterise differences in

metabolite profiles observed in acute myocardial ischemia in patients with established coronary artery disease. Myocardial ischemia was followed by increased lactate levels and changes in tricarboxylic acid cycle intermediates and breakdown products of adenosine monophosphate. The LC-MS approach provided quantitative data and allowed grading of relative degrees of ischemia.(53) Using LC-MS, similar metabolic changes were also observed in patients undergoing alcohol septal ablation as a model of planned myocardial infarction.(54)

Profiling of plasma lipids using LC-MS techniques represents a greater challenge. The chemistry required for chromatography in LC-MS can be difficult to optimise, as many lipids are not soluble in solvent systems commonly used in reverse-phase carbon 18 (C18) columns, thereby escaping subsequent MS analysis.(55) Matrix assisted laser desorption ionisation – time of flight (MALDI-TOF) MS is an emerging alternative technique for high throughout lipid analysis of complex biological samples.(56) MALDI-TOF-MS has recently been utilised for plasma lipidomic profiling in other disease states.(57, 58) Specific to atherosclerosis research, MALDI-TOF-MS has recently been applied for characterisation of plasma phospholipids of hyperlipidemic patients.(59)

Further to the analysis of the individual proteome, metabolome, and lipidome fraction, it is increasingly recognised that the combined application of proteomics, metabolomics and lipidomics offers the potential to identify emergent behaviour that cannot be observed by studying individual fractions in isolation.(60) Results from proteomics data, in conjunction with biological network analysis, can facilitate the selection of other molecules whose release profiles are highly correlated and thus have a higher probability of being regulated by common mechanism(s). This inferential analysis approach thus provide a tool which can reveal potential novel pathophysiology pathways central to a disease, as the inter-connections

between significant differentially expressed proteins can be the result of deregulations of a common component within the network. The integration of plasma "multi-omics" also has the potential utility of cross-validation of findings from each fraction, as information derived from one -omics fractions can help focus the investigation in the other fractions.(60, 61)

The value of integrating proteomic, metabolomics/lipidomic analysis is progressively recognised in the field of cardiovascular research. Existing literatures in this field has mainly focused on integrating -omics characterisation of tissue samples, as the analysis of plasma proteome poses particular challenges (the particular challenges of plasma proteomic analysis will be discussed in further detail in Chapter 5 of this thesis). For example, Mayr *et al* combined proteomic and metabolomics for the investigation of atherosclerotic vessels of Apolipoprotein E deficient ($ApoE^{-/-}$) mice(62), vascular smooth muscle cells from the arterial media of $ApoE^{-/-}$ mice (63) and microparticles isolated from human atherosclerotic plaques.(64) Similar approaches have also been applied for the profiling of human atrial fibrillation(65), atrial remodelling in congestive heart failure(66), and protein kinase C mediated cardio-protection.(67) There are rare reports of integrated -omics analysis for plasma samples, such as a recent study which reported a combined lipidomic and metabolomics approach for the characterisation of plasma in a hamster model of atherosclerosis.(68) Details of these exemplary studies on integrated proteomic, metabolomics, lipidomic profiling in cardiovascular research are summarised in Table 1.

So far there is no report of the utilisation of integrated plasma proteo-metabolo-lipidomics for the investigation of coronary atherosclerotic plaque rupture. It will be the aim of this thesis to explore the utility of such an approach for the discovery of novel biological signatures for this critical event.

1st Author	Year	Disease model (species)	Sample matrix	"-omics" analytic techniques	Main findings	Ref
Mayr	2005	Atherogenic ApoE$^{-/-}$ (Mice)	Aortic tissue	Proteomic : 2D GE, MALDI-TOF-MS, LC-MS/MS Metabolomic:^{1}H- NMR	79 proteins were altered during various stages of atherogenesis. Oxidative stress in the vasculature reflected by the oxidation status of peroxiredoxin. Decline in alanine and depletion of adenosine nucleotide pool in ApoE$^{-/-}$ mice. Plaque lesion was associated with alterations of malic enzyme	(62)
Mayr	2008	Atherogenic ApoE$^{-/-}$ (Mice)	SMCs from aorta	Proteomic: 2D GE, LC-MS/MS Metabolomic: ^{1}H NMR	Progenitors of SMCs in vascular adventitia (Sca-1^{+} cells) were distinct from wild type SMCs under both normoxic and hypoxic conditions. Key enzymes in glucose metabolism were among the proteins differentially expressed in Sca-1+ cells, resulting in faster glucose consumption and compensatory reduction in baseline IL-6	(63)
Mayr	2008	Atrial fibrillation [AF] (Human)	Atrial tissue	Proteomic: 2D GE, MALDI-MS, LC-MS/MS Metabolomic: ^{1}H NMR	Elevation of beta-hydroxybutyrate, glycine, and ketogenic amino acids observed in patients with persistent AF. Differential expression of 3-oxoacid transferase was also observed. Patient susceptible to post operative AF showed discordant regulation of energy metabolites.	(65)
Mayr	2009	Atherosclerosis (Human)	Plaque derived microparticles (MP)	Proteomic: 2D GE, LC-MS/MS Metabolomic:^{1}H NMR	Plaque MPs express surface antigens consistent with their leukocyte origin, including MHC class I and II, and induced a dose dependent stimulatory effect on T-cell proliferation. Taurine was highly enriched in plaque MPs.	(64)
Mayr	2009	Protein Kinase C epsilon transgenic (Mice)	Mitocondrial, cytosolic proteins from heart	Proteomic: 2D GE, LC-MS/MS Metabolomic: ^{1}H NMR	Creatine kinase, pyruvate kinase, lactate dehydrogenase, cytosolic form of aspartate amino transferase, and malic enzyme were differentially expressed in PKCε transgenic mice. These were dependent on PKCε activity, and had pronounced effects on glucose and energy metabolism	(67)
De Souza	2010	Ventricular-tachypacing [VTP] induced CHF (Canine)	Primary Cardio-myocytes	Proteomic: 2D GE, LC-MS/MS Metabolomic: ^{1}H NMR	Decreased antioxidant proteins (superoxide dismutase and peroxiredoxin); rapid increase in heat shock protein (HSP) 27, HSP60 and HSP70; delayed increase of GRP78, HSP90, and α-B-crystallin) were observed at 2-week VTP. Early changes in glucose and alanine persisted as CHF developed.	(66)
Jove	2013	Atherogenic diet (Golden Syrian Hamster)	Plasma, aortic tissue	Metabolomic: LC-MS/MS, Lipidomic: LC-MS/MS	Novel changes observed in PPARγ pathway, oxidative and endoplasmic reticulum stress, and cell senescence. High fat diet induces up regulation of taurocholic acid, and down regulation of taurine and phenylalanine. This effect on taurocholic was modulated by a grape seed extract.	(68)

Table 1: Summary of studies which utilised an integrated proteomics, metabolomics, or lipidomics analysis in cardiovascular research.
(Abbreviations in order of appearance**:** ApoE$^{-/-}$:Apolipoprotein E deficient, 2D GE: 2 dimensional gel electrophoresis, MALDI-TOF-MS: matrix assisted laser desorption ionisation time-of-flight mass spectrometry, LC-MS/MS: liquid chromatography tandem mass spectrometry, SMC: smooth muscle cell, NMR: nuclear magnetic resonance, CHF: congestive heart failure, PPARγ: peroxisome proliferator activated receptor gamma**)**

1.9 Hypothesis and Aims

1.9.1 Hypothesis

Stenting induced disruption of coronary atherosclerotic plaque *in vivo* mimics the natural plaque rupture event. This leads to the release of novel biomarkers and changes in plasma molecular profile that can be characterised using a selection of analytic techniques.

1.9.2 Aims

- To quantify existing candidate plasma markers implicated in acute coronary syndrome and their behaviour after a timed plaque disruption event.
- To determin the utility of intravascular imaging by optical coherence tomography (OCT) for assessment of atherosclerotic plaque pathology *in vivo*.
- To determine the feasibility of using an integrated plasma proteomics, metabolomics and lipidomics approach to identify novel biological signatures of atherosclerotic plaque rupture.

CHAPTER 2

GENERAL METHODS
AND
PRE-ANALYTIC CONSIDERATIONS

In this Chapter, a general outline of the framework for the study is presented, followed by detailed discussions on the pre-analytic considerations leading to the determination of a optimal blood preparation method applied for this research. Detailed descriptions of the individual laboratory techniques used at different stages of this thesis will be further elaborated in the corresponding chapter(s).

2.1 Ethics and regulatory approval

The study protocol was approved by the Oxfordshire Research Ethics Committee (OREC, Ethics Reference 08/H0603/41). The original study protocol allowed for recruitment of 100 patients undergoing PCI with stents. The OREC subsequently approved a protocol amendment which allowed for recruitment of 200 patients and inclusion of patients undergoing diagnostic angiography without stenting. Recruitment of university staff as Healthy Volunteers was conducted accordingly to the University of Oxford Occupational Health Policies.(69)

PCI with stent placement applies radial force to the diseased segment of coronary artery and disruption of the underlying atherosclerotic plaque. This *in vivo* model of plaque disruption allows the examination of temporal behaviour of subsequent biomarker release in reference to the defined baseline. Patients who underwent diagnostic (Dx) angiography without stenting served as control subjects in this experimental model. The steps involved for Dx angiography (arterial needle puncture/catheterisation, intra-arterial passage of guidewires, injection of contrast and acquisition of x-ray images) were the same as PCI but without stenting.

2.3 Study design

This was a prospective, single centre, cohort observational study at the John Radcliffe Hospital (JRH), Oxford. Patients aged 30-90 who were referred for non-emergency coronary angiography with the view to proceed to stenting were invited to participate in the study. The

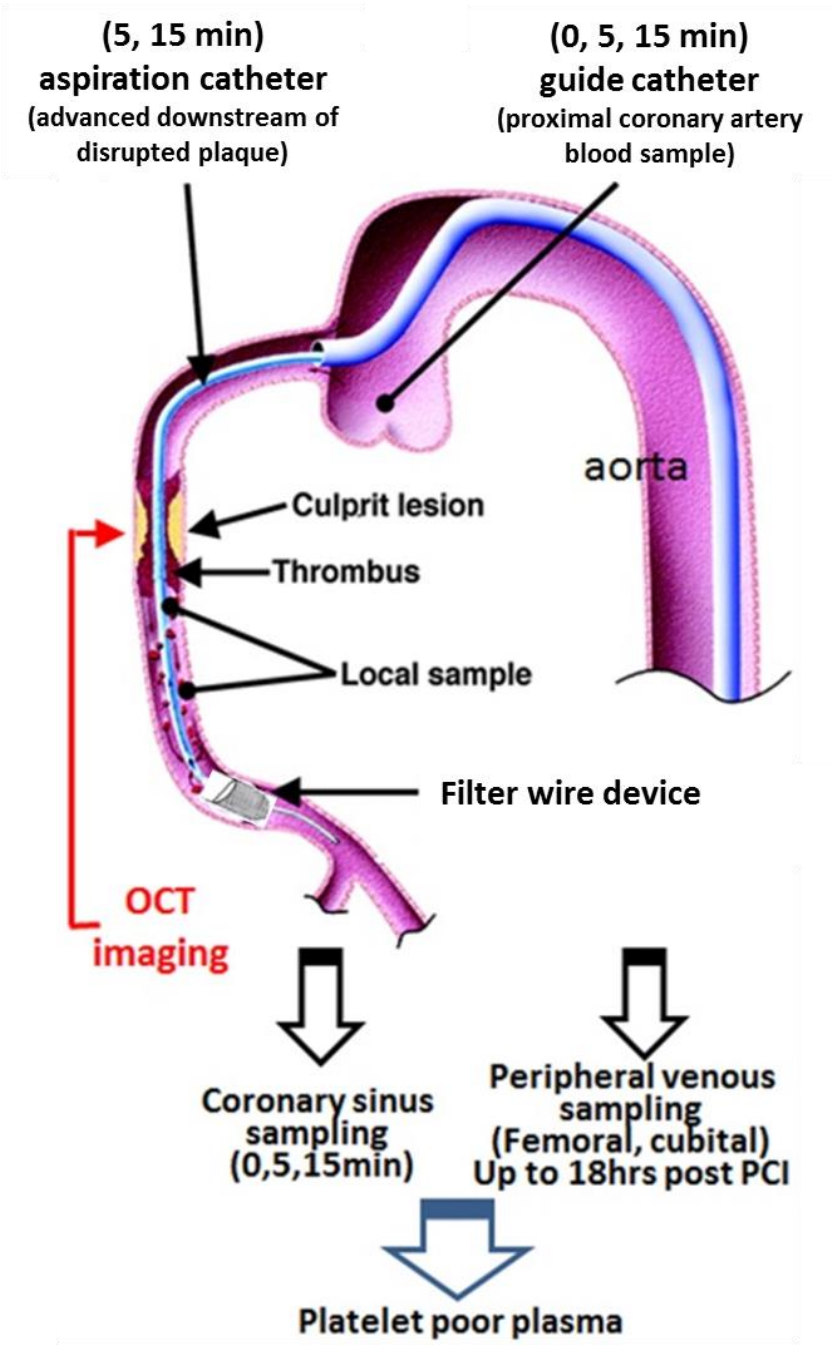
exclusion criteria included: haemodynamic instability, known history of renal impairment or anaemia, and PCI for left main coronary disease. Written informed consent was obtained from patients planned for coronary angiography with the view to proceed to PCI.

Coronary angiography procedure was performed by the interventional cardiologist(s) in accordance to routine clinical practice. Optical coherence tomography of the diseased coronary artery segment was performed prior to the deployment of stent in a subset of patients, as deemed anatomically suitable by the interventional cardiologist. Where clinically indicated, a distal protection device was used to prevent downstream embolisation and for the retrieval of cellular debris liberated by the stent placement. Blood samples were collected from targeted anatomical sites, at specific time points in reference to stent placement. This included coronary aspiration catheter for sampling of arterial blood downstream of the lesion, and/or coronary sinus sampling in a subset of subjects. Other demographic data, medical history and procedural related information were recorded. The study procedures are summarised by Figure 2. Further detailed blood sample collection schedule is described in Section 2.4.

2.4 Blood sample collection

Blood samples were collected from: coronary artery, coronary sinus, and peripheral vein (femoral/ brachial) at specific time points. Standard guiding catheters were used for blood sampling from proximal coronary artery and coronary sinus during the PCI procedure. Peripheral venous bloods were obtain from either indwelling venous catheters or fresh venepunctures. The time points for blood sampling for participants undergoing PCI with stent is summarised by Figure 2-B. Collection of blood sample downstream of plaque disruption will be described in Section 2.4.1. The same time points applied to Dx angiography patients except for stent placement, and the beginning of procedure was used as the baseline.

A.



B.

	Beginning of precedure	Stent placement (0 min)	5m	15m	30m	1hr	2hr	6hr	18hr
Coronary artery*	+		+	+					
Coronary sinus	+		+	+					
Peripheral venous	+		+	+	+	+	+	+	+

Figure 2: Summary of study procedures and blood sampling time points

2.4.1. Use of aspiration catheter for arterial sampling

In selected patients, deemed anatomically suitable by the PCI interventional cardiologist, a dedicated aspiration catheter was used for arterial blood sampling downstream of the stented lesion at 5 and 15 minutes after stent placement. Three types of aspiration catheters were used during the study [Export (Medtronic, Minneapolis, USA), Pronto LP (Vascular Solutions, Minneapolis, USA), Hunter (IHT Worldwide, Barcelona, Spain)]. In each case, the catheter was carefully passed over-the-wire downstream of the stented segment and 5mls of arterial blood aspirated. This procedure was abandoned if difficulty was encountered during the intra-arterial passage of catheter.

2.4.2 Coronary artery plaque debris retrieval by filter wire

Where clinically indicated (large native artery or vein graft with significant disease), a Filterwire device (Boston Scientific, Massachusetts,USA) was deployed downstream of the lesion in a standard matter. The umbrella-like polyurethane mesh contains 110µm pores to allow passage of blood components while trapping the debris material released during angioplasty. The filterwire was retrieved at the end of the procedure. The filter section (containing coronary artery plaque debris) was divided from the body of the guiding wire and placed in a cryovial for immediate freezing on dry ice and subsequently stored at -80°C.

2.4.3 Use of distal protection device

In a few highly selective cases (large right coronary artery and a focal plaque lesion), the Guardwire® system (Medtronic, Minneapolis, USA) was used to attempt distal arterial occlusion downstream of the lesion and for aspiration of the static column of arterial blood sample from the coronary artery. Briefly, a compliant balloon was positioned distal to the target lesion and inflated immediately prior to stent deployment. This transient occlusion of arterial flow would result in a static column of blood enriched with substances liberated by

the disrupted plaque. Aspiration of the static blood column was performed prior to release of the guarding balloon. The rest of the angiography procedure was performed as routine.

2.5 Overall strategy for the discovery workflow

As discussed in the preceding chapter, plaque disruption *in vivo* likely results in a heterogeneous pattern of biological response in individuals. This limits the applicability of traditional approaches of clinical research in search of novel biomarkers whereby the inclusion of increasing numbers of study subjects is believed to improve the statistical power for the differences observed. Assuming a dichotomous biomarker responses from the plaque disruption event, the average response observed in an overall cohort will converge towards the median (ie with no apparently biological effect). In this instance, the statistical power for the observation is actually decreased by the inclusion of larger numbers of subjects because of the heterogeneity of response intrinsic in the cohort (Figure 3).

One way to improve the statistical power in such instance is to focus the analysis on the subgroup of subjects enriched with the biological signals. In the case where there are dichotomous biomarker responses (such as group “A” and “B” in Figure 3), analysis of subjects at the extremes of the spectrum will lead to observations with higher signal to noise ratio, thereby increasing the chance of detecting the underlying differences. The subset of cohorts with enriched signals are better suited as the basis of a discovery cohort for the comprehensive plasma -omics discovery analysis. In addition, coronary plaques are a highly enriched source of potential biomarkers released after the plaque disruption event. Direct analysis of the plaque samples can provide further information to the selection of putative novel targets observed in plasma.

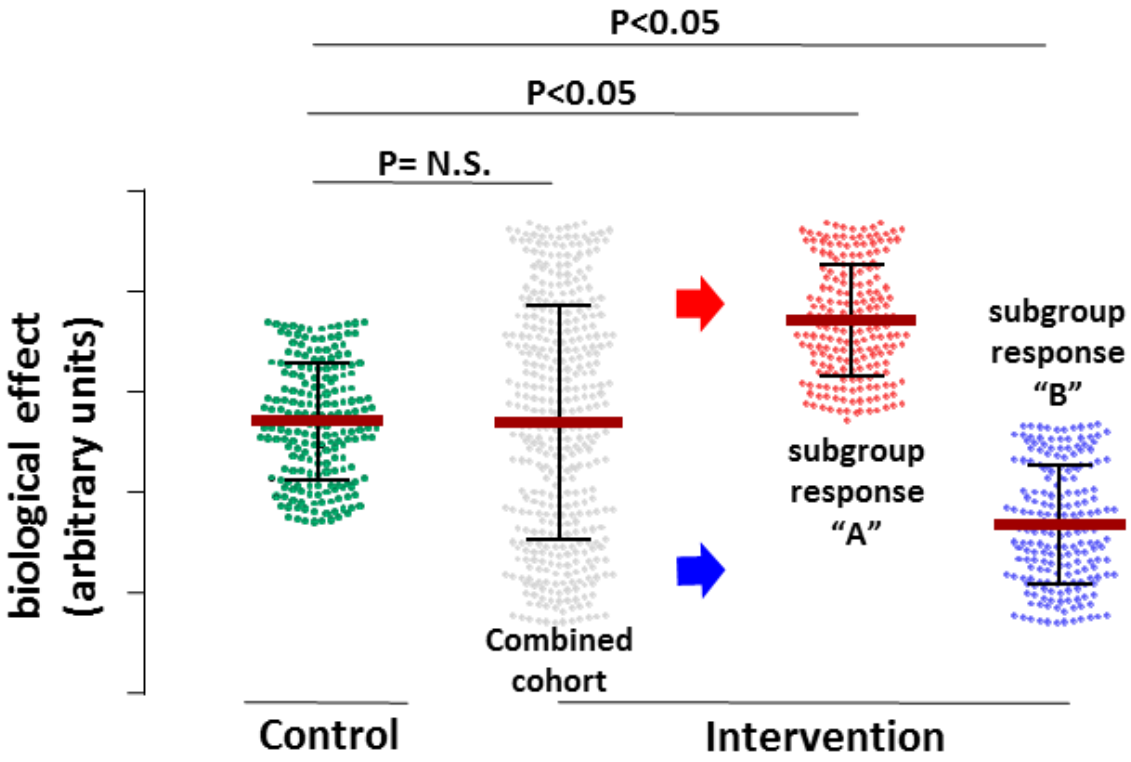


Figure 3: Failure to detect differences in a biological effect due to inappropriate grouping of subjects.

This is an illustration of how the statistical power for detecting a difference in observed effect can be diluted when there is inappropriate grouping of the subjects. The brown bar represents the mean, and the black error bars represent the standard deviation from the mean. In this scenario, there are two types of underlying biological response after an intervention in a population (response "A" and "B"). The standard deviation for the observed effect in each subgroup is smaller as compared to the standard deviation observed in the combined cohort. Without the correct consideration of subgroup, it would appear the intervention leads to no difference in biological response as compared to the control group. However, significant differences in response are clearly observed between the subgroups (A and B) as compared to control. The traditional approach to increase statistical power for detecting a difference between intervention and control group is to increase the numbers. However, this approach is counter-productive in such scenarios, as the variance (standard deviation) observed within the combined cohort will not be improved by the increase of numbers examined.

The overall biomarker discovery workflow for this thesis is summarised in Figure 4. In the first phase (*screening phase*), candidate marker analysis were performed on the overall study cohort. Based on the results of candidate marker analysis, an algorithm was devised for the selection of a subset of cohort likely to contain enriched biomarker signals to form the discovery cohort. An additional panel of candidate markers was measured in the of discovery cohort, with the view to ratify the validity of the selection algorithm. In the *discovery phase*, plasma samples from the discovery cohort and plaque debris samples collected using the filterwire device were subjected to proteomic, metabolomic and lipidomic analysis, leading to the discovery of potentially novel biological signatures of coronary atherosclerotic plaque rupture.

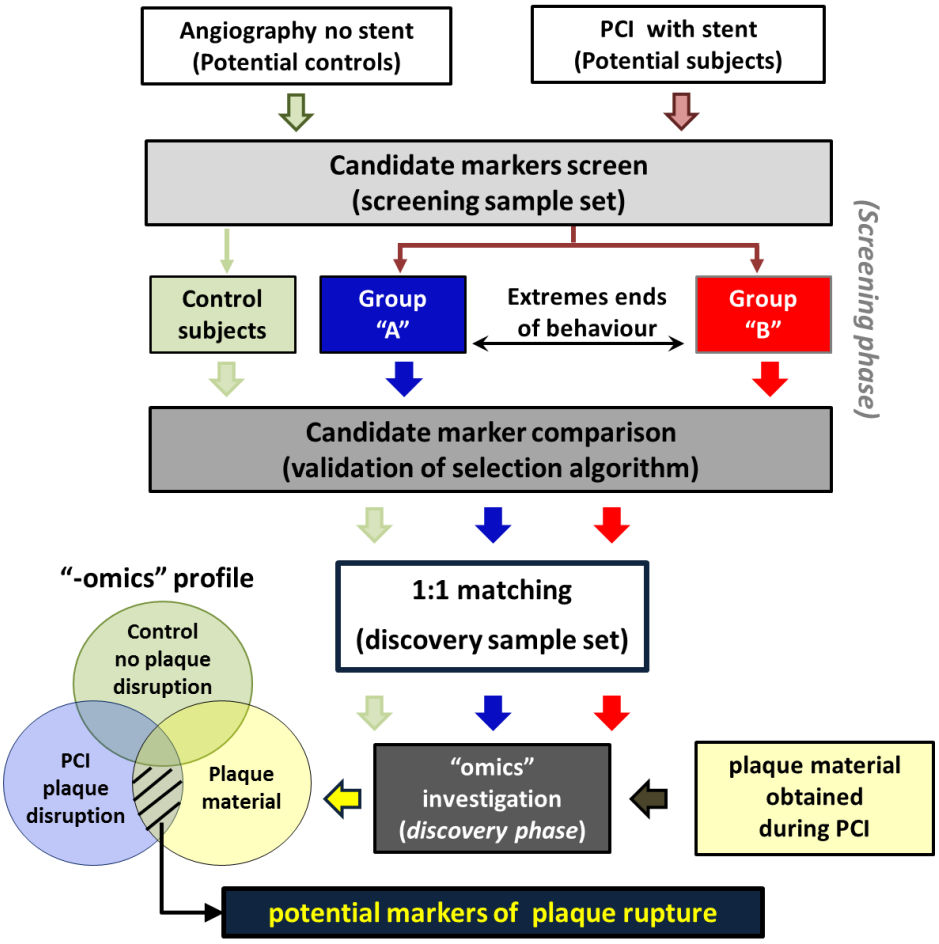


Figure 4: Flow chart of biomarker discovery workflow for this research

2.6 Pre-analytic considerations for plasma sample preparation

Pre-analytic factors can influence subsequent measurement of plasma biomarkers. These issues to consider at the time of blood sample preparation are broadly related to the type of anticoagulants used and the parameter settings during blood centrifugation to separate plasma (force, duration, temperature).(70, 71) Serum, obtained after coagulation of whole blood, contains significantly different protein and metabolite contents as compared to the plasma prepared from the same sample. This is largely due to consumption / productions of proteins involved in the coagulation pathway and *ex vivo* activation of platelets and neutrophils.(72) Based on this consideration, serum sample was considered not a suitable sample matrix for the use in this study.

2.6.1 Parameters for plasma preparation

Platelets are increasingly recognised as a source of circulating biomarkers, such as cytokines, in cardiovascular disease (CVD).(73, 74) Incomplete removal of platelets from plasma samples in clinical research may be undesirable, yet there is sparse literature describing the effect of platelet contamination on biomarker measurement in clinical studies. It is common practice in clinical studies to transfer and centrifuge blood samples at refrigerated conditions (e.g. 4°C) for preparation of plasma samples.(75-77) Higher levels of platelet derived substances observed in plasma prepared under refrigerated conditions have been thought to be due to *ex vivo* release after platelet cold activation.(70, 78) However, there is no published literature on the effect of temperature during blood sample processing and the residual platelet count in plasma samples.

An example of how residual plasma platelet may confound plasma protein marker levels in clinical studies is the measurement of soluble CD40 ligand (sCD40L). Platelet is the major source of sCD40L in circulation. sCD40L has pro-inflammatory and pro-coagulant properties

and high level of plasma sCD40L is commonly regarded as a marker of *in vivo* platelet activation and therefore associated with increased cardiovascular (CV) risks.(79) However, the reported associations between plasma sCD40L and cardiovascular risks have been inconsistent in literature. Two large, prospective studies (the CAPTURE trial(80) and the Women's Health Study(81)) published in the noughties, reported the prognostic value of sCD40L as a biomarker for predicting subsequent CV risk both in patients with established CAD and otherwise healthy individuals. However, such observations were not replicated in other subsequent large prospective cohorts. For example the Dallas Heart Study(76) and the FATE study(82) both reported lack of association between plasma sCD40L and subsequent CV risks. A review of these studies revealed significant differences between the methods of plasma sample preparation (Table 2). Interestingly, the study design of the Dallas Heart Study, published in the American Journal of Cardiology(83), described a different plasma preparation protocol as compared to the methods described by the subsequent research finding paper published in another journal.

Study	Year	Cohort type	Plasma preparation protocol as published by study	Ref
CAPTURE trial	2003	CAD	No mention	(80)
Women's Health Study	2001	HVs	EDTA plasma stored in liquid nitrogen	(81)
Dallas Heart Study	2005	CAD	EDTA plasma, centrifuged at 1430g for 15min at 4°C centrifuged at 1000g for 15min at 4°C	(76) (83)
FATE study	2005	HVs	No mention	(82)

Table 2: Summary of the plasma preparation protocols for major studies on the prognostic value of soluble CD40 ligand (sCD40L) in CAD patients and healthy volunteers

These major studies reported conflicting observations on the prognostic value of sCD40L on cardiovascular events in both CAD and HV subjects. However, the plasma preparation protocols were not reported for three of these studies. Of note, the Dallas Heart Study published incongruous sample preparation protocol in different manuscripts. (EDTA: Ethylene-diamine-tetra-acetic acid)

The residual cellular contents in plasma are dependent on the duration and force applied during plasma preparation. Indeed, centrifugation at low force for a short duration is a recognised laboratory method for the preparation of platelet enriched plasma.(84) Since platelet is the main reservoir of sCD40L, I hypothesised that the different plasma preparation protocol could confound the results of subsequent sCD40L measurement due incomplete platelet removal. I further hypothesised that preparation of plasma sample under refrigerated conditions could result in incomplete removal of platelets, which in turn affected the level of sCD40L measured.

To address the hypothesis, additional patients were recruited for a single blood sample collection. This group consisted of two *parallel* cohorts. The first cohort included 15 HVs (9 males, 6 females, age 35±8 years) who do not have any history of medical problems and not taking any current medication. The second cohort included 40 CAD patients (32 males, 8 females, age 66±12 years) admitted to the JRH awaiting non-emergency percutaneous coronary intervention or coronary artery bypass surgery (CABG).[a]

In all subjects, blood samples were collected using BD-vacutainer® SST and K_2EDTA tubes for the preparation of serum and plasma, respectively. For serum, whole blood (WB) was allowed to clot at room temperature (RT) then centrifuged at 2500g for 15 minutes. In order to obtain plasma with a varying degree of residual platelets, a staged centrifugation algorithm was applied to WB using the following protocols, illustrated by Figure 5.

[a] The CABG patients were recruited under a separate study protocol (Ethics Ref 11/SC/0140), with the assistance of Dr Alexios Antonopoulos and Dr Marios Margaritis from the Antoniades group.

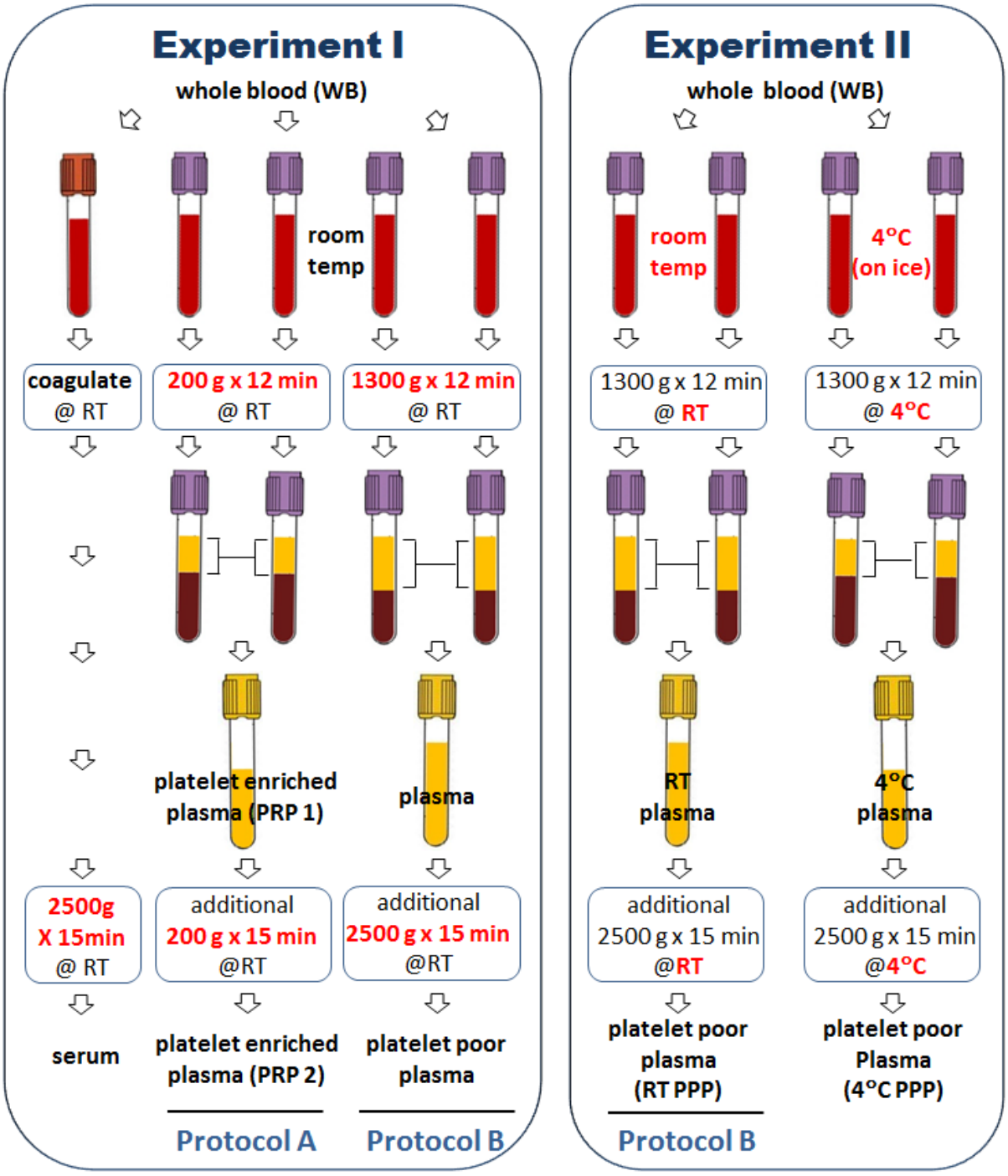


Figure 5: Flowchart for the centrifugation protocol to obtain plasma with differential residual platelet counts, and the experimental design to test the effect of residual platelet count on the level of plasma candidate markers

Protocol A was designed to obtain plasma enriched with platelets. [Platelet rich plasma (PRP)]. WB was centrifuged at 200g for 12 minutes. The supernatant (PRP1) was transferred to a BD vacutainer tube without additive. A fraction of this PRP1 was stored at -80°C. The residual fraction was subjected to an additional centrifugation at 200g for 15 minutes to obtain PRP2 and stored at -80°C.

Protocol B was designed to obtain routine plasma, and subsequently platelet poor plasma (PPP) from the same patient. WB was centrifuged at 1300g for 12 minutes. The supernatant layer, containing "routine" plasma, was transferred to a BD tube without additive. A fraction of the plasma was stored at -80°C. The residual fraction was centrifuged at 2500g for 15 minutes to obtain PPP and stored at -80°C.

To investigate the effect of centrifugation force, duration and temperature setting on residual platelet count and sCD40L measurements, I used the following experimental designs:

- Experiment I aimed to investigate the effect of residual plasma platelet on subsequent sCD40L measurement. Duplicate blood samples from each subject (HVs: n=15; CAD: n=15) were used for concurrent preparations of PRP1 and plasma, followed by concurrent preparation of PRP2 and PPP. These were performed at RT.
- Experiment II aimed to investigate the effect of temperature (during transit and centrifugation) on residual platelets and sCD40L in the resultant plasma matrix. Duplicate blood samples from each subject (CAD: n=25) were used for concurrent preparation of plasma, followed by concurrent preparation of PPP, either at RT or refrigerated (transferred on ice, centrifuged at 4°C).

Platelet counts were measured by the hospital laboratory Sysmex XE2100 analyser immediately after sample preparation. Plasma prepared using different protocols resulted in gradients of residual platelet counts in both the HV and CAD samples. After the initial

centrifugation, a proportion of the samples did not fulfil the criteria for PPP (platelet<$10x10^3/\mu l$). After the second centrifugation, all fulfilled the PPP criteria (Figure 6 – A, B). Quantification of sCD40L was performed using a Luminex® imuno-assays[b] (R&D Systems, Minneapolis, USA) according to the manufacturer's instructions. This assay had a lower limit of quantification (LLOQ) at 20pg/ml. Intra- and inter-plate variation (%CV) were both less than 10%. Given the non-normal distribution of the platelet count and sCD40L in samples, Wilcoxon matched-pairs signed rank tests were used for comparisons between the sample types within each cohort. P value of less than 0.05 was considered significant.

In both HVs and CAD patients, the centrifugation protocol resulted in significant reduction of residual platelets between PRP1/PRP2, and between plasma/PPP (Figure 6-A,B). Progressive removal of platelets also resulted in significant reduction of sCD40L between PRP1/PRP2, and between plasma/PPP (Figure 6-C,D, $P<0.001$ for all). Samples which contained more than $10x10^3/\mu l$ platelets (non-PPPs) and sCD40L level above the LLOQ were included to assess their association using Spearman Rank correlation. In both HVs and CAD patients, there was a highly significant correlation between the residual platelet and sCD40L in the sample (Figure 6–E, F; $P<0.0001$ for both).

Temperature settings had a significant effect on the residual platelet count in plasma. After the first centrifugation at 1300g for 12 minutes [the recommended setting for plasma preparation by manufacturers such as Beckon and Dickinson (BD)], 4°C-plasma contained significantly higher residual platelet compared to paired RT-plasma (Figure 7-A, $P<0.001$). Accordingly, 4°C-plasma contained higher level of sCD40L (Figure 7-B, $P<0.01$). After the additional centrifugation to obtain platelet poor plasma, no difference in sCD40L was observed between the RT-PPP and 4°C-PPP samples (Figure 7-C, D).

[b] For further description on the Luminex assays, please refer to Section 3.5.5,

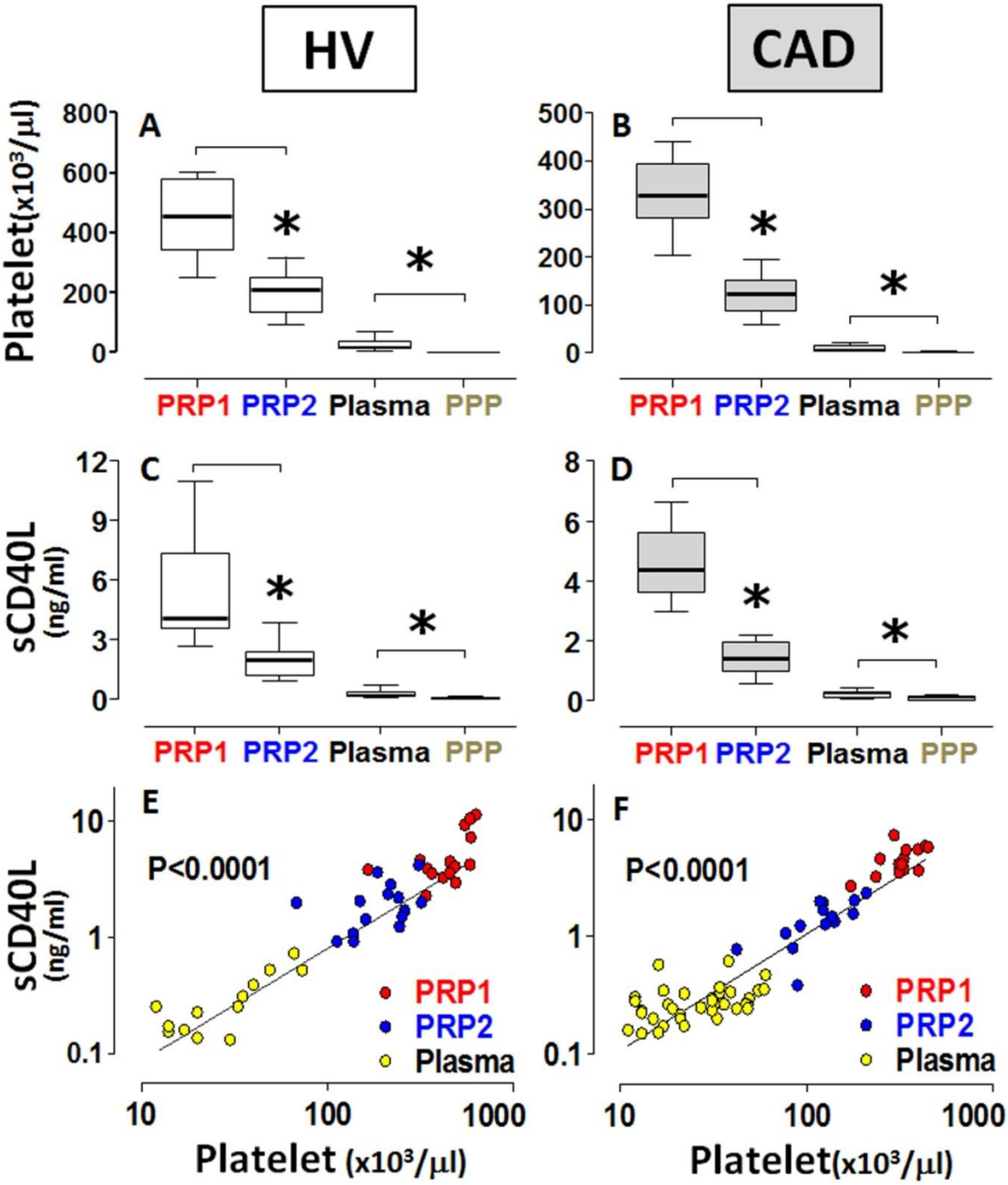


Figure 6: Significant correlations between residual plasma platelets and soluble CD40 ligand in both health volunteers and CAD patients

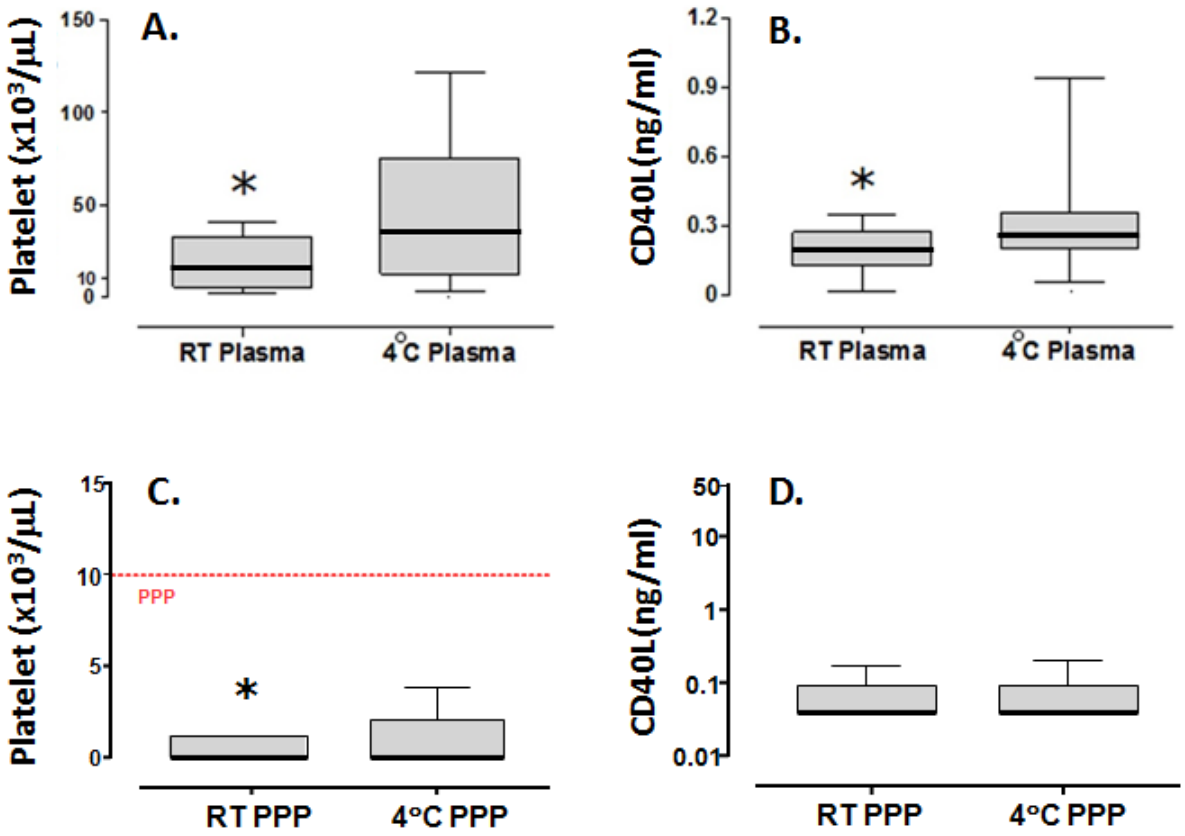


Figure 7: Effect of temperature during centrifugation on the levels of residual plasma platelets and soluble CD40 ligand

Paired plasma samples with differential residual platelet counts were collected from subjects with coronary artery disease (CAD, n=25), using the staged centrifugation protocols described in Section 2.6.1 of this thesis. Platelet counts were measured by Sysmex XE2100 analyser immediately after sample preparation. Quantification of soluble CD40 ligand (sCD40L) was performed using an enzyme-immunoassay. Wilcoxon matched-pairs signed rank tests were used for comparisons between the sample types within each cohort. P values of less than 0.05 were considered statistically significant. (Data are presented as median and inter-quartile range.)

After the first centrifugation at 1300g for 12 minutes [the recommended setting for plasma preparation by manufacturers such as Beckon and Dickinson (BD)], plasma prepared under refrigerated conditions (4°C-plasma) contained significantly higher residual platelets compared to paired plasma prepared under room temperature (RT-plasma) (Panel A), and higher levels of sCD40L (Panel B). After the additional centrifugation step at 2500g for 15 minutes, all samples fulfilled the criteria of platelet poor plasma (platelet count<<10x10^3/µl) (Panel C), and no difference in sCD40L was observed between the resultant RT-PPP and 4°C-PPP samples (Panel D).

(Lee, R., et al. Int J Cardiol, 2013 Sep 30;168(2):1648-50.(85) Figure panel A and B are reproduced with permission from Elsevier)

In experiment I, I demonstrated that sCD40L was highly correlated to *residual* platelets within the prepared plasma sample, both in HVs and CAD patients. Therefore, the real biological significance of plasma sCD40L can only be assessed in the absence of platelet contamination. Interestingly, there was no correlation between whole blood platelet counts to the level of sCD40L in either routine plasma or serum of the same subjects (data not shown). In experiment II, I demonstrated that preparation of plasma sample using time and force settings recommended by Beckon and Dickinson in refrigerated conditions, resulted in higher residual platelets compared to paired plasma sample prepared at RT. Accordingly, higher levels of sCD40L were observed in the 4°C-plasma samples.

Previous studies that observed higher levels of platelet derived substances in plasma prepared at cold temperature attributed this to be the result of *ex vivo* platelet activation.(70, 78) The findings within this thesis indicate that the higher levels of platelet derived substances (as in this case, sCD40L) observed in 4°C plasma are in fact not the result of platelet activation *(in vivo* or *ex vivo)*, otherwise the level of sCD40L would have remained the same despite further removal of platelets by additional centrifugation. Rather, freeze-thawing of samples results in cell lysis. Freeze thawing of plasma samples containing residual platelets therefore results in varying degree of platelet lysis(86) and shedding of platelet derived contents, such as sCD40L, occurs after storage.

Separation of cellular components by density gradient is a technique routinely used in laboratory practice.(87) The density of plasma is higher at 4°C as compared to at RT.(88) Although the effect of plasma density and on residual platelet count was not specifically examined, this density difference may partly explain the higher residual platelets when plasma samples are prepared under refrigerated conditions. Taken together, these results demonstrate that the common laboratory practice of preparing blood samples with single low

speed centrifugation under refrigerated conditions can result in unpredictable higher residual plasma platelets. This in turn confounds the measurement of platelet derived contents, such as sCD40L, as freeze thawing of the plasma samples lead to a varying degree of platelet lysis and release of the platelet derived contents.(85)

2.6.2 Choice of anti-coagulant for plasma preparation

Anticoagulants commonly used for preparation of clinical samples include: ethylene-diamine-tetra-acetic acid (EDTA), citrate, and heparin. The former two confer their anticoagulant property via chelation of trace metal ions such as Ca^{2+} that are required for the coagulation pathway.(89) Heparin induces a conformation change and enhances the inhibitory activity of anti-thrombin III. With the exception of factor VIIa, all coagulation factors are inhibited by anti-thrombin III.(90) Citrate anticoagulants are typically prepared in a liquid suspension in blood collection tubes, therefore a dilution correction factor has to be applied for quantitation of the plasma (or blood) contents.(91)

For this thesis, the choice between EDTA and lithium heparin (LH) as anticoagulants was considered. To investigate the effects of these two anticoagulants on subsequent measurement of plasma biomarkers, paired EDTA and LH platelet poor plasma samples were prepared using the two stage centrifugation protocol described in Section 2.7. Proteomic screening of paired PPP samples was performed for two subjects of the study.[c] The samples were analysed in technical duplicates. In this proteomic screen, over 600 proteins were measurable in the plasma samples. Principal component analysis (PCA)[d] showed distinct separations between the paired plasma prepared using EDTA or LH as anticoagulant (Figure 8-A). The majority of proteins showed no significant difference in abundance between the plasma sample types. However, the abundance of 41 proteins differed significantly between the

[c] Please refer to Chapter 5 for detailed descriptions of the plasma proteomics methods
[d] Please refer to Section 4.1.7 for further explanation on principal component analysis (PCA)

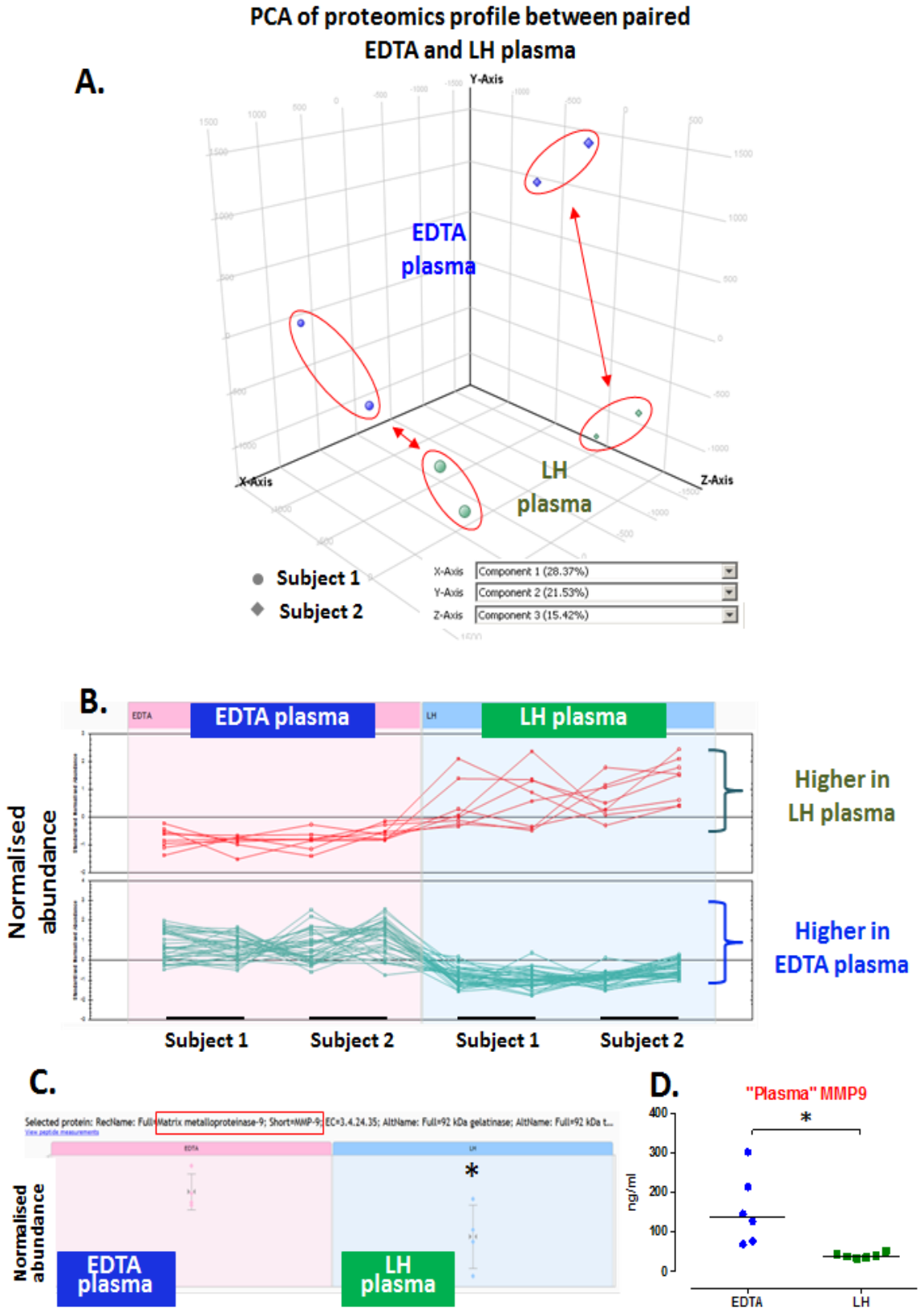


Figure 8: Comparison between protein profiles in paired plasma samples prepared using EDTA or lithium heparin as anticoagulant

paired PPP samples prepared using different anticoagulant. LH samples contained significantly lower abundance of 33 proteins, while EDTA sample had lower abundance in 8 proteins (Figure 8-B). Amongst these, MMP9 was one of the proteins found to be lower in abundance in LH samples in the proteomics screen (Figure 8-C). To confirm this observation from MS analysis, a separate experiment was performed using paired EDTA and LH PPP samples collected from patients with CAD (n=6). The levels of MMP9 were measured using Luminex® assays (HCVD1-67AK, Merck Millipore, USA). The significant difference between the two types of sample matrix was also observed (Figure 8-D, $P<0.05$).

A broad screen of the small molecules (metabolites and lipids) of the same paired PPP samples was performed according to methods described in section 4.3. In the lipid fraction, PCA scores plot revealed tight clustering of the technical replicates of the negative control samples, but a wide separation between the paired EDTA and LH samples (Figure 9-A). Similarly, PCA scores plot of the metabolite fraction also revealed tight clustering of the technical replicates, but a wide separation between the paired EDTA and LH samples (Figure 9-B). These observations provided further evidence that anticoagulants could confound measurement of small molecules in -omics analysis.

Heparin, a poly-sulfated glycosaminoglycan, is one of the most highly negatively charged compound in nature, which is associated with interactions with diverse proteins.(90) Heparin interaction with plasma proteins *ex vivo* can lead to interference with antibody-antigen binding required for enzyme immuno-assays. This can partially explain why different levels of proteins are observed in paired LH plasma samples as compared to EDTA. It is beyond the scope of this thesis to examine the exact mechanisms for the differences observed between the -omics screen in the plasma samples. Nevertheless such observations serve as a reminder of the critical importance of applying a carefully considered protocol in a clinical study.

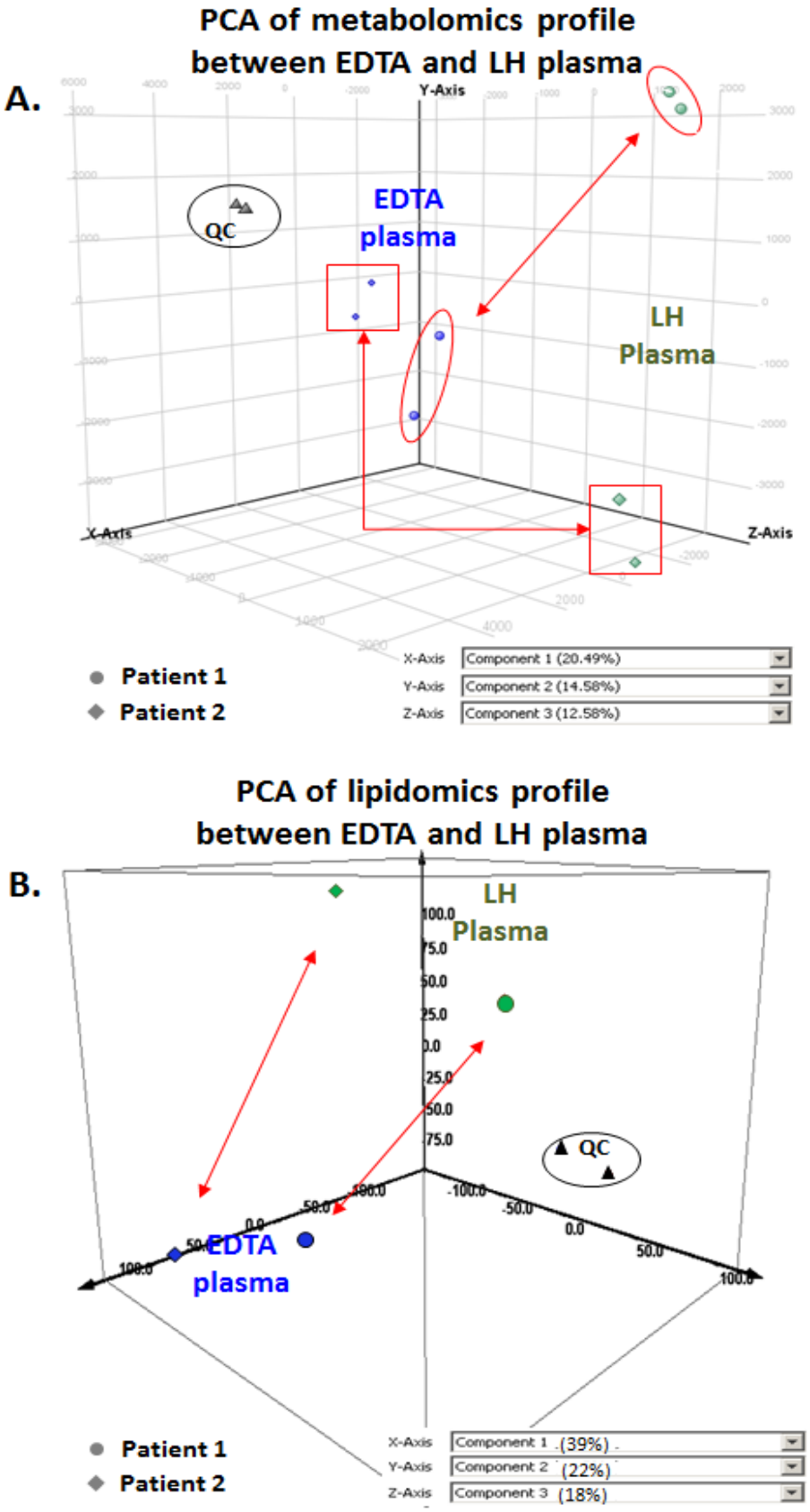


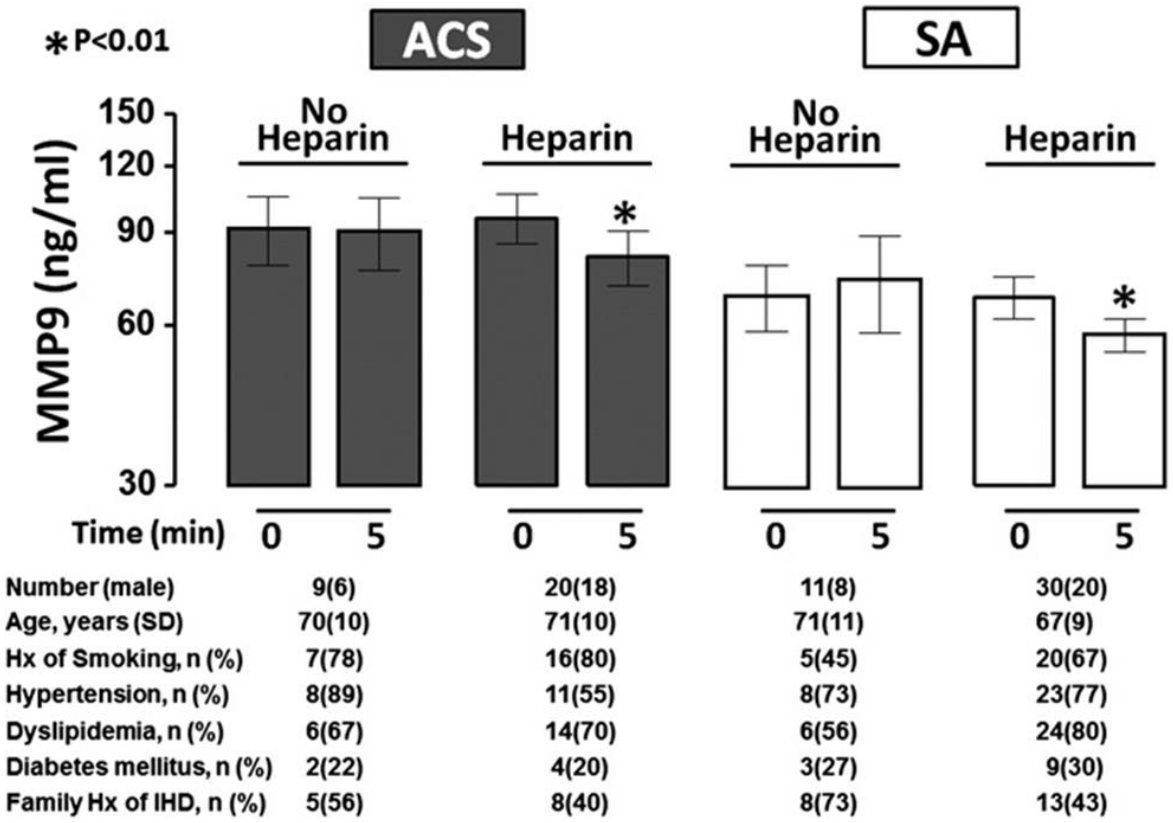
Figure 9: Comparison between metabolite and lipid profiles in paired plasma samples prepared using EDTA or lithium heparin as anticoagulant

2.6.3 *In vivo* effect of heparin administration on biomarker measurement

Having observed the *ex vivo* effect of heparin on plasma proteins, I hypothesised that systemic administration of heparin may also affect subsequent measurement of plasma biomarkers. This was an important consideration as heparin was commonly used as anticoagulant during PCIs.

To test this hypothesis, informed consent was obtained from subjects planned for coronary angiography with the view to proceed to PCI with stenting at the JRH (the majority of subjects included in this experiment also took part in the serial blood sampling protocol as described in Section 2.4). Baseline venous blood was collected at the beginning of the angiography procedure (Timepoint: 0 min). In subjects who demonstrated suitable lesion(s) for PCI [ACS: n=20, stable angina (SAP): n=30], intravenous heparin (70-100 i.u./kg) was administered after baseline blood sampling. A repeat venous blood sample was collected 5 minutes after heparin administration (Timepoint: 5 min). In subjects who were found to have significant coronary atherosclerosis but not suitable for PCI (ACS n=9, SA n=11), no intravenous heparin was administered as part of the angiography procedure, and a repeat blood sample was collected 5 minutes (5 min) after baseline. These subjects served as controls. EDTA platelet poor plasma was prepared using the same protocol as described in Section 2.7. Given the observations of *ex vivo* heparin effect on MMP9 at the proteomics screen and EIA observed in section 2.6.2, it was chosen as one of the marker for further investigation in this experiment regarding the effect of *in vivo* heparin administration.

Baseline characteristics between the treatment and control groups did not differ between the groups (Figure 10). At baseline, ACS patients had significantly higher MMP9 levels (mean=95.6±10.1ng/ml) compared to SAP (mean=68.1±6.1ng/ml) (P=0.02). However, administration of intravenous heparin resulted in significant, rapid reductions of plasma



Number (male)	9(6)	20(18)	11(8)	30(20)
Age, years (SD)	70(10)	71(10)	71(11)	67(9)
Hx of Smoking, n (%)	7(78)	16(80)	5(45)	20(67)
Hypertension, n (%)	8(89)	11(55)	8(73)	23(77)
Dyslipidemia, n (%)	6(67)	14(70)	6(56)	24(80)
Diabetes mellitus, n (%)	2(22)	4(20)	3(27)	9(30)
Family Hx of IHD, n (%)	5(56)	8(40)	8(73)	13(43)

Figure 10: Effect of systemic administration of heparin and the level of plasma MMP9 in coronary artery disease patients

Informed consent was obtained from subjects planned for coronary angiography with the view to proceed to PCI with stenting. Baseline venous blood was collected at the beginning of the angiography procedure (0 min). In subjects who demonstrated suitable lesion(s) for percutaneous coronary intervention (PCI) [ACS: n=20, stable angina (SAP): n=30], intravenous heparin (70-100 i.u./kg) was administered after baseline blood sampling. A repeat venous blood sample was collected 5 minutes after heparin administration (5 min). In subjects who were found to have significant coronary atherosclerosis but not suitable for PCI (ACS n=9, SAP n=11), no intravenous heparin was administered as part of the angiography procedure, and a repeat blood sample was collected 5 minutes after baseline. EDTA platelet poor plasma was prepared using the same protocol as described in Section 2.7 of this thesis. Plasma MMP9 level was measured by an enzyme immunoassay. At baseline, ACS patients had significantly higher MMP9 levels (mean=95.6±10.1ng/ml) compared to SA (mean=68.1±6.1ng/ml) (unpaired t-test, P=0.02). However, administration of intravenous heparin resulted in significant, rapid reductions of plasma MMP9 in both ACS and SAP groups, while No significant change in plasma MMP9 was observed in subjects who did not receive IV heparin. Importantly, heparin reduced the measurable MMP9 levels in ACS patients to levels comparable to that observed in the SA patients at baseline. (Data are presented in mean ± SEM; *=p value<0.01 by paired t-test.) (*Lee, R., et al. Int J Cardiol, 2013. 163(2): p. 212-3.(92) This figure is reproduced with permission from Elsevier.*)

MMP9 in both ACS and SA groups. No significant change in plasma MMP9 was observed in subjects who did not receive IV heparin. Importantly, heparin reduced the measurable MMP9 levels in ACS patients to levels comparable to that observed in the SA patients at baseline (Figure 10).

This experiment demonstrated the novel observation that heparin administration resulted in acute reduction of plasma MMP9 levels, in a way able to eliminate the biological difference in MMP9 levels between SA and ACS patients.(92) Amongst the potential heparin-protein interactions, heparin is known to bind to the C-terminus domain of MMPs.(76) This interaction would partially explain the acute reduction of plasma MMP9 levels after *in vivo* heparin administration, as heparin binding may interfere with antigen detection in enzyme immune-assays.

2.7 Discussion

The results presented thus far have provided several key insights pertinent to studies utilising clinical plasma samples. The parameters used for plasma sample preparation is often overlooked in clinical studies, both at the design and reporting stages. The conventional practice of transferring blood samples on ice and subsequently centrifuging blood under refrigeration has likely originated from the experimental evidence that cellular metabolism is reduced in hypothermic conditions,(93) which would in turn encourage a "homeostatic" state of the blood content until the samples are processed. These data provide evidence that variable contamination by platelets occurs when plasma is prepared under refrigerated conditions at the speed and force settings recommended by manufacturers. Such platelet contamination can confound the subsequent measurement of biomarkers, due to *ex vivo* release from lysed platelets after freeze thaw cycles. By minimising platelet contamination of

plasma samples, one will also minimise the potential confounding effect of *ex vivo* biomarker release without biological significance.

The two-stage centrifugation protocol was effective at minimizing platelet contamination, as demonstrated by achieving residual platelet of less than $10x10^3$/ul in all samples prepared. Indeed, over 60% (19 out of 30) of samples in Experiment I showed no detectable residual platelets by the Sysmex200 system after the additional centrifugation (at room temperature), thus the majority of samples prepared under this protocol were deemed platelet free plasma by definition. In contrast, plasma prepared under refrigerated conditions did not achieve the same proportion of platelet free plasma after the additional centrifugation, although there was no difference in the sCD40L levels in between the two types of platelet poor plasma.

One might suggest that preparing PPP under refrigerated conditions would result in benefits of both hypothermia (on *ex vivo* metabolism) and low residual platelets. However, cryoprecipitation of proteins occurs when blood samples are prepared at 4°C, which is a phenomenon utilised for the preparation of cryoprecipitates in transfusion services.(94) Indeed, this precipitation effect was also observed in MMP9 measured in paired RT and 4°C PPP samples, while proteins such as vascular cell adhesion molecular (VCAM) were not affected (Figure 11). Given the variable cryoprecipitation effect on plasma contents, optimisation of analysis should ideally be performed for analytes of interest in every study.

The observations regarding *ex vivo* effect by anticoagulants and subsequent plasma protein marker measurements are important. It is common for clinical studies to prepare plasma samples in different types of anticoagulant, in anticipation of potential future use in specific assays. (For example, due to the chelating properties of EDTA and citrate, EDTA and citrate plasma are not recommended for application in cell based activity assay, as incubation of the cells using EDTA or citrate plasma would lead to chelation of metal ions

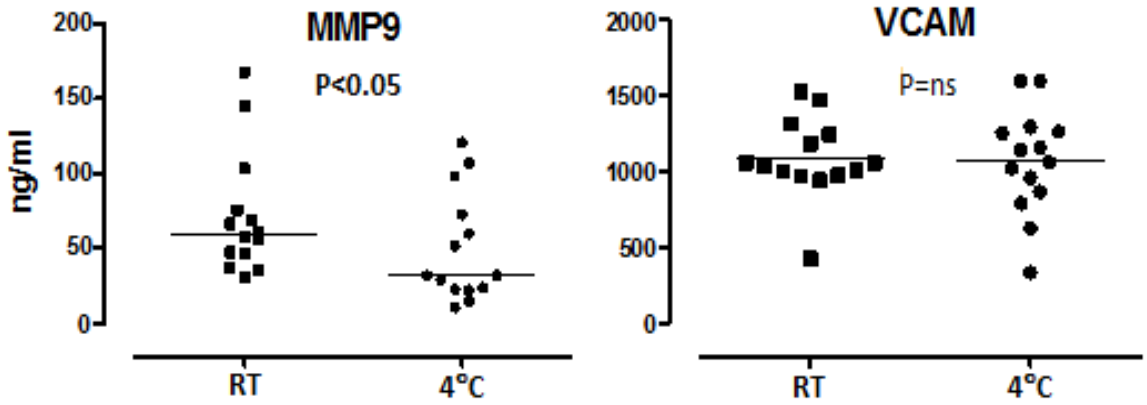


Figure 11: Effect of temperature during centrifugation on the level of plasma MMP9 and VCAM

Paired plasma samples were collected from subjects with coronary artery disease (CAD, n=14) in either room temperature (RT) or refrigerated conditions (4°C), using the staged centrifugation protocols described in section 2.6.1 of this thesis. Levels of matrix metalloproteinase 9 (MMP9) and vascular cell adhesion molecule (VCAM) were measured by enzyme immunoassays. Comparisons between the paired samples were by the Wilcoxon matched pair signed rank test. The level of MMP9 was significantly lower in plasma prepared under refrigerated conditions compared to RT. No difference was observed in the plasma level of VCAM between the two types of plasma. (Bars represents median. *: P<0.05)

required for binding to the cell culture vessel, leading to detachment of cells during subsequent washing steps.) It is imperative that when different types of plasma are stored for a study, no un-intentional (or intentional) mix-up of different plasma type occurs at the analytic stage. Otherwise the true biological differences may be undermined by the technical variability inherent to the different sample preparation type.

The *in vivo* effect of heparin administration and subsequent plasma biomarker measurement cannot be overlooked in clinical studies. When blood samples collection takes place during systemic heparin administration, such as during PCI, the definition of study time-points must be precise in reference to heparin administration. Subsequent work, which is not included as part of this thesis, has further demonstrated the confounding effect of systemic heparin administration on measurement of plasma microRNAs in patients with coronary heart disease.(95) Although the confounding effects of other medications were not investigated as part of this thesis, it was possible that such effects may also be observed to other systemically administrated medications. Clinical studies should ideally take all these variables into consideration, and ensure samples are collected at consistent time points.

The decision regarding optimal plasma preparation method for the purpose of this research was based on these considerations:

1. Blood samples were processed immediately after collection, at room temperature in the research annex of the Oxford Heart Center catheter lab.
2. EDTA was the anticoagulant of choice for the preparation of plasma.
3. Where intravenous heparin was given during the PCI procedure, the blood sample(s) collected after heparin administration was used as the baseline for comparison.

    - Platelet poor plasma was to be prepared using a two-stage centrifugation protocol: 1st spin at 1300g for 12 minutes, followed by the 2nd spin at 2500g for 15 minutes

CHAPTER 3

CANDIDATE MARKERS OF CORONARY ATHEROSCLEROTIC PLAQUE RUPTURE

3.1 Introduction

Discovery of biomarker(s) specific for the plaque rupture event may be potentially useful for early diagnosis of AMI and risk stratification in the setting of ACS. Several biomarkers have been proposed to be potential candidates based on experimental evidence showing local enrichments of these molecules in the atherosclerotic plaques. Studies have rigorously examined the utility of these candidate markers, lone or in combination, in clinical settings. Despite clear associations between many of these candidate markers in acute coronary syndrome, and in some instances offering additive prognostic values to established markers such as CRP and troponin, none has been established as a biomarker of coronary plaque rupture.(96)

Candidate marker analyses for this research were performed in two phases. During the *screening phase*, I assessed the response of a panel of the candidate markers that had been associated with plaque rupture in literature. Analysis of the candidate markers served several purposes. It was important to ascertain if any changes in biological signals were detectable in the plasma samples collected from this study cohort. Further, it was critical that the observed biological signals were consistent with findings reported in literature, as such observations would support the internal validity of this study. The candidate marker analysis would further provide information to guide the strategy for selection of a discovery subject subset for –omics analysis. Having selected a discovery subject subset based on results from the first *screening phase*, I analysed the level of additional candidate markers during a second *confirmation phase*, with the aim to ascertain the validity of my proposed slection algorithm for a discovery subject subset.

3.2 Candidate markers of atherosclerotic plaque rupture

The following section provides further discussions of the candidate markers that have been measured during this research.

3.2.1 Myeloperoxidase

Myeloperoxidases (MPO) are enzymes stored within primary granules of neutrophils and monocytes, that are released upon leukocyte activation and degranulation. MPOs regulate the formation of free radicals and diffusible oxidants, and are considered to be an important element in inflammatory responses and anti-microbial host defence.(97) With increasing recognition of a link between inflammation and the development of vulnerable plaques, cumulative evidence indicate MPO to be a potential biomarker for risk of CAD.(98)

3.2.2 Matrix metalloproteinases

Matrix metalloproteinases (MMPs) are a family of at least 28 secreted or surface bound proteases, categorised into subgroups according to their preferred substrates. Collectively, MMPs are responsible for the regulation of extra-cellular matrix homeostasis. The association between thinning of the fibrous cap and fatal plaque rupture has led to the hypothesis that collagen turnover contributes to the depletion of these extra-cellular matrix proteins.(4) Of the MMPs, MMP9 has attracted particular interest as a candidate marker of plaque rupture in many clinical studies. Increased expression and activity of MMP9 has been observed in the shoulder region of atherosclerotic plaques(99); patients with features of ruptured plaques on intravascular imaging also have higher plasma levels of MMP9(100); higher levels of MMP9 are observed in patients presenting with ACS compared to SAP (the plaque rupture event has already occurred in ACS patients)(101, 102); plasma MMP9 returns to a lower level days after the presentation with ACS and approaches the same as that observed in SAP.(101, 102) All these lines of evidence support the role of MMP9 as a potential biomarker of vulnerable

plaques. However, measurement of circulating MMPs are subject to confounding effects by pre-analytic factors, as highlighted by the findings presented in Chapter 2. Therefore the internal and external validities of published clinical studies on MMPs are challenging to establish.

3.2.3 Tissue inhibitors of MMPs

The activities of MMPs are regulated in part by their interaction with specific tissue inhibitors of MMPs (TIMPs). TIMPs bind to the active site of the MMPs in a stoichiometric 1:1 molar ratio, thereby blocking access to extracellular matrix substrates. Apart from this primary action, TIMPs may have cell-growth modulating properties and have been shown to stimulate the growth of fibroblasts.(103) Regulated expression of TIMPs has been shown to counteract MMP activity in atheroma and hence may influence plaque stability.(104) Down regulation of TIMP1 expression in human foams cells by interleukin-8 may be another mechanism through which TIMPs affect plaque stability.(105) TIMP1 in particular has been shown to be a prognostic marker for cardiovascular death amongst patients with CAD.(106)

3.2.4 Other candidate markers of plaque instability

Other candidate markers have been implicated in the pathobiology of plaque rupture. These markers are associated with plaque instability by virtue of: association with the lipid composition of plaques (OxLDL)(107); direct detection within plaque materials (lipoprotein-associated phospholipase A_2 [$LpPLA_2$](108), osteopontin(109), neutrophil gelatinase associated lipocalin [NGAL](110)); interactions with atheroma-associated cell signalling leading to plaque progression or destabilization (sCD40L)(81), growth differentiation factor-15 [GDF15](111), pregnancy-associated plasma protein A_2 [PAPP-A_2](112)). All of these markers have been shown in clinical studies to confer some additional predictive value in cardiovascular outcome in patient with CAD.(113) These markers were measured during the *confirmation phase*.

3.3 Intra-vascular assessment of plaque morphology

3.3.1 Features of vulnerable plaque

Coronary plaque composition and morphology has been extensively characterised in post mortem specimens. The accepted criterion for defining features of plaque vulnerability *in vivo* rely on a key assumption: that the lesions prone to rupture bear a strong morphological resemblance to ruptured plaques observed post mortem. These features include the presence of a thin fibrous cap (<65μm), macrophage infiltration of the fibrous cap, large necrotic core (>25% plaque area or 120% circumference), spotty calcification, intra-plaque haemorrhage, vasa vasorum proliferation and neo-intimal neovascularisation.(114)

3.3.2 Optical coherence tomography (OCT)

OCT is an imaging modality which utilises similar principles to intravascular ultrasound imaging, but uses near infra-red light to detect differences within the tissue sample. This leads to significantly higher image resolution compared to intravascular ultrasound and potentially advantageous for plaque morphology characterisation. Since OCT is not able to image through blood (or thrombus), clearing of blood either by proximal occlusion (occlusive method) or continuous flushing of contrast medium (non-occlusive method), is required for image acquisition. Selected representative features on OCT are highlighted in Figure 12. In a normal coronary artery, the vessel wall appears as a tri-laminar structure on OCT (Figure 12-A). The circular rings in the lumen are due to image artifacts from the imaging wire (Figure 12-A, white arrow). The presence of a lipid rich core can be readily differentiated from other lesions which contain mainly a calcific or fibrotic core. Necrotic lipid cores typically have a poorly delineated and diffuse distal border surrounding signal poor regions (lipid pool, Figure 12-B, white arrow). The overlying signal rich band corresponds to the fibrous cap (Figure 12-B, yellow arrow). The presence of a thin fibrous cap (<65μm) overlying a lipid pool in Figure 12-B is consistent with the morphology of a thin cap fibro-atheroma (TCFA). In contrast,

calcific contents within the plaque typically appear as well-delineated regions with relatively low reflectivity and low attenuation to light (Figure 12-C, white arrow), while fibrous plaques appear as well-delineated, homogenous regions with high back scattering (Figure 12-D, white arrow).(115)

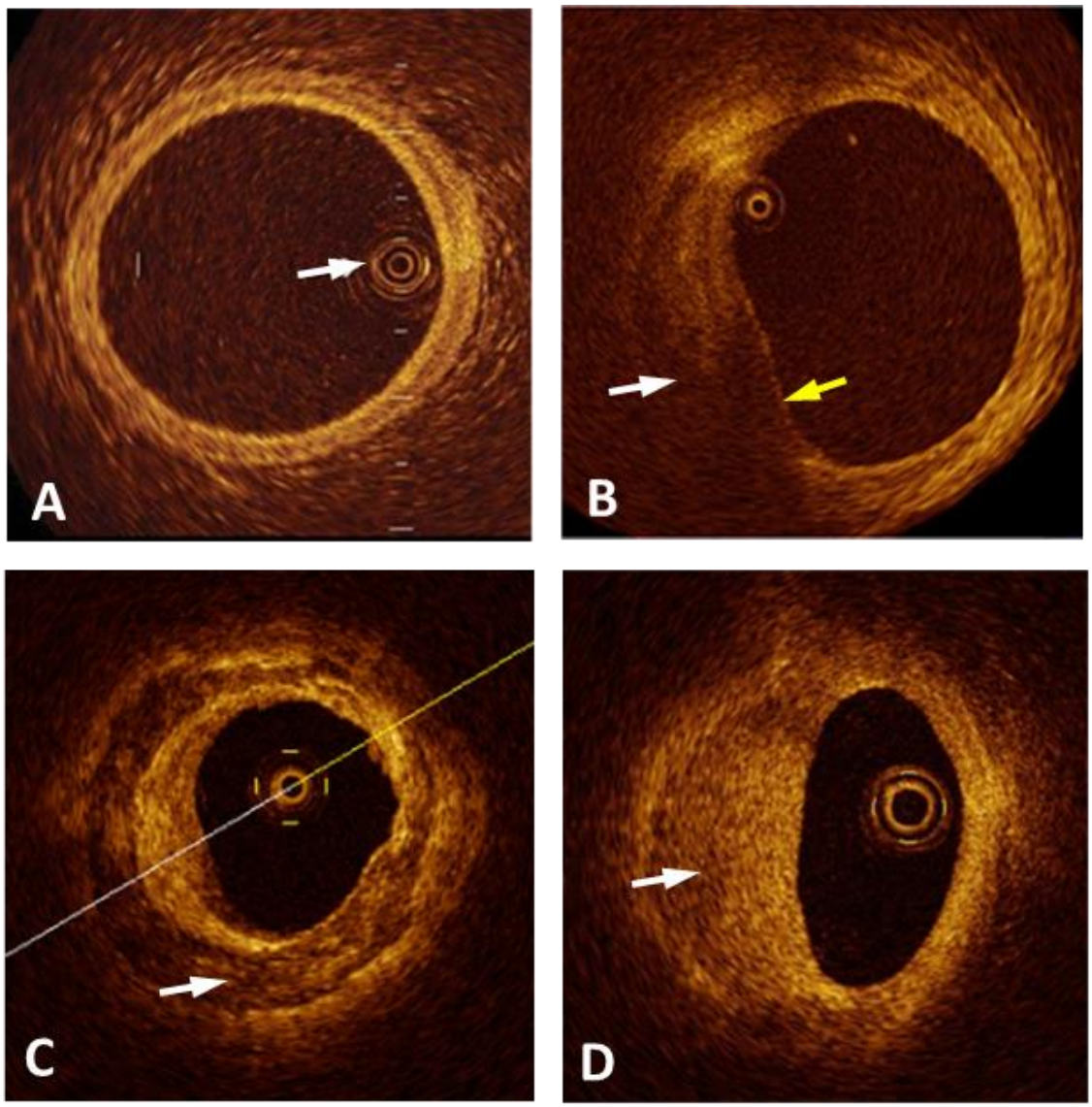


Figure 12: Representative features of coronary artery cross section obtained by intravascular optical coherence tomography imaging.

3.4 Hypotheses and Aims

The primary aim at this stage of candidate marker analysis was to determine if the plaque rupture event in this experimental model indeed resulted in changes of candidate marker signals. Specifically, I hypothesised that:

- The baseline biomarker profiles observed in this study cohort was consistent with the existing literature
- Stent induced plaque disruption would lead to acute changes in candidate markers that had been implicated in the pathophysiology of plaque vulnerability
- Plaque morphology, as defined by OCT, was a predictor of candidate marker release after plaque disruption
- It was feasible to define a subset of cohort with maximal biomarker response for the purpose of plasma -omics discovery analysis.

3.5 Methods

3.5.1 Study design and subjects

The recruitment of subjects and sample collection were described in section 2.3 and 2.4. EDTA blood samples collected from subjects were processed to obtain platelet poor plasma as described in Section 2.7. PPP samples were stored in aliquots at -80°C until subsequent analysis. Additional lithium heparin PPP samples were also collected at selected time points. These were used for measurement of clinical markers by the hospital laboratory.[e]

[e] For the rest of this thesis, uses of the term plasma refer to platelet poor plasma prepared by staged centrifugation at room temperature, as defined by Section 2.7.

3.5.2 Intravascular imaging by optical coherence tomography

3.5.2.1 OCT procedure

Two models of OCT console were used during the study: Lightlab M3 and C7 system (St. Jude Medical, Minnesota, USA). Slight variations in the procedural technique were required to adjust for the difference in catheter design for each system. The M3 system utilised an image wire, which could be advanced directly to the segment of diseased artery for image acquisition. The C7 system utilised an image catheter which required passage over an existing 0.14F guidewire. Image acquisition was considerably (5x) faster in the C7 system and allowed for a longer segment of the coronary to be imaged at once.

In both systems, the non-occlusive technique was used to achieve blood displacement by a viscous iso-osmolar contrast solution (Visipaque^{TM}, GE Healthcare, UK) to allow for image acquisition. After fluoroscopy confirmation of imagewire/catheter position, image wire/catheter pull back was performed at the highest available speed during simultaneous infusion of Visipaque^{TM} (through the guiding catheter). Typically, 20ml of Visipaque^{TM} infusion was required to complete an image acquisition. The acquired raw data was stored on the OCT console for the procedure for subsequent analysis.

3.5.2.2 Analysis of OCT images

OCT analyses were performed in batches throughout stages of the study using the terminologies defined by the expert review document. The assessors were blinded to the clinical status and other biomarker measurements of the patient[f]. The culprit lesion was categorised into two subtypes (lipid-rich and non-lipid) using a pre-defined scoring system. Discordance between observers were resolved by taking a consensus reading. A binary score was then assigned to each culprit lesion for comparison with other variables.

[f] Independent analysis of OCT images were kindly performed by Dr. David Adlam, Glenfield Heart Centre, University Hospitals of Leicester NHS Trust.

3.5.2.3 Scoring system for lesion morphology on OCT

For each culprit lesion, the image frame containing the minimal luminal area (MLA) was identified and selected as the index frame. Ten additional frames (5 antegrade + 5 retrograde) flanking the index frame were also included in the analysis. Each frame was further divided into 4 quadrants, centred from the vessel lumen. Each quadrant was assessed for the presence of lipid, calcium, or fibrous lesion(s). A score of 1 was assigned for presence of each feature in that quadrant. (eg. Lipid: 1, calcium: 0, fibrous: 0). A total score (maximum = 4) was assigned for each feature in the frame by adding the scores from all quadrants. The average score over 11 frames (index + 10 flanking) were then calculated for each feature. A lesion was defined as "lipid-rich" if the average lipid score was the highest. Lesions which have higher fibrous or calcium scores were defined as "non-lipid" plaques (Figure 13).

3.5.3 Clinical diagnostic blood tests

Measurement of plasma CRP (by a high sensitivity assay), cTnI, and CKMB, and blood cholesterol profiles were performed by the clinical biochemistry / haematology department at the JRH.

3.5.4 Single analyte measurement with enzyme linked immunosorbent assay

Enzyme linked immune-sorbent assays (ELISAs) were performed using commercially available kits, according to the manufacturer's instructions. Serum sample prepared from one healthy volunteer was stored in multiple aliquots at -80C, and used as a biological quality control (QC) sample in every assay throughout the period of this research. For each assay, an additional non-biological QC was included by diluting neat standard solution by a factor of 50x (1:50). This QC was measured as technical replicates both at the beginning and at the end of each plate, and was used to determined the intra- and inter-plate co-efficient of variation (%CV)

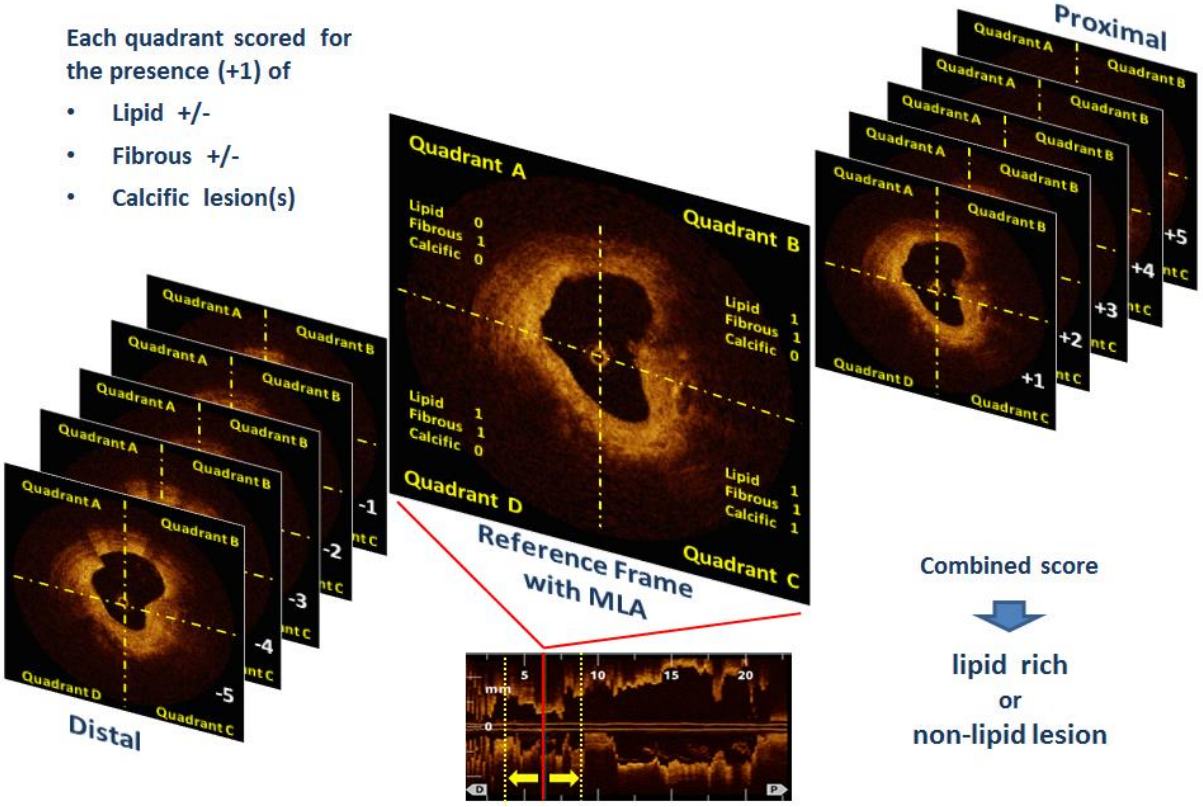


Figure 13: Graphical illustration of the scoring method for classification of plaque morphology on OCT imaging

Intravascular optical coherence tomography (OCT) imaging of coronary arteries was performed according to methods described in Section 3.5.2 of this thesis. For each culprit lesion, the image frame containing the minimal luminal area (MLA) was identified and selected as the index frame. Ten additional frames (5 antegrade + 5 retrograde) flanking the index frame were also included in the analysis. Each frame was further divided into 4 quadrants, centred from the vessel lumen. Each quadrant was assessed for the presence of lipid, calcium, or fibrous lesion(s). A score of 1 was assigned for presence of each feature in that quadrant. (eg. Lipid: 1, calcium: 0, fibrous: 0). A total score (maximum = 4) was assigned for each feature in the frame by adding the scores from all quadrants. The average score over 11 frames (index + 10 flanking) were then calculated for each feature. A lesion was defined as "lipid-rich" if the average lipid score was the highest. Lesions which have higher fibrous or calcium scores were defined as "non-lipid" plaques.

3.5.5 Multi-analyte screening with Luminex® platform

The Luminex® platform can quantify multiple analytes in a single assay by combining the principles of flow cytometry with sandwich ELISA. Instead of a flat solid phase (typically a microplate for ELISA) used for the anchoring of capture antibody, the Luminex® platform uses small polystyrene beads (5.6μm in diameter) as the solid phase. These beads are infused with varying amounts of red and infrared dyes, with the surface of beads coated with specific capture antibodies for an analyte (Figure 14-A).

The principal steps of a Luminex® assay are similar to a sandwich ELISA at the incubation stage, with the key differences at the analysis stage. In Luminex® assays, analysis of samples occurs after aspiration of the individual beads in suspension through a flow chamber on millisecond time scales. Due to the hydrodynamic influence of the fluid, these beads form a single file line as they flow through the fluidic chamber. At this stage, two lasers are used to cause excitation of the dye inside the beads. The first red laser (635nm) causes emission of fluorescence at different wavelengths based on the composition of the dyes. This confirms the identity of the beads (corresponding to the antibody coated to the surface). The second green laser (532nm) excites the reporter molecules bound to the secondary antibody. (Figure 14-B) The intensity of fluorescence emitted by the reporter molecule determine the abundance of antigen bound on each bead, therefore allowing quantification of the amount of analytes present. Since the beads carrying bound analytes are read singularly, in sequence, more than one type of beads (carrying different types of primary antibody) can be used in one experiment. This allows quantification of multiple analytes in the same experiment.

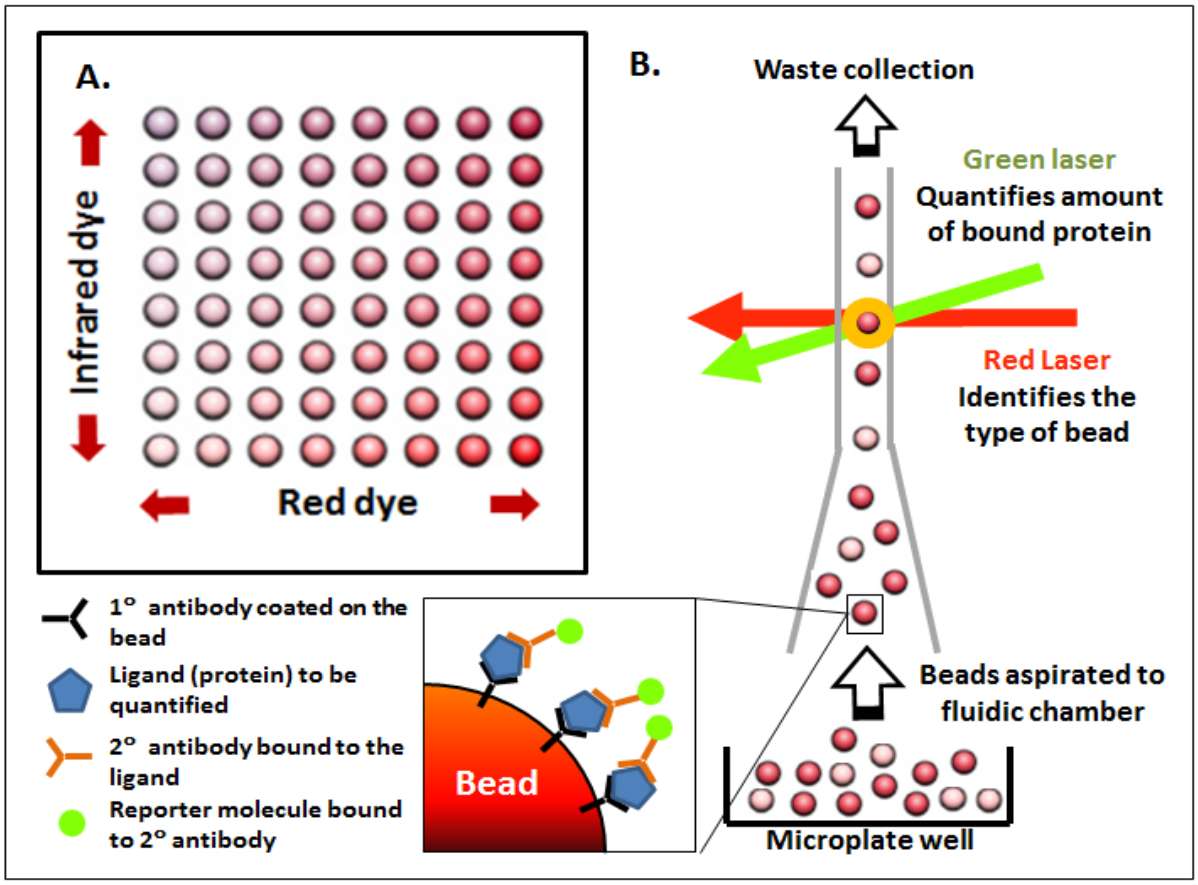


Figure 14: Principles of multi-analyte profiling by the Luminex® platform

Panel A: The Luminex® platform uses small polystyrene beads (5.6µm in diameter) as the solid phase coated with primary antibody against an analyte (eg. a protein). These beads are infused with varying amounts of red and infrared dyes, with the surface of beads coated with specific capture antibodies for an analyte.

Panel B: In Luminex® assays, analysis of samples occurs after aspiration of the individual beads in suspension through a flow chamber. Due to the hydrodynamic influence of the fluid, these beads form a single file line as they flow through the fluidic chamber. At this stage, two lasers are used to cause excitation of the dye inside the beads. The first red laser (635nm) causes emission of fluorescence at different wavelengths based on the composition of the dyes. This confirms the identity of the beads (corresponding to the antibody coated to the surface). The second green laser (532nm) excites the reporter molecules bound to the surface of the beads. The intensity of fluorescence emitted by the reporter molecule determine the abundance of antigen bound on each bead, therefore allowing quantification of the amount of analytes present. Since the beads carrying bound analytes are read singularly, in sequence, more than one type of beads (coated with different types of primary antibody) can be used in one experiment. This allows quantification of multiple analytes in the same experiment.

3.5.6 List of candidate markers measured

The following were amongst the candidate markers measured by Luminex® assays during the *Screening Phase*:

- MPO, MMP9: (HCVD1-67AK, Merck Millipore, USA)
- MMP 2,3,7,8: (Flurokine MAP Luminex kit, LMP000, RnD Systems, UK)
- TIMP 1,2,3,4: (Flurokine Map Luminex Kit, LKT003, RnD Systems, UK)

The following assays were performed during the *Confirmation Phase* by either ELISA or Luminex® assays:

- LpPLA (Quantikine ELISA kit, DPLG70, RnD Systems, UK)
- Oxidised LDL (ELISA, 10-1143-01, Mercodia, Sweden)
- GDF15, PaPPA, sCD40L (Flurokine Map Luminex kit, LUCA975, RnD systems, UK)
- NGAL, Osteopontin: (BeadPlex kit, BPHKT002-4, Merckbioscience. USA)

3.5.7 Data analysis – general considerations

Subjects were characterised by clinical parameters, OCT findings, and the candidate biomarker response. Exploratory data analysis was performed for variables to obtain the appropriate summary statistics. Transformation of data was performed for comparison where appropriate. Normalisation of plasma levels of a candidate marker at subsequent time points was performed by dividing it against the baseline value to obtain fold change. Area under the curve (AUC) from *venous* time course response of each candidate marker was calculated for individual subjects using the fold change values for each time point.

Independent variables (clinical presentation, OCT characteristics, volume of stent deployed during PCI etc.) with potential influence on the candidate marker response after plaque disruption by PCI were used to stratify patients into subgroups for comparison. Other methods for stratifying candidate markers response were also explored, such as grouping the subjects according to the AUC observed in a candidate marker. Dependent on the normality

of sample distribution, comparisons between two groups were performed by either parametric or non-parametric t-tests. Analysis of variance (ANOVA) was performed for comparison between 3 or more groups or to test the effects of repeated measures. These analysis were performed using Graphpad Prism (Version 5.0, San Diego California USA, www.graphad.com). Linear regression modelling of the effects between variables was performed using IBM SPSS Statistics (Version 19.0. Armonk, NY: IBM Corp) Statistical significance was defined by a p value of <0.05, with correction for multiple testing where appropriate.

Spearman rank correlation coefficients (rho-values) were calculated for the extent of correlation between candidate markers. To account for the effect of multiple testing in comparison between candidate markers, significant correlation was determined by two standard methods. The first was to convert the Spearman rho-values to p-values by calculating a z-score from the Fischer transformation of the rho-value. These p values were then adjusted using the Boneferroni correction method for multiple testing, and a p-value less than 0.01 considered to be significant. In addition, a permutation test was performed to estimate the lower and upper bounds of the distribution of rho-values under a null hypothesis of no change. In brief, 10,000 permutations of the data set (in which the collected data points are re-ordered at random for each candidate marker) were created, and Spearman rho values for all comparisons were re-calculated for each permutation. The average 0.5^{th} and 99.5^{th} percentiles of these permutation comparisons were calculated to form lower and upper bounds of a 99% confidence interval for the null hypothesis rho-value. Correlations with rho-values outside these bounds were considered significant. These were performed using R scripts.[g]

[g] The correlation analysis using R script was kindly designed and performed by Dr Philip Charles at the Centre of Cellular and Molecular Physiology (CCMP), Oxford.

3.6 Results

3.6.1 Study population

One hundred and nine patients undergoing non-emergency coronary angiography were recruited to the study (PCI: 84, Dx: 25). Of the recruited PCI subjects, 26 were excluded from subsequent analysis for to the following reasons: different plasma preparation protocol (n=11, subjects 1 to 11); vein graft angioplasty (n=4); in-stent restenosis due to neo-intimal formation (n=1), no post heparin blood available (n=4); blood sampling ceased due to complication from PCI procedure (n=5); ACS post thrombolysis (n=1). Two Dx angiography patients did not have angiographic evidence of atheroma and were excluded from subsequent analysis. Baseline characteristics of the subjects included in the *screening phase* were summarised in Table 3. The venous plasma samples for all time points were analysed during the *screening phase*.

3.6.2 Baseline comparisons of candidate biomarkers according to clinical status

Of the candidate markers measured during the *screening phase*, significant differences between ACS and SAP subjects at baseline were observed in MMP8, MMP9, TIMP1 and TIMP4. No significant differences were observed in MMP2, MMP3 and TIMP2 (Figure 15). The levels of MMP7 and TIMP3 were below the LLOQ for the respective assays.

3.6.3 Myeloperoxidase

In most cases, baseline levels of MPO were below the LLOQ for the Millipore Luminex® assay. Minutes after heparin administration, a rapid increase in plasma MPO level was observed. This rapid increase was observed in both ACS and SAP subjects. The peak increase was observed by 30 minutes after stenting and the levels returned to baseline by 6 hours after the procedure in most of the subjects (Figure 16). No changes were observed in subjects who underwent Dx angiography without receiving systemic heparin.

	PCI	Diagnostic Angiography
Number (male)	58 (46)	23 (16)
Age, years (SD)	66 (11)	68 (10)
Acute coronary syndrome, n (%)	21 (36)	13 (57)
Smoking status, n (%)		
Current smoker	16 (28)	3 (13)
Ex-smoker > 1 month	25 (43)	13 (57)
Never smoked	17(29)	7 (30)
Past History of CAD, n (%)		
MI/ACS	22 (38)	7 (30)
Stable angina	15 (26)	7 (30)
Hypertension, n (%)	39 (67)	19 (83)
Hypercholesterolemia, n (%)	45 (78)	13 (57)
Diabetes mellitus, n (%)	14 (24)	4 (17)
Family history of CAD, n (%)	29 (50)	12 (52)
Regular medication, n (%)		
Aspirin	40 (69)	17 (74)
Thienopyridine	23 (40)	11 (48)
Statin	47 (81)	20 (87)
β-blocker	33 (57)	14 (61)
Angiotensin converting enzyme inhibitor	38 (65)	19 (83)
White Ethnicity, n (%)	55 (95)	23 (100)
Procedural related, n		
IV heparin administered for procedure	58	7
IV adenosine administered	4	4
IIb/IIIa antagonist administered	2	0
Optical coherence tomography	36	n/a
Aspiration catheter sample collection	30	n/a
Coronary sinus sample collection	22	5
Coronary artery treated		
Left anterior descending / diagonal	22	n/a
Circumflex / obtuse marginal	18	n/a
Right coronary artery	15	n/a
Intermediate	3	n/a

Stent Volume in mm^3, median (interquartile range)	170 (119-258)	n/a

Table 3: Characteristics of study subjects included in the *screening phase* of the study

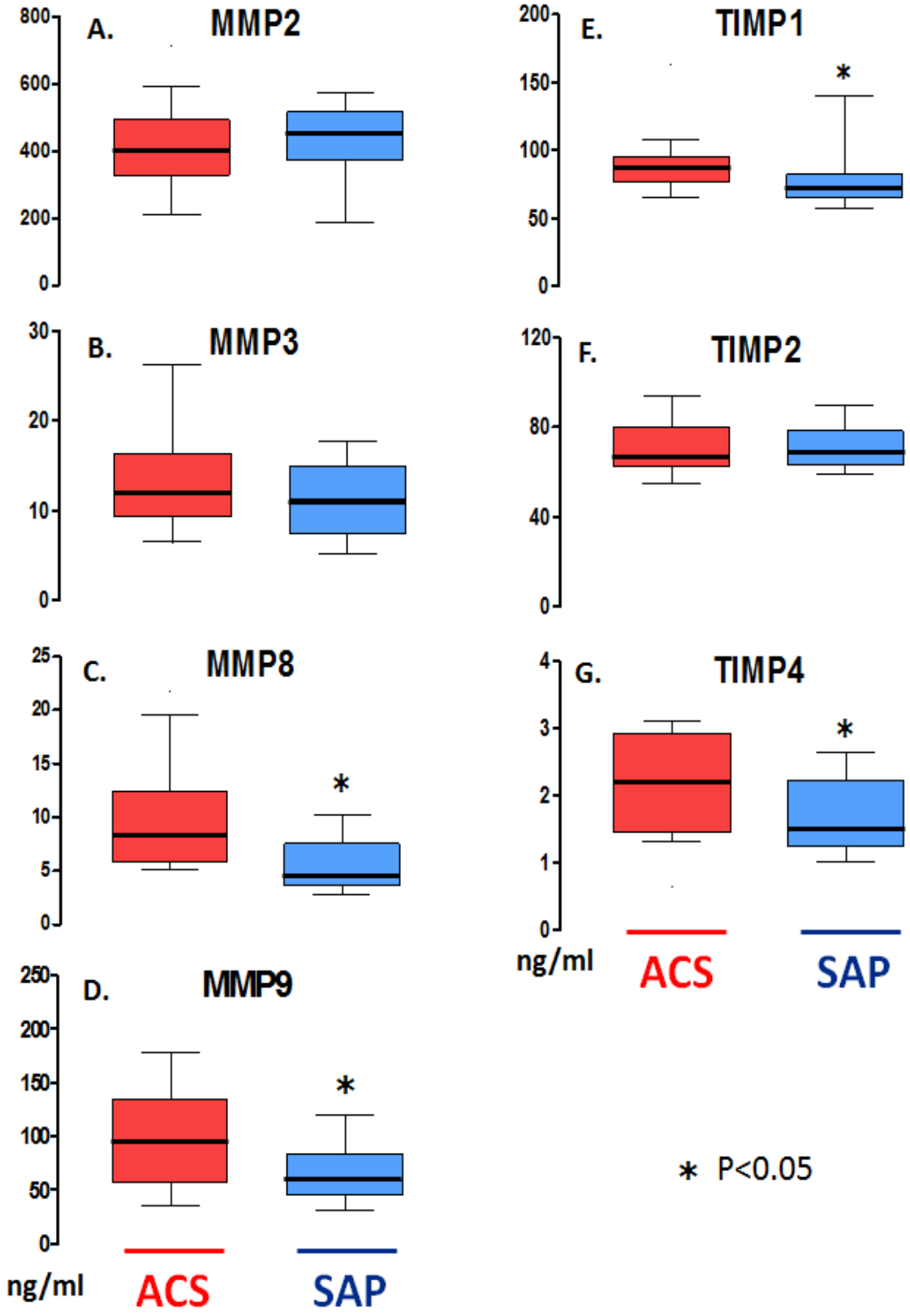


Figure 15: Baseline comparison of candidate marker levels between CAD patients who presented with acute coronary syndrome or stable angina

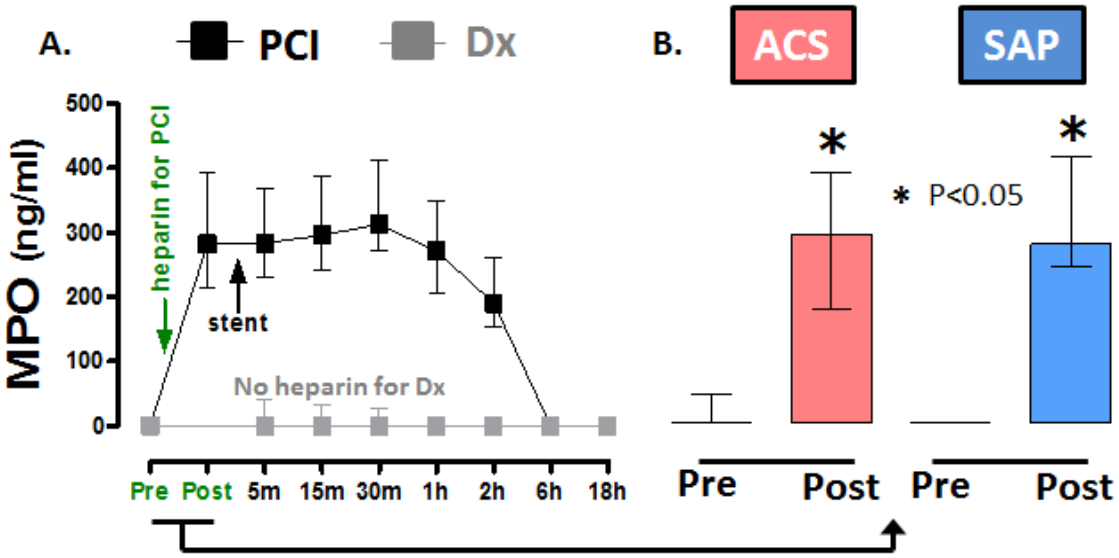


Figure 16: Effect of systemic administration of heparin and the plasma level of myeloperoxidase in CAD patients after PCI induced plaque disruption

Peripheral venous blood was collected from subjects with coronary artery disease undergoing either percutaneous coronary intervention (PCI) or diagnostic (Dx) angiography according to methods described in Section 2.3 and 2.4 of this thesis. For subjects undergoing PCI, bloods samples were collected before ("Pre-"), and 5 minutes after heparin administration ("Post-") at the beginning of procedure. Diagnostic angiography subjects did not receive heparin for the procedure. Plasma levels of myeloperoxidase (MPO) were measured using Luminex® assays. Comparison within group was performed Wilcoxon matched pair signed rank test. P values less than 0.05 were considered statistically significant. (Data are presented in median with interquartile range.)

In most cases, plasma MPO was below the lower limit of quantification for this assay. However, plasma MPO level significantly increased soon after heparin administration, before the stent was deployed (Panel A). The acute elevations were observed in both subgroups of subjects who presented with acute coronary syndrome (ACS) of stable angina pectoris (SAP) (Panel B). The peak increase in the PCI group was observed by 30 minutes, with the level returning towards baseline by 6 hours. No changes were observed in subjects who underwent Dx angiography only.

3.6.4 Evidence of myocardial injury and systemic inflammation after PCI

Baseline levels of CKMB, cTnI and CRP were significantly higher in the subjects who presented with ACS as compared to those who presented with SAP (Figure 17-B, D, F). Amongst the subjects who received PCIs, plasma level of CKMB and cTnI were significantly increased by 18 hours after the procedure (Figure 17 - A, C). These changes were particularly pronounced in the SAP group after PCI (Figure 17 - B, D). Similar patterns of change were also observed for CRP (Figure 17 - E, F). No Significant changes in CKMB and cTnI were observed in the control subjects without plaque disruption, although significant increase in CRP was also observed in the control group at 18 hours after the diagnostic angiography (Figure 17 - E). Amongst all subjects who underwent PCI, the AUC for CKMB and TnI correlated significantly with the AUC of CRP (Figure 17- G, H).

3.6.5 Plasma levels of MMP8 and MMP9 after plaque disruption

Amongst the candidate markers measured, significant increases in venous plasma levels of MMP8 and MMP9 were observed at various time points. For MMP9, significant elevation was observed as soon as 30 minutes after plaque disruption (Figure 18 - A); for MMP8, the significant elevation was observed by 2 hours after plaque disruption (Figure 18 - B). When examined in subgroups according to clinical status, there was differential response of MMP8 and MMP9 between patients who presented with ACS or SAP (Figure 18 - C,D,E,F). For both markers, significant elevations after plaque disruption were observed earlier in ACS patients. The peak levels of MMP8 and MMP9 in SAP patients were observed at 6 hours after plaque disruption, and reached similar levels observed at baseline in ACS patients. Upward trends were observed within the diagnostic angiography patients, but did not reach statistical significance (Figure 18 - G, H).

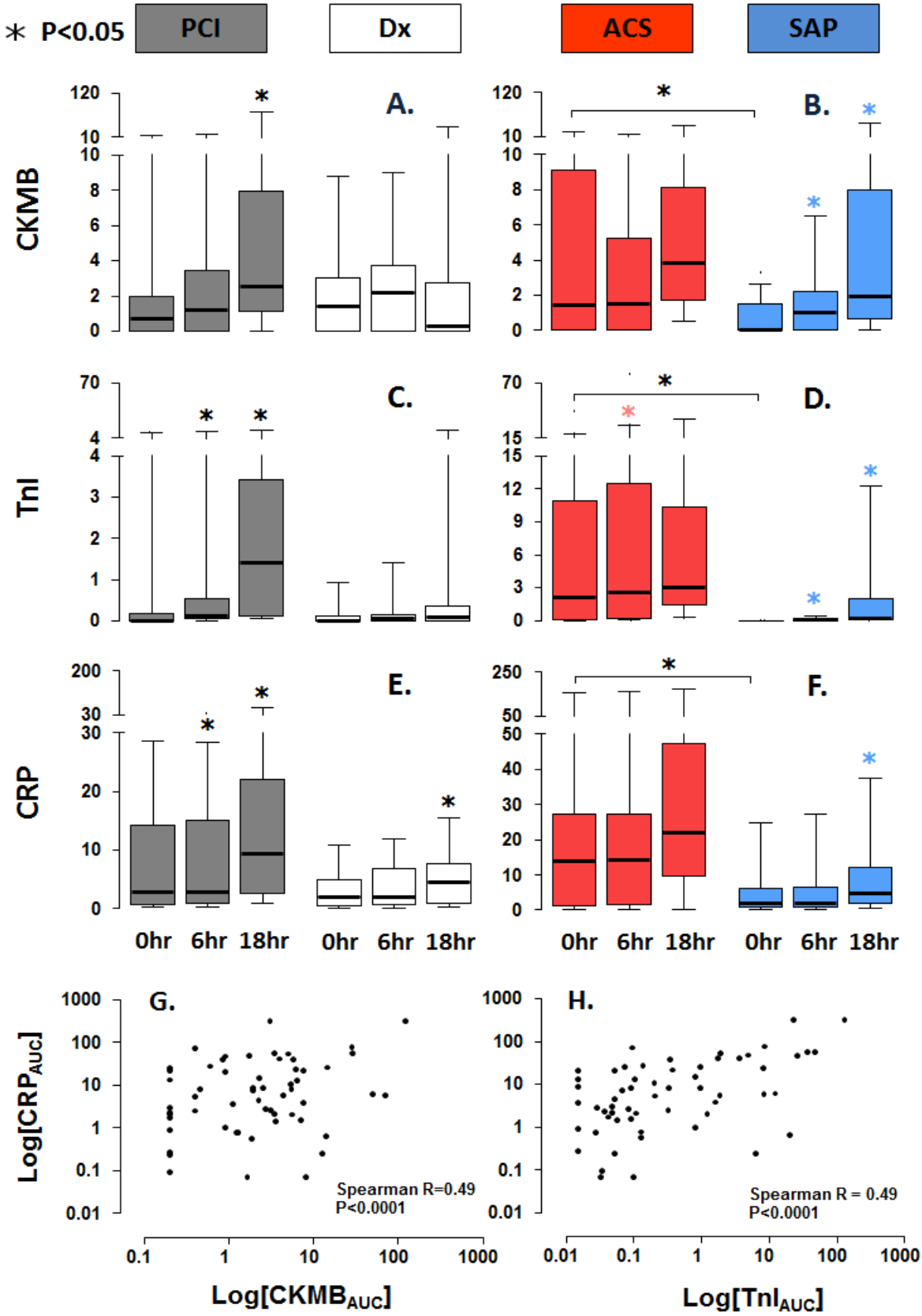


Figure 17: Evidence of myocardial injury and systemic inflammation after stent induced plaque disruption

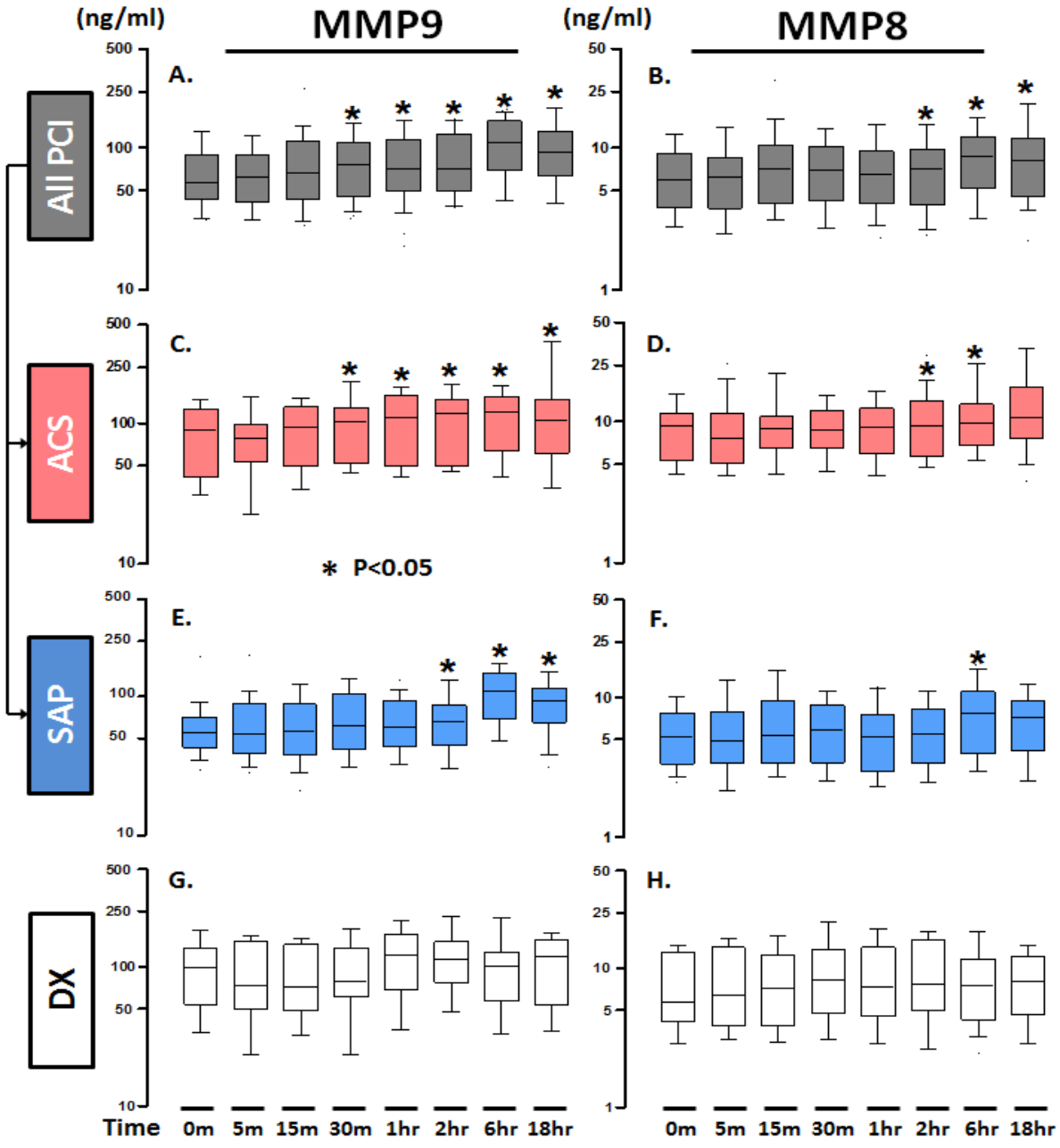


Figure 18: Plasma levels of MMP8 and MMP9 after stenting induced plaque disruption

3.6.6 Plasma levels of other candidate markers after plaque disruption

Different trends throughout the time course after plaque disruption were observed for MMP2, MMP3, TIMP1, TIMP2 and TIMP4, both in the combined cohort group and according to grouping by clinical status. However, when the level of these markers at individual time points were compared against the subjects own baseline value, none of the changes reached statistical significance by paired t-tests.

3.6.7 Candidate marker response after plaque disruption according to clinical status, using fold change values

Data presented in Section 3.6.2 (Figure 15) showed heterogeneity of baseline levels of the candidate markers. To account for such heterogeneity between individuals, the observed levels at each timepoint time were normalised against each individual's baseline to obtain fold change vlues. The fold change values at each time point were used to calculate AUC for the overall time course response of candidate markers after plaque disruption. Comparisons between groups were made according to the presenting clinical status of ACS or SAP. Although significant elevation for plasma MMP8 was observed by 6 hours after plaque disruption in both the ACS and SAP groups (as show in Figure 18), there was no significant difference between either of these subgroups and control subjects (Dx angiography) when the comparison of MMP8 was based on the AUC incorporating all time points (Figure 19-C). AUC of MMP9 ($MMP9_{AUC}$) was significantly higher in the ACS subjects after plaque disruption compared to control subjects, but was not different between the SAP and control subjects (Figure 19-D). Amongst the other candidate markers, significant difference between the ACS and Dx subjects (by ANOVA) was observed only in $MMP3_{AUC}$ (Figure 19-B). There was no statistically significant difference in the AUC between SAP and ACS subjects, or the AUC between SAP and Dx subjects, in all the candidate markers measured during the *Screening Phase* (Figure 19).

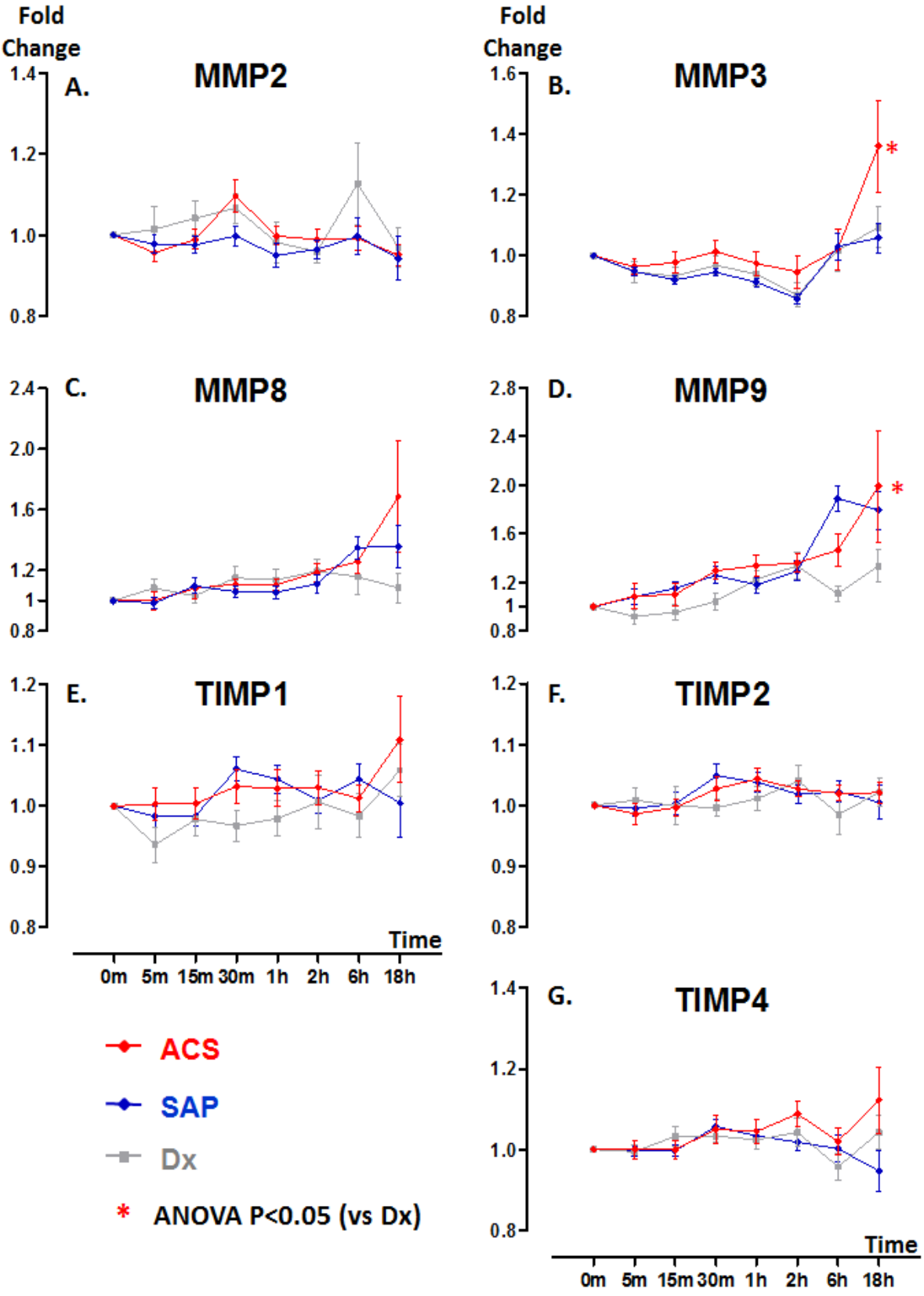


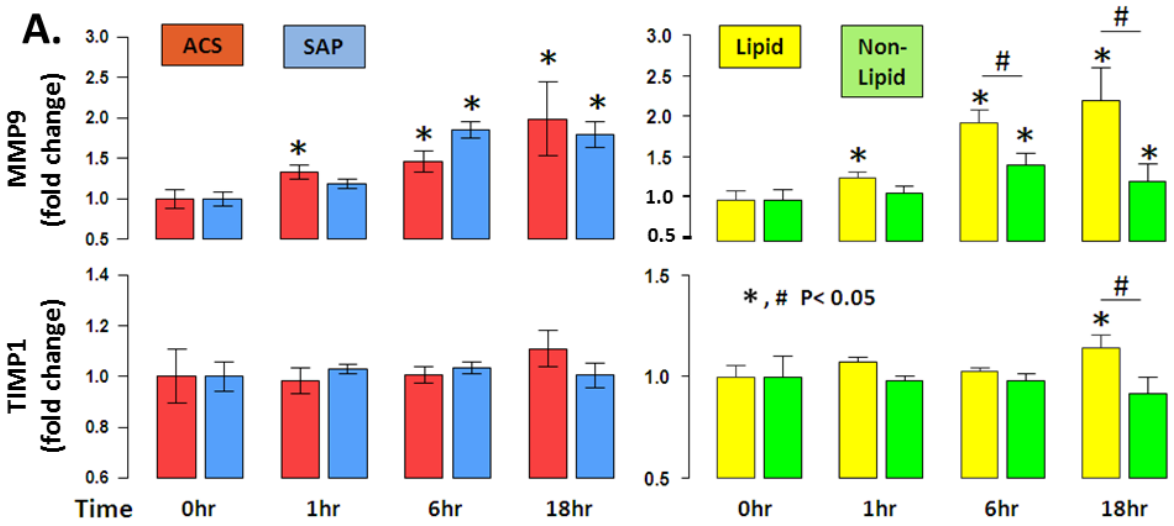
Figure 19: Plasma levels (fold change) of MMP2, MMP3, MMP8, MMP9, TIMP1, TIMP2, and TIMP4 after stenting induced plaque disruption

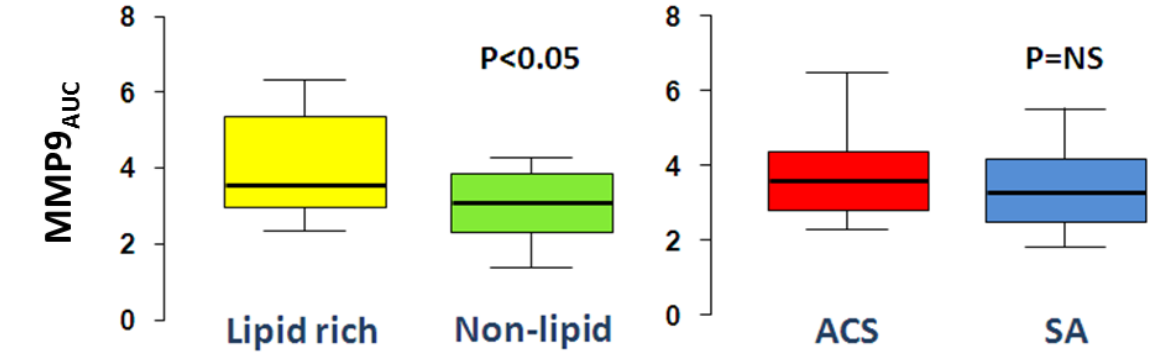
3.6.8 Candidate marker response according to plaque morphology

OCT images were obtained from 36 PCI subjects. Based on the scoring system outlined in Section 3.5.2.3, 23 target lesions were classified as containing predominantly lipid rich plaque(s). There were no differences between the proportions of subjects with lipid rich or non-lipid plaques in term of their clinical presentation. (31% of subjects with a lipid rich plaque presented with ACS; 38% of subjects with a non-lipid rich plaques presented with ACS. p=ns by Fisher exact test.) The changes observed for MMP9 and TIMP1 amongst subjects with lipid rich plaques, whereby earlier elevation of MMP9 subsequently followed by a significant increase in plasma TIMP1 at 18 hours after plaque disruption, closely mimicked the trend of the patients presenting with ACS. This pattern was not observed in subjects with non-lipid plaques. Higher fold changes at 6 and 18 hours after plaque disruption were observed in lipid rich plaques (Figure 20-A). No significant differences were observed between subjects with lipid or non-lipid plaques over the time course for the other candidate markers measured.

When comparing the MMP9 change by AUC over the entire time course after plaque disruption, $MMP9_{AUC}$ was significantly higher for patients with lipid rich plaques; whereas no significant difference was observed in $MMP9_{AUC}$ between subjects who presented with ACS or SAP (Figure 20-B).

Logistic regression analysis was performed using the two independent variables (clinical status and plaque morphology) in a backward elimination approach to assess their effect on MMP9 release after plaque disruption (as reflected by $MMP9_{AUC}$). Plaque morphology, not clinical status, was the only significant predictor of MMP9 release after plaque disruption, having accounted for the clinical status of each individual subject (Figure 20-C, $P<0.05$).





C.

Variables Entered/Removed[b]

Model	Variables Entered	Variables Removed	Method
1	Lipid=1, nonlipid=2, SA=1 ACS=2	.	Enter
2	.	SA=1 ACS=2	Backward (criterion: Probability of F-to-remove >= .100).

a. All requested variables entered.
b. Dependent Variable: MMP9_0_1_6_18hr_AUC

ANOVA[c]

Model		Sum of Squares	df	Mean Square	F	Sig.
1	Regression	9.253	2	4.627	2.495	.098[a]
	Residual	61.189	33	1.854		
	Total	70.442	35			
2	Regression	8.059	1	8.059	4.392	.044[b]
	Residual	62.383	34	1.835		
	Total	70.442	35			

a. Predictors: (Constant), Lipid=1, nonlipid=2, SA=1 ACS=2
b. Predictors: (Constant), Lipid=1, nonlipid=2
c. Dependent Variable: MMP9_0_1_6_18hr_AUC

Figure 20: Comparison of MMP9 and TIMP1 after plaque disruption according to clinical status and plaque morphology

3.6.9 Candidate markers response in relation to plaque volume disrupted

The volume of stent (SV) deployed was calculated as a cylinder ($SV=\pi r^2 h$; r=diameter of balloon used for post dilatation; h=length of stent), and used as a surrogate index of plaque volume disrupted. No correlation was observed between SV and any candidate markers at the time point of maximal response, or the cumulative response according to AUC.

3.6.10 Candidate markers response according to stratification by AUC

I reasoned that for a candidate marker to be related to plaque disruption, the AUC response observed in the PCI group should differ from the control group. For all MMPs and TIMPs analysed, significant differences in AUC were observed between PCI subjects within the highest AUC tertile ($PCI^{upper1/3}$) and control subjects within the lower ½ of AUC ($Dx_{lower1/2}$).[h] However, significant difference between the $PCI^{upper1/3}$ and the Dx subjects within the upper AUC half ($Dx^{upper1/2}$) was only observed in MMP9 and MMP8 (Figure 21). There was no statistically significant difference between the $PCI^{upper1/3}$ and $Dx^{upper1/2}$ for the others.

3.6.11 Correlations of candidate markers with CRP, CKMB, and cTnI

Correlations between the AUC of candidate markers were assessed. Using Bonferroni-corrected p-values, at a significance level of p<=0.01, MMP2, MMP3, TIM1, TIMP2 and TIMP4 were significantly correlated with CRP, and/or CKMB, and/or cTnI. Permutation testing gave the bounds of the 99% confidence interval of the null hypothesis to be -0.344021 to 0.345041. MMP2, MMP3, MMP8, TIMP1, TIMP2 and TIMP4 were significantly correlated with at least one of CRP, CKMB, or cTnI. MMP2, MMP3 and TIMP1 were only significantly correlated with CKMB and cTnI, and MMP8 was only significantly correlated with cTnI. MMP9 was the only candidate marker that did not show statistically significant correlation to CRP, CKMB or cTnI (Figure 22).

[h] Due to the lower number of subjects reruited in the Dx group, stratification of this group by median split was performed (instead of stratification by tertiles) to achieve a more comparable number as the PCI tertile group.

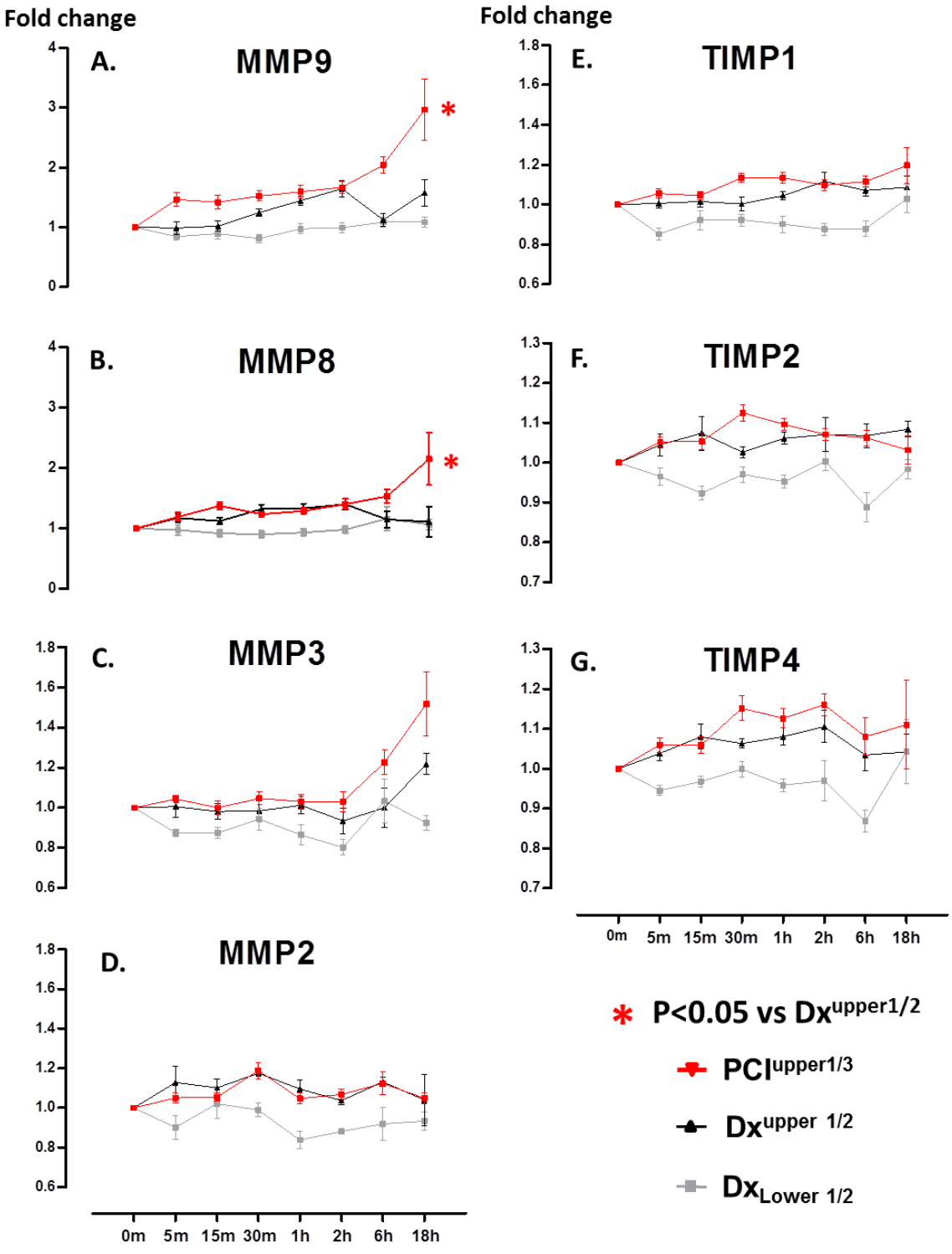


Figure 21: Candidate marker response after plaque disruption, stratified by area under curve over the entire time course.

A.

Spearman rho by permutation testing

	CRP_{AUC}	$CKMB_{AUC}$	$cTnI_{AUC}$
$MMP2_{AUC}$	0.155603	0.470820	0.594944
$MMP3_{AUC}$	0.298384	0.455773	0.625897
$MMP8_{AUC}$	0.148115	0.296172	0.358561
$MMP9_{AUC}$	0.089486	0.220188	0.266170
$TIMP1_{AUC}$	0.310078	0.377615	0.452748
$TIMP2_{AUC}$	0.436730	0.437944	0.565913
$TIMP4_{AUC}$	0.436853	0.457285	0.533303

P value (with Bonferroni correction)

	CRP_{AUC}	$CKMB_{AUC}$	$cTnI_{AUC}$
$MMP2_{AUC}$	1.000000	0.026413	0.000431
$MMP3_{AUC}$	0.480962	0.006805	0.000003
$MMP8_{AUC}$	1.000000	0.503660	0.119969
$MMP9_{AUC}$	1.000000	1.000000	0.912019
$TIMP1_{AUC}$	0.374781	0.072976	0.007541
$TIMP2_{AUC}$	0.012793	0.012302	0.000077
$TIMP4_{AUC}$	0.012743	0.006462	0.000342

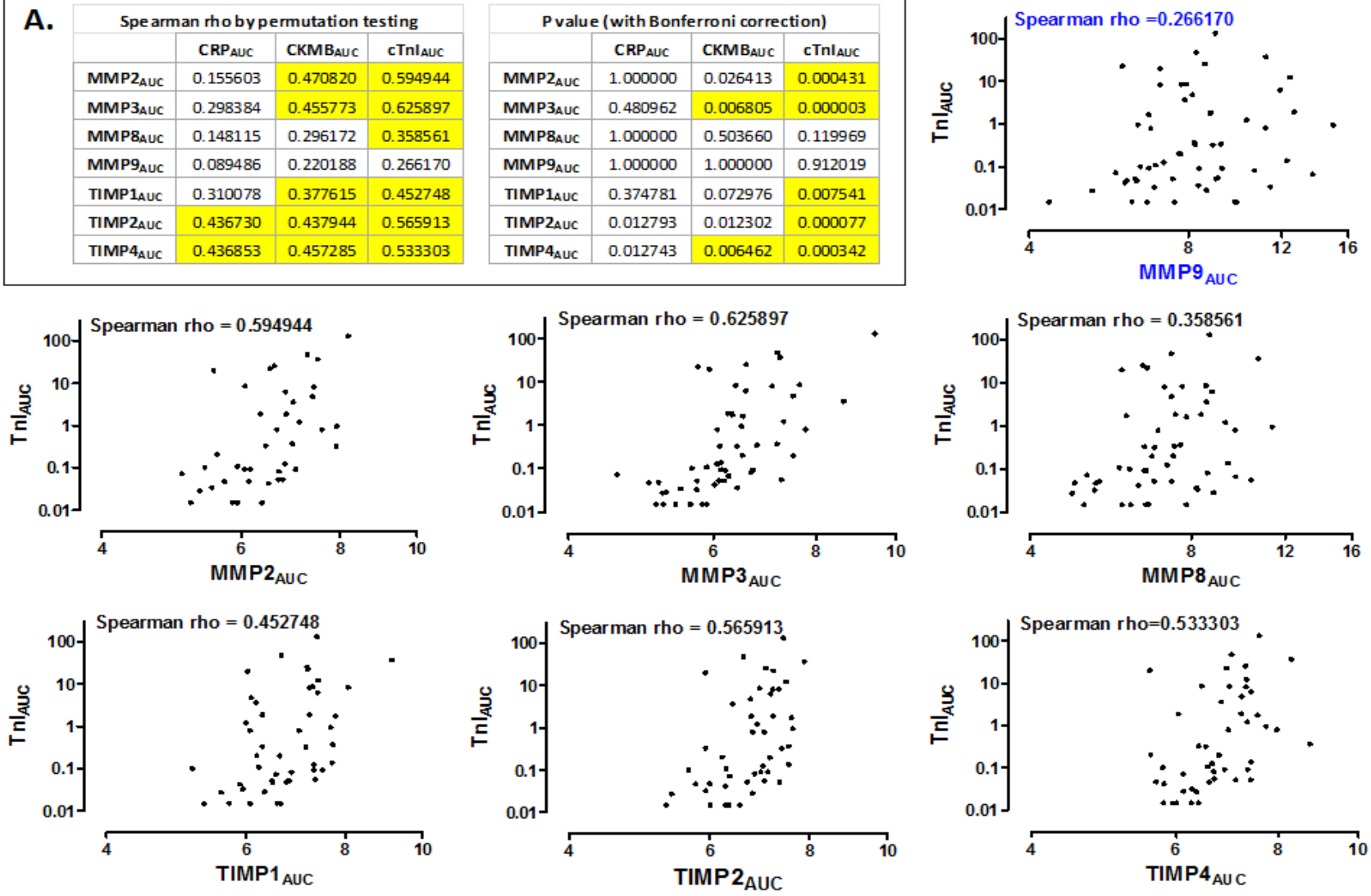


Figure 22: Correlations between MMPs, TIMPS to CRP, CKMB and cTnI

3.6.12 Arterial plasma MMP9 levels at early time points after plaque disruption

Of the candidate markers measured, a robust signal after plaque disruption was observed in MMP9. Therefore, in addition the the venous plasma samples, the level of MMP9 was also measured in coronary *arterial plasma samples* collected at the early time points (5 and 15 minutes) after plaque disruption. I reasoned that analysis of these samples could provide further insight in terms of temporal or anatomical gradients of MMP9 release, as a subset of these samples (n=30) were collected using an aspiration catheter advanced downstream of the disrupted lesion (therefore containing potentially enriched biological signals). Correlates of the arterial MMP9 with the presenting clinical status or plaque morphology on OCT were also assessed. These information could be useful to ascertain the the utility of a algorithm for the selection of a discovery subject subset. For example, if the presenting clinical status or plaque morphology were indeed useful for stratifying the subjects with enriched biological signals from plaque disruption, one would expect to observe further enrichment of the signal in the arterial blood samples collected immediately downstream of the disrupted plaque in these subjects.

Amongst the PCI subjects, no significant change in plasma MMP9 was observed in arterial blood aspirated from the coronary artery guide catheter at 5 or 15 minutes (Figure 23-A). No difference was observed amongst the subgroup of patients in whom coronary blood sampling at these time points were performed by an aspiration catheter advanced downstream of the stented lesion (Figure 23-B).

Grouping of the subjects by clinical status revealed no changes of arterial MMP9 levels in the ACS group within 15 minutes of plaque disruption. In contrast, significant elevations of MMP9 in distal coronary artery blood (collected by an aspiration catheter) were observed 15 minutes after plaque disruption amongst the SAP subjects (Figure 23-C, D). This observation

was also incongruous to the prior assumption that patients presenting with ACS have inherently more vulnerable plaques and would therefore have a more pronounced biomarker signal after plaque disruption.

When the subjects were grouped according to plaque morphology (lipid rich vs non-lipid plaques, Figure 23-E,F), there was no difference in MMP9 level of arterial plasma collected either from proximal coronary sampling (by a guide catheter) or from downstream of the disrupted plaque (by an aspiration catheter) within the first 15 minutes.

The reasons for comparing the candidate marker response according to subgroups according to AUC over the time course were discussed in Section 3.6.10. [Note that significant differences in AUC were observed between PCI subjects within the highest AUC tertile for venous MMP9 ($PCI^{upper1/3}$) and Dx subjects within the upper AUC half for venous MMP9 ($Dx^{upper1/2}$) (Figure 21)]. Amongst the $PCI^{upper1/3}$ subjects who did not undergo downstream arterial aspiration, no significant change was observed for *arterial* MMP9 at 5 or 15 minutes after plaque disruption (Figure 23-G). In comparison, significant acute elevation in arterial MMP9 was observed in $PCI^{upper1/3}$ subjects whose samples were collected from downstream of the disrupted plaque as early as 5 minutes after plaque disruption. This was not observed in those subjects with a low MMP9 response ($PCI_{lower1/3)}$ after plaque disruption (Figure 23-H).

3.6.13 Other anatomical gradients of candidate markers in the *Screening Phase*

Coronary sinus blood samples were successfully collected from 22 of the PCI subjects. Of the candidate marker panels analysed during the *Screening Phase*, no significant differences were observed in paired comparisons between coronary arterial versus coronary sinus, coronary arterial versus peripheral venous, or coronary sinus versus peripheral venous plasma samples at each time point (baseline, 5min, 15min). There was no significant temporal change observed in the coronary sinus serial samples.

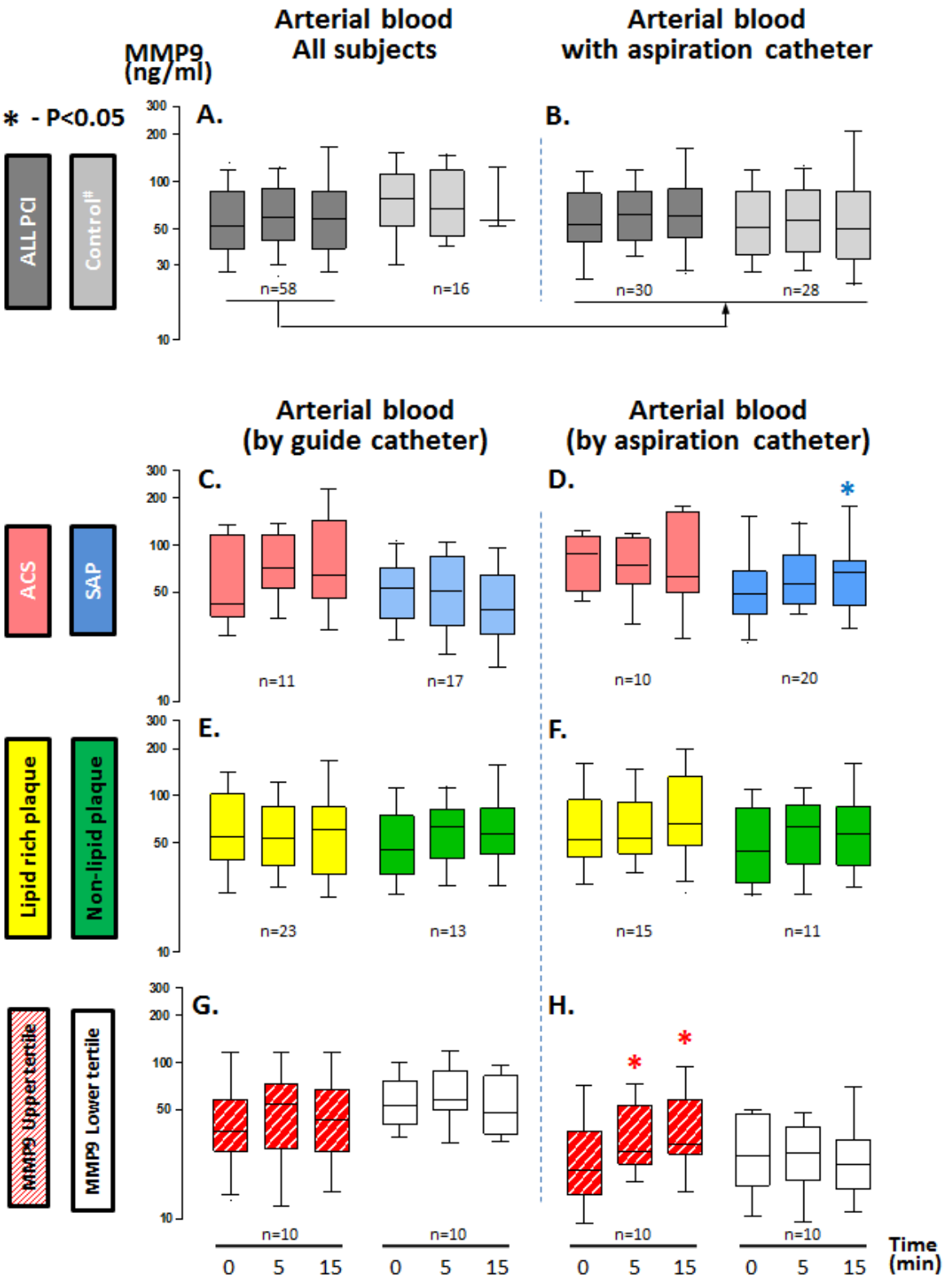


Figure 23: Changes in arterial MMP9 at early time points after plaque disruption.

3.6.14 Additional notes

1. The use of distal protection device (Medtronic Guardwire) was unsuccessful after several trial attempts due to the inability to achieve distal occlusion of the artery. This procedure was not attempted further for the remainder of the study.
2. There were no correlations between the stent volume and any of the candidate markers measured.

3.6.15 Selection of a discovery subject subset

There is a wealth of evidence which indicate differential profiles of soluble biomarkers in patients with diabetic patients compared to non-diabetics. Perturbations of metabolic pathways (such as protein synthesis, protein degradation, and oxidative stress) have been observed in patients with type I diabetes.(116) Proteomic analysis of different body fluids have revealed significant differences in many proteins between diabetic with or without complications, as compared to healthy individuals.(117) It has also been shown that loss of endothelial specific miRNA in type II DM patients, suggesting the possibility of altered response to vascular injury.(118) Based on these considerations, patients with a history of diabetes as confirmed by fasting plasma glucose level were further excluded from the final selection of a discovery set cohort. Out of the remaining subjects in the $PCI^{upper1/3}$, $PCI_{lower1/3,}$ and $Dx_{lower1/2}$ groups, the highest (or lowest) 10 subjects from each of these groups were included in the discovery sample set. **These final 10 subjects selected from each of the $PCI^{upper1/3}$, $PCI_{lower1/3,}$ and Dx angiography groups will be respectively referred to as the $PCI_{MMP9High}$, $PCI_{MMP9Low}$, and $CONTROL_{Dx}$ group for subsequent sections of the thesis.** Demographic characteristics of the discovery subject subset are presented in Table 4.

	PCI $MMP9_{High}$	PCI $MMP9_{Low}$	$CONTROL_{Dx}$	P value
Number (male)	10(7)	10(7)	10(5)	0.56
Age, years (SD)	66(8)	68(11)	67(12)	0.88
Acute coronary syndrome (ACS), n	5	3	6	0.39
Smoking status, n				
Current smoker	1	1	1	1
Past history of smoking (>1month)	7	5	4	0.39
Never smoked	2	4	5	0.37
Past History of CAD, n				
MI/ACS	2	4	5	0.37
Stable angina	4	4	0	0.07
Hypertension, n	6	6	8	0.55
Hypercholesterolemia, n	8	10	6	0.08
Diabetes mellitus, n	0	0	0	1
Family history of CAD, n	6	3	5	0.39
Regular medication, n				
Aspirin	6	7	8	0.62
Thienopyridine	3	3	4	0.86
Statin	7	9	9	0.38
β-blocker	5	6	6	0.87
ACE inhibitor	6	5	7	0.66
Plasma lipid profile (mmol/L**)**				
Total cholesterol (SD)	3.7(0.4)	3.8(0.9)	3.8(1.39)	0.94[#]
HDL (SD)	1.0(0.3)	1.1(0.61)	0.9(0.3)	0.50[#]
LDL (SD)	2.0(0.3)	2.1(0.8)	2.3(1.0)	0.75[#]
Triglyceride (SD)	1.5(0.7)	1.1(0.3)	1.5(0.6)	0.32[#]
Procedural related, n				
Aspiration catheter for arterial blood	4	5	-	1
Optical coherence tomography	5	7	-	0.65
Predominantly lipid plaque	4	2	-	0.63
Vessel treated				
LAD / diagonal	2	6	-	0.17
Circumflex / OM	5	3	-	0.65
RCA	3	1	-	0.58

Table 4: Characteristics of the discovery subject subset for the *discovery phase* of the study

([#]These comparisons were made using ANOVA, the rest of the comparisons were made using the Fisher exact test) CAD: coronary artery disease, MI: myocardial infarction, ACE: angiotensin converting enzyme HDL: high density lipoprotein, LDL: low density lipoprotein, LAD: left anterior descending coronary artery, OM: obtuse marginal artery, RCA: right coronary artery.)

3.6.16 Results from the *Confirmation Phase*

Measurement of candidate markers during the subsequent *Confirmation Phase* was only performed in the discovery subject subset as defined in the previous section. Venous blood collected at baseline, 30 minutes and 6 hours after plaque disruption were chosen as representative early and late time points for analysis during this phase of analysis.

3.4.16.1 NGAL

Significant elevation of NGAL was observed in the PCI subjects ($PCI_{MMP9High}$ + $PCI_{MMP9Low}$, n=20) at 6 hours after plaque disruption, which was not observed in the $CONTROL_{Dx}$ group. $NGAL_{AUC}$ was significantly higher in the $PCI_{MMP9High}$ groups compared to the others (ANOVA $P<0.05$). When the trends for individual group were compared according to fold changes of NGAL at subsequent time points, the levels observed in the $PCI_{MMP9High}$ group was significantly higher at 30 minutes as compared to $PCI_{MMP9Low}$ and $CONTROL_{Dx}$ ($P<0.01$ and $P<0.001$ on two-way ANOVA, respectively) (Figure 24-A).

3.4.16.2 GDF15

Significant elevation of GDF15 was observed in both the PCI and $CONTROL_{Dx}$ angiography subjects at 6 hours after plaque disruption. However, $GDF15_{AUC}$ was significantly higher in $PCI_{MMP9High}$ group compared to the others. When the trends for individual groups were compared according to fold changes of GDF15 at subsequent time points, the levels observed in the $PCI_{MMP9High}$ group was significantly higher at 6 hours as compared as compared to $PCI_{MMP9Low}$ and $CONTROL_{Dx}$ ($P<0.05$ and $P<0.001$ on two-way ANOVA, respectively) (Figure 24-B).

3.4.16.3 LpPLA, Oxidised LDL, PaPPA, sCD40L, Osteopontin

For these markers, no significant changes were observed in either the combined PCI group, or individual subgroups ($PCI_{MMP9High}$ or $PCI_{MMP9Low}$), at 30min or 6 hrs after plaque disruption.

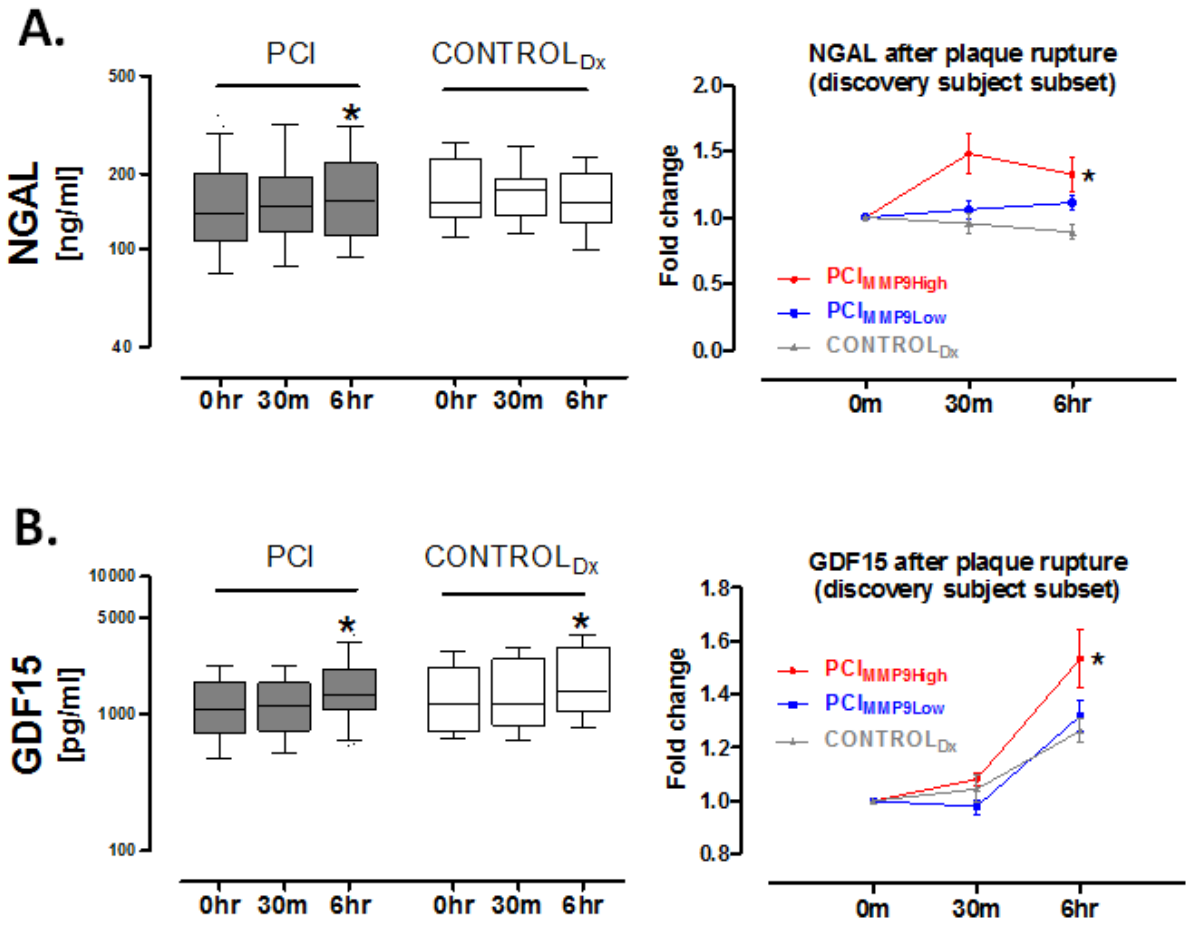


Figure 24: Plasma levels of NGAL and GDF15 in the discovery subject subset after plaque disruption

3.7 Discussion

The results presented so far demonstrated the presence of positive candidate marker signals after plaque disruption in the study cohort. Although several interesting observations emerged from the pilot data, the focus at this stage of the project was to select a discovery subject subset with potentially the highest signal-to-noise ratio of novel biomarker release for subsequent discovery phase -omics analysis.

The observation on MPO further illustrated the importance of pre-analyic issues laid out in Chapter 2. Since the seminal article by Brennan *et al*. that reported a single initial measurement of plasma MPO independently predicted early risk of myocardial infarction and subsequent major adverse cardiac events(119), there had been inconsistent reports on MPO level and association with cardiovascular risks.(120) Without the measurements from blood samples obtained prior to heparin administration, I would have reached a very different set of observations: it would appear that MPO levels were higher in patients undergoing PCI as compared to the patients undergoing diagnostic angiography only. Following plaque disruption, a gradual decrease of MPO was observed from 30 minutes after the event in the plaque disruption cohort, and eventually returned to a level that was similar to the Dx subjects (which were below the LLOQ). However, when MPO levels were further measured in the sample obtained prior to intravenous administration of heparin, the effect of heparin *in vivo* became apparent. Indeed MPO levels were bordering/below the LLOQ of the assay for all subjects, except in those who received low molecular weight heparin (LMWH) as part of their clinical management within the last 24 hours. These observations were consistent with the literature where administration of unfractionated heparin (UF) or LMWH were both shown to lead to acute elevations in plasma MPO levels.(121, 122) It was possible that pre-analytical LMWH or UF administration may be a confounding factor in previous clinical

studies, as both forms would be frequently used in the management of ACS or thromboembolism prophylaxis for in-patients awaiting cardiac investigation.(11)

The panel of candidate markers measured in the *Screening Phase* had all been implicated in the pathophysiology of ACS. The observations that baseline levels of MMP8, MMP9, TIMP1 and TIMP4 were higher in ACS patients provided the first evidence that candidate marker signals observed in this cohort were consistent with literature. Significant elevations were further observed at various time points after plaque disruption for MMP8 and MMP9. Elevation of CKMB, TnI and CRP confirmed the presence of concurrent peri-procedural myocardial injury and systemic inflammatory response after plaque disruption in this experimental model.

Observations thus far supported the hypothesis that this model of plaque rupture led to acute changes in plasma molecular profiles. This was a strong evidence to support the presence of associated release of novel biomarkers in this experimental model. However, as the PCI procedure would also evoke downstream events in terms of myocardial injury and systemic response, further attempts were required to tease out the subset of subject/samples (the discovery subject subset) with the most enriched molecular signals which were specific to the upstream plaque disruption event, and with minimal confounding signals from the ensuing myocardial injury and systemic inflammation, down stream of the plaque disruption.

A central hypothesis of this thesis was that plaque disruption could result in disparate patterns of biomarker release. Hence, the first challenge in the selection of a subset of discovery subject subset was to identifying those subjects who represented the extremes of the spectrum of biomarker release. One approach to select the discovery subject subset utilised the comparison between candidate marker changes according to patient dependent variables such as clinical status at the time of recruitment. The hypothesis was that ACS patients had

presented to the hospital as a result of a preceding significant plaque rupture event, hence the inherent "vulnerability" of the target (culprit) lesion being disrupted during stenting. One would arguably expect to observe differences in candidate markers at baseline, and/or in the pattern of candidate marker profiles after stenting induced plaque disruption in ACS patients, as compared to subjects who presented with stable symptoms and presumably more stable plaques. This approach of subject stratification led to several promising observations, particularly in relation to MMP8 and MMP9. Trends initially observed in this cohort supported the assumption that clinical status may be helpful in predicting biomarker response after further stent induced plaque disruption.

A second approach for selection of a discovery subject subset was to compare candidate marker changes according to plaque morphology defined by OCT. In this experimental model, plaque disruption was induced by stent placement *in vivo*, rather than a spontaneous *de novo* event. I therefore reasoned that the plaque composition would bear more influence on the biomarker response after stenting, rather than the presence of a thin fibrous cap. Presence of a lipid rich, necrotic core is a recognised feature of plaque vulnerability. Such feature can be readily distinguished on OCT. Therefore the lesions were grouped into two broad categories of lipid rich or non-lipid plaques.

Similar to the grouping by clinical status, differential release of candidate markers after plaque disruption was also observed according to the plaque type. Disruption of lipid rich plaques (irrespective of the clinical status) resulted in changes in MMP9 and TIMP1 that were similar to disruption of "vulnerable" plaques in ACS patients. Plaque morphology, rather than clinical status, was the independent predictor of $MMP9_{AUC}$ after plaque disruption in multivariate analysis. This observation strongly supported the hypothesis that plaque composition may be another useful tool for guiding the selection of a discovery subject subset. However, anatomical and procedural factors limited the acquisition of OCT images

for every subject. As a result, only 36 of the 58 subjects in the study underwent OCT imaging. To rely on OCT analysis for guiding the selection of a discovery subject subset would mean exclusion of almost half of the recruited cohort, which was undesirable.

Another challenge in the *Screening Phase* was the selection of a specific time point(s) during the entire time course which could represent the time of maximal biomarker released after plaque disruption. Initial data on MMP9 pointed towards 6-hours after stenting as a time point where maximal biomarker response was likely to be observed. This was indeed also observed in MMP8 (Figure 17). However, the differential temporal changes observed amongst the subgroups according to clinical status or plaque morphology challenged this selection, as maximal changes were also evident in earlier time points in a subset of subjects. In this regard, serial blood sampling within each subject allowed for the calculation of AUC during the whole time course after plaque disruption. By comparing AUC of the time course, rather than comparing the levels between individual time points, it was possible to get a more accurate comparison of the temporal changes in a particular candidate marker between individuals.

Given the heterogeneity of the baseline values of each candidate marker between individuals, AUC calculation of each candidate biomarker would be heavily biased without some form of correction against individual's own baseline. The correction methods considered for this thesis included calculation of the difference ($\Delta_{\text{candidate marker}}$) between time points, or by fold change values against the baseline ("y"/baseline). The utility of using $\Delta_{\text{candidate marker}}$ as a corrected value for AUC calculation was similarly limited, as $\Delta_{\text{candidate marker}}$ would also be influenced by the variance of the baseline values observed between individuals. I therefore reasoned the fold change at a given time point would be a more appropriate index to allow for comparison of combined time course comparison *between* subjects, as this would minimise the issue of heterogeneity within the cohort.

Subsequent re-examination of the existing data using fold change values at each time point revealed new observations for MMP8 and MMP9: the differential time course response seen in clinical subgroups (Figure 17) became less evident in this comparison (Figure 18). Taking MMP9 as an example, the time course based on fold change for ACS patients was closely paralleled by SAP patients within the first 2 hours, contrary to the trends suggested by the box plot of raw data. Furthermore, the time course based on fold change for the Dx subjects revealed a similar upward trend at 1 to 2 hours after diagnostic angiography without stenting (Figure 18-B), although the raw data for Dx subjects at these time points did not significantly differ from baseline on paired t-tests.

When the cumulative temporal response was compared (using AUC), significant differences between ACS and Dx subjects were only observed in $MMP9_{AUC}$ and $MMP3_{AUC}$. This later finding contradicted my earlier observation that clinical status affected MMP8 and MMP9 release after plaque disruption, where the measured value at a given time point was used for statistical comparison against its baseline value without accounting for the inherent heterogeneity. It became apparent that other objective means of "phenotyping" the plaque disruption response had to be explored, as the characteristics (clinical status, plaque morphology, stent volume) of an individual provided little insight to which subjects were likely to have release of novel biomarkers specific to the plaque disruption event.

A "backward" selection approach was subsequently applied in search of a different strategy for selection of the discovery subject subset. I further hypothesised that subjects could be stratified according to changes of a candidate marker for plaque disruption, instead of using patient dependent baseline characteristics, and that those at the extremes of candidate marker response specific to the plaque disruption event would also convey the maximal signals for novel signatures for plaque rupture.

In addition, I reasoned that:

A. Diagnostic angiography may also result in arterial injury and related biomarker response may be observed in control subjects.
B. For a plasma marker to be associated with plaque rupture, certain trends could be expected:
    1 The baseline level should be higher in subjects presenting with ACS compared to SAP (plaque rupture event has naturally occurred).
    2 Time course response after such markers after plaque disruption (PCI) should differ from control subjects who did not have plaque disruption (Dx angiography only).
    3 Its release should be independent to events downstream of plaque disruption, such as myocardial injury and systemic inflammation.
    4 If there was local release of molecules after plaque disruption, the blood sample collected downstream of the plaque should be enriched in these molecules.
    5 Conversely, a method which "correctly" stratified patients for their response to plaque disruption should also detect the maximal differences between the samples collected from proximal coronary artery (by guide catheter) and from the enriched samples collected downstream of the disrupted plaque (by aspiration catheter).
C. Release of biomarkers after plaque disruption may be observed throughout different phases:
    i. Early: from to acute liberation of *in situ* cellular contents
    ii. Later: due to *de novo* synthesis of such markers (either as a direct response of plaque rupture, or as a result of epi-phenomenon downstream to plaque rupture)
D. For a molecule to be acutely liberated *in situ* from the plaque, it should be present in the plaque material.

Of the candidate markers which fulfilled assumption B-1 (MMP8, MMP9, TIMP1 and TIMP4), only MMP8 and MMP9 showed significantly higher AUC levels between the $PCI^{upper1/3}$ and $Dx^{upper1/2}$ subjects (met assumption B-2). Between them, MMP9 was the only candidate marker which did not correlate to marker of systemic inflammation (CRP) or myocardial injury after PCI (CKMB, cTnI) (met assumption B-3). This data suggested that MMP9 release (amongst the candidate markers measured) would be the most objective index for a plaque disruption response.

The levels of MMP9 measured in *arterial* plasma samples at early time points further supported the backward selection approach for a discovery subject subset. Judging by the trends observed in venous plasma levels of MMP9, where the time course for ACS and SAP patients was mirrored by trends observed according to plaque morphology (as shown in Figure 20), one would expect to observe a similar trend in arterial plasma samples at early time points (5min and 15min). However this was not the case. Differential MMP9 release between clinical status and plaque morphology subgroups was not evident, even in subjects from whom "enriched" coronary artery blood was collected using coronary aspiration catheters (as shown in Figure 23).

In contrast, when subjects were stratified by *venous* plasma AUC response, acute and persistent elevations were observed in plasma collected using aspiration catheter in subjects with the highest *venous* $MMP9_{AUC}$. This was distinctly different from the subjects in the lowest *venous* $MMP9_{AUC,}$ who also had downstream blood sampling by aspiration catheters. Since the arterial sample levels of MMP9 were measured independently to the venous sample measurement, the fact that grouping of subjects by venous AUC also predicted similar trends in arterial plasma MMP9 levels strongly supported the "backward" selection approach proposed in this thesis.

Of the candidate markers screened, alterations in plasma MMP9 appeared to be an objective index for the plaque disruption phenotype in this experimental model. This observation reflected existing literature that MMP9 could be a useful marker for plaque rupture event(s). However, one could also argue against the validity of this observation as studies have also reported contradictory findings on MMP9 as a candidate marker of plaque rupture.(123-125)

One explanation for the disparity of findings in clinical studies of MMP9 in CAD might be due to the pre-analytic issues already alluded to in the previous Chapter. The lack of stringent quality assurance in large scale clinical studies could have introduced pre-analytic bias. Not only would the choice of anticoagulant and timing of baseline sample collection in reference to intravenous heparin administration influence the levels of MMP9, delay in blood sample preparation could also lead to variable levels of MMP9 measured in plasma.(126) Neutrophils(125) and platelets(127) are major sources of MMP9 release *ex vivo*, therefore serum typically contains higher level of MMP9 as compared to plasma samples.(71) The stringent plasma sample preparation protocol applied in this study likely had a positive influence on the ability to measure acute changes of MMP9 in this cohort.

The observed MMP9 changes after plaque disruption in this thesis were in close parallel to a previous study, which also reported acute elevation of MMP9 in coronary artery blood sample collected from downstream of the lesion using aspiration catheters.(128) Taken together, these data strongly suggested the utility of MMP9 as candidate marker of acute plaque disruption. However, its potential clinical application would be limited, due to the heterogeneity observed between individuals, and also because of its involvement in a wide range of pathological processes which involve abnormal turnover of extra cellular matrix such as neoplasms. Nevertheless, normalising serial measurement against individual's

baseline allowed for correction of between-subject heterogeneity, and the $MMP9_{AUC}$ provided an objective index of the plaque disruption response.

To assess the robustness of the selection algorithm, further candidate marker screen on selected time-points in the discovery subject subset (0 min, 30 min, and 6 hours) were performed, using a different panel of candidate markers that had been implicated in the pathophysiology of plaque vulnerability. Significant changes after plaque disruption were observed in two of the candidate markers, NGAL and GDF15, during this *Confirmation phase*. The release patterns of these markers were as predicted by the discovery subject subset selection algorithm: a divergent response should be observed between the two groups predicted to be at the extremes after plaque disruption ($PCI_{MMP9High}$ and $PCI_{MMP9Low}$).

The changes observed in NGAL aptly illustrated the concept discussed in Section 2.5 and Figure 3, that nondescript grouping of subjects could results in "masking" of an underlying significant difference. When the two groups ($PCI_{MMP9High}$ and $PCI_{MMP9Low}$) were combined for analysis, there appears to be no change at 30 minutes after plaque disruption. However, when the trends were examined according to each subgroup, it was evident that a divergent response was observed by 30 minutes after plaque disruption (Figure 24). Similarly for GDF15, even though the overall patterns based on raw value comparison appeared similar between the combined PCI group and $CONTROL_{Dx}$ group, there was actually underlying divergent trends between the $PCI_{MMP9High}$ and $PCI_{MMP9Low}$ subgroups.

Osteopontin, oxLDL, and LpPLA had all been directly observed in atherosclerotic plaque lesions. Interestingly, there were no significant changes in these candidate markers observed after plaque disruption either in the combined cohort, or in the subgroups defined by *venous* MMP9. For example, the necrotic core of an established plaque should be enriched in oxLDL(129) and previous studies reported acute elevations of circulating oxLDL after

coronary angioplasty(130) and also in patients who presented with ACS(131). Therefore, one would expect to observe an increase in circulating oxLDL level after plaque disruption in this cohort. However, oxLDLs consist of a family of complex proteins and difference between the primary (capture) antibody would result in recognition of different subtypes of oxLDL.(132) This was one explanation as to why no changes in oxLDL were observed in my cohort.

The observation that plasma levels of sCD40L were below the lower limit of quantification (of this R&D assay) for most subjects was not completely unexpected. These subjects all received intensive dual antiplatelet therapy as part of the preparation for the coronary angiography, therefore minimal platelet activation was observed during the peri-procedural period. This finding further highlighted the virtue of preparing platelet poor plasma for the purpose of biomarker research in the settings of coronary artery disease. My data showed that in the absence of residual platelet contamination, there should be minimal or no measurable sCD40L in HVs' or CAD patients' plasma.

In summary, the results from the candidate marker screen showed a candidate marker profile of this cohort consistent with literature. After plaque disruption, acute changes in biomarkers were observed in the cohort. Although plaque morphology was a useful predictor for subsequent biomarker release, the cautious application of OCT for research in clinical settings limited its use as the selection criteria for a discovery sample set. Calculation of AUC using fold change values allowed for correction of the heterogeneity between individuals and comparison of candidate marker between subjects based on the combined temporal release. Of the candidate markers measured during the *Screening phase*, MMP9 release after plaque disruption was the most objective index of the plaque disruption phenotype. The validity of the discovery sample set selection, based on MMP9 release, was further confirmed by measurement of an additional panel of candidate markers.

CHAPTER 4

SMALL MOLECULE PROFILING OF CORONARY ATHEROSCLEROTIC PLAQUE DISRUPTION (LIPIDOMIC AND METABOLOMIC SCREEN)

4.1 Introduction

There are several platforms of mass spectrometry (MS) based analytic techniques applicable to cardiovascular research. Irrespective of the type of platform, the same principles underpin key stages of the mass spectrometry workflow (Figure 25). At the sample processing stage, the small molecule fractions are extracted from the biolocial samples. At the MS stage, molecules in the sample preparation are first converted into gas phase and ionised by an energy source, and guided towards a mass analyser. A mass analyser differentiates the ions by its mass to charge ratio (m/z) and directs them to a mass detector, which determines the mass, charge, and abundance of each ion. The abundance signals for ions are integrated to produce mass spectra which can be analysed. An overview of individual MS platforms utilised in this thesis will be further provided in the corresponding sections.

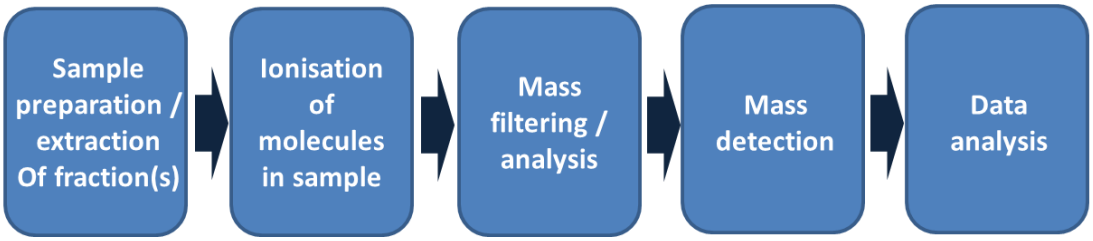


Figure 25: Typical work flow for untargeted –omics experiments

4.1.1 Principles of LC-MS data acquisition

It is common practice to subject the extracted sample through liquid chromatography (LC) prior to the mass spectrometry step. In addition to MS analysis, the use of liquid chromatography provides a valuable means of reducing mass spectral complexity via the different retention properties and elution time for each molecules in the sample. Reversed phase liquid chromatography, which uses a hydrophobic stationary phase such as a C18 column, is a mainstream method and widely adopted for the MS analysis of metabolites.(133) After the chromatography elution step, a typical method of ionisation of molecules is by

applying an electric voltage to the sample as it is injected as a fine spray through the ionisation source – a process referred to as "electro spray ionisation" (ESI). Sequential quadrupoles are used as mass filters and analysers. A "quadrupole" usually consists of 4 metallic poles positioned orthogonal to each other. When opposing electric currents are applied to the metallic poles, charged ions flying through the channel can be attracted out of its direct flight path sequentially depending on its m/z ratio. By adjusting the electric currents applied to the quadrupole, molecules with different m/z ratios can be filtered out, before reaching the mass detector. The mass detector detects the number (intensity) of charged ions that has passed through the quadrupole (which corresponds to a specific m/z as determined by the electric current applied).

4.1.2 Principles of MALDI-TOF-MS data acquisition

In MALDI-TOF-MS (Matrix assisted laser desorption ionisation, time-of-flight mass spectrometry), matrix solution is first added to the sample and directly spotted on a target plate. A laser is then used as the energy source for ionisation of molecules. The energy applied by laser is "desorbed" by the matrix solution and transferred to the sample, resulting in ionisation of molecules (hence the acronymous name of "MALDI"). These ions are guided through a flight channel and a time-of-flight (TOF) mass analyser differentiates the m/z ratio based on the time it takes each ion to fly through the channel. Lighter ions and / or ions with higher charge state (z) fly through the channel more quickly than the heavier ions and reach the mass detector first. To improve resolution of the mass spectra, the flight path can be increased using a reflector. A schematic diagram for MALDI-TOF-MS is presented in Figure 26. Many lipid species are not soluble in solvents used for reverse phase chromatography, therefore cannot be analysed using LC-MS.(134) MALDI-TOF-MS has a unique role in lipidomics research and provides the advantage that samples can be ionised directly, without the requirement to be solubilised and separated using an acqueous phase first.

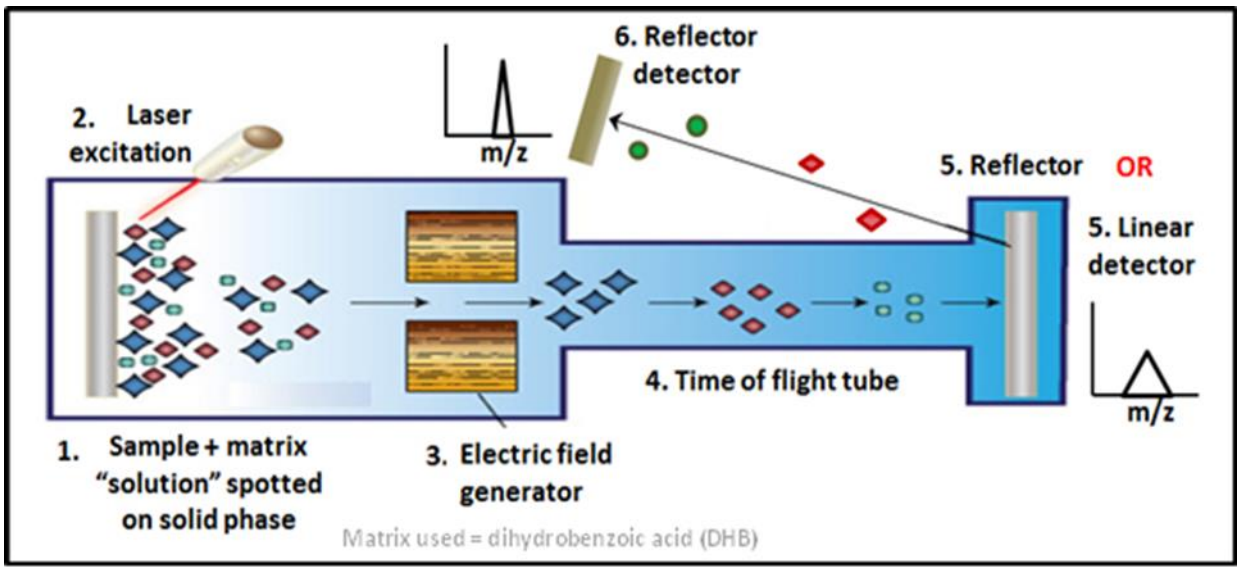


Figure 26: Schematic diagram for MALDI-TOF-MS

In MALDI-TOF-MS (matrix assisted laser desorption ionisation, time-of-flight mass spectrometry), matrix solution is first added to the sample and directly spotted on a target plate. A laser is then used as the energy source for ionisation of molecules. The energy applied by laser is "desorbed" by the matrix solution and transferred to the sample, resulting in ionisation of molecules (hence the eponymous name of "MALDI"). These ions are guided through a flight channel, and a time-of-flight (TOF) mass analyser differentiates the m/z ratio based on the time it takes each ion to fly through the channel. Lighter ions and/or ions with higher charge state (z) fly through the channel quicker than the heavier ions, and will reach the mass detector first. To improve resolution of the mass spectra, the flight path can be increased using a reflector. (*This figure is adapted with permission, from Sigma-Aldrich. http://www.sigmaaldrich.com/*)

4.1.3 Principles of post processing for untargeted small molecules MS analysis

Irrespective of the platform of mass spectral acquisition, similar principles of data post processing and analysis are required as part of the workflow. For qualitative analysis, spectra can be visually inspected for the spectral differences between samples. In a two dimensional spectral data (x axis: m/z, y axis: intensity) such as those acquired from MALDI-TOF-MS, it may be feasible to visually distinguish the presence or absence of mass features between samples (Figure 27). However, where 3 dimensional spectral data is acquired (with the three axes consisting of m/z, intensity and retention time) or when large numbers of samples are analysed, visual comparison of individual spectra across the group is not feasible. In order to make comparison between large number of samples and to perform semi-quantitative comparison between groups, post processing of data is required. A typical post processing workflow includes the following key steps: spectral alignment, filtering of background noise, normalisation of spectral intensity, selection of spectral signal ("peak picking"), extraction of signals, and data analysis.(133)

4.1.4 Conferring the identity of small molecules

One of the challenges in untargeted small molecule profiling is confirming the identity for the mass peaks of interest. Unlike untargeted proteomics analysis (this will be discussed in the following chapter), where the identities of proteins can be inferred from the peptide sequences, methods for conferring identities of metabolites and lipids based on their fragment ions are less established. The difficulties encountered for confirming the small molecule identity is underpinned by the presence of isobaric species – whereby multiple metabolites or lipids may have the same molecular weight or formula, yet differ completely in molecular structure (Figure 28). Therefore these isobaric species may not be distinguishable using information of mass alone. This particular challenge further underpins the inherent high false discovery rate (FDR) of untargeted small molecule profiling.(135)

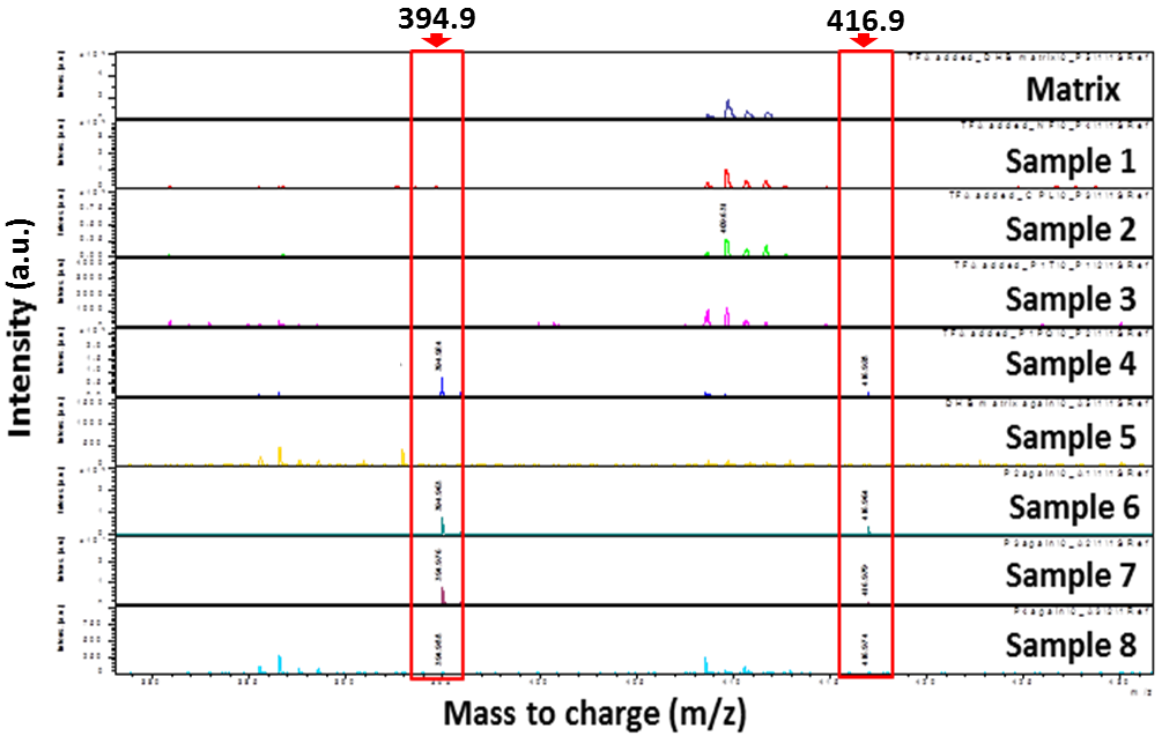


Figure 27: Comparison of MALDI-TOF-MS spectra between different samples

Representative spectra of biological samples acquired using an Ultraflex MALDI-TOF-MS (Bruker Daltonics, Bremen, Germany), and displayed using the Flexanalysis™ software (Bruker Daltonics, Bremen, Germany, Version 2.4) without post processing. The X-axis presents mass to charge ratio (m/z) of a molecular feature, and the Y-axis presents the intensity of the mass feature (arbitrary units). For qualitative analysis, spectra can be visually inspected for the presence or absence of spectra in a each sample. Analysis of the matrix solution (matrix) used for the experiment allows the exclusion of background noise. For example, mass features with the m/z of 394.9 and 416.9 are present in 4 out of the 8 samples, and are both not detected in the matrix.

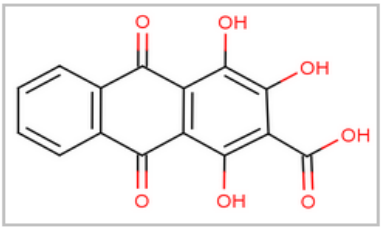
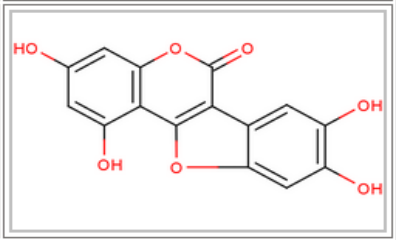
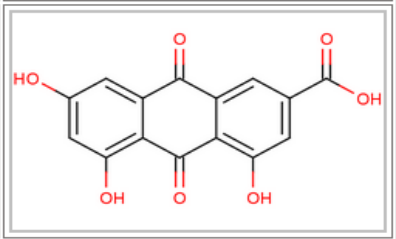
METLIN ID	MASS	Δppm	NAME	MS/MS	STRUCTURE
68301	300.0270	0	**Pseudopurpurin** *Formula:* C15H8O7 *CAS:* 476-41-5	NO	
48355	300.0270	0	**Demethylwedelolactone** *Formula:* C15H8O7 *CAS:*	NO	
43825	300.0270	0	**EMODIC ACID** *Formula:* C15H8O7 *CAS:* 478-45-5	View	

Figure 28: Presence of isobaric species for small molecules raises challenges for confirming identification based on mass

A small molecule mass feature detected by mass spectrometry can be searched against online databases such as the Metlin database used for this particular search (www.metlin.scripps.edu/). However, information on the mass of a molecule often is not sufficient to allow identification of a small molecule (metabolite or lipids) because of the presence of isobaric species. In this example three different compounds, each with different molecular structure, all have the exact same mass of 300.0270, with 0 ppm error. These molecules cannot be differentiated based on the mass alone. This highlights the potential challenges of metabolite identification in small molecules screen.

4.1.5 Sample size considerations for -omics analysis

Sample size consideration in comparative -omics research, whereby samples are compared according to a disease condition (such as before and after plaque disruption) to screen for up or down regulation of "novel/unknown" molecular signatures, is different from the traditional power calculation approach for "known" candidate markers. The traditional approach of sample size calculation, which requires prior knowledge of the variance observed in a particular measurement, is not feasible in discovery –omics workflow. Instead, the biological variance (differences observed between patients) and technical variance (differences observed between replicates) predominate in the consideration of sample size.(136) Assuming the combined biological and technical variance of 100% between samples, the sample size of 10 in each arm of the study will be sufficient to detect a 2.25 fold change (up or down regulation) in a given protein/metabolite with 80% power and α of 0.05 (Figure 29).(137) The ability to detect lower fold change with a given number of samples can be improved if the technical variance can be minimised.

4.1.6 Pooling of plasma samples for -omics analysis

Pooling of samples for omics analysis has the advantage of reducing the intrinsic biological variation observed between samples, making the substantive features easier to detect.(138) Sample pooling can also reduce the total number of samples analysed and reduce the overall requirement of computational power for the analysis and the constraints imposed by instrument throughput and cost considerations.(139) The disadvantage with sample pooling is the inability to estimate within population variation, or to retrospectively identify and exclude "outliers" from the dataset.(138) In this thesis, pooled plasma samples were used for the analysis in each -omics fraction. Based on the discovery phase data, putative targets were selected for further technical replication using individual patient samples.

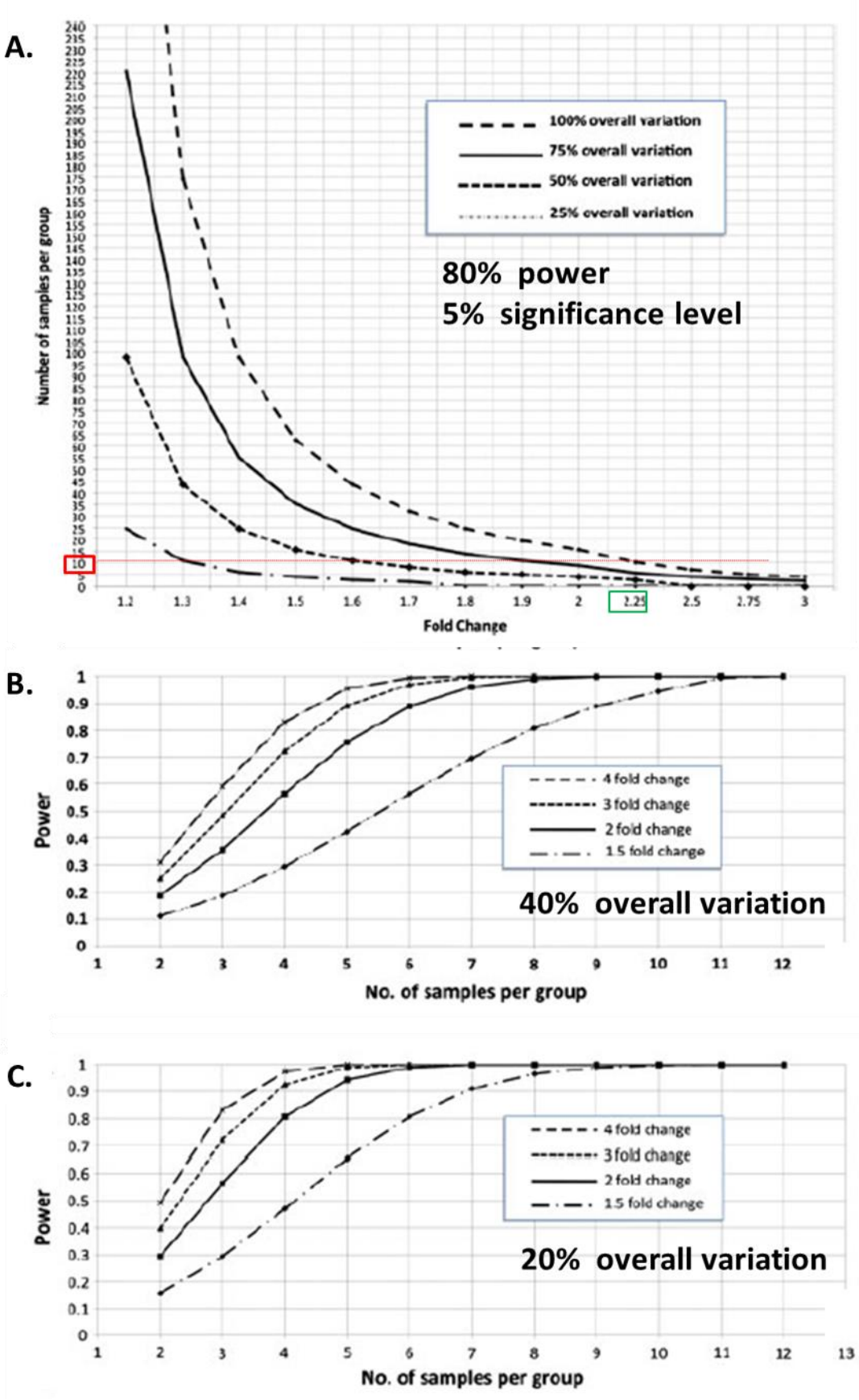


Figure 29: Sample size consideration for discovery -omics research

4.1.7 Principal component analysis – an overview

Traditional statistical tools are often inadequate at summarising and presenting the complexities inherent to datasets which contain a large amount of variables for each observation/samples. PCA is a robust tool widely used for extraction and visualisation of the features contained within such complex datasets. The mathematical concept behind PCAs is similar to that of a regression analysis. In linear regression, a line of best fit to a dataset is created through the dataset. Likewise, a principal component is defined by a vector which contains as much data variability due to the features (protein, metabolite, or lipid features). While in linear regression the relationship between the line of best fit and the observations (samples) is defined by one variable, more than one variable can be included to define each principal component in PCA. Therefore PCA is a powerful tool to reduce the number of original features into a small set of principal components, with each principal component oriented orthogonal to each other in the n-dimensional space, and each accounting for the residual variances yet explained by the previous principal components. In theory, the maximum number of principal components that can be defined for an analysis equates to 1 less the total number of features. In practice, PCA scores plot are typically presented using 2 (2D) or 3 (3D) principal components.(140) A conceptual illustration for performing a PCA is present in Figure 30.

PCA is an extremely useful tool for visual assessments of the inter-relations of among a set of features. On a PCA score plot, samples which are similar to each other (thus containing less variance between them) will be closer to each other, as compared to samples which are different to each other which will separate further in space. This spatial separation is a key feature that allows the utilisation of PCAs as a data visualisation tool, as the samples collected from different conditions (biological variation, different disease type, samples collected before/after intervention, etc.) may be distinguishable by spatial separation. The

opposite observation, whereby samples are positioned close to each other on a PCA score plot, indicates similarity between the samples (good technical replicates, same type of disease, small effect of intervention, etc.). However, it is important to note that PCA does not give information regarding the *statistical significance* between the patterns observed.(140)

4.2 Hypotheses and Aims

The purpose of the work in this chapter was to assess the acute changes of plasma small molecules after stenting induced plaque disruption using untargeted metabolomics and lipidomics approach.

Specifically, I hypothesised that:

- Plaque disruption leads to acute changes in plasma small molecules profiles
- The acute changes in plasma small molecule profile can be characterised using untargeted MALDI-TOF-MS and LC-MS analysis

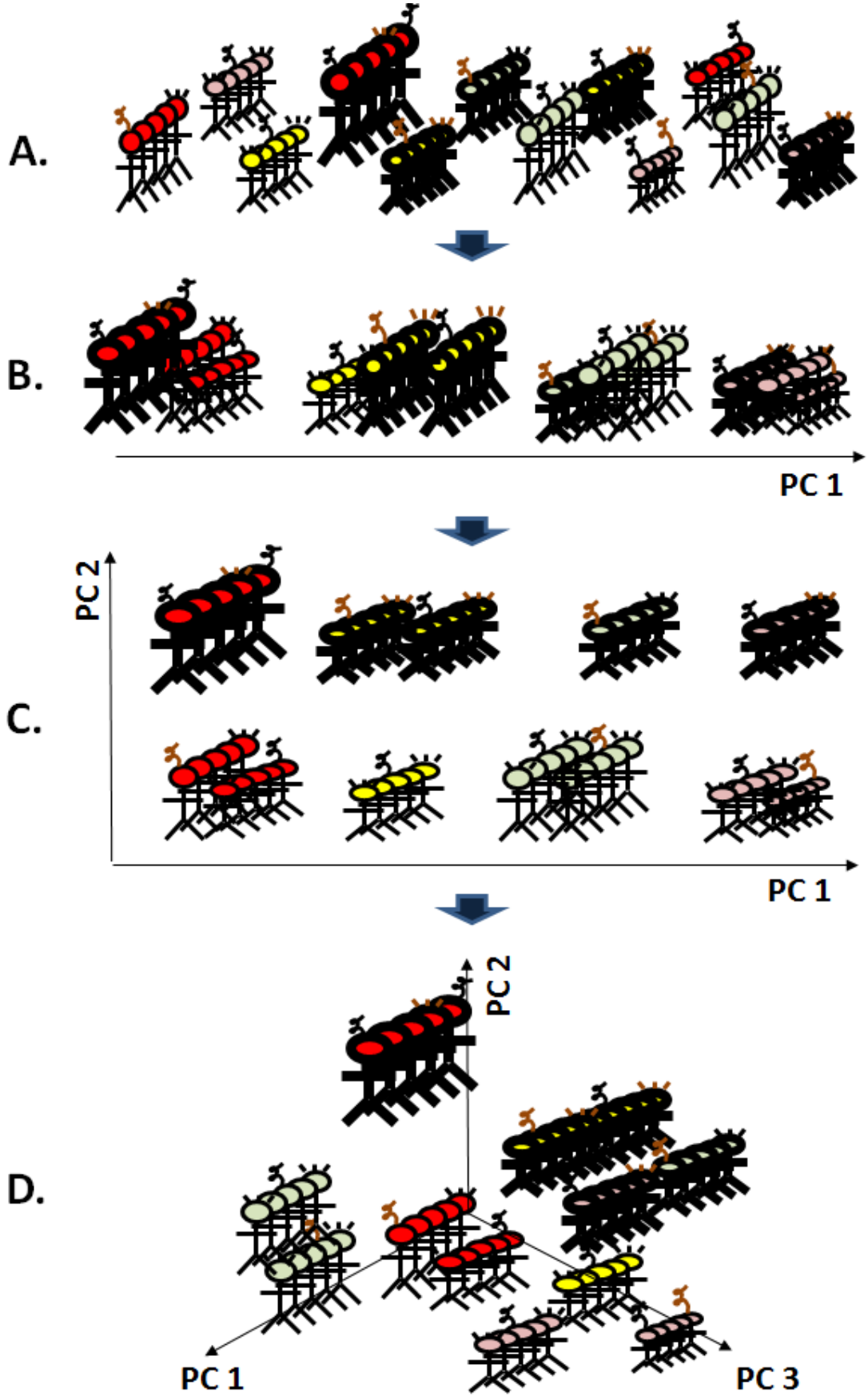


Figure 30: Conceptual illustration of how a PCA is performed

4.3 Methods

4.3.1 Plaque debris for analysis

Collection of coronary plaque debris was performed in using methods described in Section 2.4.2. To assess if blood components in circulation (other than coronary plaque debris) would adhere to the filterwire during the PCI procedure, therefore giving rise to artifactual signals unrelated to coronary plaque debris, a paired filterwire device was prepared as matched control. After the diagnostic angiography confirmed suitability for stenting with filterwire distal protection, an additional 10 ml of arterial blood was aspirated from the coronary guide catheter and transferred into a 15 ml falcon tube. A filterwire was then positioned downstream of the coronary lesion followed by the PCI procedure. Concurrently, an unused filterwire was placed in the falcon tube containing the individual's blood. This was then immediately transferred to a water bath and incubated at 37.5°C for the duration of the stenting procedure (Figure 31-A). At the end of the PCI procedure, both filterwires (one containing plaque debris, and one from *ex vivo* incubation) were retrieved and immediately frozen on dry ice and stored at -80°C for subsequent analysis.

4.3.2 Plasma samples for analysis

Plasma samples analysed during the *Discovery Phase* included 30 subjects selected from the *Screening Phase,* as detailed in Section 3.6.15. This consisted of 10 subjects in each of the $PCI_{MMP9High}$, $PCI_{MMP9Low}$, and $CONTROL_{Dx}$ group. To capture the earliest changes in the plasma proteins, plasma collected from the coronary artery at *5 minutes* after plaque disruption were used for comparison against the baseline sample collected from the coronary artery prior to stent (0 min). Plasma samples from 10 healthy volunteers without any prior medical history were also included. The final composition of the discovery subject subset for plasma samples is represented in Figure 31-B. The demographic data for the discovery subject set has been presented in Table 4.

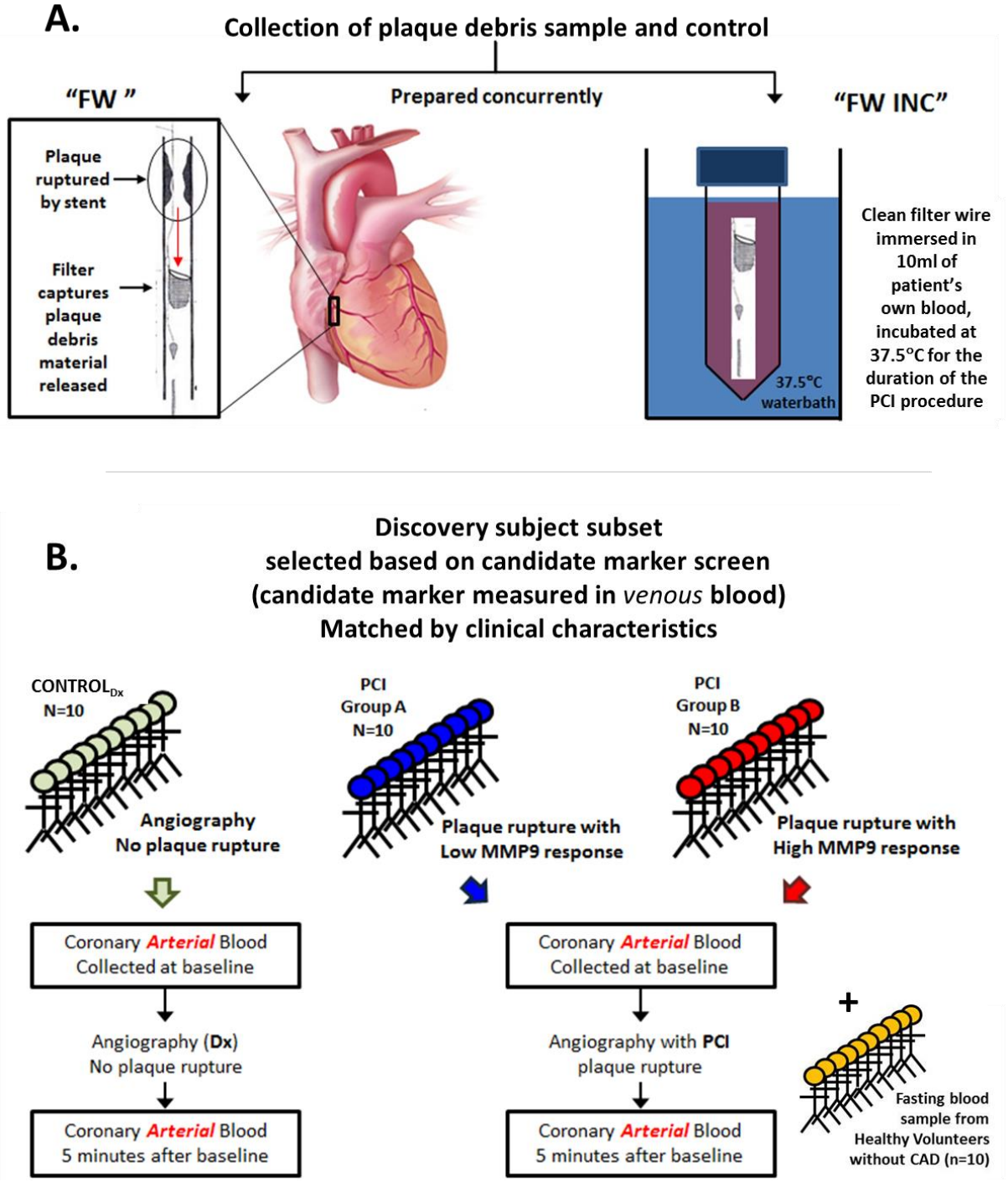


Figure 31: Sample analysed during the discovery phase of this research

4.3.3 Additional samples and controls used for MALDI-TOF-MS and LC-MS analysis

In order to minimise false discovery during this phase of experiment, a negative control (NC) sample was use in each analysis. The negative control sample consisted of a new filterwire device, prepared through the same organic extraction protocol as the rest. This non-biological sample was then subjected to the same analysis workflow as the other samples. For MALI-TOF-MS, the matrix solution (DHB - dihyrobenzoic acid) used for sample suspension was also analysed as a blank sample which contained intrinsic matrix peaks (noise). *In addition to the pooled plasma samples, lipidomic fraction from individual samples of each patient were also analysed by MALDI-TOF-MS.*

4.3.4 Extraction of lipid and metabolite fractions from FW and FW INC samples

The filterwire device containing plaque debris was first transferred to a 2ml eppendorf tube and immersed in 500µl of H_2O. The sample was subjected to sonication in a water bath for 2 minutes to achieve cell lysis. The tissue lysate was retrieved for the staged extraction of each of the protein, metabolite and lipid fraction using an organic extraction protocol with sequential concentration gradients of methanol, chloroform and H_2O as illustrated in Figure 32.[i] This protocol utilised the variable miscibility of lipids according to the concentration of methanol in the organic solvent.(141) Using this protocol, the metabolite portion was extracted in the aqueous phase, followed by separation of the lipid and protein fractions after an additional step of methanol extraction.

After the first stage of methanol and chloroform extraction, the aqueous phase supernatant (containing the polar metabolites) was filtered using a molecular weight cut off spin column (Corning® Spin-X UF 6mL concentrator). The filtrate was diluted 1 in 10 with 0.2% trifluroacetic acid (TFA), followed by sequential washes of Buffer A (consisting of 0.1%

[i] This protocol was designed in collaboration with Dr Benedikt Kessler's group at the CCMP, Oxford.

TFA) and Buffer B (consisting of 0.1% TFA with 65% acetonitrile) to remove inorganic salt. The final eluent was aliquoted and vacuumed dried, then stored at -80°C for subsequent analysis. After extraction of the aqueous phase, a further 1125μL of methanol was added to the residual organic phase, vortexed, and centrifuged at 16000g for 2 minutes to precipitate proteins. The supernatant contained the lipid fraction. Each of the final fractions was vacuum dried and stored at -80°C for subsequent analysis.

4.3.5 Data acquisition for lipidomic fraction

Matrix solution was prepared by dissolving 50mg of DHB in 1ml solution containing 50% methanol, 49% water, and 1% TFA. The dried samples were re-suspended using 20μl of methanol (100%) and mixed thoroughly. After mixing the DHB matrix solution with the re-suspended sample (1:1 ratio), 1μL of the final mixture was spotted on the MALDI Anchorchip target plate (Bruker Daltonics, Bremen, Germany) and allowed to dry. Mass spectra of spotted samples were acquired using an Ultraflex MALDI-TOF-MS (Bruker Daltonics, Bremen, Germany) mass analyser. Mass calibration of the instrument was performed using standards (Bruker Daltonics, Bremen, Germany) covering the range of 1-12KDa prior to sample data acquisition. Positive ion spectra were acquired in reflectron mode, between the m/z range of 80 to 1060. The laser power was set to 20%, and 100 lasers shots were automatically summed per acquisition. For each sample, 16 laser acquisitions were collected from random areas within each sample spot, and the intensities from the 16 acquisition were summed to give rise to the final mass spectra for each sample. To ascertain the technical reproducibility between different spectral acquisitions, replicate spectra were obtained from the HV sample.

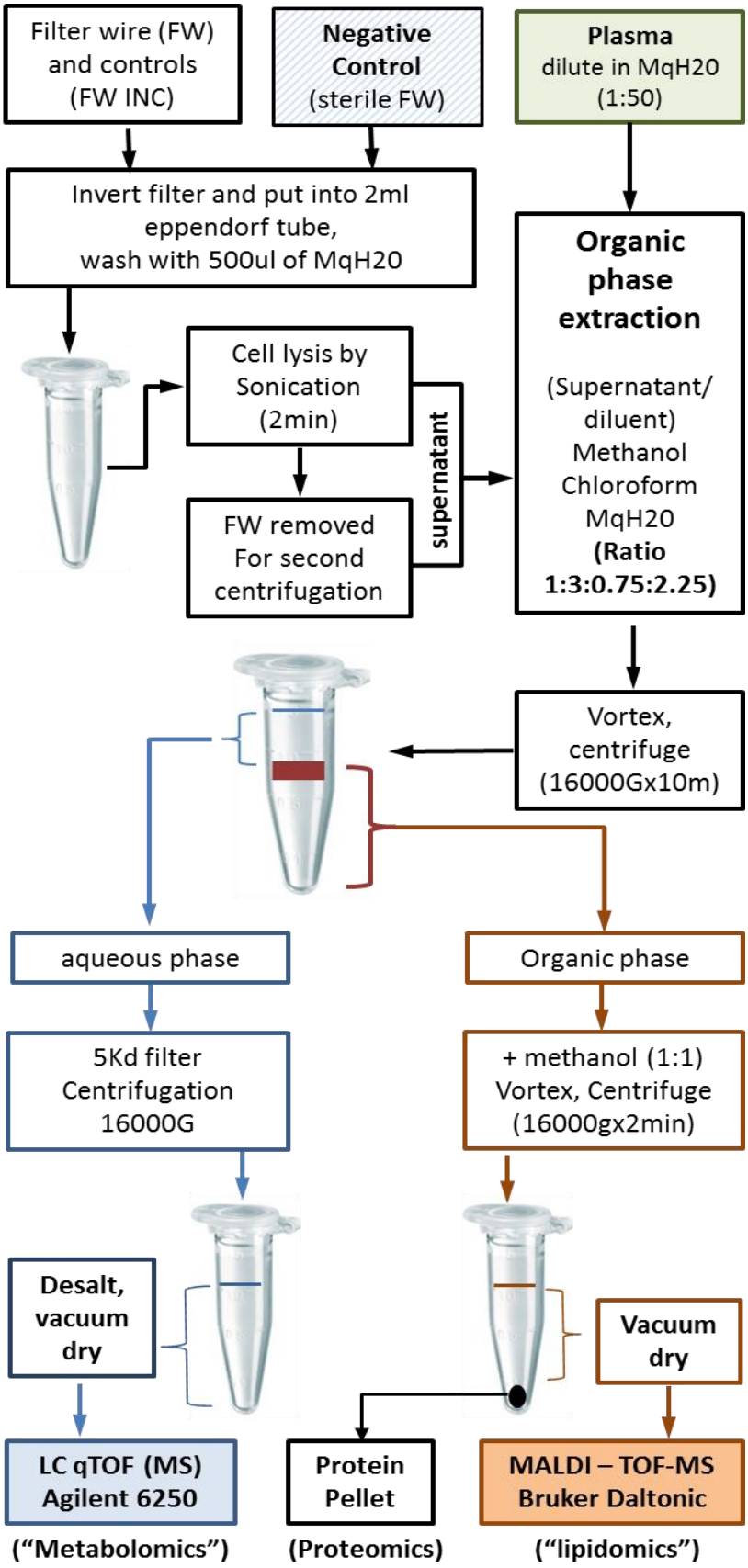


Figure 32: Summary of the organic extraction protocol used for the extraction of lipid and metabolite from plaque debris and plasma samples

4.3.6 Data acquisition for metabolomics fraction

The metabolite fractions prepared from Section 4.3.4 were re-suspended in 10μL of aqueous buffer containing 0.1% formic acid and 2.5% acetonitrile. A QC sample was prepared by pooling 1.5μL from each of the re-suspended samples. The samples were subjected to mass spectrometry using a nano-flow reverse phase LC system coupled to an ESI Q-TOF MS/MS (Agilent 6250, Agilent Technologies, Santa Clara, USA). Acquisitions of sample spectra were performed according to a randomised worklist, in technical triplicates. Acentonitrile runs were used as column washing injections in between biological samples. Pooled QC samples were run at regular intervals. Mass calibration was performed using internal reference mass of m/z 83.0603 and 445.1200. Each sample (0.5μL) was loaded to the ultrahigh capacity chip (Agilent Technologies, G4240-65010) packed with Zorbax-80SB-C18 5μm particle (enrichment column: 25mm, 500nl; analytic column: 75μm internal diameter x 15cm length) at a flow rate of 0.4μL/min. Chromatographic separation was achieved by a 15 minute gradient using Buffer B which contained 95% acetonitrile and 0.1% formic acid (from 0% to 40% in 11minutes, from 40% to 100% in 2 minutes, this chromatographic condition was kept for 1 minute, then returned to 0% in 1 minute). Every analysis was preceded by column equilibration flow of Buffer B for 15 minutes. Each sample analysis was followed by equilibration of the column with a further 10 minute gradient using Buffer B. Small molecules were ionised in positive mode operating in full scan mode between the m/s range of 50 to 1000 in an extended dynamic range (2GHz), using N_2 as nebuliser gas (1.5L/min, 350°C). The capillary voltage was set at 2050V, with a scan rate of 1.37scan/s with a fragmentor voltage of 100V.[j] The full scan mass spectra data were acquired by Mass Hunter Data Acquisition Software (Agilent Technologies, Santa Clara, USA, Version 0.2.064.0).

4.4 Data analysis

[j] This metabolomics workflow was optimised by Dr. Alessandro Valli at the CCMP, University of Oxford

4.4.1 Data analysis for MALDI-TOF lipidomics

4.4.1.1 Qualitative analysis by visual inspection of spectra

Mass spectra data files (generated in .d format) were directly imported to Flexanalysis™ (Bruker Daltonics, Bremen, Germany, Version 2.4). Visual inspection of the entire spectra was performed with the following samples aligned side by side: DHB, NC, FWs, FW INCs, and pooled plasma samples as illustrated by Figure 27 in Section 4.4.1.1. This analysis allowed for detection of mass peaks which were visually present in the biological samples, but absent in the non-biological controls.

4.4.1.2 Semi-quantitative analysis

Mass spectra data files (generated in .d format) were directly imported to Medicwave Spectrolyser (Version 1.0.19, Halmstad, Sweden) for analysis. For each data file, subtraction of baseline noise was performed using a signal to noise ratio (SNR) of 10 to the average noise at baseline as cut off. Normalisation of data intensity was then performed using Total Ion Current (TIC) normalisation algorithm. The peak intensity for each mass peak was normalised to a total of $1x10^9$ arbitrary units per whole spectra of the sample. Automatic peak extraction was performed between the m/z range of 80 to 1060, with further filtering of potential noise signal using SNR of 2 to the minimum noise at baseline. Alignment of the extracted mass peaks was performed through the program's binning algorithm (density method, using the highest peak for multiple peak resolution, maximum/minimum bin width set to 1 and 0.1 Da respectively).

After the alignment stage, all mass peaks that were observed in the DHB matrix and NC sample (non-biological mass peaks) were excluded from the biological samples using the custom feature selection algorithm. The residual peaks, containing biological mass peak signals, were log transformed prior to further analysis. PCA was performed for exploratory data analysis. Mass peaks which had low variance within an individual sample group were

further excluded. Comparisons of the same mass peaks within individual group (0min and 5min) were performed using paired t-tests. The cluster of 15 mass peaks which were most significantly changed after plaque disruption (in the PCI group) were selected through the Spectrolyzer's Multiple Biomarker Detection algorithm. Mass spectra for individual patients were also exported after the alignment step for off-line analysis by Perl script (version 5.12.4), in addition to the Spectrolyser analysis. This Perl script analysis followed the same steps of mass peak exclusion (of non-biological mass peaks), data transformation, and paired t-tests of mass peaks within individual groups. Multiple testing corrections were performed by Benjamini-Hochberg test.[k]

4.4.2 Data analysis for LC-MS metabolomics

4.4.2.1 Non- targeted analysis of metabolomics profile

Non-targeted extraction of molecular features within each spectra were performed using the MassHunter Qualitative Analysis software "*Find Compounds by Molecular Feature*" algorithm, using the following settings: retention time restriction 3.5-18min; peak filter minimum of 200 counts; allowing $[M+H]^+$, $[M+Na]^+$, $[M+K]^+$ and $[M+NH_4]^+$ adduct ions; peak spacing tolerance=0.0025 m/z, plus 15ppm; limit assigned charge states to a maximum of 1. The molecular features extracted from each spectra were exported as .CEF format files and uploaded to MassHunter Mass Profiler Professional Software (Version B12.05, Agilent Technologies, Santa Clara, USA) for further analysis. Only ion features with minimum abundance of ≥2000 were included in the import. Molecular features across different samples were aligned using these alignment parameters: retention time window slope and intercept (5%, 0.3min), mass window slope and intercept (50ppm, 50). Z-transformation was applied to each spectral data file as the way to normalise data acquired from different sources.

[k] Perl script analysis was kindly performed by Dr. Philip Charles at the CCMP, Oxford

For exploratory data analysis, PCAs based on metabolite abundance levels were performed all experimental groups. For comparison between samples, features which were detected in *any* negative control (NC) sample replicates (background noise) were first excluded. Of the remaining features, only common features found in at least 70% of the pooled QC sample replicates (biological signal in this experiment) were included in the analysis. Statistical comparisons were made between the following groups: FW and FW INC samples (2 pairs), Dx (0min and 5min), $PCI_{MMP9Low}$ (0min and 5min), $PCI_{MMP9High}$ (0min and 5min). P values were calculated using paired t-tests, with Benjamini-Hochberg Multiple Testing Correction. The P value of <0.05 was considered statistically significant.

4.4.4.2 Targeted search of molecular features

The MassHunter Qualitative Analysis software (Version B0.5.00, Agilent Technologies, Santa Clara, USA) was used to analyse the raw data files generated from Section 4.3.6. The molecular formula and weight of compounds of interest were searched against online repository sites including Metlin (http://metlin.scripps.edu), HMDB (http://www.hmdb.ca) and Lipid Maps Lipidomics Gateway (http://www.lipidmaps.org). Targeted searches for individual compounds in the experimental data files were performed using the "*Find Compound by Formula*" algorithm of the MassHunter Qualitative Analysis software software (142) by inputting the empirical formula of a particular compound using default settings: The ion adduct species allowed for were: +H, +Na, +K, -H, and neutral loss of H_20; peak spacing toleration was set a 0.0025 for m/z and 7.0 for ppm; A charge state of 1 was set as the limit. A list of compounds for targeted search was decided based on biological pathways of potential relevance to the experiment observations.

4.5 Results

4.5.1 MALDI-TOF MS lipidomic screen

4.5.1.1 Qualitative analysis by visual inspection of spectra

Visual inspection of the spectra using Flexanalysis^{TM} software revealed several peaks which were consistently observed in biological samples, but absent in the matrix and NC. One of the mass peaks present in all biological samples was m/z 369.00 which was consistent with cholesterol (-H_2O) (Figure 33–I). There were mass peaks unique to plaque debris collected from the native coronary artery (Figure 33–II) or plasma (Figure 33-III). One of the mass feature (m/z 919.37) was absent in the plaque debris and baseline plasma samples, but appeared in plasma after plaque disruption in both PCI groups (Figure 33–IV).

4.5.1.2 Semi-quantitative analysis

4.5.1.2.1 Plaque debris and pooled plasma samples

PCA scores plot for all lipid features showed tight clustering of the HV sample technical replicates, while clear separation was observed between the different sample types (Figure 34-A). PCA scores plot for the plasma samples showed a distinct pattern: a greater separation was observed between the plasma samples before and after plaque disruption in the $PCI_{MMP9High}$ group, while lesser separation was observed in the $PCI_{MMP9Low}$ group. This was in contrast to the $CONTROL_{Dx}$ group, in which minimal separation was observed between the plasma samples taken at baseline and 5 minutes after (Figure 34-B).

4.5.1.2.2 Individual plasma samples

A total of 1440 different mass peaks were observed in the 60 individual plasma samples using the extraction algorithm detailed in Section 4.4.1.2. The 15 most significantly changed mass peaks at 5 minutes after baseline for each group were selected by the Spectrolyser^{TM} Multiple Biomarker Detection algorithm. These are summarised by a correlation matrix in Figure 35. However, correction for multiple testing was not available within the Spectrolyser^{TM} software. The analysis was therefore repeated off-line by Perl script. After applying the Benjamini-Hochberg multiple testing corrections, none of the changes observed in the individual mass features remained statistically significant.

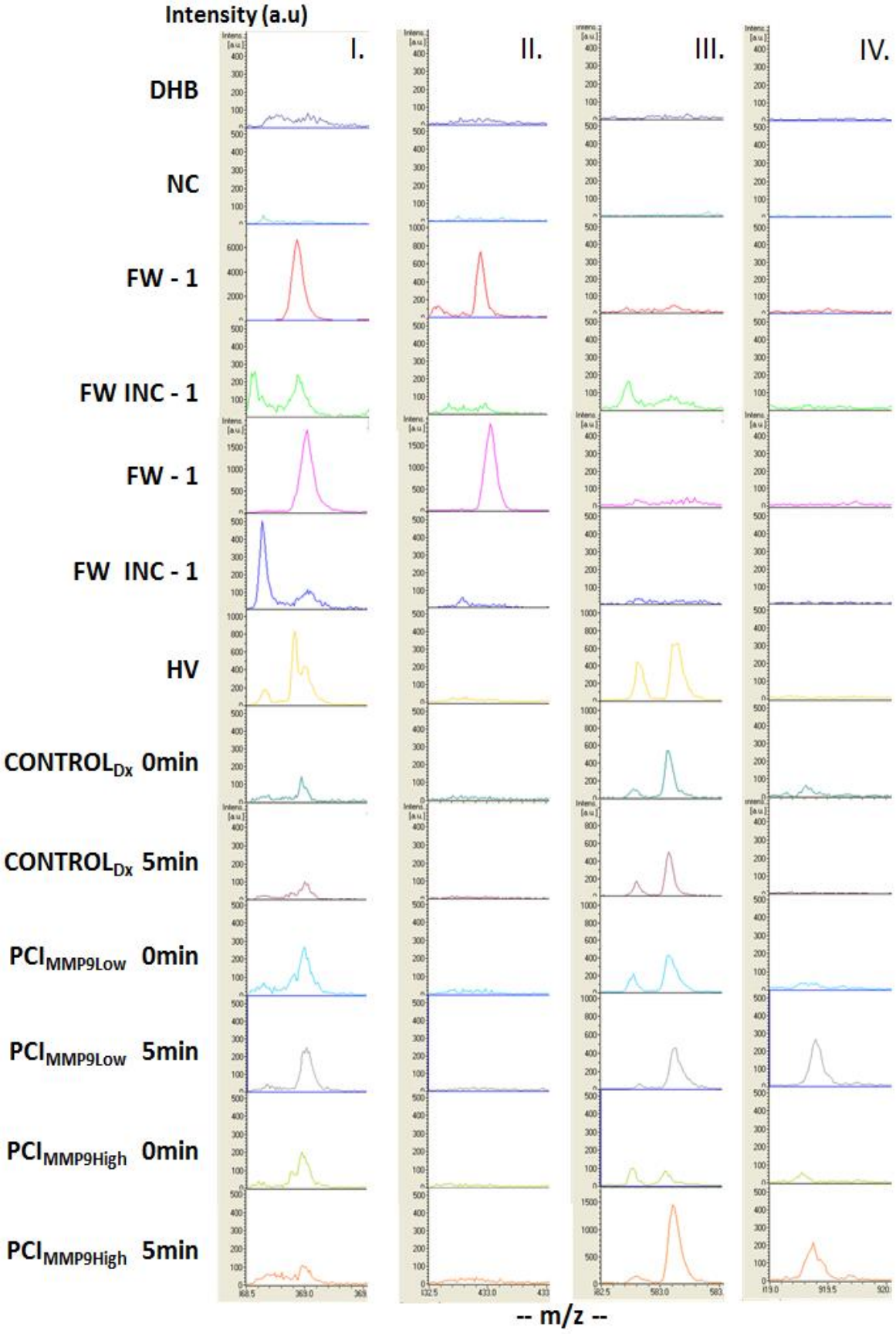


Figure 33: MALDI-TOF-MS spectra showing unique features in biological samples analysed during the discovery phase

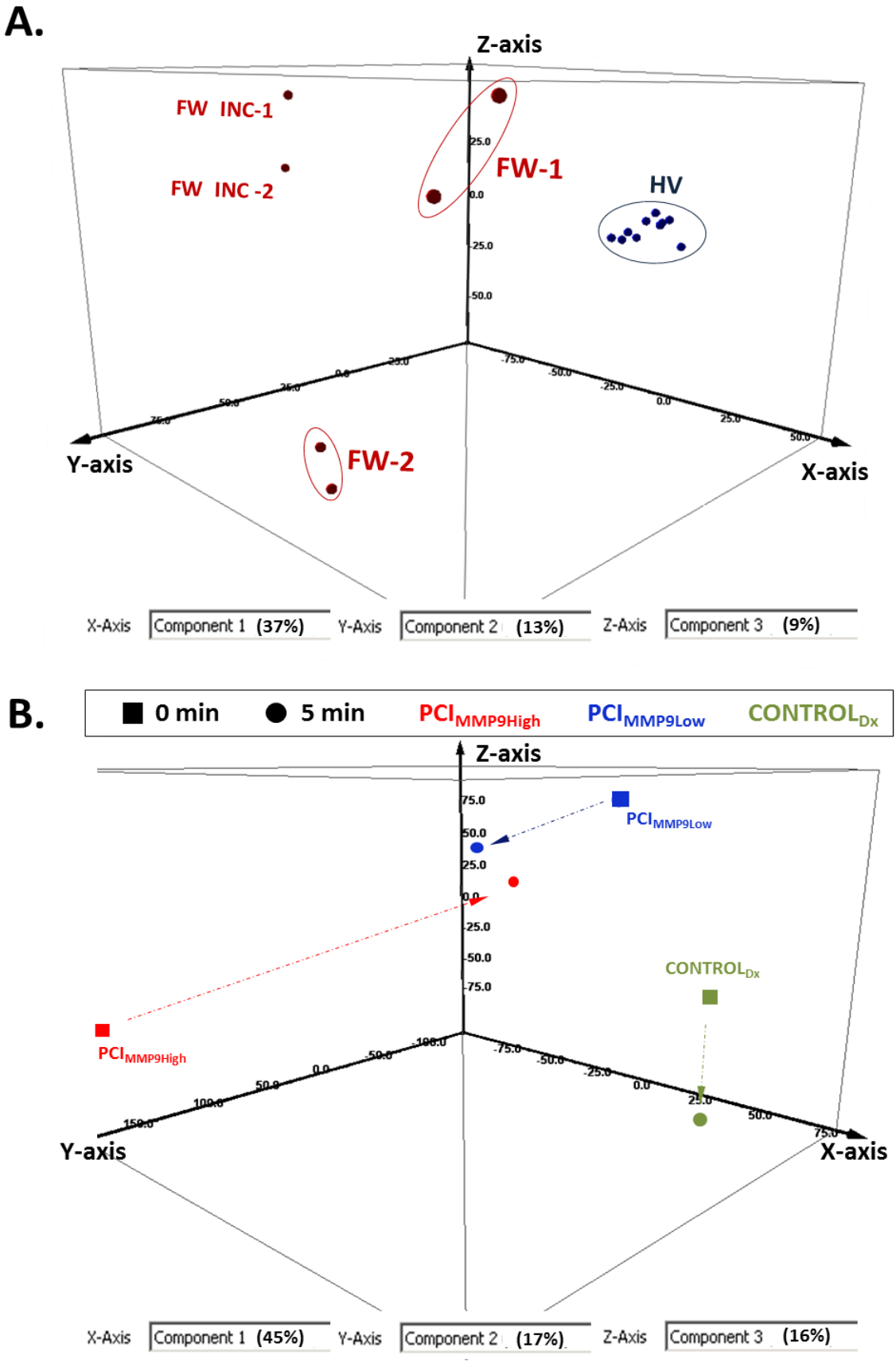


Figure 34: Lipidomic profiles differ between the types of samples, and in plasma samples before and after plaque disruption

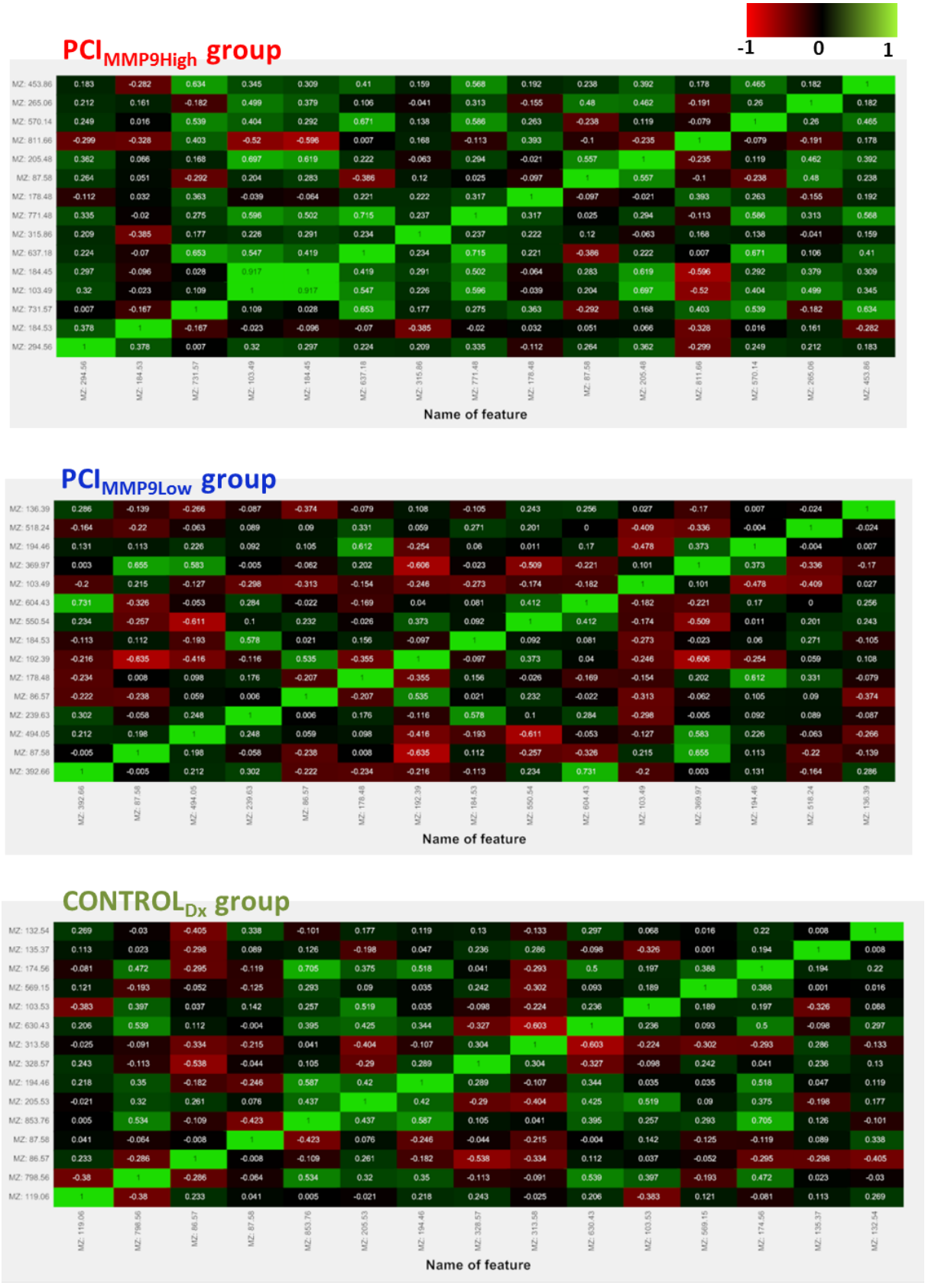


Figure 35: Correlation matrix of the 15 most significantly changed mass features selected by the Medicwave Spectrolyzer™ software in the plasma samples from the discovery subject subset

4.5.2 LC-MS metabolomic screen

4.5.2.1 Untargeted metabolomics analysis

PCAs were performed for the experimental groups. PCA scores plot of the QC sample spectra showed tight clustering between the technical replicates and clear separations between the different sample types of plasma, FWs, and FW INCs (Figure 36-A). The averaged intensity of individual features observed over the technical triplicates were used for principal component analyses. PCA scores plot for the plasma samples before and after plaque disruption showed distinct patterns: greater separation was observed between the plasma samples before and after plaque disruption in the $PCI_{MMP9Low}$ group. Lesser separation was observed between the plasma in the $PCI_{MMP9High}$ group before and 5 minutes after plaque disruption, which was similar to the separation observed in the control Dx group (Figure 36-B).

A total of 27045 small molecule features were observed in the overall dataset. Features detected in one or more of the technical replicates in the negative control sample were excluded (n=12314). Of the residual small molecule features, 415 were observed in at least 70% of the QC samples. The levels of 44 features differed significantly between the FW and FW INC samples. Amongst these, significantly higher levels of 17 features were observed in FW samples compared to the FW INC samples (Figure 37-A). Comparison between the plasma samples at 5 minutes versus 0 minutes showed significant changes ($P<0.05$, after multiple testing correction) within each of the experimental group ($CONTROL_{Dx}$, $PCI_{MMP9Low}$, $PCI_{MMP9high}$). Amongst these, significant changes in 5 features were observed consistently in all three groups, while significant changes of 17 and 82 features were uniquely observed in the $PCI_{MMP9High}$ and $PCI_{MMP9Low}$ group, respectively. The patterns of significantly changed features in the individual PCI groups are summarised by the heatmaps in Figure 37, panel B and C.

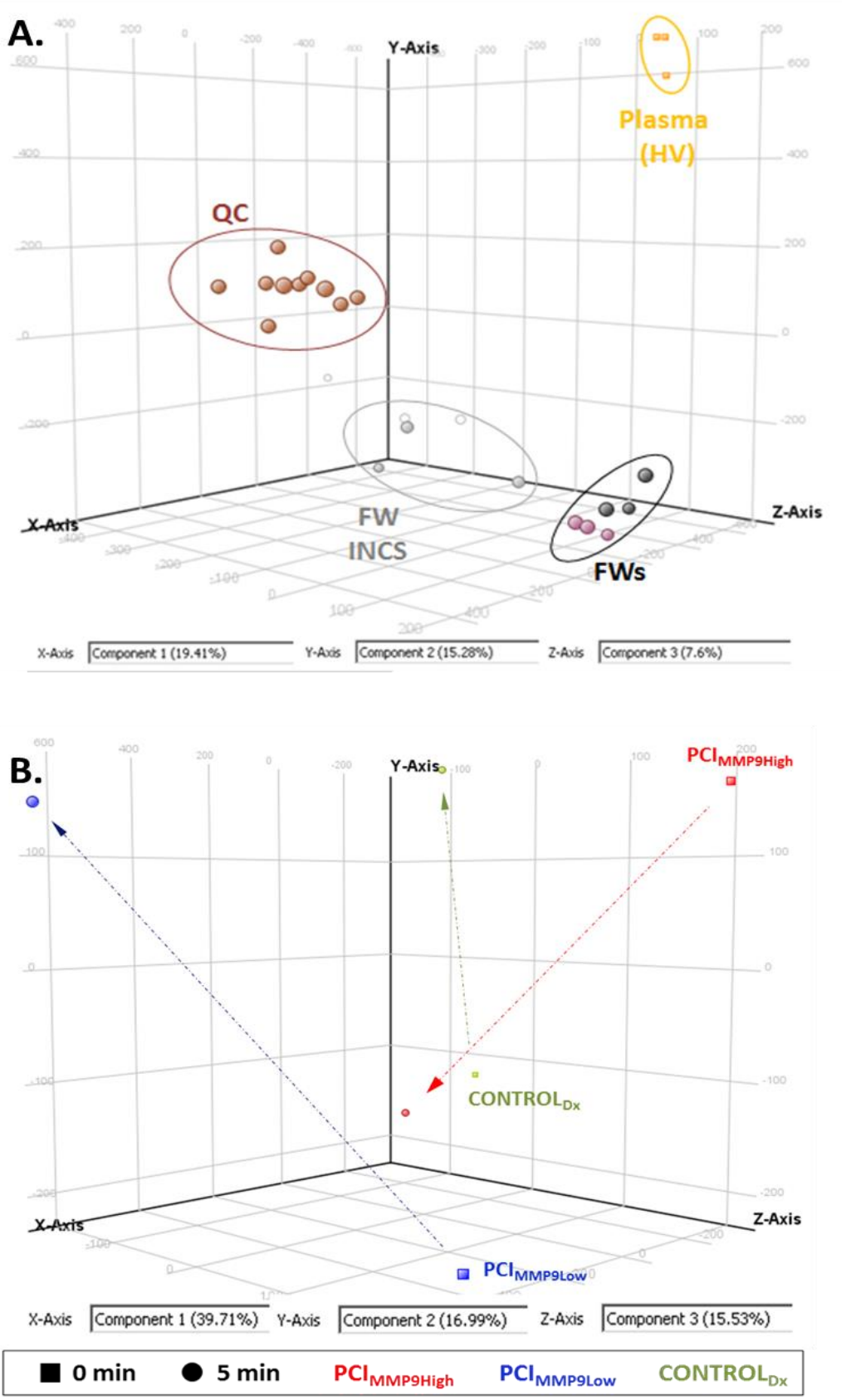


Figure 36: Metabolomic profiles differ between types of samples, and in plasma samples before and after plaque disruption

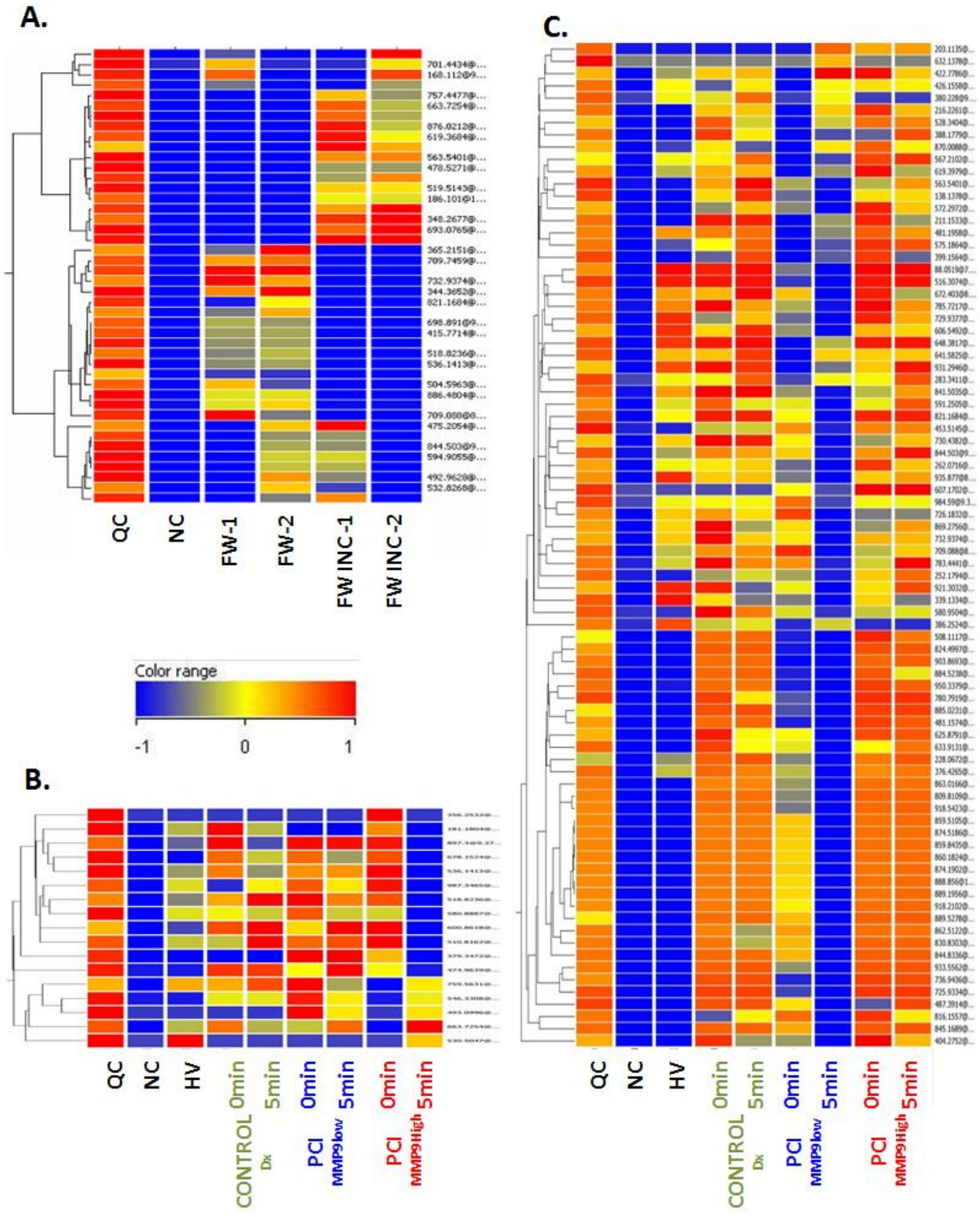


Figure 37: Metabolite features which were differentially detected in plaque debris, and in plasma after plaque disruption

4.5.2.2 Targeted metabolomics search

Given the observations from the MALDI-TOF-MS analysis, where marked separation of lipidomics profiles were observed after plaque disruption particularly in the $PCI_{MMP9High}$ group, targeted searches were performed for compounds involved with fatty acid and cholesterol biosynthesis pathways. Mass features which were consistent (within 5 ppm) with the following compounds were observed in pooled plasma samples dataset: acetyl-CoA ($C_{23}H_{38}NO_{17}P_3S$), coenzyme-A ($C_{21}H_{36}N_7O_{16}P_3S$), acetoacetyl-CoA ($C_{25}H_{40}N_7O_{18}P_3S$), 3-hydroxy-3-methylglutaryl-CoA ($C_{27}H_{44}N_7O_{20}P_3S$), mevalonate ($C_5H_{12}O_4$), 3-hydroxybutanoyl-CoA ($C_{25}H_{42}N_7O_{18}P_3S$), crotonyl-CoA ($C_{25}H_{40}N_7O_{17}P_3S$), and NADH ($C_{21}H_{29}N_7O_{14}P_2$). In addition, there were several mass features which were present in plasma of CHD patients at 0 minute, but became undetectable at 5 minutes in $PCI_{MMP9Low}$ group (Figure 38).

4.6 Discussion

Profiling of the lipidomic and metabolomic fractions revealed several important observations. It was feasible to characterise these two fractions from biological samples using a relatively uncomplicated sample processing protocol to extract the small molecules in both plasma and plaque debris samples. Gross differences in small molecule profiles between different sample types were observed, which was an evidence for the internal validity of the experiment. In both small molecule fractions, results from the PCAs indicated greater changes were observed in the plaque disruption groups as compared to no plaque disruption. Importantly, divergent patterns of small molecule release were observed after plaque disruption, dependent on the experimental group. More marked separation in the MALDI-TOF-MS lipidomic fraction after plaque disruption was observed in the $PCI_{MMP9High}$ group; whereas the $PCI_{MMP9Low}$ group showed more distinct changes in the LC-MS metabolomics fraction after plaque disruption.

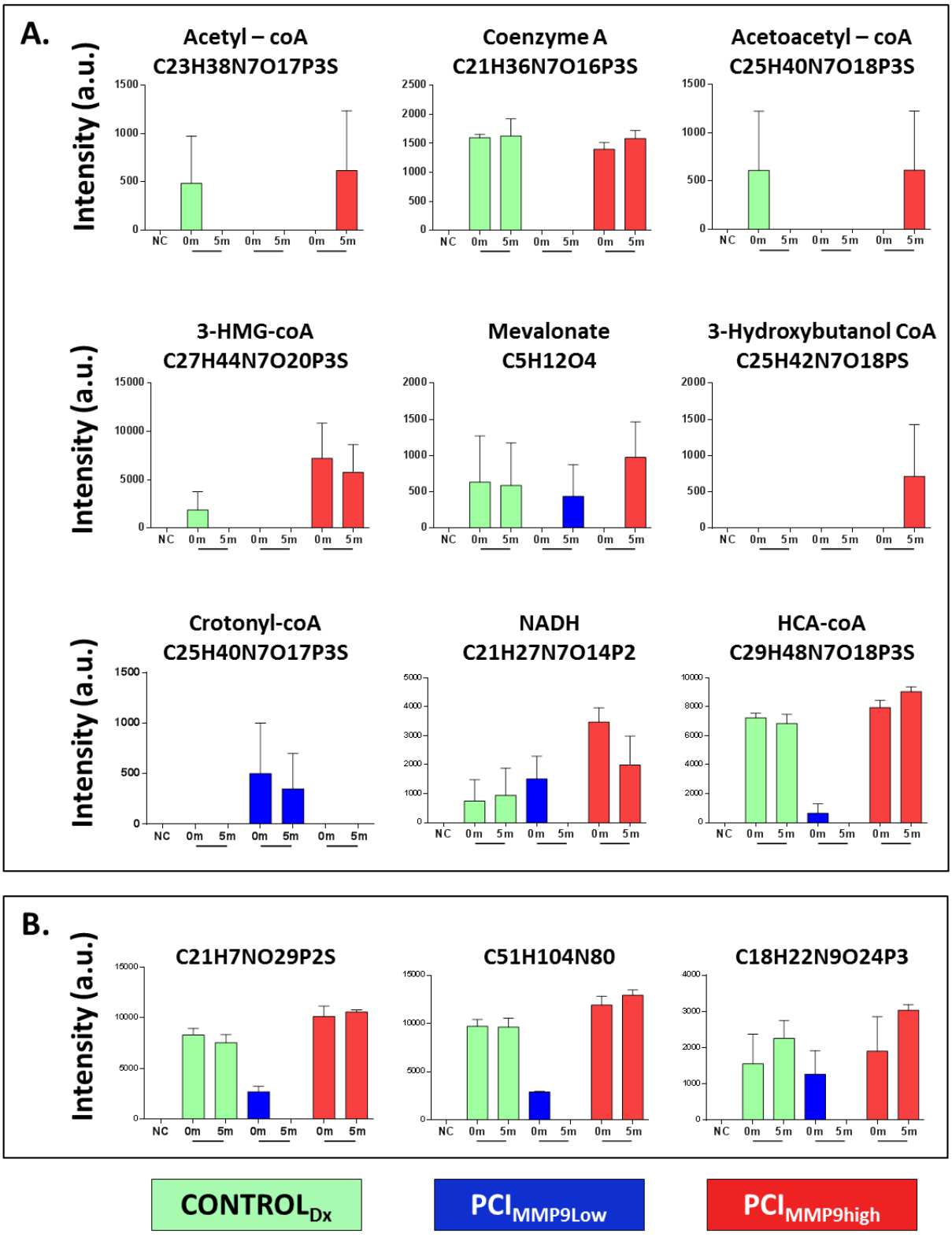


Figure 38: Mass features which demonstrate distinct patterns in plasma samples analysed during the *discovery phase*

In order to control for the intrinsic high rate of false discovery in small molecule screen, additional negative controls were included using a non-biological sample processed through the identical sample processing and experimental workflow. Noise/artifactual mass spectra signals observed in the negative control samples were excluded from the biological dataset prior to further analysis. Using this approach, a high proportion of mass spectra was excluded in both the MALDI-TOF-MS and LC-MS dataset. The use of negative control in this manner has not been routinely reported in literature, but is becoming recognised as one approach to minimise false discovery in untargeted small molecule profiling (personal communication with Dr. Elizabeth Want at Imperial College, London).

Data presented in the preceding chapter showed that disruption of lipid rich plaque was associated with earlier changes of plasma markers such as MMP9, compared to non-lipid plaques. That subjects with the overall highest $MMP9_{AUC}$ change after plaque disruption also demonstrated the most apparent separation in lipidomics profile within 5 minutes of plaque disruption was another highly encouraging observation. It corroborated with the findings on disruption of lipid rich plaque and subsequent differential MMP9 release, and was consistent with the central role of lipid metabolism in plaque biology. This prompted subsequent MALDI-TOF-MS analysis of the *individual* plasma samples, with the aim to elucidate mass features that were significantly changed at 5 minutes after plaque disruption. Even though none of the individual MALDI-TOF-MS mass features reached statistical significance after correction for multiple testing, the global profile changes in the lipidomic fraction remained valid. These findings warrant further investigation.

In this thesis, MALDI-TOF-MS was chosen as the platform for lipid fraction analysis for several reasons. MALDI-TOF-MS negated the need to keep sample in solution, as ionisation of molecules was achieved by desorption of laser energy (lipid species extracted from the

organic fraction migh not be soluble in solvents optimised for the LC-MS platforms available to me during this period of research.) The MS acquisition workflow per sample was significantly shorter for MALDI-TOF-MS compared to other techniques, therefore allowing the analysis of individual plasma samples in this project. However, the high throughput nature of MALDI-TOF-MS was countered by a loss in resolution. Without the chromatography separation step, it lacked the ability to resolve lipid species which shared the same mass to charge ratio. It was possible that some of the more hydrophilic lipid species may were retained in the aqueous phase after organic extraction steps. Therefore the aqueous phase, subsequently analysed by LC-MS in this thesis, might indeed also provided coverage of a subset of lipid species.(68)

In the LC-MS analysis, reverse phase chromatography with a C18 nano-column was used for the chromatographic separation of metabolites extracted in the aqueous fraction, and ionisation was induced by positively charged electric currents ("positive mode"). This is an accepted method for LC-MS analysis of small molecules, but can only capture a fraction of the small molecules which favour such chromatography and ionisation techniques. The use of alternative chromatography methods (such as hydrophilic interaction liquid chromatography) and negatively charged electric current ("negative mode") for ionisation can provide additional coverage of other small molecules in the aqueous fraction. Given the promising data observed so far, exploration of these additional techniques is warranted and will form part of the future work. The combined use of different chromatography and ionisation methods will also provide a more comprehensive coverage of small molecule profile in the biological sample.

In both the MALDI-TOF-MS and LC-MS analysis, unique mass features were observed in the coronary plaque debris samples (FWs) which were not present in the paired controls (FW

INCs). The pooled plasma analysis clearly demonstrated inherent changes in small molecule profiles within 5 minutes of plaque disruption, as compared to the control group ($CONTROL_{Dx}$). Further, the LC-MS analysis provided evidence that significant changes could be detected for individual mass features in plasma. However, identification of these features remained a significant challenge, as highlighted in Section 4.1.4. The strategy to ascertain identity of a mass feature is to perform tandem MS (MS/MS) of the differentially expressed mass features. Matching of MS/MS spectra, molecular weight, and retention time (in the case of LC-MS), between a mass feature and analytical standards, may be sufficient to confer identity of a mass feature.(143) The MS experiments described thus far provide information on putative targets for further interrogation against analytical standard compounds. However, it can be still difficult to select the "correct" analytical standard for direct comparison using mass information alone, due to the existence of isobaric species.

In order to improve the probability of "correct" selections of analytical standards for identity confirmation, I proposed a method using pathway association to guide subsequent target selection during my research. I reasoned that small molecules associated with biological pathways implicated in the experimental conditions were more likely to demonstrate significant changes. Therefore, when the molecular weight of a putative mass feature matched to small molecules associated in the particular pathway, the likelihood of it being the correct match was increased. Indeed similar approaches were recently reported in literature by the time of writing this thesis.(61, 144) These emerging literatures supported my own reasoning above. Using this approach of "inferential pathway analysis", several mass features could be matched (by mass) to small molecules implicated in lipid synthesis pathways. Confirmation of the identity of these mass features will be an immediate goal for the future work.

CHAPTER 5

PROTEOMIC SIGNATURES OF CORONARY ATHEROSCLEROTIC PLAQUE DISRUPTION

5.1 Introduction

5.1.1 Brief overview of untargeted proteomics for biological samples

Untargeted proteomics (also referred to as "shotgun" proteomics) is commonly used for comparison between samples without *a priori* assumptions. This technique allows for characterisation of the maximal number of proteins in one experiment, where the "maximal" number is limited by various parameters related to the experiment. Specific to the type of workflow applied to this thesis, there are several key steps which highlight the basic principles of shotgun proteomics. Insights to these key steps involved are important, as it puts in context various challenges and the respective solutions throughout the workflow. The follow section contains a brief overview of the workflow, which is illustrated in Figure 39.

Proteins are first extracted from the samples and digested by a protease (such as trypsin) to form peptides. This step can be performed while the sample matrix remains in solution ("in-solution" digest) or after separation of protein fractions by gel electrophoresis ("in-gel" digest). The resultant peptides are subjected to liquid chromatography to separate out the peptides according to their biochemical properties prior analysis by the mass spectrometer steps. An ionisation source is applied to the peptides to form charged molecules (or precursor ions). These charged ions are analysed by a mass spectrometer, which determines the mass to charge ratio (m/z) ratio of the ions, and the abundance (intensity) of each precursor ions. The steps so far are similar to the metabolomics work flow, and commonly referred to as liquid chromatography – mass spectrometry (LC-MS).

In order to identify the individual peptides (and infer the identity of the protein from which the tryptic peptides are derived), select peptides from the precursor ion scan are further fragmented by an energy source and subjected to an additional MS scan (hence the term "tandem MS", or "MS/MS"). Using the pattern of fragment ions generated, it is feasible to

computationally determine the individual peptide sequences. Certain peptide sequences are unique to the parent protein and allow the "identification" of its parent protein.(145) This identification step is typically performed through a web-based engine, one of which is the Mascot online portal (Matrix Science, Boston, USA).

Because the identity of a protein is inferred from the fragment ions of its composite peptide, the identity of protein is probability based. For every protein "identified", there are probability scores to denote the likelihood of a false identification for each protein. In addition, false discovery rate can be determined for each peptide/protein, or for the combined experimental dataset.

In shotgun proteomics workflows, internal standards are not applied to the samples. Therefore, it is not feasible to provide absolute quantification of individual proteins in a given sample. Characterisation of the protein profile for individual samples is only qualitative. However, the relative abundance between proteins within an individual sample can be inferred by mathematical algorithms such as the emPAI (exponentially modified protein abundance index) score(146), or by spectral counting of the total number of spectra identified for a protein.(147)

Semi-quantitative comparison of protein abundance between samples can be achieved in shotgun proteomics through post processing of data, using algorithms to perform data normalisation. This can be performed by direct computation with coding software such as R, which requires informatics programming skills. For this thesis, a proprietary software tool has been used (Progenesis LC-MS^{TM}, Non-linear Dynamics, Newcastle, UK).

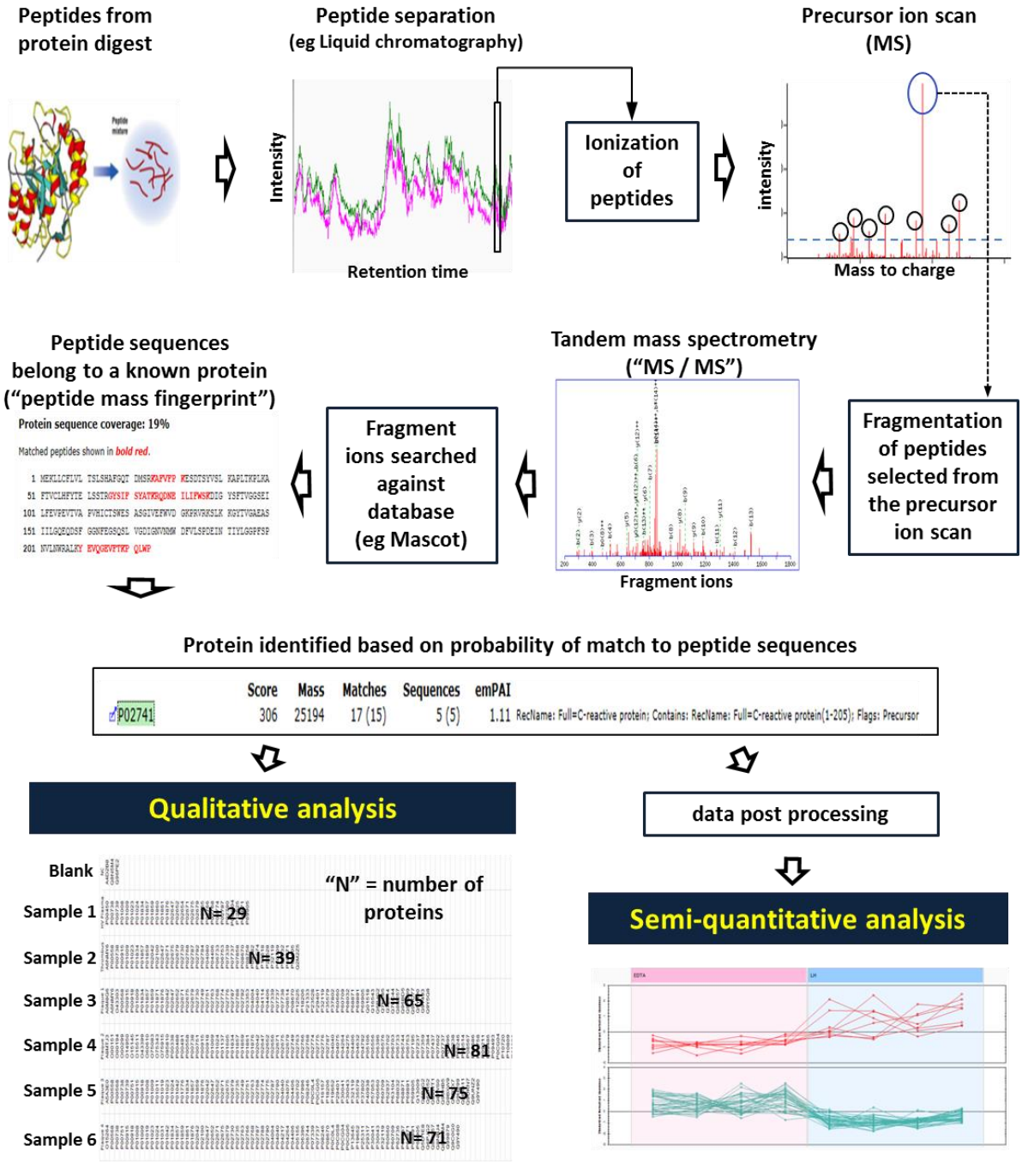


Figure 39: Overview of an untargeted "shotgun" proteomics workflow

5.1.2 Dynamic range of human proteome and its implications for shot gun proteomics

Human plasma is one of the most complex biological samples in terms of protein composition. In addition to classical soluble proteins, plasma also contains tissue "leakage" proteins such as troponin and prostate specific antigen. The dynamic range of plasma proteome in terms of protein concentration can span more than 10 orders of magnitude, ranging from the most abundant proteins such as albumin, which exhibits concentration in the mg/ml range, to low abundant proteins such as interleukins and cytokines, that have concentrations in the pg/ml range (Figure 40-A).(148)

This presents particular challenges for shotgun proteomic analysis of plasma, as the more abundant proteins will result in higher abundance of tryptic peptides. The most abundant ions will attract proportionally more charges during electrospray ionisation, making it less likely for low level peptides to get ionised – a phenomenon referred to as *ionic suppression*. At the precursor ion scan stage, these peptides in higher abundance are likely to be preferentially selected for subsequent tandem MS leading to *under-sampling* of the low abundance peptide sequences (Figure 40-B). Under-sampling can also result from the inability of a given mass spectrometer to select all precursor ions because of sample complexity. Specific strategies are needed to improve coverage across the dynamic range in a given shotgun proteomics experiment. Some of these will be discussed in the following section.

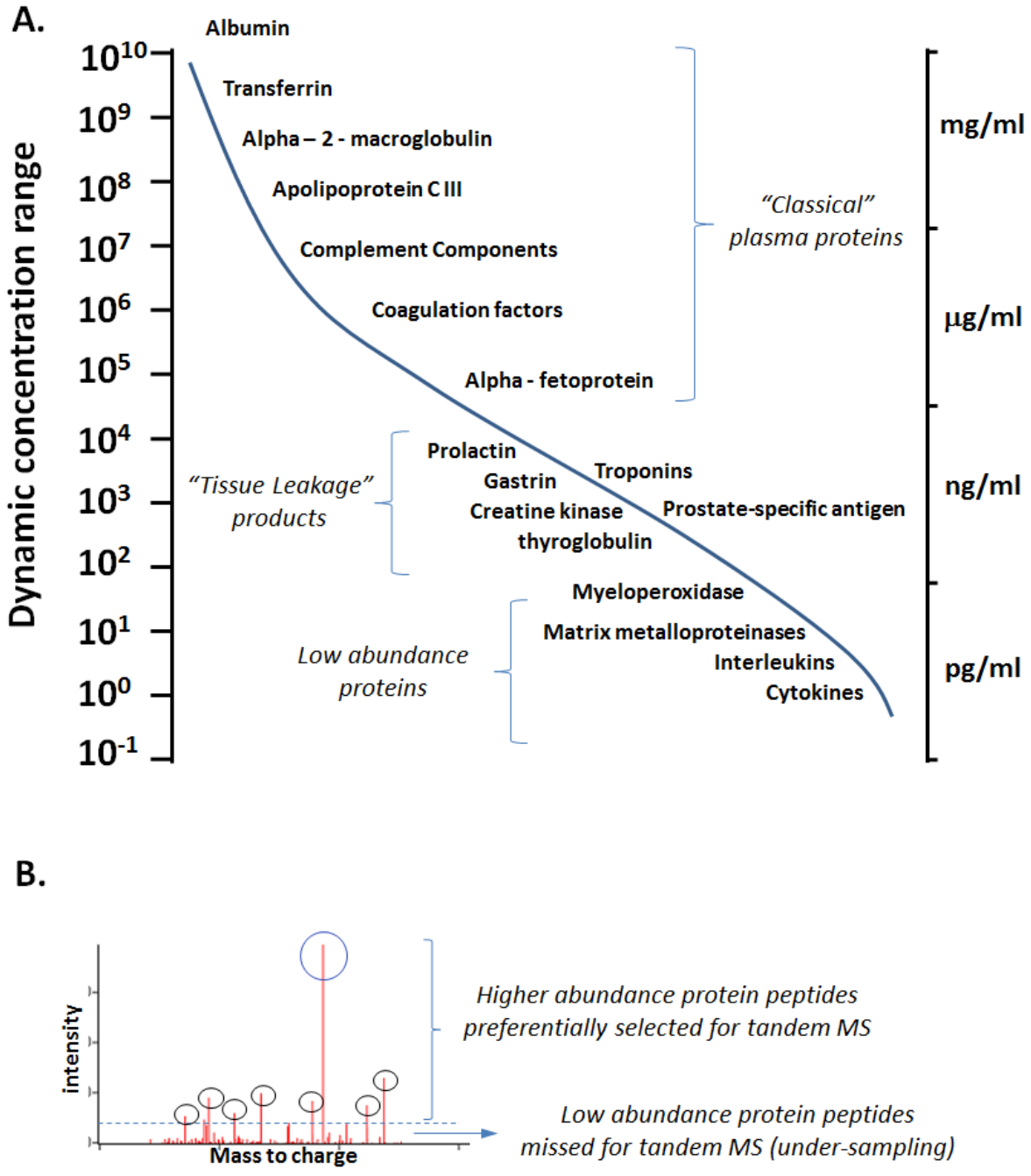


Figure 40: The wide dynamic range of human plasma proteome, predisposing under sampling of low abundance protein peptides by shotgun proteomics

5.1.3 Strategies for improving coverage for plasma proteomics analysis

In broad terms, improvement of protein coverage in proteomics analysis can be achieved by: (a) depletion of proteins of little biological relevance to the scientific question; (b) separation of protein / peptides into smaller fractions; (c) increase detection / sensitivity at the mass spectrometer; (d) improved post processing parameters. Several methods that have been optimised by Dr Kessler's group were utilised in this thesis .

Briefly, the plasma samples were depleted of the two most abundant plasma proteins (albumin and IgG) prior to tryptic digest (to address point "a"). At the liquid chromatography step, an optimised long separation gradient (2 hours) was performed. This meant fewer peptides were eluted at a given point in time, therefore the resultant eluent contained relatively fewer peptides to be analysed as compared to a shorter separation gradient (to address point "b"). The samples were analysed in duplicates, with separate mass range included for subsequent tandem MS analysis in each analysis which were then combined. This improved the chances of lower abundant peptides being selected for MS/MS (to address point "C"). The latter two strategies are further illustrated in Figure 41.

At the post processing stage, the Progenesis LC-MS^{TM} software has several built in feature to improve detection. One specific example was to apply the identified peptide data from samples (which have higher abundance of such peptide/proteins) to all samples within the experiment (some of which may have lower abundance of such peptide/proteins, and therefore missed MS/MS due to ionic suppression or under-sampling).

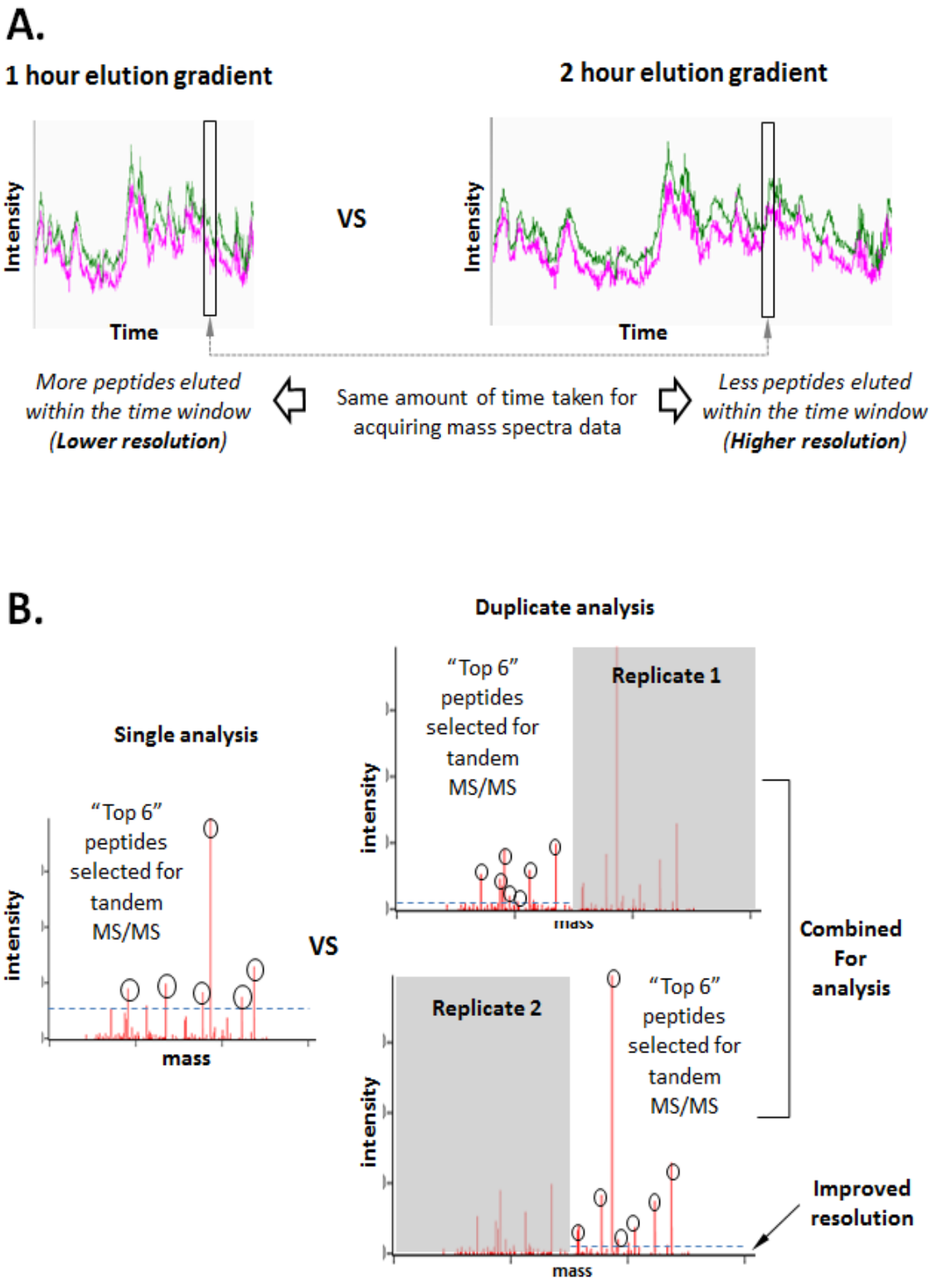


Figure 41: Two strategies utilised in this thesis for improving protein peptide coverage for shotgun proteomics analysis

5.1.4 Pathways and integrated -omics analysis

In addition to semi-quantitative comparison between samples to determine a list of proteins that are significantly changed at 5 minutes, the complete protein dataset was analysed using Ingeunity Pathway Analysis (IPA) (Ingenuity® Systems, Redwood City, USA, www.ingenuity.com) to ascertain the canonical pathways most implicated by this dataset. Briefly, IPA compares the number of proteins observed in the dataset, and maps them to the existing knowledgebase of curated canonical pathways. Based on the number of proteins in the dataset that are known to participate in a particular pathway, and the total number proteins that are known to be associated with the pathway in the Reference Dataset (i.e. the IPA Knowledge Base), IPA determines the likelihood that the association between the proteins in the experiment to a given pathway is due to random chance, and assigns a significance value using a right-tailed Fisher exact test. Using this approach, the most significantly represented canonical pathways can be selected for further examination.

Data from the proteomics analysis can be utilised to help further interrogations of the small molecular screen performed in the previous chapter. After the acute release of substances from the disrupted plaque, other acute changes in the plasma molecular profile may be due to the downstream effects mediated by the acutely released proteins, which leads to acute activation of enzymatic pathways; alternatively, the acutely released proteins can lead to activation of receptor mediated mechanisms, leading to downstream release of small molecules. Using the identified proteins as a guide, it may be feasible to direct further investigations of the small molecules by way of their association in a known biological pathway implicated by the protein data (Figure 42). This approach of inferring identity of the unknown small molecules by using the experimental data of known biological pathway involvements in the samples is a novel strategy for integration of different plasma –omic fraction analysis, and has been discussed in the previous chapter.

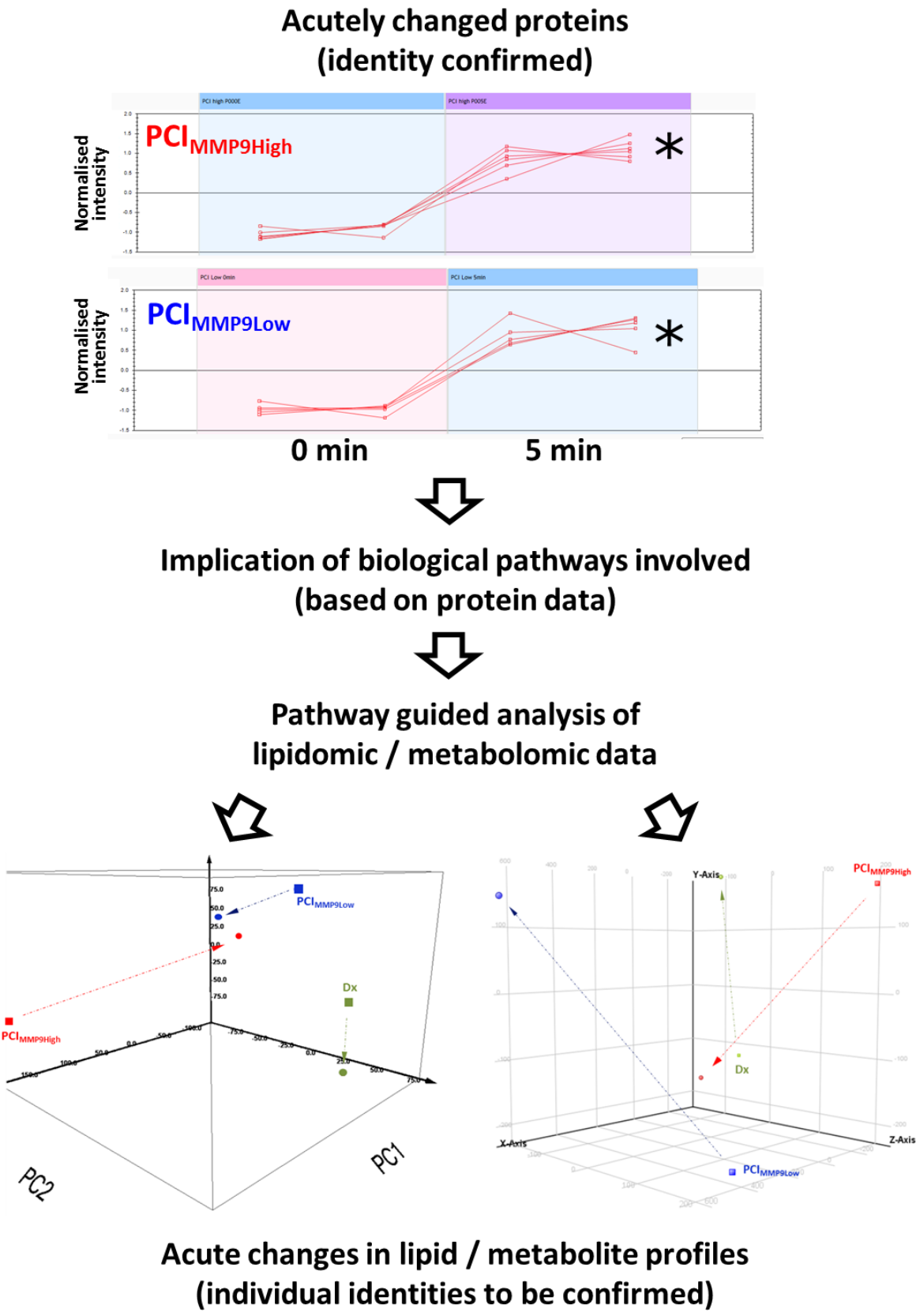


Figure 42: The concept of inferential pathway analysis

5.2 Hypotheses and Aims

The aim of this chapter was to assess the feasibility of plasma proteome characterisation in the model of stenting induced plaque disruption using a shotgun proteomics approach.

Specifically, I hypothesised that:

- Plaque rupture would lead to acute release of plaque protein contents
- The acutely released proteins could be detected in plasma samples by shotgun proteomics analysis
- For a protein to be acutely liberated *in situ* from the plaque, it should be present in the plaque material
- It should be feasible to integrate the protein and small molecules data using a pathway analysis approach

5.3 Methods

5.3.1 Samples analysed

The clinical samples used for this analysis were the same as those analysed in the small molecules screen. For technical validation of the individual protein targets selected by the analysis algorithm described in Section 3.6.15, the protein levels in *individua*l patients were measured by ELISA. Demographic data of this cohort was presented in Table 4.

5.3.3 Extraction of protein fraction from plaque debris samples

Extraction of protein fraction from plaque debris sample was performed using the same protocol as previously described in Section 4.3.4 Extraction of lipid and metabolite fractions from FW and FW INC samplesand Figure 32. The protein pellet retrieved at the end of the extraction procedure was subjected to in-solution trypsin digest as described in the later Section 5.3.5

5.3.4 Extraction of protein fraction from plasma samples

Depletion of the two most abundant plasma proteins, albumin and IgG was perfomed in the plasma samples, using a protocol optimised by Dr Roman Fischer at the CCMP.(149) Briefly, plasma aliquots were first centrifuged at 16000g for 15min at RT to separate lipid layers. A fine pipette tip was used to aspirate 50µl from the middle layer of plasma. IgG depletion was performed by precipitation using agarose beads (Thermo Scientific ID# 20398). The beads were prewashed (1:2 volume) with 0.15mM NaCl (1:2 volume) to remove ethanol, then reconstituted with 0.15mM NaCl (1:1.5 volume). The reconstituted bead (150µL), 50µL of delipidated plasma, and 100µL of 0.15mM NaCl were transferred to a mini spin column (Costar 8161 Spin-X) and mixed thoroughly by a rotating mixer at RT for 1hr.

Subsequent steps for albumin depletion were performed in the cold room at 4°C. Plasma diluent (200µL) from the above step were transferred to a new Eppendorf tube and allowed to equilibrate to 4°C by gentle mixing on a rotating mixer for 1hr. To the 200µL of chilled plaque diluent, 158.5µL of 95% ethanol were added to achieve a final concentration of 42% ethanol. The mixture was centrifuged at 16000g x 20min at 4°C. The supernatant fraction contained albumin which remained in solution after the above procedures and was removed. The residual pellet was washed using 42% ethanol to remove any residual water, and centrifuged again at 16000g x 20min at 4°C. The pellet, containing albumin depleted protein fraction, was retrieved for the subsequent in-solution trypsin digest as described in the following section.

5.3.5 In-solution trypsin digest for protein

The protein pellets were processed to obtain peptide fragments using the protocol established in CCMP. Briefly, 50µl of 6M urea was added to protein pellets retrieved. This was vortexed

and sonificated for 2 minutes. Dithiothreitol (DTT, 2.5μL, Sigma Aldrich) was added to the solution and incubated at RT for 30 minutes. Next, iodoacetamide (10μL, Sigma Aldrich) was added and the solution incubated in dark for 30 minutes at RT. Further 10μL of dithiothretiol was added to deactivate iodoacetamide, and the mixture was incubated at RT for 30 minutes. Subsequently, 388μL of 100mM TEAB buffer (Triethylammonium bicarbonate, Fluka analytical) was added as a base buffer. Trypsin (Promega, sequencing grade, Ref V5113) was diluted 1:50 and added to the solution. The final mixture was incubated overnight at 37°C in a shaker at 600rpm.

5.3.6 Desalting and purification of peptides

Buffer A (0.1% trifluoroacetic acid) and buffer B (0.1% trifluroacetic acid with 65% acetonitrile) were prepared for the desalting step. The trypsin digested samples from section were sonicated for 1 minute, and centrifuged at 16000g x 5min to precipitate non-peptide debris. The SEP-PAK C18 columns (Thermo Scientific SOLA tube SPH-300-010Q) were conditioned sequentially using Buffer B and Buffer A (1ml each). The solution containing peptides were loaded to the column in equal volume of Buffer A (500ul each). The column was then washed with 1ml of Buffer A. The peptides were eluted from the column with 300μL of Buffer B. The eluent was vacuum dried and stored in -80°C until analysis.

5.3.7 Data acquisition for shot gun proteomics by LC MS/MS

(*This was kindly performed by Dr Roman Fischer, CCMP, University of Oxford*.) The desalted tryptic peptides were re-suspended in 10μL of formic acid for LC MS/MS analysis. Each sample (0.5μL) was separated on a nanoflow reverse phase LC system (Nano Acquity, Waters) and eluted with a 2 hours linear gradient (from 3% acetonitrile plus 0.1% formic acid to 40% acetonitrile) at a flow rate of 250nl/min. The column (C18 BEH, 75μm internal diameter x 25cm length, 1.7μm particle size) was coupled to an electrospray ionisation source

in positive mode. Spectra were collected from an ion trap mass analyser (LTQ-orbitrap Velos, Thermo Fisher Scientific). Technical duplicates were obtained from full ion scans acquired in two different m/z ranges (300-609 and 609-2000). MS/MS was performed on the top 20 ions in each MS scan using the data-dependent acquisition mode with dynamic exclusion enabled. Fragmentation was recorded in collision induced dissociation mode in the iontrap at the collision energy of 35V with resolution 15000 at M/Z 400. The precursor ion full scan and subsequent MS/MS spectra were acquired at a resolution of 60000 profile mode and 7500 centroid mode, respectively. Poly-dimethylcyclosiloxane (m/z = 445.120025), generated in the ESI process from ambient air, was used the reference mass for real time internal calibration throughout the experimental workflow. MS/MS spectra were extracted from raw files and converted to MGF-format peak lists by Proteo Wizard (Version 2.1.0).

5.3.8 Data analysis

5.3.8.1 Qualitative analysis

For qualitative analysis, MS/MS peak lists from the two technical replicates were first merged and searched against the human database (Uniprot/Swissprot, Release 2012.09.07, 20,306 protein entries) using Mascot search engine (http://www.matrixscience.com/, version 2.4.0). Carboxyamido-methylation of cysteine was chosen as a fixed modification. Oxidation of methionine and deamination of asparagine or glutamine were allowed as variable modifications. One missed cleavage and 10ppm/0.5Da mass deviation were allowed in MS and MS/MS. The same search was also performed against a decoy database in which the peptide sequences for each protein were randomised. FDRs of MS/MS peptide identification were calculated by the comparing the total number of spectra matched to the Uniprot_Swissprot database against the number spectra matched to the decoy database. FDR for the peptide identification was defined by: FDR=decoy matches/(decoy matches+database matches). Only proteins with a protein score of >20 were accepted in the Mascot analysis.

5.3.8.2 Semi-quantitative analysis for proteins

For label-free protein quantitation, raw data were first imported to Progenesis LC-MS^{TM} and processed through the default workflow. The data files between samples were first aligned by allowing a retention window of 0.05min. A maximum charge of 5 was allowed for automated mass peak extraction. The selected peptide peaks were exported using default settings (200 most intense MS/MS peaks, no de-convolution or de-isotoping). These were searched against the human database as described in the previous section. Mascot generated protein identification lists were re-imported into Progenesis LC-MS^{TM} for statistical analysis, using the routine work flow (Figure 44).

Proteins were grouped and only protein features which were identified by 2 or more tryptic peptides were included for identification. For unbiased exploratory data analysis of individual experiments, PCA was performed using the identified proteins as the observed variables. For the assessment of technical reproducibility between samples, technical replicates were individually included in the corresponding PCA; for the assessment of biological variation between sample groups, the averaged intensity values for the sample replicates were included in the corresponding PCA. Statistical comparisons were made in the following experimental groups: FW vs FW INC samples, $CONTROL_{Dx}$ (0min vs 5min), $PCI_{MMP9Low}$ (0min vs 5min), $PCI_{MMP9High}$ (0min vs 5min). P values for comparison were calculated by the Progenesis LC-M^{TM} software, were based on paired t-tests (two sample ANOVA), and the value of <0.05 was considered the cut-off point for selection of a putative protein feature for further examination.

FDR of the protein identification was further performed by uploading the converted MGF files to the Central Proteomics Facilities Pipeline (CPFP, version 1.3.0), which combined the searches against the human databases using three different search engines (Mascot, OMSSA,

and X!TANDEM k-score).(150) The FDR for each protein was cross referenced between CPFP output file and Progenesis LC-MS^{TM} data. Of these proteins which had a P value less than 0.05, only those which fulfilled a FDR of less than 1% according to Central proteomics Facilities Pipeline analysis were considered for the final protein target selection. Proteins which were significantly changed in the $CONTROL_{Dx}$ group (at 5 minutes aginst baseline) were excluded from subsequent analysis.

5.3.8.3 Pathway analysis by Ingenuity Systems Pathways Analysis (IPA)

Two approaches were used for IPA. Firstly, protein features which significantly changed at 5 minutes after plaque disruption (in either the $PCI_{MMP9High}$ or $PCI_{MMP9Low}$ group) were individually searched against the Ingenuity Pathway Analysis Knowledge Base for their known implications in curated canonical pathways. In addition, the complete protein dataset for the individual experimental groups were further exported from Progenesis LC-MS^{TM} in .xls format. These were uploaded to IPA for identification of protein compartment localisation (for FW and FW INC samples) and pathway analysis (for plasma samples), using the standard IPA workflow. For each dataset, the following values were assigned as an observation in IPA: protein accession number, Anova p-value, fold change at 5 minutes (compared to 0 minutes). Canonical pathways implicated by the plasma proteins in the sample groups were assessed using the over-representation technique in IPA. This analysis provided the significance p-value based on likelihood of representation and the percentage representation of proteins detected in the dataset. Benjamini Hochberg correction for multiple testing was applied to the p values.

5.3.9 Technical validation of putative protein targets

Technical validation of the putative protein targets were attempted by measuring the protein level in the individual samples, using commercially available ELISA kits. The ELISA procedures were performed according to manufacturer's protocols.

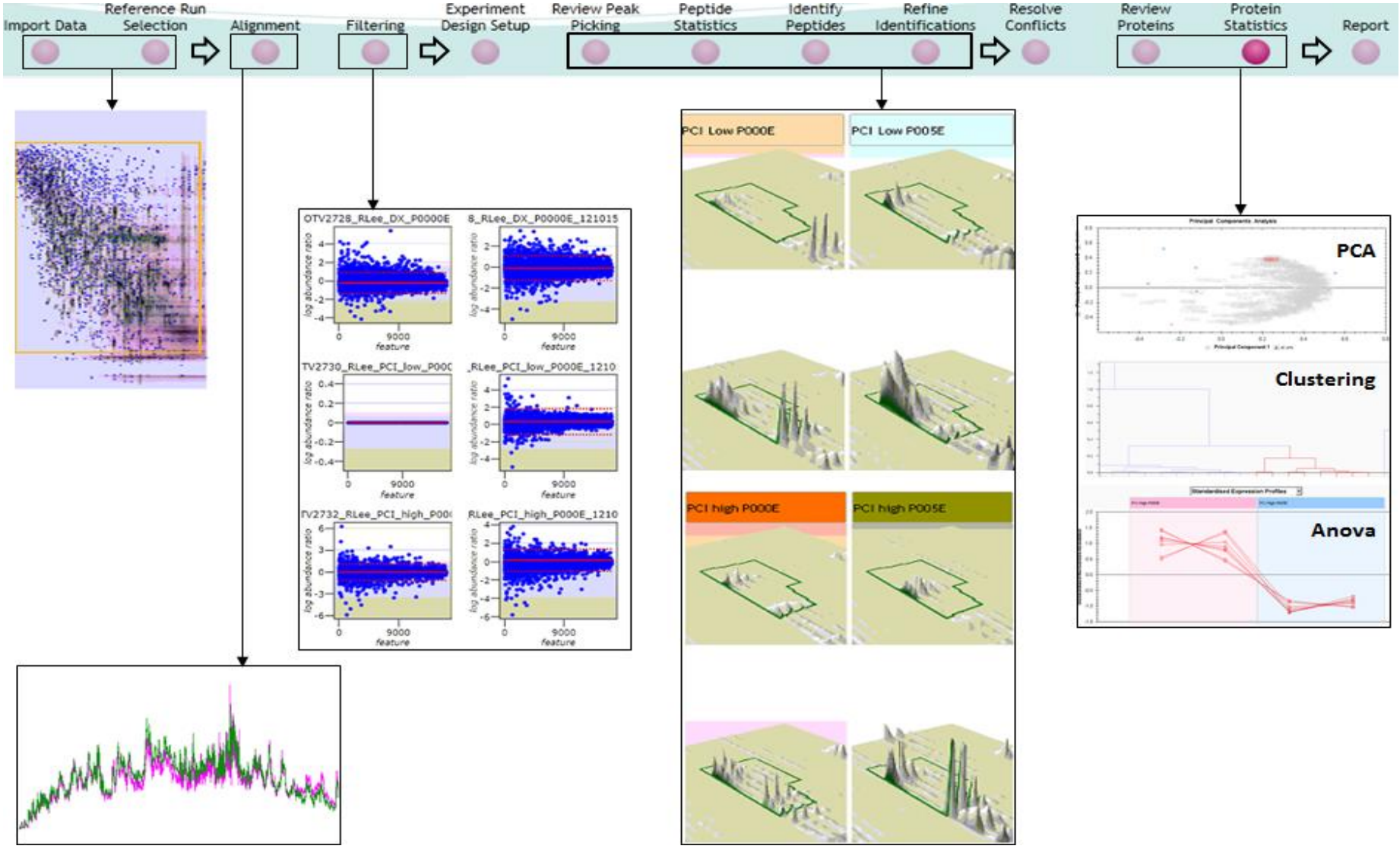


Figure 43: The Progenesis LC-MS™ workflow

5.4 Results

5.4.1 Proteomics profile of samples analysed - qualitative analysis

The number of proteins identified by Mascot search for each sample is summarised in Figure 45. When the Mascot search was performed using individual sample's raw data, more proteins were identified from the plaque debris samples as compared to plasma samples. Over 1,000 proteins were identified for each of the plaque debris samples (FW 1, n=1016; FW 2, n=1175). However, a number of proteins were also detected in the paired incubated control samples (FW INC 1, n=509; FW INC 2, n=410). Alpha- and Beta-actin are examples of two ubiquitous cellular protein (Uniprot accession number P68133 and P60709) which were detected in all FW and FW INC samples (Figure 45, black and red bars), but were not detected in any of the plasma. Despite the common presence of these proteins, different abundances of the actin protein peptides were detected in individual samples, resulting to their different emPAI scores (Figure 45-blue boxes). Calponin (accession number P99439, Figure 44 - blue bars), an actin binding protein and a marker of smooth muscle cells, was detected in both FW1 and FW2 samples, but also present in one of the FW controls (FW INC-1).

Despite the plasma albumin and IgG depletion step described in section, albumin (Figure 44 - orange bars) was still detected in all samples, while CRP (accession number P02741, Figure 44 - green bars) was one of the proteins detected in only patients who underwent PCI induced plaque disruption, but not in the plasma of HVs or patients who underwent diagnostic angiography only. Interestingly, MMP9 (accession number P14780, Figure 44 - purple bars) was detected in the FW and FW INC samples, but not in the plasma samples according to the Mascot search.

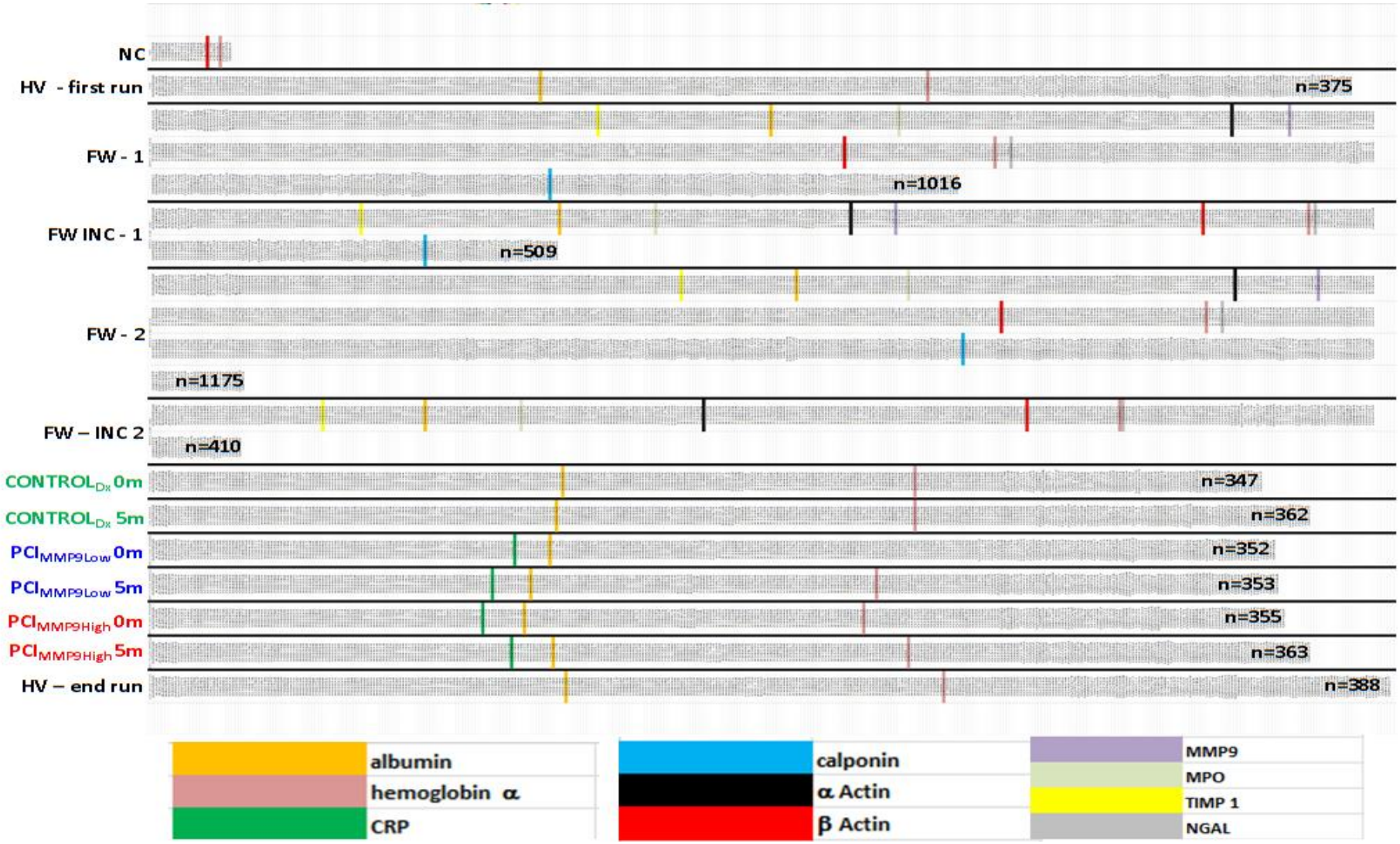


Figure 44: Qualitative proteomics profile of samples analysed during the *discovery phase*

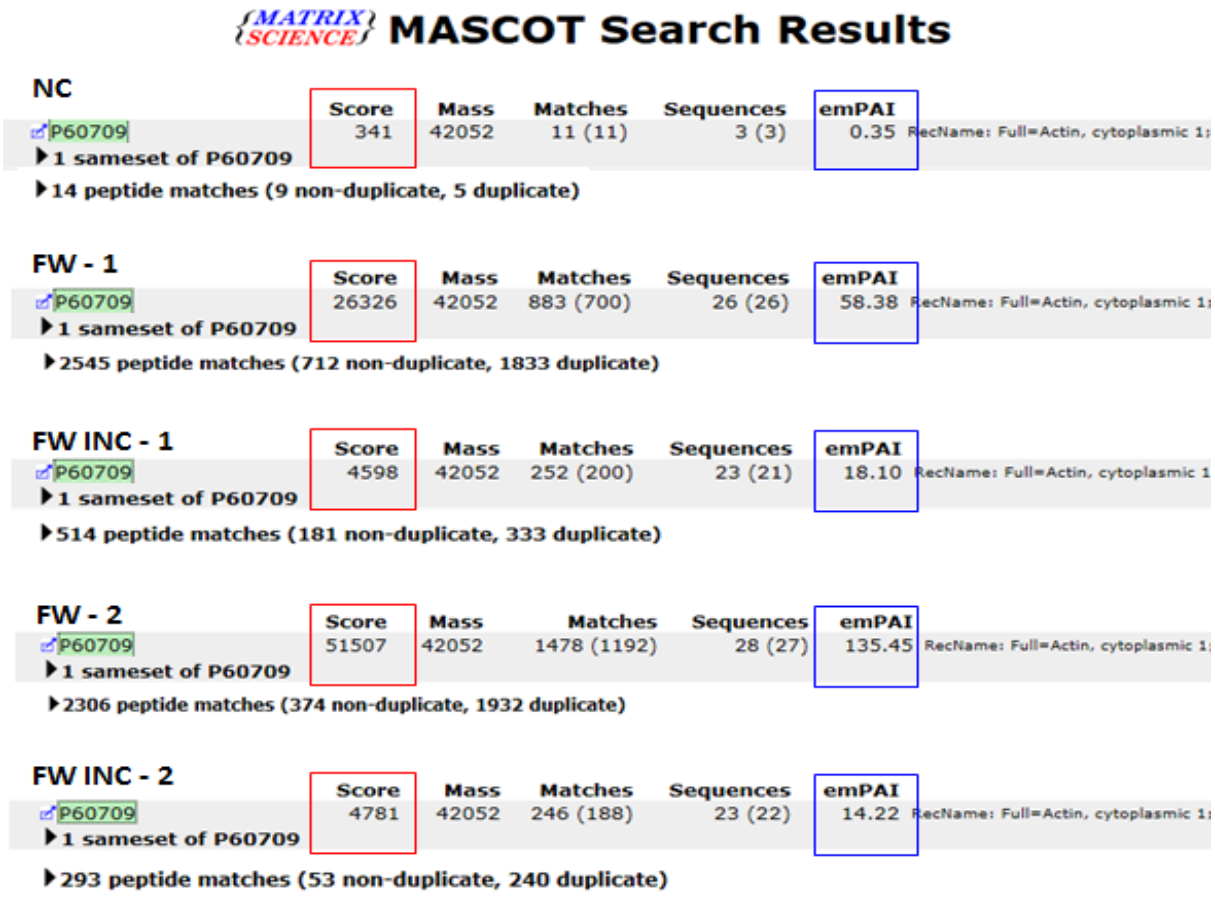


Figure 45: emPAI scores for individual samples highlight one limitation of qualitative proteomic analysis in a shotgun proteomics design

5.4.2 Proteomics profiles – semi quantitative analysis

Following the Progenesis LC-MS^{TM} workflow described in Figure 43, a total of 22836 out of 31357 spectra could be matched to the Uniprot_Swissprot human database using a significance threshold of P<0.05. Of these, 911 decoy hits were identified indicating a FDR of 3.99% at the level of peptide identification. Mascot protein identifications were grouped into 679 proteins based on the highest scoring protein in each group.

The pooled HV sample was analysed as technical replicates both at the beginning and at the end of the mass spectrometry acquisition work flow as quality control, in addition to the lock mass (Poly-dimethylcyclosiloxane) analysed for real time calibration. PCA scores plot of the proteins detected in the experimental group containing quadruplicate HV samples, duplicate FW samples and duplicate FW INC samples showed close clustering of the technical replicates, indicating technical reproducibility between mass spectra acquisitions. There were also clear separations between the plasma and non-plasma samples, and between the FW and FW INC samples (Figure 46).

5.4.2.1 Analysis of plaque debris

Based on the analysis by Progenesis LC-MS^{TM}, as described in Section 5.3.8.2, significantly higher abundance (denoted by a p-value of less than 0.05 compared to the FW INC controls) of 423 proteins were observed in the plaque debris samples. These proteins were considered to be plaque specific. Using IPA, these proteins were assigned to the following cellular compartments: nucleus (n=17), cytoplasmic (n=191), cellular membrane (n=58) or extracellular space (n=135). The residual 15 proteins could not be assigned by IPA. MPO, MMP9, TIMP1, NGAL were amongst the proteins present in the plaque debris (for a complete list of the proteins present in plaque debris, refer to Appendix Table 1).

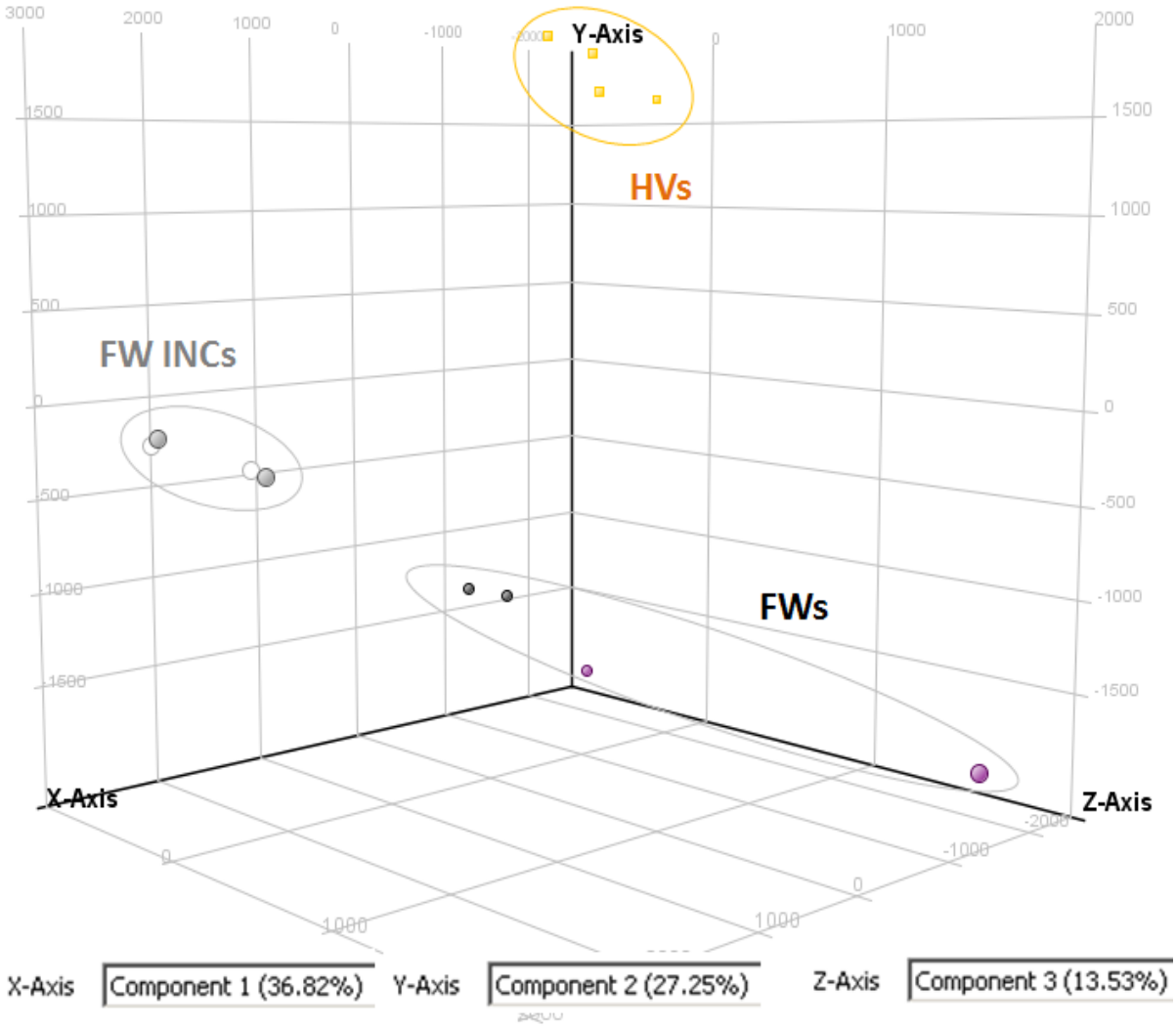


Figure 46: Proteomic profiles differ between plaque debris and plasma

5.4.2.2 Analysis of plasma

5.4.2.2.1 CAD vs HV

All patients included in the discovery set had established coronary atherosclerosis. Therefore the baseline plasma samples from all CAD subjects (n=30) represents a heterogeneous group of CAD patients. Comparison between CAD and HV was performed as an assessment of the internal validity of this analysis. In this dataset 17 proteins were significantly higher in the CAD patients; while 10 proteins were significantly higher in HVs compared to CAD patients. CRP was amongst the proteins that are significantly higher in CAD patients, while the level of apolipoprotein A2 was higher in HVs. These are listed in Table 5.

5.4.2.2.2 Plasma protein after plaque disruption

PCA of plasma samples was performed using the averaged value observed in the technical replicates. This demonstrated separation of the samples between baseline (0min) and 5min in both the plaque disruption groups ($PCI_{MMP9High}$, $PCI_{MMP9Low}$) and the $CONTROL_{Dx}$ group. However the separations within the plaque disruption groups were wider than the control group, indicating greater differences observed between plasma after plaque disruption compared to baseline (Figure 47). After exclusion of the proteins which showed acute changes in the $CONTROL_{Dx}$ group, 13 proteins showed significant changes at 5 minutes after plaque disruption in the $PCI_{MMP9High\ group}$ (Table 6) while 11 proteins showed significant changes in the $PCI_{MMP9Low}$ group (Table 7). Of these proteins, 6 were acutely increased in the $PCI_{MMP9High}$ group and 5 in the $PCI_{MMP9Low}$ group. Amongst the proteins which were acutely elevated in the plaque disruption groups, lipopolysaccharide binding protein (LBP), cytochrome B5 reductase 3 (CYB5R3), tight junction protein 2 (TJP2), and chloride intracellular channel protein 4 (CLIC4) were also significantly enriched in the plaque debris samples as compared to the incubated controls (Table 6 and 7).

significantly higher in Healthy Volunteers				
Uniprot Accession Number	**Peptide count**	**Anova (p value)**	**Max fold change**	**Description**
O14791	16	0.022	1.55	Apolipoprotein L1
O60610	13	0.027	1.65	Protein diaphanous homolog 1
O95445	3	0.020	1.92	Apolipoprotein M
P01814	2	0.046	1.91	Ig heavy chain V-II region OU
P02652	8	0.049	1.46	Apolipoprotein A-II
P02765	9	0.044	1.52	Alpha-2-HS-glycoprotein
P09493	13	0.049	2.53	Tropomyosin alpha-1 chain
P09496	2	0.002	16.29	Clathrin light chain A
P47756	7	0.026	1.76	F-actin-capping protein subunit beta
Q9NZN3	11	0.021	1.31	EH domain-containing protein 3

significantly higher in CAD patients				
Uniprot Accession Number	**Peptide count**	**Anova (p value)**	**Max fold change**	**Description**
P02741	6	0.035	7.10	C-reactive protein
P02747	4	0.038	1.61	Complement C1q subcomponent subunit C
P02749	22	0.034	1.65	Beta-2-glycoprotein 1
P02750	12	0.019	1.91	Leucine-rich alpha-2-glycoprotein
P02774	39	0.018	1.93	Vitamin D-binding protein
P08519	10	1E-04	6.59	Apolipoprotein(a)
P11678	6	0.004	Infinity	Eosinophil peroxidase
P18428	6	0.019	2.81	Lipopolysaccharide-binding protein
P20742	28	0.001	4.29	Pregnancy zone protein
P23229	5	0.016	2.63	Integrin alpha-6
P29401	6	0.049	1.53	Transketolase
P36980	9	0.001	3.94	Complement factor H-related protein 2
P40121	2	0.037	4.63	Macrophage-capping protein
Q02985	3	0.006	3.21	Complement factor H-related protein 3
Q03591	19	0.026	2.90	Complement factor H-related protein 1
Q06033	22	0.017	1.41	Inter-alpha-trypsin inhibitor heavy chain H3
Q96C24	4	0.046	1.49	Synaptotagmin-like protein 4

Table 5: List of proteins which differed between the healthy volunteers and the CAD patients of the discovery subject subset

Pooled plasma were prepared from the HVs and CAD patients as described in section 4.3.2. Plasma collected at baseline for CAD patients (consisting of $PCI_{MMP9High}$, $PCI_{MMP9Low}$, and $CONTROL_{Dx}$, n=30 in total), were further combined for comparison against the HV pooled plasma (n=10). Proteomics data were acquired and analysed according to Section 5.3. Proteins were sorted alphanumerically according to the Uniprot database accession number.

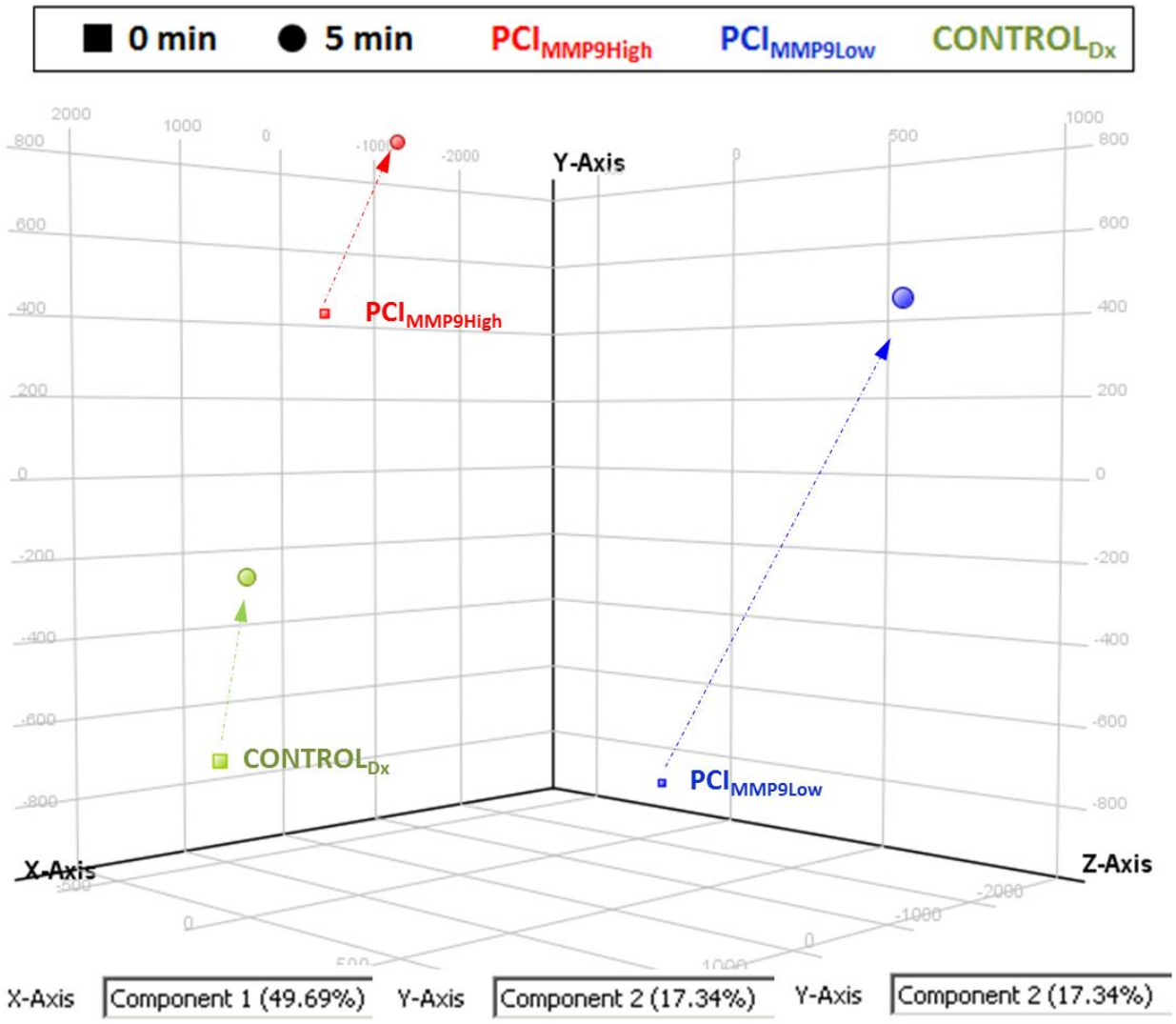


Figure 47: Rapid changes in the global proteomic profile are observed after plaque disruption

5.4.3 Ingenuity pathway analysis

In the first step of IPA, each of the significantly changed proteins in both the $PCI_{MMP9High}$ (n=13) and $PCI_{MMP9Low}$ (n=11) group was manually searched against the IPA Knowledge Base to ascertain its involvement in curated canonical pathways. In addition, the overall dataset for plasma proteins in the PCI groups was analysed using the standard IPA workflow. Canonical pathways which were flagged up by both of these analyses were subjected to further examination. To further minimise the likelihood of random observation, the additional criteria of $P<0.0001$ [i.e. $-\text{Log}(\text{P value}) \geq 4$] and percentage representation greater than 20% were applied. Based on this approach, two pathways were highlighted: LXR/RXR activation [-Log(P value) = 4.2, 36% representation] and acute phase response signalling pathway [-Log(P value) = 4.1, 30% representation]. Importantly, three of the significantly changed proteins [HPX, A1BG ($PCI_{MMP9Low}$) and LBP ($PCI_{MMP9High}$)] 5 minutes after plaque disruption were all part of the LXR/RXR pathway. These are summarised in Table 6 and 8.[l]

PCAs of proteins specific to canonical pathways (which were detected in the plasma samples) revealed unique patterns in these samples (Figure 48). PCA scores plot of proteins involved with the LXR/RXR activation and acute phase response signalling pathways demonstrated a greater separation between the $PCI_{MMP9Low}$ plasma at baseline and 5 minutes after plaque disruption. Although similar extents of separation were observed between the $PCI_{MMP9High}$ and $CONTROL_{Dx}$ patients in both of these pathways, the direction of individual protein change were distinctly different. This could be illustrated by superimposing the fold change observed at 5 minutes for each protein on the LXR/RXR pathway (Figure 49-51).

[l] Due to the low number of proteins which were significantly changed at 5 minutes after plaque rupture, network analysis by IPA was considered inappropriate and therefore not performed.

Plasma proteins significantly changed at 5 minutes after plaque disruption in the $PCI_{MMP9High}$ group

Individual protein data							Representation of the canonical pathway by overall proteins detected in $PCI_{MMP9High}$ group	
Uniprot accession number	Protein name	Increase or decrease	Maximum fold change	ANOVA P value	Protein present in FW?	Canonical Pathway Implicated	-Log [P value]	percentage representation
P18428	LBP	Increase	1.75	0.0159	Yes	LXR/RXR activation	4.2	36.00%
						Acute phase response Signaling	4.1	30.00%
						Hepatic fibrosis / stellate cell activation	2.69	8.22%
						Actin cytoskeleton signalling	1.5	14.00%
						LPS/IL 1 mediated inhibition of RXR function	0.74	4.15%
						IL 6 signaling	0.675	4.84%
						iNOS signalling	0.32	3.85%
						IL10 signaling	0.32	3.85%
						LPS stimulated MAPK signalling	0.29	3.66%
						Toll like receptor signalling	0.18	3.23%
						Hepatic Cholestasis	0.15	2.30%
P00387	Cytochrome B5 reductase 3	Increase	3.88	0.0401	Yes	γ Lionleate biosynthesis	0.24	4.20%
						mitochondiral dysfunction	1.86	5.70%
P08758	Annexin A5	Increase	2.41	0.0143	Yes	not mapped by IPA	-	-
P63241	Eukaryotic translation intiation factors	Increase	2.28	0.0218	Yes	not mapped by IPA	-	-
O75558	Syntexin 11	Increase	3.04	0.0222	Yes	not mapped by IPA	-	-
Q9UIB8	CD84	Increase	7.18	0.0486	No	not mapped by IPA	-	-
P52566	Rho GDP dissociation inhibitor 2	Decrease	1.36	0.0187	Yes	Rho GDI signalling	8.43	11.60%
Q08380	Galectin 3 binding protein	Decrease	1.69	0.0341	Yes	not mapped by IPA	-	-
P02750	Leucine rich alpha 2 glycoprotein	Decrease	1.59	7.50E-04	Yes	not mapped by IPA	-	-
P05543	Thyroxine binding globulin	Decrease	1.13	0.0158	Yes	not mapped by IPA	-	-
P22797	Carboxypeptidase N	Decrease	1.82	0.00225	Yes	not mapped by IPA	-	-
P04220	Ig Mu heavy Chain	Decrease	1.49	0.0303	No	not mapped by IPA	-	-
P11678	Eosinophil peroxidase	Decrease	500	0.0185	No	not mapped by IPA	-	-

Table 6: List of proteins significantly changed after plaque disruption in the $PCI_{MMP9High}$ group

Plasma proteins significantly changed at 5 minutes after plaque disruption in the $PCI_{MMP9Low}$ group

Individual protein data							Representation of the canonical pathway by overall proteins detected in $PCI_{MMP9Low}$ group	
Uniprot accession number	Protein name	Increase or decrease	Maximum fold change	ANOVA P value	Protein present in FW?	Canonical Pathway Implicated	-Log [P value]	percentage representation
P02790	Hemopexin	Decrease	2.75	0.0383	Yes	LXR / RXR Activation	4.2	36.00%
						Acute phase response	4.1	30.00%
O04217	Alpha 1B glycoprotein	Decrease	2.95	0.0252	No	LXR / RXR activation	4.2	36.00%
P01859	Ig Gamma-2 chain	Decrease	2	0.0352	Yes	SLE signalling	4.09	7.60%
						Primary immunodeficienty signaling	4.09	14.50%
						Hematopoiesis from pluripotent stem cells	3.36	12.70%
						Autoimmune thyroid disease	2.1	9.80%
						Communication between innate and adaptive immune cells	1.84	7.34%
						Allograft rejection	1.55	
						Dendritic cell maturation	0.62	3.83%
						role of macrophage, fibroblasts and endothelial cells in RA	0.45	3.27%
P01617	Ig Kappa Chain V-II	Decrease	1.63	0.0363	Yes	Not mapped by IPA	-	-
P04220	Ig Mu heavy chain	Decrease	1.35	0.044	No	Not mapped by IPA	-	-
P04827	Sex hormone binding protein	Decrease	1.5	0.0477	No	Androgen signalling	1.03	4.83%

Table 7: List of proteins significantly changed after plaque disruption in the $PCI_{MMP9Low}$ group.

Plasma proteins significantly changed at 5 minutes after plaque disruption in the $PCI_{MMP9Low}$ group - Cont.

Individual protein data							Representation of the canonical pathway by overall proteins detected in $PCI_{MMP9Low}$ group	
Uniprot accession number	**Protein name**	**Increase or decrease**	**Maximum fold change**	**ANOVA P value**	**Protein present in FW?**	**Canonical Pathway Implicated**	**-Log [P value]**	**percentage representation**
Q9y696	Chloride intracellular channel protein 4	Increase	1.9	0.0063	Yes	not mapped by IPA	-	-
Q9UDY2	Tight Junction protein 2	Increase	2.86	0.012	Yes	Sertoli cell sertoli cell junction signalling	3.25	7.70%
						Tight Junction signaling	2.35	7.50%
						Hepatic cholestasis	0.15	2.30%
P47756	F- Actin capping protein	Increase	1.68	0.0255	Yes	Not mapped by IPA	-	-
P05141	ADP/ATP carrier protein	Increase	3.13	0.0103	Yes	Induction of apoptosis by HIV 1	0.17	3.10%
P04439	HLA Class 1	Increase	Infinity	0.0011	NO	Caveolar mediated endocytosis	6.94	16.50%
						Virus entry via endocytic pathways	5.93	15.00%
						CDC42 signaling	4.19	9.00%
						Neuroprotective role of the THOP1 in Alzheimer disease	4.09	14.80
						SLE signalling	4.09	7.60%
						Antigen presentation	2.62	15.00%
						Autoimmune thyroid disease	2.1	9.80%
						Communication between innate and adaptive immune cells	1.84	7.34%
						Allograft rejection	1.55	7.29%
						Protein ubiquitination pathway	1.19	4.85%
						Crosstalk between dendritic cells and natural killer cells	1	6.25%
						Dendritic cell maturation	0.62	3.83%
						cytotoxic T lymphocyte mediated apoptosis	0.48	4.65%
						Type I DM signalling	0.27	3.33%
						Graft versus host disease	0.26	4.00%
						OX40 Signaling	0.22	3.16%

Table 7: List of proteins significantly changed after plaque disruption in the $PCI_{MMP9Low}$ group – cont.

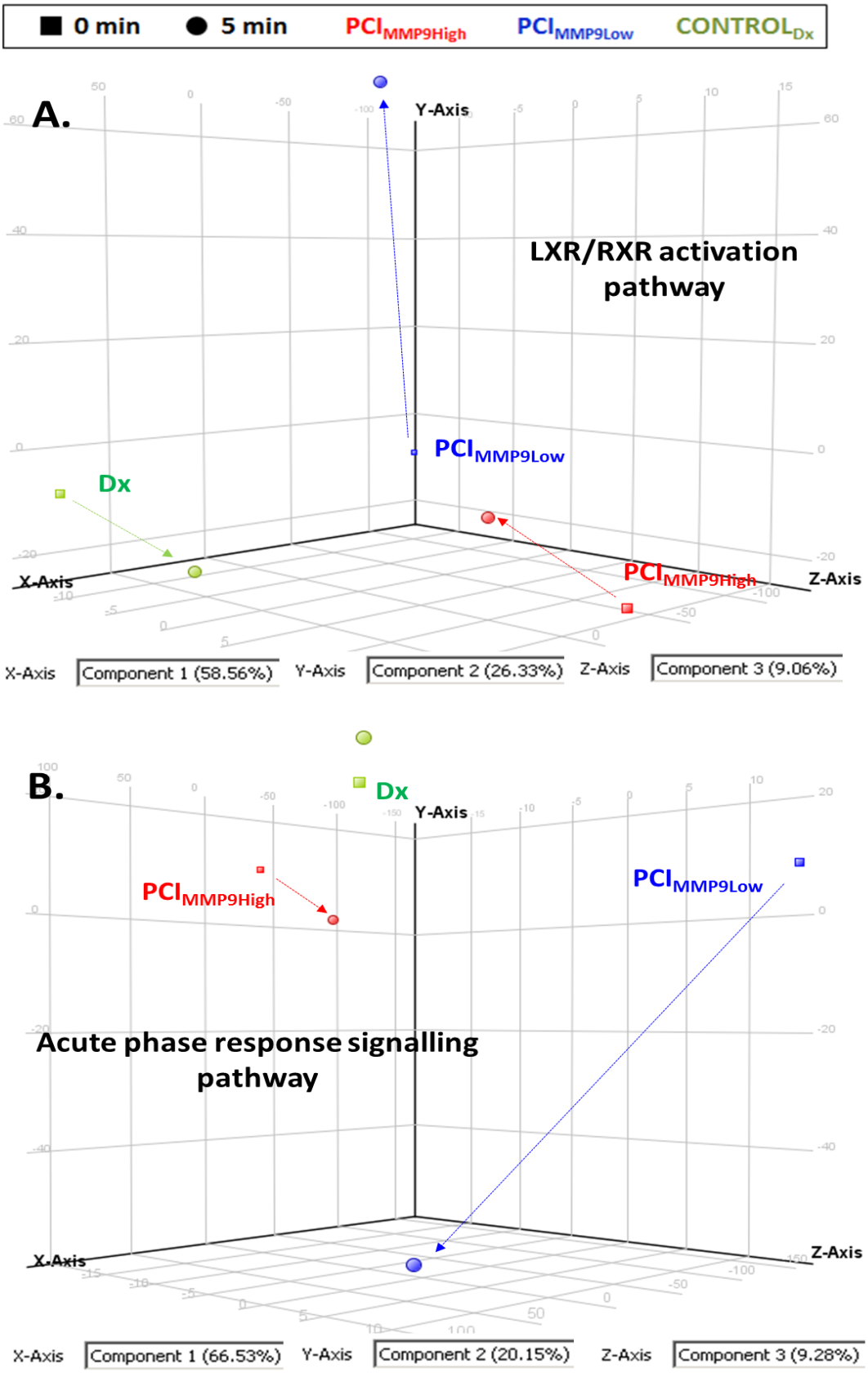


Figure 48: Rapid changes of the LXR/RXR activation and acute phase response signalling pathways for the PCI and CONTROL$_{Dx}$ samples before and after plaque disruption

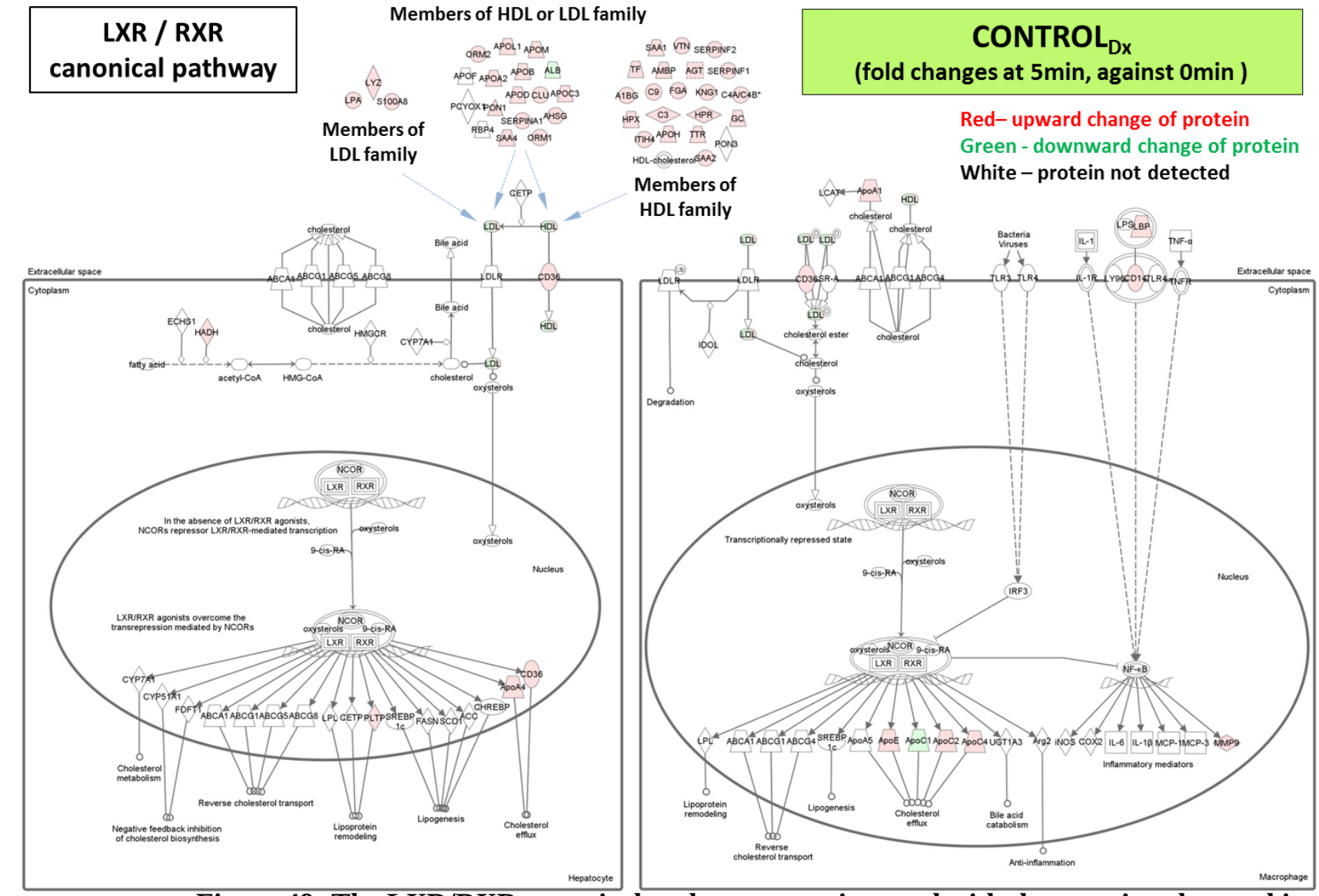
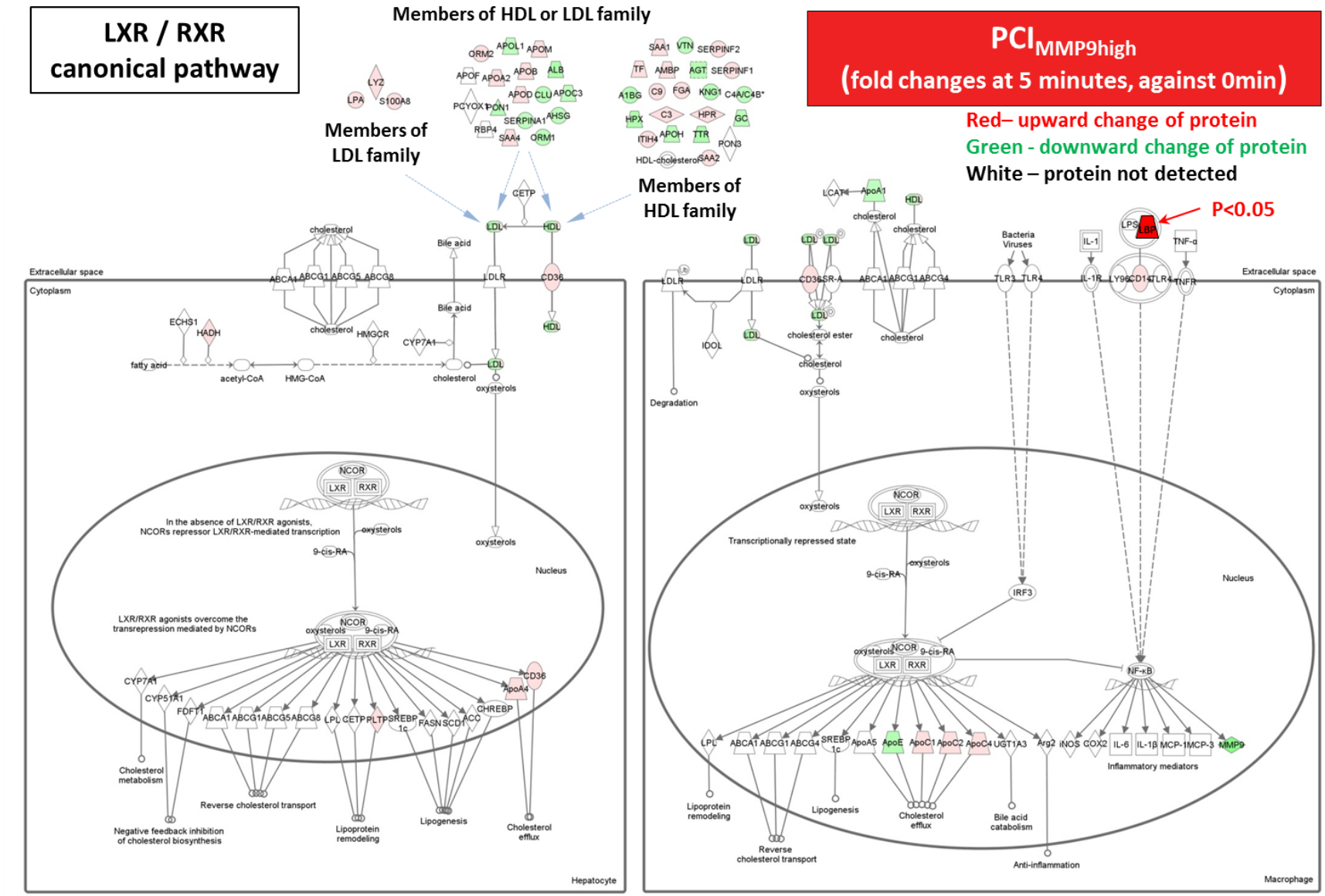
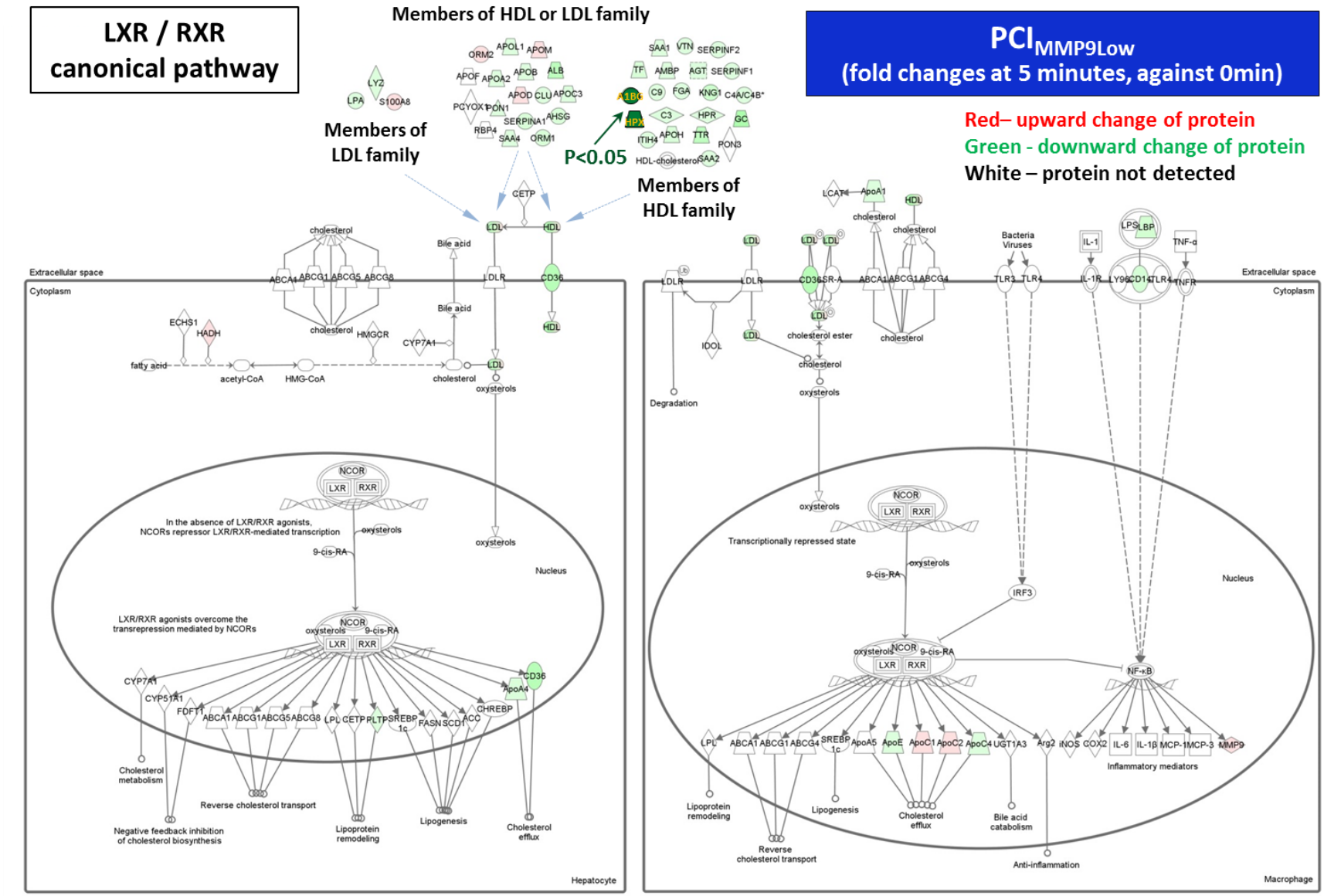


Figure 49: The LXR/RXR canonical pathway, superimposed with the proteins observed in the CONTROL$_{Dx}$ group.



© 2000-2012 Ingenuity Systems, Inc. All rights reserved.

Figure 50: The LXR/RXR canonical pathway is implicated after coronary atherosclerotic plaque disruption in the $PCI_{MMP9High}$ group



© 2000-2012 Ingenuity Systems, Inc. All rights reserved.

Figure 51: The LXR/RXR canonical pathway is implicated after coronary atherosclerotic plaque disruption in the $PCI_{MMP9Low}$ group

5.4.4 γ -Linoleate biosynthesis pathway

CYB5R3 was present in the plaque debris samples and acutely increased in plasma at 5 minutes after plaque disruption in the $PCI_{MMP9High}$ group. CYB5R3 is an enzyme which belongs to the family of linoleoyl-CoA desaturase (E.C. 1.13.19.3). This enzyme is central to the conversion between linoleoyl-CoA to γ-linolenoyl-CoA. The molecular weight for linoleoyl CoA and γ-linolenoyl-CoA are 1029.96Da and 1027.94Da, respectively. However, mass peaks matching the same molecular formula / weight were not detected in the MALDI-TOF-MS or LC-MS experiments presented in Chapter 4. (Of note, the acquisition of data was set to the mass range of 50 – 1000 m/z in the experiment described in Section 4.3.6.) However, mass peaks which matched to upstream substrates in the γ-linoleate biosynthesis pathway [linoleate (280.24 Da) and coenzyme-A (767.53 Da)] were observed in this data set (Figure 52).

5.4.5 Technical validation of protein targets by ELISA

The selection of putative target proteins for technical validation was driven by several considerations: (1) significant change in plasma ($P<0.05$ by Progenesis LC-MS^{TM} analysis) observed within 5 minutes of plaque disruption in either $PCI_{MMP9High}$ or $PCI_{MMP9Low}$ group; (2) implication of canonical pathways according to IPA analysis; (3) availability of commercial ELISA assay kits.

Based on these considerations, the following ELISA assays were purchased from Mybiosource [LBP, CYB5R3, CD84, hemopexin, alpha-1b-glycoprotein (A1BG)]. In addition, hydroxyl-acyl CoA dehydrogenase (HADH) ELISA was purchased based on its involvement in fatty acid metabolism and involvement in the LXR/RXR pathway (enzyme involved for conversion of fatty acid to acetyl CoA), although the level of change at 5 minutes did not reach statistical significance at the Progenesis LC-MS^{TM} analysis.

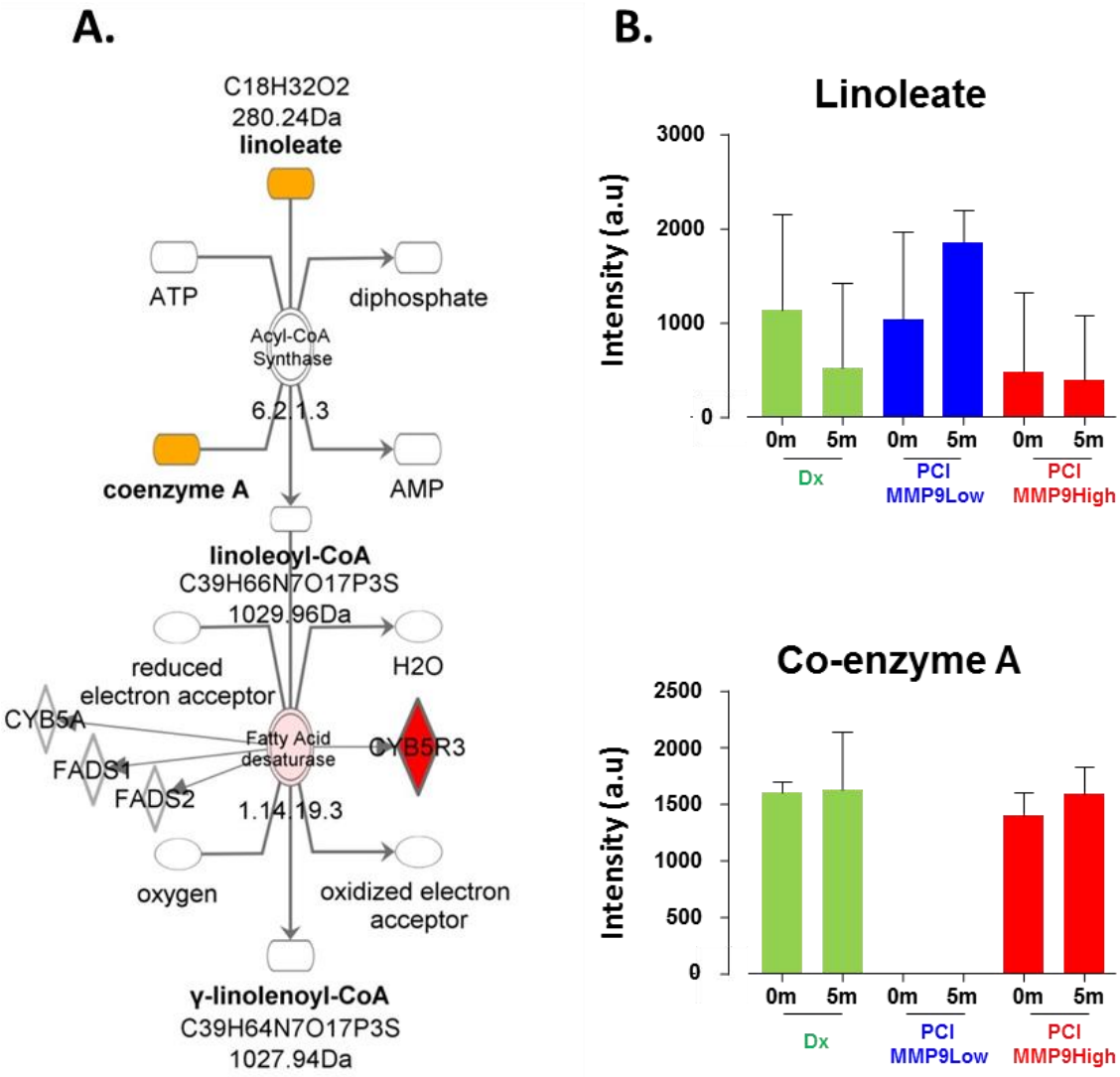


Figure 52: γ-Linoleate biosynthesis pathway may be implicated after coronary atherosclerotic plaque disruption

Although human plasma samples were listed as an acceptable sample type for measurement by each one of these assay kits, the manufacturer recommended using lithium heparin plasma for ELISA measurement. EDTA plasma was collected for this study, therefore further experiments were required to determine the optimal dilution factor for each of the analytes. For each analyte, the highest and lowest points of the standard curves were constructed using the supplied standard stocks. Serial dilutions of plasma samples were created using PBS (at 1:1, 1:2, 1:20, and 1:50). For CYB5R3, HADH, and CD84, non-linear results were observed in serially diluted samples, with progressive increases in optical density despite further plasma dilution in the first optimisation experiment (Figure 53-A). These observations prompted questions regarding the linearity of assays and whether the further dilution of the sample was required. Therefore a second experiment for each was performed.

In the second attempt, a serial dilution of the standard stock solution was performed (1:1, 1:10, 1:100, 1:200, 1:300) using PBS to constitute the standard curve. In addition, serial dilution of plasma from one representative CAD patient was performed using PBS (1:1, 1:2, 1:20, 1:50, 1:100, 1:500, 1:1000, 1:5000, 1:10000, 1:500000, 1:10000000). Further, plasma from a healthy volunteer was spiked with the standard stock solution and serial dilution performed using neat plasma from the same HV (1:20, 1:50, 1:100, 1:500, 1:1000) to test for recovery of protein. Although each of the standard curves demonstrated a linear range (Figure 53-B), serial dilutions of standard stock using HV plasma did not show linear recovery (Figure 53-C). Further, the levels of each protein was below or bordering the LLOQ for each assay regardless of the dilution factor (Figure 53-D) and did not demonstrate linearity within the dilution range tested. Based on the results, these commercially available assay kits were deemed unsuitable for measurement of human EDTA plasma samples as advertised by the manufacturers, and further measurements of plasma samples were not performed using these kits.

The same optimisation experiments demonstrated dilution linearity of analyte measurement in LBP, HPX, and A1BG. Using the recommended dilution factor (for LBP: 50ul of plasma undiluted; for HPX: plasma diluted 1:40000; for A1BG: 100ul of plasma undiluted), the observed optical densities (O.D.) were in the middle range of the standard curve. These kits were considered suitable for plasma measurement. However A1BG measurement was not performed for the individual samples, as the level of A1BG in the pooled plasma sample was close to the LLOQ for this assay and it would require 100µl (an entire aliquot) of plasma for the technical validation of one protein target. This was uneconomical use of the limited sample aliquots remaining.

The ELISA measurements of LBP and HPX from individual patient samples confirmed the same patterns as detected by the MS proteomics screen of the pooled samples. Within 5 minutes of plaque disruption there was acute, significant elevation of plasma LBP in the $PCI_{MMP9High}$ group. There were no significant changes in LBP in the $PCI_{MMP9Low}$ and $CONTROL_{Dx}$ group (Figure 54).

Likewise, levels of HPX were significantly reduced in the $PCI_{MMP9Low}$ group at 5 minutes after plaque disruption, while the HPX levels remain unchanged in the $PCI_{MMP9High}$ and $CONTROL_{Dx}$ group (Figure 54). Significant correlations were further observed between the fold change of LBP at 5 minutes after plaque disruption to both the fold change of HPX (at 5 minutes) and the subsequent $MMP9_{AUC}$ after plaque disruption (Figure 55).

A.

CYB5r3		HADH		CD84	
Sample	O.D.	Sample	O.D.	Sample	O.D
Standard 7	1.872	Standard 7	3.5	Standard 7	3.486
Standard 1	0.678	Standard 1	2.846	Standard 1	0.879
Plasma 1:1	0.145	Plasma 1:1	0.27	Plasma 1:1	0.468
Plasma 1:2	0.095	Plasma 1:2	0.413	Plasma 1:2	0.399
Plasma 1:20	0.152	Plasma 1:20	0.646	Plasma 1:20	0.233
Plasma 1:50	0.493	Plasma 1:50	2.115	Plasma 1:50	0.614

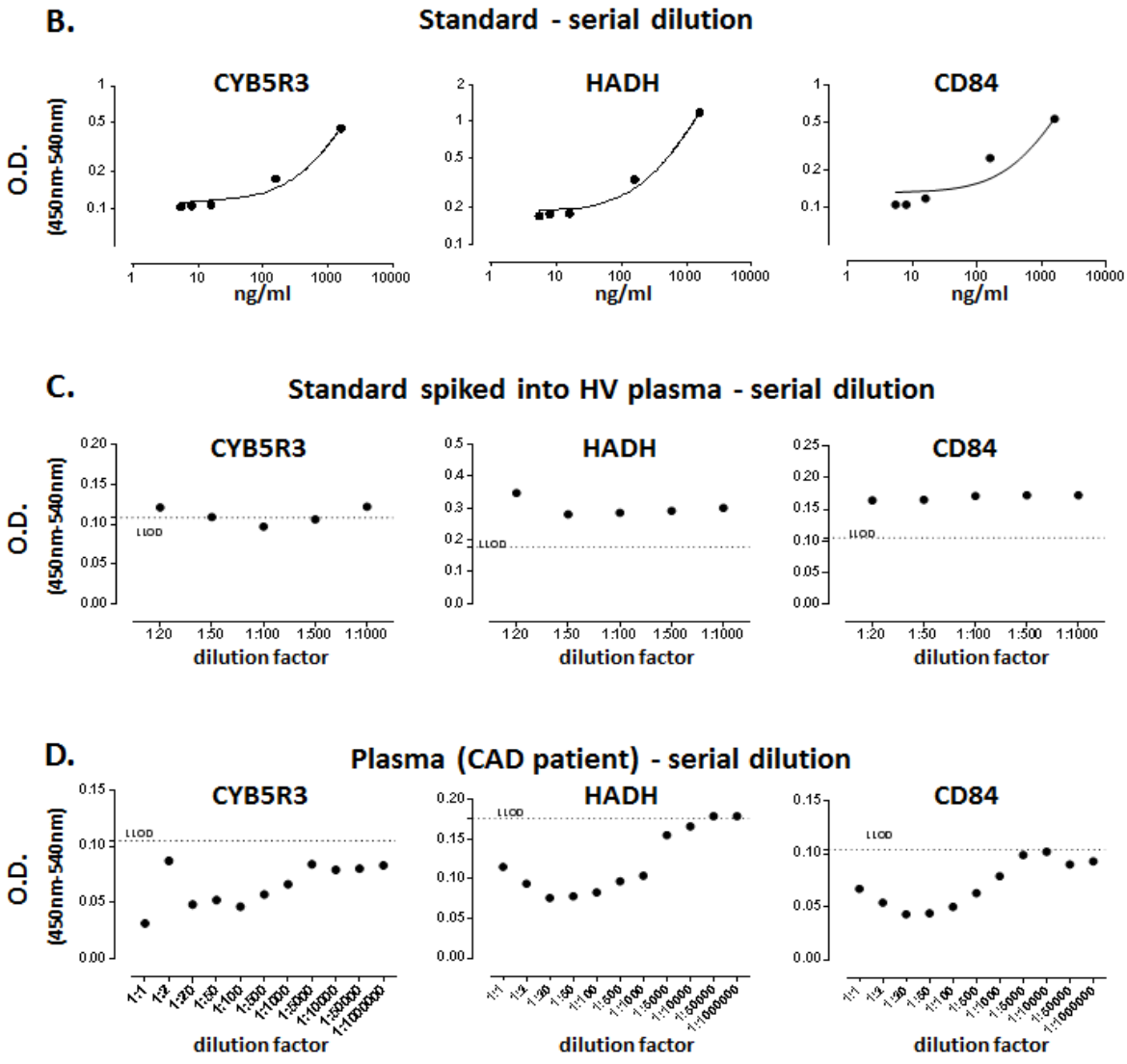


Figure 53: Non-performance of the commercially available ELISA kits for CYB5R3, HADH and CD84

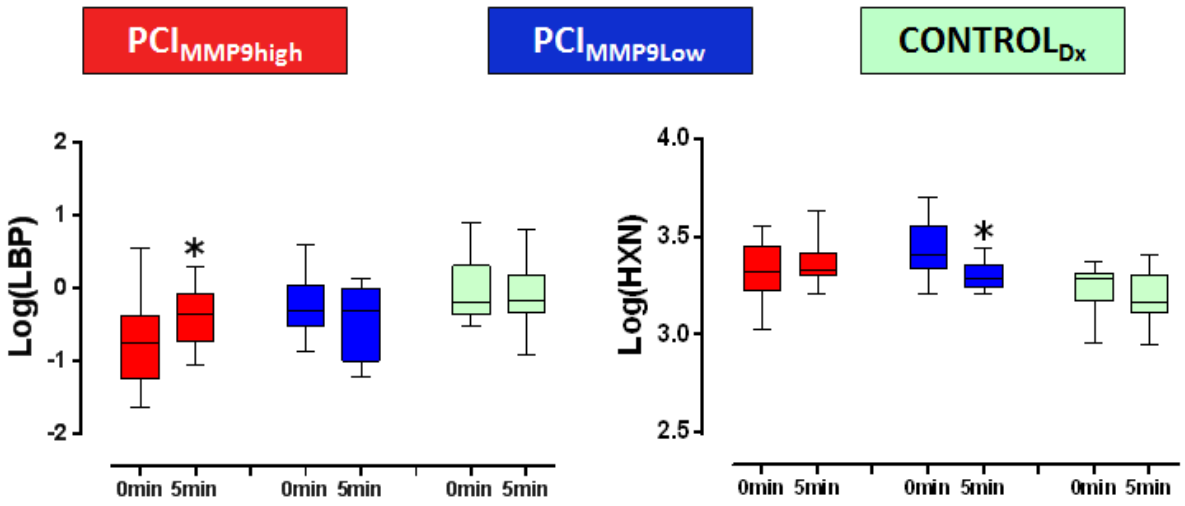


Figure 54: Acute changes of plasma LBP and HPX after coronary atherosclerotic plaque disruption

Arterial plasma levels of LBP and HPX at baseline (0 min) and 5 minutes (5 min) in *individual patients* were measured by ELISA in the discovery subject subset. Log transformation of data was performed and comparison between time points were performed using paired t-tests. P-value of less than 0.05 was considered significant. Within 5 minutes of plaque disruption, there was acute, significant elevation of plasma LBP in the $PCI_{MMP9High}$ group. There were no significant changes in LBP in the $PCI_{MMP9Low}$ and $CONTROL_{Dx}$ group. Likewise, levels of HPX were significantly reduced in the $PCI_{MMP9Low}$ group at 5 minutes after plaque disruption, while the HPX levels remain unchanged in the $PCI_{MMP9High}$ and $CONTROL_{Dx}$ group. (Data are presented in median with interquartile range.)

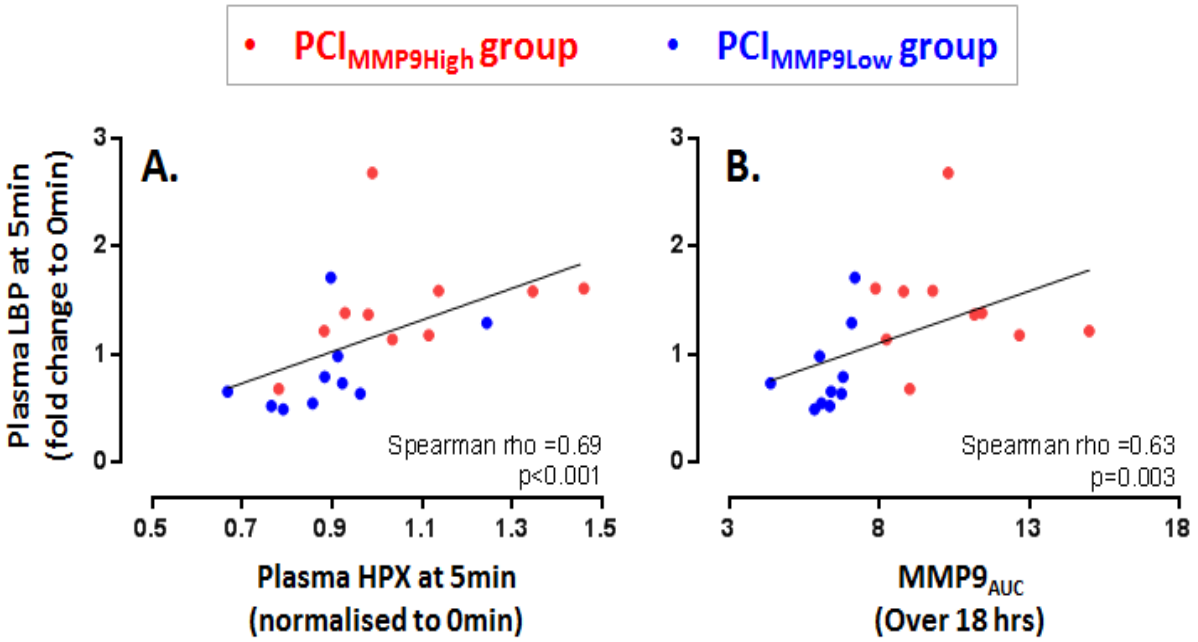


Figure 55: Plasma LBP correlates with plasma HPX and $MMP9_{AUC}$ after coronary atherosclerotic plaque disruption

Arterial plasma levels of LBP and HPX at baseline (0 min) and 5 minutes (5 min) were measured by ELISA in the discovery subject subset. Correlations between the fold change of LBP and HPX (at 5 minutes) and between the fold change of LBP and venous $MMP9_{AUC}$ were assessed using Spearman rank correlation. P-value of <0.05 was considered to be significant. Significant correlations were observed between the fold change of LBP at 5 minutes after plaque disruption to both the fold change of HPX (at 5 minutes) and the subsequent $MMP9_{AUC}$ throughout the post procedural period.

5.5 Discussion

5.5.1 Key findings of proteomics analysis

Several key findings have were presented in this proteomics analysis. Firstly, it was feasible to characterise the proteomics profile of plaque debris retained by filterwires even though there were typically only microscopic amount of materials retrieved. The proteomics profile of plaque samples was distinct from the matched experimental controls (FW INCs) and distinct from plasma, which reflected the intrinsic differences between sample types. This was to be expected and supports the internal validity of this experiment. Further supporting evidence for the internal validity was derived from the comparison between HV and CAD patients' baseline plasma. In this small cohort, CAD subjects showed higher levels of CRP than the HVs, but lower levels of several members of the HDL family (APO-A2, APO-L, APO-M). Such observations are consistent with the associations between these lipoprotein subclasses and the risk of developing CAD.

Plaque disruption resulted in changes of proteomics profile compared to the control group. This was evident through examination by PCAs of all proteins, and also the unique patterns associated with the key canonical pathways. In addition, several proteins that were present in plaque debris are also acutely increased in circulation minutes after plaque disruption. This argued strongly that such proteins may indeed be acutely released from the plaque after plaque disruption. Technical validation of the significantly changed proteins (at 5 minutes) according to mass spectrometry measurement was achieved for two targets (LBP and HPX) using ELISA. The reproducibility of results for two proteins is strong evidence for validity of the other changes observed in the overall proteomics dataset.

5.5.2 Spectrum of proteomics profile changes after plaque disruption

Another key finding relates to the spectrum of proteomics changes observed in this model of plaque rupture. PCA of all proteins detected in this experiment demonstrated greater differences in the $PCI_{MMP9Low}$ group before and after plaque disruption, as compared to the $PCI_{MMP9High}$ group. Similar patterns were also observed for PCAs of proteins specific to the most highly implicated canonical pathways after plaque disruption. The results from proteomics analysis mirrored those from the LC-MS metabolomics screen, where the widest separation on PCA scores plot of metabolites was also observed in the $PCI_{MMP9Low}$ group after plaque disruption. These findings suggested likely interactions between plasma proteins and metabolites at early moments after plaque disruption in the $PCI_{MMP9Low}$ group.

On the other hand, it was counterintuitive that smaller magnitudes of change in proteomic profile were observed in patients with the highest $MMP9_{AUC}$ after plaque disruption. Findings from the candidate marker analysis indicated MMP9 release to be least confounded by the downstream myocardial injury and systemic inflammation, hence its potential utility as an index of response after plaque disruption. The later observations from proteomics analysis further supported the assumptions that plaque disruption could indeed lead to disparate patterns of biomarker release, otherwise one would observe little changes in the proteomic and metabolomic profile in those with little changes in MMP9 ($PCI_{MMP9Low}$ group) after plaque disruption. Importantly, the dramatic differences observed in the MALDI-TOF-MS lipidomic profile in the $PCI_{MMP9High}$ group drew parallels with the observations related to plaque morphology and subsequent MMP9 release (that disruption of lipid rich plaques resulted in more rapid elevations in plasma MMP9). Given the central role of lipids in atherogenesis, results from the $PCI_{MMP9High}$ group suggest cross-talks between lipid metabolism and downstream MMP9 changes.

Results from individual proteins might provide mechanistic explanations for the spectrum of proteomic changes after plaque disruption. Of the significantly changed proteins detected by shotgun proteomics, three (LBP, HPX, A1BG) were implicated in the top canonical pathway associated with this dataset - the LXR/RXR activation pathway. Closer examination of this pathway revealed compartmental activity of these three targets. Peripheral activation of LXR/RXR pathway in neutrophil / monocytes can be triggered by binding of LBP to toll like receptor 4 (TLR4) resulting in activation of NFκB (nuclear factor kappa light chain enhancer of activated B cells), which subsequently stimulates the release of MMP9 (Figure 56). On the other hand, activation of the LXR/RXR pathway can be triggered via CD36 signalling. HPX and A1BG are both members of the HDL family, which can interact with cell surface scavenger CD36 (Figure 50, 51).

Findings reported in this thesis suggest that when plaque rupture is associated with acute release of LBP, activation of the LXR/RXR pathway in monocytes and neutrophils result in subsequent release of MMP9, likely through NFκB mediated signalling. In contrast, when plaque rupture is not accompanied by acute LBP release, there is no activation of LXR/RXR pathway in the circulating monocytes/macrophages, and no MMP9 release is observed in this group. In such cases, acute decrease in HPX and A1BG after plaque rupture are observed. Importantly, HPX binds heme with the highest affinity of any known protein(151), with the main biological function as a scavenger for heme released by the turnover of heme proteins such as hemoglobin. Intra-plaque haemorrhage is a recognised event throughout the lifecycle of plaques.(152) One can hypothesise that disruption of plaque with dominant intra-plaque haemorrhage phenotype results in the acute consumption of circulating HPX.

5.5.3 Integration of proteomics and small molecules data

It was the final aim in this chapter to explore the feasibility of integrating data derived from the small molecules screen with information gained from proteomics analysis. Two pathways were examined using this approach: γ-linoleate biosynthesis pathway and glutary-CoA degradation pathway.

5.5.3.1 CYB5R3 and γ-linoleate biosynthesis pathway

According to the proteomics analysis, CYB5R3 was present in the plaque samples and was acutely elevated in plasma within 5 minutes of plaque disruption in the $PCI_{MMP9High}$ group. The key enzymatic role of CYB5R3 in fatty acid oxidation pathway could be one explanation for the results observed in the MALDI-TOF-MS lipidomics data, whereby $PCI_{MMP9High}$ group exhibited the most dramatic changes in MALDI-TOF-MS lipidomic profile after plaque disruption (Figure 34). However, technical validation of the proteomics data on CYB5R3 using ELISA was unsuccessful, as the only commercially available assay did not perform for EDTA plasma measurements. At the time of writing, there was no literature which reported the measurement of CYB5R3 in human plasma, as this enzyme had only been examined as a cellular component in literature.

Although the immediate substrates upstream and downstream of CYB5R3 (linoleoyl-CoA and γ-linoleoyl-CoA) were not detected in the metabolomics experiment described in Chapter 4 (due to acquisition mass range set to below 1000 m/z), mass peaks with a close match to the parent substrate (linoleate) in this pathway were detected in this experiment (Figure 52). Importantly, in a retrospective analysis of pilot data acquired in early experiments (not included in this thesis) where the upper limit of acquisition mass range was set to 1100m/z, mass peaks which matched the molecular formula of linoleoyl-CoA were indeed detected in plasma. This suggests the likelihood to be able to detect this particular mass feature in future

experiments with a broader mass acquisition window. This pathway warrants further investigation as it may provide novel insights to the mechanisms of acute lipidomic profile changes observed in the $PCI_{MMP9high}$ group.

The findings regarding acute release of LBP and CYB5R3 after plaque disruption, and their potential roles in downstream activation of the respective biological pathways, are summarised by Figure 56.

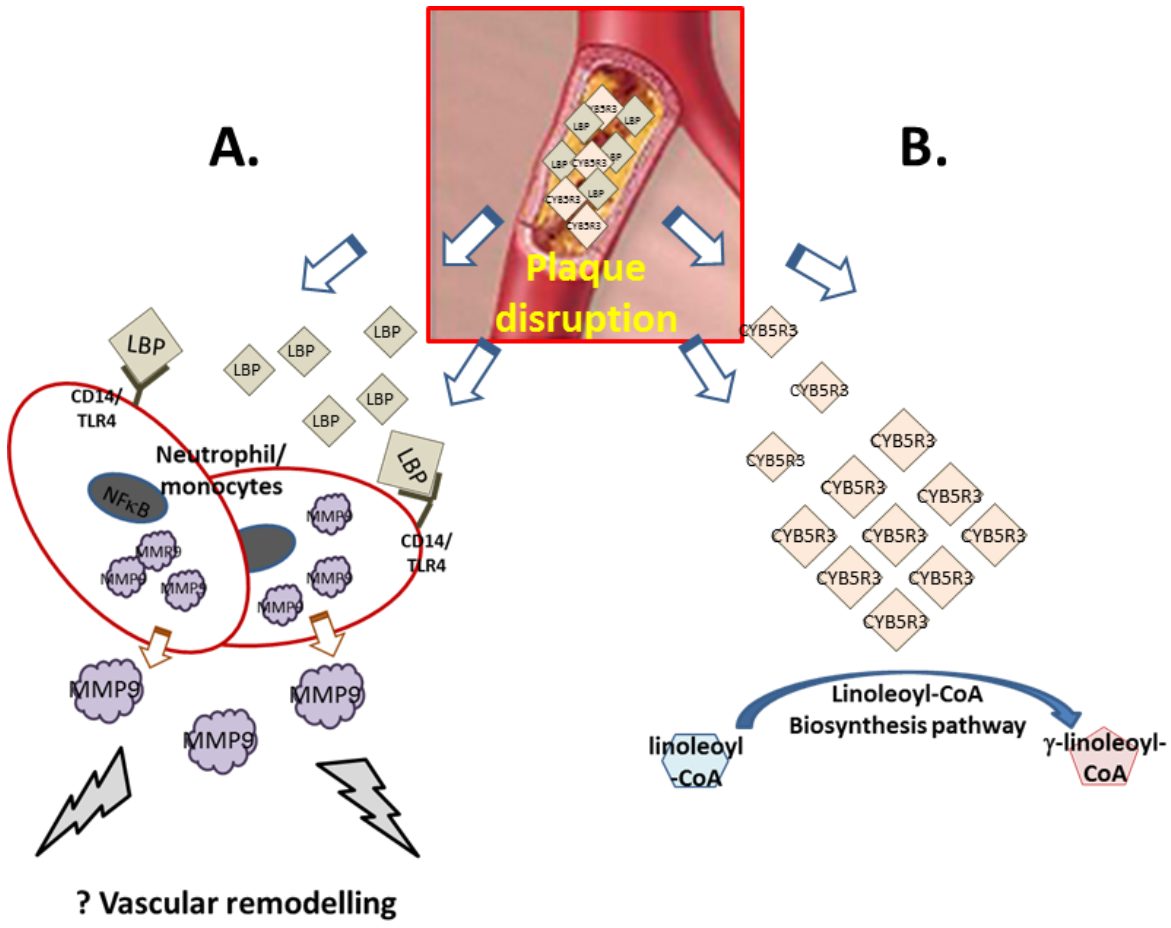


Figure 56: Potential mechanisms of biological pathway activations after plaque disruption due to the acute release of LBP and CYB5R3

5.5.3.2 Glutaryl –CoA degradation pathway

Three proteins that belong to the enzyme hydroxyacl-CoA dehydrogenase family (EC 1.1.1.35) were detected in the proteomics analysis: hydroxyl-CoA dehydrogenase (HADH), hydroxysteroid dehydrogenase 17 B10 (HSD17B10), and hydroxysteroid dehydrogenase 17 B4 (HSD17B4) (Figure 57). This family of enzymes are central to final step of glutaryl-CoA degradation pathway whereby (s)-3-hydroxybutanoyl-CoA is degraded by β-oxidation to form acetoacetyl-CoA. In the metabolomics analysis, mass peaks of several features which matched the molecular formula of substrates in this pathway were detected: acetyl-CoA, coenzyme A, acetoacetyl-CoA, NADH, (s)-3-hydroxybutanoyl-CoA, and Crotonyl CoA (Figure 38). Although the changes of these three proteins at 5 minutes did not reach statistical significance in the proteomics analysis, the patterns of change between the plaque disruption and control groups were distinct. With increased numbers (by measuring the individual samples from this cohort), statistically significant changes of these three proteins may be observed. Of note, the attempt at measuring the level of HADH for individual samples has not been successful, due to the issues encountered with the only commercially available ELISA assay.

Glutaryl-CoA is a common intermediate in the degradation of several different compounds such as lysine and tryptophan. Tryptophan metabolism pathway has been implicated in cardiovascular disease risk. Products of tryptophan metabolism (kynurenic acid and anthranillic acid) have been shown in a previous metabolomics study to be associated with metabolic risk factors of obesity, insulin resistance and dyslipidaemia.(153) Kynurenine has also been shown to be an endothelium derived relaxing factor produced during inflammatory stimuli.(154) In the LC-MS metabolomics experiment, several other mass peaks which had molecular feature matching to substrates for parts of the tryptophan to glutaryl Co-A pathway were observed (formylkynurenine, kynurenine, oxoadipate, NADPH, NADH, FAD and

FADH2 – Figure 58). Taken together, there is a high probability that members of this pathway contribute towards the signature of plaque rupture, and further investigation of this pathway is warranted.

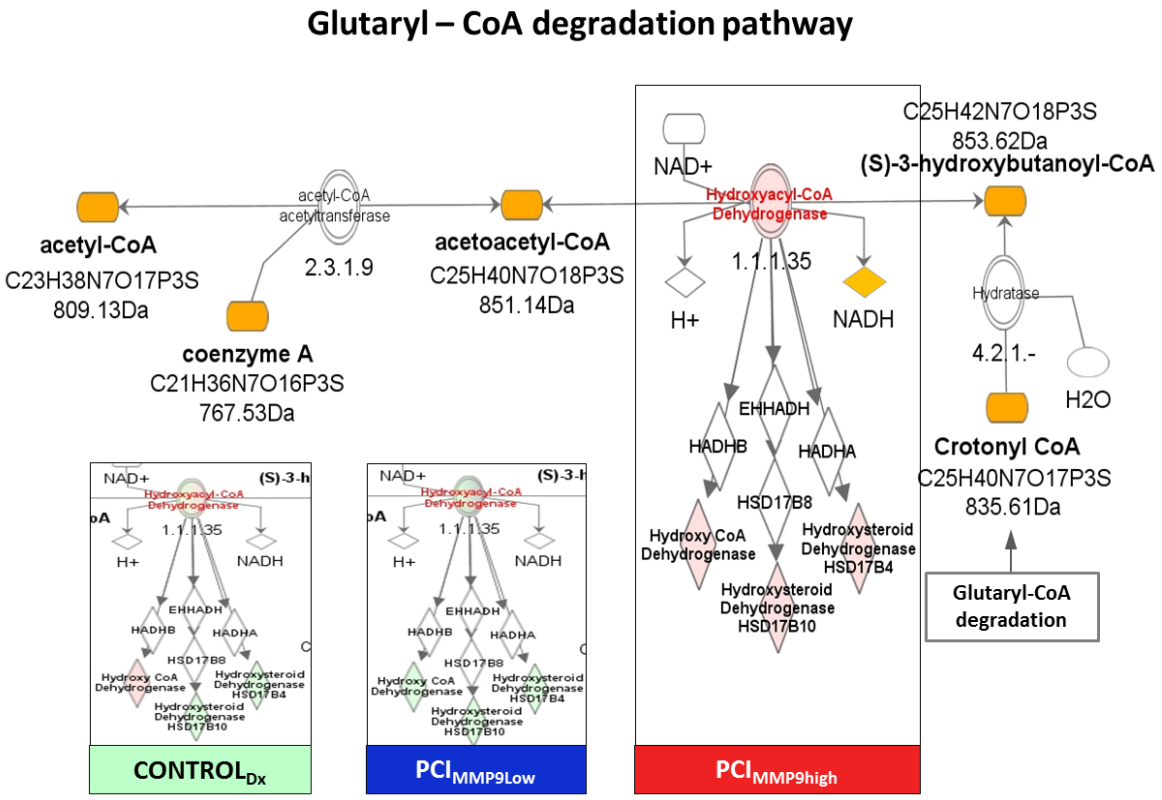


Figure 57: Glutaryl–CoA degradation pathway may be involved after coronary atherosclerotic plaque rupture

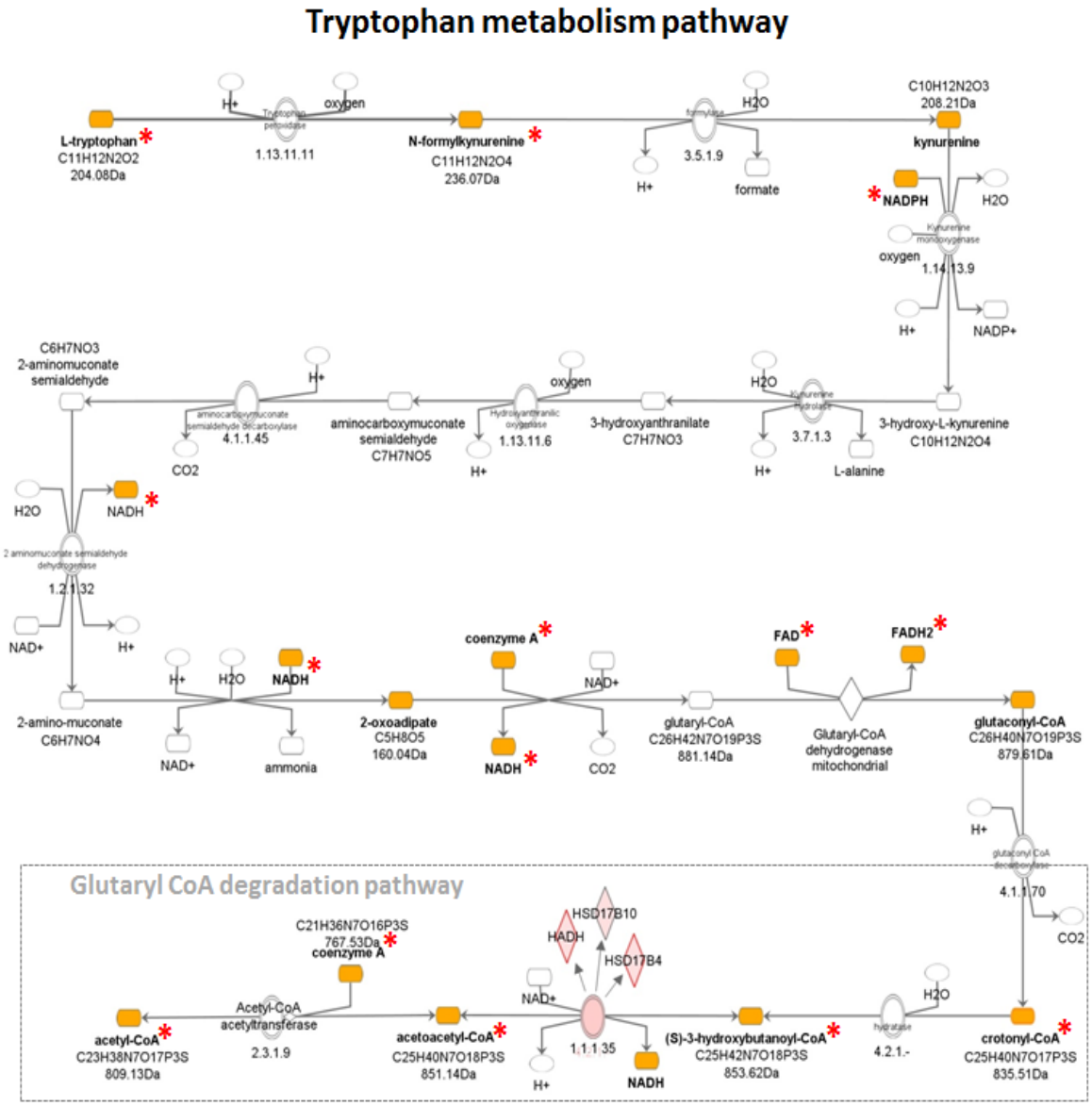


Figure 58: Tryptophan metabolism pathway may be involved after coronary atherosclerotic plaque rupture

CHAPTER 6

GENERAL DISCUSSION

6.1 Original hypotheses and aims

The central hypotheses for this thesis were that plaque rupture *in vivo* would lead to the release of novel plasma biomarkers, that macro/micro-molecules acutely released after plaque rupture should be also detectable in the plaque debris, and that such acutely released molecules could be detected and characterised by mass spectrometry based techniques. I further hypothesised that plaque rupture encompassed more than a singular phenotype and that a spectrum of biomarker release profile may be observed. The greater purpose for this search of novel plasma biomarkers was to utilise such maker(s) as a vehicle to improve our understanding of the biological processes surrounding plaque rupture events. To achieve this, PCI induced plaque disruption was used as the human model of plaque rupture, which enabled collection coronary plaque debris, and plasma samples from different anatomical locations in a temporal fashion. These samples were subsequently characterised using a range of techniques.

6.2 Principal findings of research

1. Pre-analytic issues can significantly confound biomarker measurements in clinical studies. Specifically, low force, short duration centrifugation of blood samples at refrigerated conditions leads to residual platelets in the plasma samples both in healthy volunteers and subjects with established coronary atherosclerosis. Residual platelets in plasma are a source of biomarker (such as sCD40L) release *ex vivo*, giving rise to artifactual biomarker measurements.
2. Platelet poor/free plasma prepared using EDTA as an anticoagulant at room temperature immediately after sample collection is a robust sample matrix the purpose of biomarker measurements.
3. Significant changes in existing candidate markers are observed after induced plaque disruption. Elevation of MMP9 after plaque disruption does not correlate with markers of

downstream myocardial injury (measured by changes in TnI and CKMB) or systemic inflammatory response (measured by changes in CRP). Therefore MMP9 is a biologically distinct index of the response to plaque disruption in this experimental model.

4. In a subgroup of patients, significant elevation of plasma MMP9 is observed by 5 minutes after plaque disruption. This implicates MMP9 to be a biomarker of specific plaque rupture phenotype.
5. Plaque morphology, as defined by OCT, predicts biomarker release after induced plaque disruption. Disruption of lipid rich plaques leads to earlier significant elevation of MMP9 compared to non-lipid plaques. This is independent to the clinical presentation of the individual patients. However, performance of OCT in every participant has not been feasible due to safety consideration.
6. Acute changes in the global plasma metabolite, lipid, and protein profiles are observed by 5 minutes after plaque disruption.
7. Ingenuity pathway analysis of the plasma proteomic profile after plaque disruption highlights the involvement of LXR/RXR pathway activation. These upstream changes result in differential release of MMP9 in systemic circulation.
8. Several of the acutely elevated plasma proteins after plaque disruption are also present in the plaque debris material, suggesting it to be directly released from the ruptured plaque. Amongst these proteins, the changes in plasma LBP levels have been technically replicated by ELISA measurement of individual samples in the discovery subject subset.
9. Distinct patterns of acute protein changes can be identified after plaque disruption. In one pattern, the acute release of LBP leads to TLR4 mediated activation of the LXR/RXR pathway in the circulating neutrophils or monocytes. This results in NFκB activation, and triggers downstream systemic MMP9 release. In another pattern, plaque disruption is associated with acute depletion of circulating HPX and differential activation of the

LXR/RXR pathway. These disparate acute changes are reflected by differential MMP9 release downstream.

6.3 Future directions

The work in this thesis provides compelling new evidence that coronary atherosclerotic plaque disruption is associated with release of novel proteins and alterations in global metabolite and lipid profiles that are detectable in the peripheral circulation. Technical validation of mass spectrometry data by measurement of individual samples has been confirmed for two targets (LBP and HPX). Further technical validation of other putative targets by ELISA has been restricted by the availability of reliable commercial assays. As such, alternative techniques for technical validation of the other protein targets need to be explored.

Over the course of this research, new methods for targeted proteomics analysis (as compared to the untargeted proteomics screen utilised in the experiment) have emerged and are gaining main stream recognition.(155) In particular, a new method called "Sequential Window Acquisition of all Theoretical Mass Spectra - MS" (SWATH-MS) offers promise to minimise the problem of ionic suppression observed in data dependent analysis by sequentially acquiring all mass spectra data in a data-independent fashion.(156) Using this method, it is theoretically feasible to acquire the tandem MS data for *all* precursor ions in a complex sample mixture such as plasma, thus creating a complete library of the peptides in the sample for subsequent data mining.

This technique has recently become available to the Kessler lab and is currently being optimised. One focus of my future work will be to analyse the *individual* plasma samples of the discovery cohort using the SWATH-MS technique. This will provide technical validation

of the findings observed in the untargeted proteomics screen and potentially reveal further putative targets in the pathways described thus far.

Small molecule screens using MALDI-TOF-MS and LC-MS also demonstrate evidence of global changes within 5 minutes of plaque disruption. The results demonstrate mass peaks in the LC-MS experiment with close match to the molecular features of substrates in key fatty acid oxidation pathways that are jointly implicated by the proteomics data. In order to confirm the identity of these small molecules, it will be necessary to compare the tandem mass spectra and chromatographic profile of the putative targets against those of an analytic standard. Mass spectrometry characterisation of analytic standard of a metabolite will give the information to identity the small molecules with greater confidence. This is a pre-requisite for semi-quantitative analysis for changes observed after plaque disruption, and to allow corroboration of information regarding the biological pathways involved. Therefore, the second focus of future work will involve acquisition of tandem mass spectra of the analytic standards, followed by re-analysis of the discovery subject subset samples. Alternative chromatography techniques (gas chromatography, hydrophilic interaction chromatography) and negative charge mode ionisation should also be attempted for the analysis of these samples to capture a more comprehensive small molecule profile.

Given the small number of plaque debris samples analysed so far, the validity of novel proteins identified in plaque debris and their subsequent release in plasma should be confirmed by analysis of additional samples. This will require recruitment of additional subjects who undergo filterwire retrieval of plaque debris, coupled with the same protocol of serial plasma sampling. Targeted protein analysis will be performed in the additional plaque debris samples using various techniques, such as western blotting, ELISA measurement of

the tissue lysates, or measurement by targeted proteomics using SWATH-MS. Ideally OCT should be performed in each of the additional participants.

$MMP9_{AUC}$ has been used as the index for stratifying subjects in this thesis, based on the considerations detailed in Chapter 3. Specifically, changes in plasma MMP9 after plaque disruption are not correlated to cTnI or CRP and therefore it is least likely to be confounded by changes due to downstream myocardial injury and systemic inflammatory response in this experimental model of plaque rupture. Results presented in this thesis demonstrate the feasibility of detecting plasma molecular profile changes within minutes of plaque disruption. Exploration of alternative indices for stratifying subjects should be attempted for future analysis of SWATH-MS data acquired from individual subjects. For example, changes in cTnI after plaque disruption may itself be another index of the plaque rupture phenotype, as subjects with greater microembolic burden after plaque disruption are likely to have greater micro-vascular ischaemia and myocardial necrosis.(157) At this early time point systemic changes in plasma molecular profile should not be confounded by potential biological signatures related to myocardial ischaemic injury (which manifest later in the time course).

There is also scientific merit in attempting to replicate the results using a different model of plaque rupture in human. A similar protocol can be applied to angioplasty with stenting in the lower limb (femoral/popliteal), whereby sampling of femoral arterial and venous blood throughout the procedural period can be readily collected as part of the procedure. Although acute lower limb ischemia is commonly triggered by cause other than plaque rupture, with the predominant aetiology being acute arterial embolism, spontaneous plaque rupture in the ilio-femoral arteries is not an uncommon event.(158) Given that atherogenic process is similar throughout the entire vasculature, it will beneficial to demonstrate that comparable biomarker changes are observed from plaque rupture in the peripheral circulation.

In addition to investigating plaque rupture in non-emergency clinical scenarios, patients presenting with acute STEMI as an emergency most likely have experienced a culprit plaque rupture event, and are therefore intrinsically enriched in biomarker signals of plaque rupture *de novo*. These cohorts provide an unique model for assessing the associations between the upstream plaque rupture event to the downstream myocardial injury and clinical outcomes. However, recruitment of STEMI patients presenting as an emergency to a research study is traditionally challenging due to ethical considerations regarding the capacity of such patients to provide informed consents.(159) During my DPhil research, I played a key role in estabslihing a new research program to allow recruitment of STEMI patients presenting for primary PCI treatment at the Oxford Heart Centre. The Oxford Acute Myocardial Infarction (OxAMI) Study (Ethics Ref: 11/SC0397) has commenced recruitment, and will facilitate further investigations of the novel markers reported in this thesis.

It has been an aspiration for this work to lead to the identification of novel biomarkers of atherosclerotic plaque rupture that may ultimately be applicable to clinical practice. Notwithstanding the recent advances in high sensitivity troponin assays and their impact on the management of patients presenting with ACS, there remain layers of challenges before these reported novel biological signatures can transend beyond the role as a research tool and be considered clinical biomarkers. The findings reported in this thesis will first need to be replicated in larger cohorts, ideally recruited in a prospective manner using the same stringent sample preparation protocol and with recording of long term outcome data. There may be opportunities to test for these targets in other existing / retrospective cohorts with banked plasma samples. However, other pre-analytic issues can affect the measurement of candidate markers in plasma samples under long term storage, and it will be crucial to assess the reproducibility and accuracy of biomarker measurements after a prolong period of storage before further analyses are performed.(160)

Further investigation of the biological roles of these novel proteins of plaque rupture are warranted. The differential biomarker response observed in this research could give further insight to why certain coronary plaque ruptures lead to significant clinical sequelae by way of significant thrombosis, while other plaque ruptures result in minimal clinical consequence. The distinct patterns of pathway activation observed in the plaque disruption groups, as highlighted by the pathway guided PCAs, provide evidence that differential activation of pathways are preceded by divergent profiles of proteins released after plaque disruption. One approach to examine the potential role these acutely released proteins in terms of subsequent differential activation of pathways is the use of animal model of plaque rupture, by co-administration of antibodies to the protein of interest. However, there are limitations of using mouse model for the study of plaque rupture. For example, atherosclerotic lesions in the commonly used genetic mice seldom develop plaque rupture with thrombosis, which is the mechanism that results in complication in human disease. Murine atherosclerotic plaques develop in the aorta and proximal great vessels, which is different from human disease where clinical consequences typically arise from coronary and peripheral arteries.(161) Alternative animal models, such as rabbit (162) or porcine (163) models for plaque rupture exist and can be explored for the purpose of this investigation.

The findings that plaque disruption leads to prompt release of a range of plaque related proteins and results in disparate activation of downstream pathways raise further questions as to the role of such proteins in atherogenesis. Differential expression / uptake of these proteins during the atherogenic process may alter the plaques phenotype, thereby indirectly affecting the downstream consequences of plaque rupture. One approach to test the causal role of these novel proteins is to employ gene targeted animal models to assess first if gene deletion of the target leads to alterations in atherogenesis, and if so how it may affect the subsequent plaque and rupture phenotypes.

6.4 Conclusion

I have demonstrated the feasibility of detecting novel plasma molecular signatures after disruption of human coronary atherosclerotic plaque *in vivo* in carefully and consistently prepared clinical samples. Plaque rupture leads to the release of plaque proteins and acute changes in the global plasma lipid and metabolite profile, which are detectable using a combination of mass spectrometry techniques. These novel proteins give insight to the involvement of LXR/RXR pathway activation, amongst others, in the early moments after plaque rupture. Multi-omics analysis can provide further clues to the mechanisms underpinning the differential biological sequelae after a plaque rupture event.

CHAPTER 7

DATA APPENDIX

Uniprot Accession number	Peptide count	Confidence score	Fold change	Anova (p)	Description	Location
Q9BR76	3	106.5	3633.2	0.00270	Coronin-1B	cytoplasmic
P05141	4	108.9	1247.3	0.03966	ADP/ATP translocase 2	cytoplasmic
P26641	6	198.1	1076.7	0.00057	Elongation factor 1-gamma	cytoplasmic
P51606	2	103.6	1002.2	0.00471	N-acylglucosamine 2-epimerase	unknown
Q96AA8	2	54.1	759.7	0.02199	Janus kinase and microtubule-interacting protein 2	extracellular
Q13094	2	72.9	744.1	0.00796	Lymphocyte cytosolic protein 2	cytoplasmic
P50991	3	101.7	689.6	0.00168	T-complex protein 1 subunit delta	cytoplasmic
P43304	4	113.7	506.0	0.00503	Glycerol-3-phosphate dehydrogenase	cytoplasmic
P11413	6	306.5	490.9	0.00029	Glucose-6-phosphate 1-dehydrogenase	cytoplasmic
P55058	2	54.5	350.1	0.00132	Phospholipid transfer protein	extracellular
P48444	2	54.4	298.6	0.00189	Coatomer subunit delta	cytoplasmic
P31150	7	488.4	298.2	0.00050	Rab GDP dissociation inhibitor alpha	cytoplasmic
P16671	8	319.1	258.6	0.00024	Platelet glycoprotein 4	membrane
P62993	3	157.6	253.6	0.00003	Growth factor receptor-bound protein 2	cytoplasmic
O15020	3	97.7	252.9	0.00142	Spectrin beta chain, non-erythrocytic 2	cytoplasmic
Q9Y624	2	75.6	243.6	0.02787	Junctional adhesion molecule A	membrane
P22392	4	128.5	238.8	0.01647	Nucleoside diphosphate kinase B	nucleus
O14745	2	74.4	237.1	0.02447	Na(+)/H(+) exchange regulatory cofactor NHE-RF1	membrane
Q9NY65	12	1132.0	232.3	0.01757	Tubulin alpha-8 chain	cytoplasmic
Q96KN2	2	93.0	228.5	0.01669	Beta-Ala-His dipeptidase	cytoplasmic
P07355	4	149.4	227.3	0.00083	Annexin A2	membrane
O15143	4	211.9	223.7	0.00015	Actin-related protein 2/3 complex subunit 1B	cytoplasmic
P22352	3	142.3	216.3	0.00323	Glutathione peroxidase 3	extracellular
P61204	5	265.1	216.0	0.00001	ADP-ribosylation factor 3	cytoplasmic
P50148	3	147.6	205.1	0.00019	Guanine nucleotide-binding protein G(q) subunit α	membrane
O43707	26	1692.3	203.2	0.00009	Alpha-actinin-4	cytoplasmic
P11226	2	84.9	197.1	0.03308	Mannose-binding protein C	extracellular
P52565	2	86.0	194.7	0.00026	Rho GDP-dissociation inhibitor 1	cytoplasmic
O75874	4	153.3	193.7	0.00436	Isocitrate dehydrogenase	cytoplasmic
P41218	4	124.3	192.2	0.00007	Myeloid cell nuclear differentiation antigen	nucleus
P14770	6	305.3	189.2	0.00068	Platelet glycoprotein IX	membrane
Q9ULV4	7	259.3	180.0	0.00002	Coronin-1C	cytoplasmic
Q99832	2	61.0	178.7	0.00069	T-complex protein 1 subunit eta	cytoplasmic
P30044	3	124.2	169.6	0.00071	Peroxiredoxin-5, mitochondrial	cytoplasmic
Q16851	3	93.2	167.8	0.00120	UTP--glucose-1-phosphate uridylyltransferase	cytoplasmic
P01889	2	159.5	167.2	0.00169	HLA class I histocompatibility antigen	membrane
P01814	2	70.4	166.5	0.00540	Ig heavy chain V-II region OU	unmapped
Q86YW5	2	134.0	160.4	0.00024	Trem-like transcript 1 protein	membrane
P80108	3	108.5	158.5	0.00015	Phosphatidylinositol-glycan-specific phospholipase D	cytoplasmic
P04844	3	240.6	157.0	0.00003	Dolichyl-ligosaccharide-protein glycosyltransferase	cytoplasmic
P16284	4	218.3	151.5	0.00031	Platelet endothelial cell adhesion molecule	membrane
P53618	3	112.9	135.7	0.00212	Coatomer subunit beta	cytoplasmic
O43396	3	128.8	134.1	0.00051	Thioredoxin-like protein 1	cytoplasmic

Appendix Table 1: Proteins present in the plaque debris

Uniprot Accession number	Peptide count	Confidence score	Fold change	Anova (p)	Description	Location
P11169	5	247.9	133.6	0.00219	Solute carrier family 2, member 3	membrane
P25705	7	374.2	132.8	0.00001	ATP synthase subunit alpha	cytoplasmic
P59998	4	128.3	129.9	0.00073	Actin-related protein 2/3 complex subunit 4	unmapped
P21291	5	188.9	128.4	0.00007	Cysteine and glycine-rich protein 1	nucleus
P23229	5	172.1	127.5	0.00072	Integrin alpha-6	membrane
P51659	3	204.2	123.0	0.00011	Peroxisomal multifunctional enzyme type 2	cytoplasmic
Q14974	5	223.2	121.2	0.00001	Importin subunit beta-1	nucleus
O75915	2	73.5	114.1	0.00002	PRA1 family protein 3	cytoplasmic
P35241	6	283.8	113.1	0.00066	Radixin	cytoplasmic
Q9H939	5	198.1	112.0	0.00627	Proline-serine-threonine phosphatase-interacting protein 2	cytoplasmic
P13224	3	130.1	112.0	0.01060	Platelet glycoprotein Ib beta chain	membrane
P26447	4	183.1	111.8	0.00026	Protein S100-A4	cytoplasmic
Q9UDY2	3	134.3	110.4	0.00900	Tight junction protein ZO-2	membrane
Q13418	18	1028.7	109.4	0.00008	Integrin-linked protein kinase	membrane
P00739	27	1780.1	101.2	0.00389	Haptoglobin-related protein	extracellular
Q9HBI1	9	818.7	100.9	0.00002	Beta-parvin	cytoplasmic
P09496	2	53.4	98.4	0.00225	Clathrin light chain A	membrane
P07195	12	710.2	93.8	0.00002	L-lactate dehydrogenase B chain	cytoplasmic
P18085	5	253.8	91.1	0.00010	ADP-ribosylation factor 4	cytoplasmic
P12814	58	4237.5	89.7	0.00009	Alpha-actinin-1	cytoplasmic
P07900	16	643.5	89.4	0.00003	Heat shock protein HSP 90-alpha	cytoplasmic
Q14247	5	280.3	87.2	0.00989	Src substrate cortactin	membrane
P78417	5	213.0	87.0	0.00010	Glutathione S-transferase omega-1	cytoplasmic
P62258	7	484.4	86.8	0.00002	14-3-3 protein epsilon	cytoplasmic
P30153	2	56.8	86.5	0.00103	Serine protein phosphatase 2A regulatory subunit A	cytoplasmic
P04899	4	179.0	86.5	0.00001	Guanine nucleotide-binding protein G(i) subunit α2	membrane
Q5JSH3	2	90.0	84.0	0.03369	WD repeat-containing protein 44	cytoplasmic
Q9NZP8	4	232.5	83.8	0.00442	Complement C1r subcomponent-like protein	extracellular
P30048	2	49.7	81.2	0.00048	Thioredoxin-dependent peroxide reductase	cytoplasmic
P29350	4	178.9	78.6	0.00005	Tyrosine-protein phosphatase non-receptor type 6	cytoplasmic
P99999	3	127.8	77.5	0.00914	Cytochrome c	cytoplasmic
P31948	4	141.7	77.4	0.00012	Stress-induced-phosphoprotein 1	cytoplasmic
P14625	14	657.9	77.4	0.00019	Endoplasmin	cytoplasmic
Q15833	10	495.9	74.5	0.00180	Syntaxin-binding protein 2	membrane
Q13423	3	120.4	74.5	0.00182	NAD(P) transhydrogenase	cytoplasmic
A6NL28	4	248.0	73.2	0.00958	Putative tropomyosin alpha-3 chain-like protein	unmapped
O15144	10	363.6	72.0	0.01694	Actin-related protein 2/3 complex subunit 2	cytoplasmic
P22314	4	168.7	69.9	0.00646	Ubiquitin-like modifier-activating enzyme 1	cytoplasmic
P00387	2	50.9	69.0	0.04348	NADH-cytochrome b5 reductase 3	cytoplasmic
P00740	5	246.7	67.9	0.00449	Coagulation factor IX	extracellular
P48735	11	508.5	67.8	0.00004	Isocitrate dehydrogenase	cytoplasmic
P05160	8	305.9	67.1	0.03699	Coagulation factor XIII B chain	extracellular
Q13201	30	1740.2	66.8	0.00068	Multimerin-1	extracellular

Appendix Table 1: Proteins present in the plaque debris – cont.

Uniprot Accession number	Peptide count	Confidence score	Fold change	Anova (p)	Description	Location
P40197	13	661.2	66.7	0.00096	Platelet glycoprotein V	membrane
P61106	5	305.7	66.2	0.00012	Ras-related protein Rab-14	cytoplasmic
P16109	4	205.4	65.5	0.00202	P-selectin	membrane
P37837	4	164.8	64.4	0.00160	Transaldolase	cytoplasmic
P63104	15	1165.9	64.3	0.00011	14-3-3 protein zeta/delta	cytoplasmic
P18054	5	328.8	63.6	0.00059	Arachidonate 12-lipoxygenase	cytoplasmic
Q16181	4	171.0	63.4	0.02090	Septin-7	cytoplasmic
O00194	10	551.3	62.6	0.00032	Ras-related protein Rab-27B	cytoplasmic
P00491	8	491.3	61.5	0.00009	Purine nucleoside phosphorylase	nucleus
P50395	7	507.9	60.1	0.01213	Rab GDP dissociation inhibitor beta	cytoplasmic
P27348	11	596.8	60.0	0.00082	14-3-3 protein theta	cytoplasmic
P0DJI9	10	707.9	59.9	0.00047	Serum amyloid A-2 protein	extracellular
P60709	40	3640.6	59.6	0.00007	Actin	cytoplasmic
P07996	42	3320.5	59.5	0.00003	Thrombospondin-1	extracellular
Q9Y613	3	90.3	58.5	0.02893	FH1/FH2 domain-containing protein 1	nucleus
P60981	3	192.0	58.1	0.00266	Destrin	cytoplasmic
O60610	13	578.0	57.3	0.00240	Protein diaphanous homolog 1	membrane
Q9Y696	2	103.8	56.0	0.00273	Chloride intracellular channel protein 4	membrane
P18206	61	3893.5	56.0	0.00014	Vinculin	membrane
Q15691	6	298.9	55.4	0.00002	Microtubule-associated protein RP/EB family member 1	cytoplasmic
Q58FF6	2	66.2	55.2	0.01189	Putative heat shock protein HSP 90-beta 4	unmapped
P14780	3	136.5	54.6	0.03171	Matrix metalloproteinase-9	extracellular
P67936	23	1722.5	54.4	0.00001	Tropomyosin alpha-4 chain	cytoplasmic
Q86UX7	29	1985.2	54.0	0.00015	Fermitin family homolog 3	cytoplasmic
P05771	3	157.1	53.5	0.00026	Protein kinase C beta type	cytoplasmic
P68363	22	1850.2	53.4	0.00060	Tubulin alpha-1B chain	cytoplasmic
P30740	4	148.8	53.1	0.00100	Leukocyte elastase inhibitor	cytoplasmic
P00558	20	905.6	53.1	0.00000	Phosphoglycerate kinase 1	cytoplasmic
P61224	13	859.1	52.8	0.00010	Ras-related protein Rap-1b	cytoplasmic
P18669	5	177.0	52.8	0.00022	Phosphoglycerate mutase 1	cytoplasmic
P80188	2	123.4	52.6	0.00416	Neutrophil gelatinase-associated lipocalin	extracellular
P46109	4	174.1	52.2	0.00018	Crk-like protein	cytoplasmic
P08238	11	508.3	52.2	0.00094	Heat shock protein HSP 90-beta	cytoplasmic
P05106	22	1079.9	51.4	0.00013	Integrin beta-3	membrane
Q14697	8	328.9	51.0	0.00064	Neutral alpha-glucosidase AB	cytoplasmic
P07359	12	627.0	51.0	0.00021	Platelet glycoprotein Ib alpha chain	membrane
Q9Y490	147	12033.8	50.9	0.00001	Talin-1	membrane
P01871	24	2289.6	50.7	0.00275	Ig mu chain C	membrane
Q93084	8	393.6	50.6	0.00009	Sarcoplasmic/endoplasmic reticulum calcium ATPase 3	cytoplasmic
P30041	11	491.8	50.0	0.00024	Peroxiredoxin-6	cytoplasmic
P09211	4	317.1	49.4	0.00030	Glutathione S-transferase P	cytoplasmic
Q9NRC6	3	80.6	49.1	0.00146	Spectrin beta chain	membrane
O15145	5	243.1	48.9	0.00556	Actin-related protein 2/3 complex subunit 3	cytoplasmic

Appendix Table 1: Proteins present in the plaque debris – cont.

Uniprot Accession number	Peptide count	Confidence score	Fold change	Anova (p)	Description	Location
P50990	4	147.7	48.8	0.00146	T-complex protein 1 subunit theta	cytoplasmic
P08514	30	1838.0	48.6	0.00026	Integrin alpha-IIb	membrane
P14618	24	1736.9	48.6	0.00003	Pyruvate kinase isozymes M1/M2	cytoplasmic
P08670	16	758.2	48.4	0.00147	Vimentin	cytoplasmic
Q14766	3	90.4	48.4	0.01459	Latent-TGF β–binding protein 1	extracellular
P35579	141	10432.7	47.7	0.00001	Myosin-9	cytoplasmic
P24557	5	205.4	47.1	0.00202	Thromboxane-A synthase	membrane
Q6DD88	2	68.4	46.5	0.01767	Atlastin-3	cytoplasmic
P09493	13	748.0	45.9	0.00077	Tropomyosin alpha-1 chain	cytoplasmic
O75083	22	1352.0	45.8	0.00005	WD repeat-containing protein 1	extracellular
P00338	11	586.0	45.8	0.00001	L-lactate dehydrogenase A chain	cytoplasmic
O75636	4	259.4	45.7	0.00135	Ficolin-3	extracellular
P07203	3	130.4	45.3	0.00001	Glutathione peroxidase 1	cytoplasmic
P09486	4	208.6	44.0	0.00046	SPARC	extracellular
P68366	23	2001.7	43.7	0.00009	Tubulin alpha-4A chain	cytoplasmic
P40926	4	160.0	43.6	0.01505	Malate dehydrogenase	cytoplasmic
Q8N392	2	102.5	43.4	0.03621	Rho GTPase-activating protein 18	cytoplasmic
P36959	3	116.5	43.1	0.00410	GMP reductase 1	cytoplasmic
P07384	11	464.7	42.9	0.00015	Calpain-1 catalytic subunit	cytoplasmic
P04075	22	1318.7	42.8	0.00001	Fructose-bisphosphate aldolase A	cytoplasmic
P11021	20	1051.1	42.7	0.00004	78 kDa glucose-regulated protein	cytoplasmic
P37235	2	69.2	42.3	0.00012	Hippocalcin-like protein 1	cytoplasmic
P24844	9	757.2	41.9	0.00007	Myosin regulatory light polypeptide 9	cytoplasmic
O15511	4	164.0	41.9	0.00003	Actin-related protein 2/3 complex subunit 5	cytoplasmic
Q6PJW8	2	76.8	41.7	0.00228	RecName: Full=Consortin;	cytoplasmic
P30405	8	399.5	41.6	0.00254	Peptidyl-prolyl cis-trans isomerase F	cytoplasmic
P06753	14	841.0	41.5	0.00050	Tropomyosin alpha-3 chain	cytoplasmic
P30040	2	103.5	41.3	0.01356	Endoplasmic reticulum resident protein 29	cytoplasmic
O00151	14	864.1	41.3	0.00005	PDZ and LIM domain protein 1	cytoplasmic
P09382	4	250.6	41.2	0.00181	Galectin-1	extracellular
P61160	12	628.6	40.8	0.00043	Actin-related protein 2	membrane
P68036	2	76.6	40.8	0.01101	Ubiquitin-conjugating enzyme	nucleus
P0CG39	9	475.1	40.7	0.01954	POTE ankyrin domain family member J	unknown
Q0ZGT2	4	186.9	40.7	0.00128	Nexilin	membrane
P55209	2	174.8	40.6	0.00255	Nucleosome assembly protein 1	nucleus
P07339	3	133.0	40.0	0.00190	Cathepsin D	cytoplasmic
Q9NR31	2	88.1	39.1	0.00360	GTP-binding protein SAR1a	cytoplasmic
P00488	27	2052.5	38.2	0.00005	Coagulation factor XIII A chain	extracellular
P06733	19	1271.1	38.0	0.00006	Alpha-enolase	cytoplasmic
P52209	4	195.0	38.0	0.00417	6-phosphogluconate dehydrogenase	cytoplasmic
P63241	6	243.5	37.8	0.00151	Eukaryotic translation initiation factor 5A-1	cytoplasmic
P08311	3	94.0	37.4	0.00290	Cathepsin G	cytoplasmic
Q15404	13	564.7	37.4	0.00034	Ras suppressor protein 1	cytoplasmic

Appendix Table 1: Proteins present in the plaque debris – cont.

Uniprot Accession number	Peptide count	Confidence score	Fold change	Anova (p)	Description	Location
P37840	5	310.1	37.3	0.00248	Alpha-synuclein	cytoplasmic
P26038	21	1136.7	35.7	0.00006	Moesin	membrane
A0M8Q6	4	314.6	35.2	0.00051	Ig lambda-7 chain C region	unmapped
P20700	4	186.8	34.7	0.00547	Lamin-B1	nucleus
Q9NQC3	5	382.5	34.2	0.00178	Reticulon-4	cytoplasmic
P61586	6	329.3	33.9	0.00196	Transforming protein RhoA	cytoplasmic
P04179	8	473.3	33.9	0.00020	Superoxide dismutase	cytoplasmic
P00748	15	935.5	33.8	0.00023	Coagulation factor XII	extracellular
P27105	15	932.8	33.5	0.00002	Erythrocyte band 7 integral membrane protein	membrane
P04792	7	309.9	33.3	0.00057	Heat shock protein beta-1	cytoplasmic
P11216	5	157.4	33.2	0.00044	Glycogen phosphorylase	cytoplasmic
P06744	11	586.0	33.1	0.00327	Glucose-6-phosphate isomerase	extracellular
Q15555	8	453.8	32.9	0.00006	Microtubule-associated protein RP/EB family member 2	cytoplasmic
P05090	2	55.5	32.8	0.00303	Apolipoprotein D	extracellular
P02743	4	172.4	32.7	0.00091	Serum amyloid P-component	extracellular
Q15084	6	404.3	32.6	0.00023	Protein disulfide-isomerase A6	cytoplasmic
Q05682	14	656.8	32.3	0.00010	Caldesmon	cytoplasmic
P06576	12	676.8	32.3	0.00005	ATP synthase subunit beta	cytoplasmic
P60660	12	1078.5	31.9	0.00020	Myosin light polypeptide 6	cytoplasmic
P08567	20	1409.5	31.5	0.00002	Pleckstrin	cytoplasmic
P21333	150	12027.2	31.2	0.00004	Filamin-A	cytoplasmic
P23528	12	1158.7	31.1	0.00037	Cofilin-1	nucleus
P29401	6	319.3	31.0	0.00550	Transketolase	cytoplasmic
Q13011	2	79.5	30.7	0.00053	Delta(3,5)-Delta(2,4)-dienoyl-CoA isomerase	cytoplasmic
Q6ZNJ1	5	213.1	30.4	0.00127	Neurobeachin-like protein 2	cytoplasmic
Q9BXR6	2	98.3	30.1	0.01106	Complement factor H-related protein 5	extracellular
P10599	5	204.8	29.9	0.00071	Thioredoxin	cytoplasmic
O95810	15	1011.7	29.8	0.00021	Serum deprivation-response protein	membrane
P43652	3	86.8	29.1	0.00852	Afamin	extracellular
P02775	6	526.6	29.0	0.00122	Platelet basic protein	extracellular
Q9UK55	3	79.8	28.8	0.00003	Protein Z-dependent protease inhibitor	extracellular
Q06830	4	211.5	28.5	0.01595	Peroxiredoxin-1	cytoplasmic
P37802	14	1038.0	28.5	0.00015	Transgelin-2	cytoplasmic
Q9H4B7	28	1793.4	28.2	0.00011	Tubulin beta-1 chain	cytoplasmic
P30101	22	1444.1	28.1	0.00002	Protein disulfide-isomerase A3	cytoplasmic
Q04917	10	575.5	28.1	0.00029	14-3-3 protein eta	cytoplasmic
P08107	11	587.3	27.9	0.00007	Heat shock 70 kDa protein 1A/1B	unmapped
Q9BS26	2	76.3	27.8	0.00002	Endoplasmic reticulum resident protein 44	cytoplasmic
P50552	16	976.4	27.8	0.00013	Vasodilator-stimulated phosphoprotein	membrane
P10720	5	423.8	27.7	0.00801	Platelet factor 4 variant	extracellular
P04433	2	71.4	27.5	0.00569	Ig kappa chain V-III region VG	unmapped
P58546	3	344.5	27.5	0.00314	Myotrophin	nucleus
P61604	5	188.2	27.4	0.00252	10 kDa heat shock protein	cytoplasmic

Appendix Table 1: Proteins present in the plaque debris – cont.

Uniprot Accession number	Peptide count	Confidence score	Fold change	Anova (p)	Description	Location
P07737	12	920.8	27.4	0.00001	Profilin-1	cytoplasmic
P31949	3	188.0	26.5	0.00044	Protein S100-A11	cytoplasmic
P52907	7	333.0	26.2	0.00021	F-actin-capping protein subunit alpha-1	cytoplasmic
O00429	11	705.0	25.9	0.00148	Dynamin-1-like protein	cytoplasmic
P23284	9	495.7	25.6	0.00017	Peptidyl-prolyl cis-trans isomerase B	cytoplasmic
P52566	8	591.9	25.5	0.00562	Rho GDP-dissociation inhibitor 2	cytoplasmic
P47756	7	309.4	25.4	0.01108	F-actin-capping protein subunit beta	cytoplasmic
P10809	6	311.2	25.3	0.00097	60 kDa heat shock protein	cytoplasmic
Q00610	23	1120.2	25.2	0.00200	Clathrin heavy chain 1	membrane
P00742	3	162.7	24.7	0.02735	Coagulation factor X	extracellular
Q9Y277	5	195.8	24.5	0.00973	Voltage-dependent anion-selective channel protein 3	cytoplasmic
Q01518	19	1261.2	24.5	0.00036	Adenylyl cyclase-associated protein 1	membrane
P62937	14	905.9	24.3	0.00039	Peptidyl-prolyl cis-trans isomerase A	cytoplasmic
Q70J99	14	652.4	23.9	0.00013	Protein unc-13 homolog D	cytoplasmic
P02776	4	403.4	23.8	0.00207	Platelet factor 4	extracellular
P80511	4	258.4	23.8	0.00167	Protein S100-A12	cytoplasmic
P01860	16	1005.4	23.6	0.00591	Ig gamma-3 chain C region	extracellular
P04275	34	1791.9	23.1	0.00033	von Willebrand factor	extracellular
P55072	15	747.3	23.0	0.00325	Transitional endoplasmic reticulum ATPase	cytoplasmic
P55056	4	142.4	22.7	0.00015	Apolipoprotein C-IV	extracellular
Q6IBS0	4	293.6	22.7	0.00897	Twinfilin-2	cytoplasmic
P01877	20	1910.7	22.3	0.00366	Ig alpha-2 chain C region	extracellular
P62158	7	660.5	22.2	0.00005	Calmodulin	unmapped
P60174	12	833.8	22.2	0.00139	Triosephosphate isomerase	cytoplasmic
P05155	19	1453.4	22.0	0.00115	Plasma protease C1 inhibitor	extracellular
P01033	2	101.7	22.0	0.02676	TIMP 1	extracellular
P02730	2	137.1	21.7	0.01242	Band 3 anion transport protein	membrane
Q3ZCW2	4	161.4	21.4	0.00992	Galectin-related protein	unmapped
Q92954	8	472.5	21.1	0.01781	Proteoglycan 4	extracellular
P08758	4	245.3	20.9	0.04075	Annexin A5	membrane
P02747	4	186.1	20.8	0.01241	Complement C1q subcomponent subunit C	extracellular
P00918	10	471.9	20.6	0.00094	Carbonic anhydrase 2	cytoplasmic
Q14847	4	121.7	20.3	0.00028	LIM and SH3 domain protein 1	cytoplasmic
Q15942	22	1389.1	20.3	0.00500	Zyxin	membrane
P27797	17	920.7	20.2	0.00026	Calreticulin	cytoplasmic
P02792	3	152.3	20.2	0.03339	Ferritin light chain	cytoplasmic
P48047	2	88.0	20.0	0.01293	ATP synthase subunit O	cytoplasmic
P02794	4	146.9	19.8	0.01102	Ferritin heavy chain	cytoplasmic
P07237	16	629.5	19.7	0.00010	Protein disulfide-isomerase	cytoplasmic
P05543	10	480.4	19.6	0.00186	Thyroxine-binding globulin	extracellular
P07225	26	1668.9	19.3	0.00000	Vitamin K-dependent protein S	extracellular
Q99623	3	147.4	19.3	0.01376	Prohibitin-2	cytoplasmic
Q9H4M9	8	362.8	17.9	0.00011	EH domain-containing protein 1	cytoplasmic

Appendix Table 1: Proteins present in the plaque debris – cont.

Uniprot Accession number	Peptide count	Confidence score	Fold change	Anova (p)	Description	Location
P02654	6	336.9	17.5	0.00026	Apolipoprotein C-I	extracellular
Q9NZN3	11	430.6	17.3	0.00064	EH domain-containing protein 3	cytoplasmic
P27824	9	404.5	16.9	0.00096	Calnexin	cytoplasmic
P23083	3	159.0	16.3	0.00049	Ig heavy chain V-I region V35	unmapped
P20851	4	207.4	16.2	0.00409	C4b-binding protein beta chain	extracellular
P22626	2	63.2	16.0	0.03601	Heterogeneous nuclear ribonucleoproteins A2/B1	nucleus
P02042	14	1348.3	16.0	0.01377	Hemoglobin subunit delta	unknown
O75390	3	135.4	15.9	0.00403	Citrate synthase	cytoplasmic
P13796	8	322.9	15.9	0.00127	Plastin-2	cytoplasmic
Q8TF42	3	144.2	15.8	0.00354	Ubiquitin-associated/SH3 domain-containing protein B	unmapped
P27169	13	1082.7	15.7	0.00859	Serum paraoxonase/arylesterase 1	extracellular
Q99459	2	58.7	15.7	0.04226	Cell division cycle 5-like protein	nucleus
P04196	7	340.9	15.7	0.00165	Histidine-rich glycoprotein	extracellular
P02671	80	6416.7	15.6	0.00021	Fibrinogen alpha chain	extracellular
P61981	16	782.7	15.4	0.00292	14-3-3 protein gamma	cytoplasmic
P02679	46	4231.5	15.3	0.00028	Fibrinogen gamma chain	extracellular
P02649	20	1523.3	15.3	0.00070	Apolipoprotein E	extracellular
Q9Y251	9	502.1	15.2	0.00043	Heparanase	membrane
P08571	6	270.7	15.1	0.00188	Monocyte differentiation antigen CD14	membrane
P61626	6	231.4	14.9	0.00400	Lysozyme C	extracellular
P41226	3	126.7	14.7	0.00176	Ubiquitin-like modifier-activating enzyme 7	cytoplasmic
P49407	2	92.8	14.3	0.04805	Beta-arrestin-1	cytoplasmic
P07437	25	1770.9	14.2	0.00932	Tubulin beta chain	cytoplasmic
P10909	19	1263.6	14.2	0.00007	Clusterin	cytoplasmic
O75558	5	207.3	14.2	0.04697	Syntaxin-11	membrane
Q13642	7	308.7	13.5	0.01323	Four and a half LIM domains protein 1	cytoplasmic
Q9Y6C2	9	494.9	13.4	0.01159	EMILIN-1	extracellular
O00299	11	492.2	13.3	0.00285	Chloride intracellular channel protein 1	nucleus
P24158	4	201.1	13.0	0.00532	Myeloblastin	extracellular
O43866	14	889.3	12.8	0.00054	CD5 antigen-like	membrane
P02675	69	6277.2	12.8	0.00008	Fibrinogen beta chain	extracellular
P35858	11	818.3	12.7	0.00035	ILGF-binding protein complex acid labile subunit	extracellular
P04083	6	354.3	12.6	0.00641	Annexin A1	membrane
P06727	24	1821.4	12.6	0.00015	Apolipoprotein A-IV	extracellular
Q07960	4	144.1	12.5	0.00233	Rho GTPase-activating protein 1	cytoplasmic
P02647	36	2729.9	12.4	0.00021	Apolipoprotein A-I	extracellular
Q9H299	6	354.7	12.1	0.04063	SH3 domain-binding glutamic acid-rich-like protein 3	nucleus
P62805	5	322.5	11.7	0.01828	Histone H4	unmapped
P06396	33	2506.4	11.6	0.00046	Gelsolin	extracellular
P36980	9	489.9	11.4	0.00352	Complement factor H-related protein 2;	extracellular
P12259	13	452.1	11.4	0.00028	Coagulation factor V	membrane
Q16836	4	223.1	11.3	0.00526	Hydroxyacyl-coenzyme A dehydrogenase	cytoplasmic
P48059	18	970.4	11.3	0.00009	LIM and senescent cell antigen-like protein 1	membrane

Appendix Table 1: Proteins present in the plaque debris – cont.

Uniprot Accession number	Peptide count	Confidence score	Fold change	Anova (p)	Description	Location
P26927	7	387.6	11.3	0.00004	Hepatocyte growth factor-like protein	extracellular
P01591	5	289.4	11.2	0.00141	Immunoglobulin J chain	extracellular
Q99497	10	534.5	11.1	0.01030	Protein DJ-1	nucleus
P01861	14	933.7	11.0	0.00969	Ig gamma-4 chain C region	extracellular
P04040	17	907.1	10.9	0.00240	Catalase	cytoplasmic
P05452	6	345.3	10.8	0.00020	Tetranectin	extracellular
P08697	16	1167.5	10.5	0.00100	Alpha-2-antiplasmin	extracellular
P11142	23	1209.3	10.5	0.00758	Heat shock cognate 71 kDa protein	cytoplasmic
P03952	20	1102.3	10.3	0.00097	Plasma kallikrein	extracellular
P05109	9	511.2	10.3	0.01043	Protein S100-A8	cytoplasmic
P68871	18	2033.6	10.2	0.00675	Hemoglobin subunit beta	cytoplasmic
P30043	6	213.8	10.2	0.00686	Flavin reductase (NADPH)	cytoplasmic
P04264	20	1301.0	10.1	0.02730	Keratin, type II cytoskeletal 1	cytoplasmic
P04004	14	1021.8	10.0	0.00007	Vitronectin	extracellular
P13671	35	2473.8	9.8	0.00045	Complement component C6	extracellular
P69905	21	2228.9	9.7	0.00786	Hemoglobin subunit alpha	unmapped
Q15019	3	147.4	9.5	0.00755	Septin-2	cytoplasmic
Q16610	3	130.6	9.3	0.01512	Extracellular matrix protein 1	extracellular
P05164	28	1477.9	9.1	0.00078	Myeloperoxidase	cytoplasmic
P08133	2	66.5	9.1	0.00394	Annexin A6	membrane
Q99439	4	198.8	9.0	0.00864	Calponin-2	cytoplasmic
P01611	2	124.9	9.0	0.02338	Ig kappa chain V-I region Wes	unmapped
P61769	5	253.0	9.0	0.00198	Beta-2-microglobulin	membrane
P23219	6	280.0	8.9	0.02428	Prostaglandin G/H synthase 1	cytoplasmic
P61158	10	561.0	8.9	0.00867	Actin-related protein 3	membrane
P01766	3	242.2	8.8	0.02111	Ig heavy chain V-III region BRO	unmapped
Q96PD5	11	635.8	8.8	0.00026	N-acetylmuramoyl-L-alanine amidase	membrane
Q8NBS9	4	161.2	8.8	0.00924	Thioredoxin domain-containing protein 5	cytoplasmic
P19652	4	276.8	8.7	0.00342	Alpha-1-acid glycoprotein 2	extracellular
P29622	14	817.6	8.6	0.00124	Kallistatin	extracellular
P0C0L4	110	9581.8	8.6	0.00608	Complement C4-A	extracellular
P02765	9	834.7	8.6	0.00048	Alpha-2-HS-glycoprotein	extracellular
P0C0L5	110	9680.3	8.5	0.00052	Complement C4-B	extracellular
P08185	8	561.2	8.4	0.00425	Corticosteroid-binding globulin	extracellular
P02788	34	2681.5	8.4	0.00030	Lactotransferrin	extracellular
P23142	3	137.1	8.4	0.04137	Fibulin-1	extracellular
P01834	10	1298.6	8.4	0.03183	Ig kappa chain C region	extracellular
P36871	3	123.3	8.4	0.00697	Phosphoglucomutase-1	cytoplasmic
P02750	12	681.7	8.3	0.00027	Leucine-rich alpha-2-glycoprotein	extracellular
P02655	4	194.2	8.3	0.00195	Apolipoprotein C-II	extracellular
Q02985	3	193.3	8.2	0.02190	Complement factor H-related protein 3	extracellular
P02748	23	1976.8	8.2	0.00003	Complement component C9	extracellular
P32119	13	661.8	8.1	0.01885	Peroxiredoxin-2	cytoplasmic

Appendix Table 1: Proteins present in the plaque debris – cont.

Uniprot Accession number	Peptide count	Confidence score	Fold change	Anova (p)	Description	Location
P35542	9	499.5	8.1	0.00355	Serum amyloid A-4 protein	extracellular
Q13576	13	669.7	8.0	0.00675	Ras GTPase-activating-like protein	cytoplasmic
P07357	24	1860.5	8.0	0.00002	Complement component C8 alpha chain	extracellular
P04114	326	24490.4	8.0	0.00004	Apolipoprotein B-100	extracellular
P31946	10	622.4	7.9	0.03288	14-3-3 protein beta/alpha	cytoplasmic
P05546	25	1610.9	7.8	0.00048	Heparin cofactor 2	extracellular
P06681	23	1364.3	7.7	0.01100	Complement C2	extracellular
P0DJI8	8	690.7	7.7	0.00003	Serum amyloid A-1 protein	extracellular
P01617	3	254.0	7.6	0.00016	Ig kappa chain V-II region TEW	unmapped
P01008	29	1977.1	7.4	0.00722	Antithrombin-III	extracellular
P15169	10	849.7	7.4	0.00545	Carboxypeptidase N catalytic chain	extracellular
P01714	3	195.5	7.4	0.02768	Ig lambda chain V-III region SH	unmapped
P18428	6	372.9	7.3	0.04981	Lipopolysaccharide-binding protein	membrane
P49748	3	119.5	7.3	0.03397	Very long-chain specific acyl-CoA dehydrogenase	cytoplasmic
P02766	13	1224.9	7.1	0.00125	Transthyretin	extracellular
Q08380	3	111.3	7.1	0.03160	Galectin-3-binding protein	membrane
P00736	22	1515.9	7.0	0.00081	Complement C1r subcomponent	extracellular
P00915	15	929.5	7.0	0.00940	Carbonic anhydrase 1	cytoplasmic
P19827	42	3364.9	7.0	0.00434	Inter-alpha-trypsin inhibitor heavy chain H1	extracellular
P00747	55	4321.0	6.8	0.00025	Plasminogen	extracellular
P19823	36	2961.5	6.6	0.00008	Inter-alpha-trypsin inhibitor heavy chain H2	extracellular
P01042	28	2148.4	6.6	0.00007	Kininogen-1	extracellular
P35908	18	1153.6	6.4	0.00772	Keratin, type II cytoskeletal 2 epidermal	cytoplasmic
P06702	12	821.2	6.2	0.00411	Protein S100-A9	cytoplasmic
P51884	7	513.3	6.2	0.00414	Lumican	extracellular
P02751	92	7623.4	6.1	0.00004	Fibronectin	extracellular
P02652	8	533.0	6.1	0.00499	Apolipoprotein A-II	extracellular
P19971	3	103.0	6.1	0.02261	Thymidine phosphorylase	extracellular
P08519	10	709.0	6.1	0.00946	Apolipoprotein(a)	extracellular
P04003	23	1501.3	6.0	0.00233	C4b-binding protein alpha chain	extracellular
O75369	10	512.2	6.0	0.04560	Filamin-B	cytoplasmic
P02763	5	378.8	6.0	0.01407	Alpha-1-acid glycoprotein 1	extracellular
P01011	27	2140.0	5.9	0.00064	Alpha-1-antichymotrypsin	extracellular
P08603	79	5735.2	5.8	0.00019	Complement factor H	extracellular
P68402	2	101.2	5.8	0.00151	Platelet-activating factor acetylhydrolase IB subunit β	cytoplasmic
B9A064	7	653.9	5.7	0.01407	Immunoglobulin lambda-like polypeptide 5	membrane
P07358	25	1849.9	5.7	0.00039	Complement component C8 beta chain	extracellular
P01857	22	1682.8	5.7	0.04832	Ig gamma-1 chain C region	extracellular
P00738	36	2794.6	5.6	0.01545	Haptoglobin	extracellular
Q9Y4L1	3	105.1	5.6	0.02476	Hypoxia up-regulated protein 1	cytoplasmic
P02787	83	7365.1	5.5	0.00279	Serotransferrin	extracellular
P01833	9	408.9	5.3	0.00164	Polymeric immunoglobulin receptor	membrane
P00751	52	4349.2	5.2	0.00003	Complement factor B	extracellular

Appendix Table 1: Proteins present in the plaque debris – cont.

Uniprot Accession number	Peptide count	Confidence score	Fold change	Anova (p)	Description	Location
P01602	3	239.1	5.2	0.04801	Ig kappa chain V-I region HK102	extracellular
Q14520	14	725.1	5.1	0.01273	Hyaluronan-binding protein 2	extracellular
P35527	12	718.0	5.0	0.01381	Keratin, type I cytoskeletal 9	cytoplasmic
P01620	5	446.2	4.9	0.02103	Ig kappa chain V-III region SIE	unmapped
P05154	5	314.0	4.9	0.03894	Plasma serine protease inhibitor	extracellular
P59665	4	201.5	4.9	0.02638	Neutrophil defensin 1	unmapped
P00734	33	2657.9	4.8	0.00564	Prothrombin	extracellular
P20742	28	1712.9	4.8	0.00043	Pregnancy zone protein	extracellular
P01024	177	15402.1	4.7	0.00085	Complement C3	extracellular
P00450	42	2918.7	4.7	0.00037	Ceruloplasmin	extracellular
P36955	14	813.6	4.7	0.00198	Pigment epithelium-derived factor	extracellular
P10412	3	151.7	4.6	0.02548	Histone H1.4	nucleus
P02749	22	1785.3	4.5	0.00216	Beta-2-glycoprotein 1	extracellular
P01009	55	4703.4	4.4	0.00517	Alpha-1-antitrypsin	extracellular
P10643	19	1270.1	4.3	0.01092	Complement component C7	extracellular
P31146	11	644.7	4.2	0.00604	Coronin-1A	cytoplasmic
P02760	15	1152.2	4.1	0.00441	Protein AMBP	extracellular
P03951	7	353.8	4.0	0.01375	Coagulation factor XI	extracellular
P01023	132	11171.4	4.0	0.00088	Alpha-2-macroglobulin	extracellular
P01031	85	5963.0	4.0	0.00568	Complement C5	extracellular
P02768	78	6874.3	3.8	0.02121	Serum albumin	extracellular
P01859	15	701.8	3.5	0.02532	Ig gamma-2 chain C region	membrane
P01019	16	1517.9	3.3	0.01021	Angiotensinogen	extracellular
P02790	36	2327.1	3.1	0.00096	Hemopexin	extracellular
Q96IY4	2	113.6	3.1	0.01016	Carboxypeptidase B2	extracellular
P05156	17	1238.6	3.0	0.03075	Complement factor I	extracellular
P02774	39	2985.5	3.0	0.00643	Vitamin D-binding protein	extracellular
Q14624	47	4304.9	3.0	0.00754	Inter-alpha-trypsin inhibitor heavy chain H4	extracellular
P07360	8	770.4	3.0	0.03299	Complement component C8 gamma chain	extracellular
P22792	9	468.8	2.9	0.02573	Carboxypeptidase N subunit 2	extracellular
P01880	7	380.1	2.9	0.00987	Ig delta chain C region	extracellular
Q06033	22	1218.3	2.7	0.04222	Inter-alpha-trypsin inhibitor heavy chain H3	extracellular
P01876	25	2232.7	2.3	0.02935	Ig alpha-1 chain C region	extracellular
P09871	28	1722.3	2.1	0.00723	Complement C1s subcomponent	extracellular
O95445	3	104.5	2.0	0.02105	Apolipoprotein M	membrane
O14791	16	858.7	1.9	0.02960	Apolipoprotein L1	extracellular

Appendix Table 1: Proteins present in the plaque debris – cont.

CHAPTER 8

APPENDICES

8.1 Timing and venue of research

The experiments detailed in this thesis were conducted between October 2009 and July 2013. Participants in this study were recruited from the Department of Cardiology at John Radcliffe Hospital, Oxford. Laboratory experiments were performed in the University of Oxford Department of Cardiovascular Medicine laboratory at John Radcliffe hospital, and Dr Kessler's laboratory at Center of Cellular and Molecular Physiology laboratory, Wellcome Trust Centre of Human Genetics. Dr Kessler's laboratory subsequently re-located to the Target Discovery Institute, where some of the experiments were performed.

8.2 Sources of funding

The Plaque Imaging and Biomarker Study was funded by the NIHR Oxford Biomedical Research Centre and supported by the British Heart Foundation Centre of Research Excellence at Oxford.

Regent Lee was further funded by the Royal Australasian College of Surgeons through the following Scholarships:

2011 Lumley Surgical Research Fellowship

2012 Foundation of Surgical Research Scholarship

2013 Surgeon Scientist Scholarship

2014 Foundation of Surgical Research Scholarship

8.3 Attributions

Apart from the exceptions described below, the Author is directly responsible for the conduct of research underpinning this Thesis.

The protocol for the Plaque Imaging and Biomarker study was written and submitted for regulatory approvals by Dr David Adlam, who also independently analysed the OCT images for the study. Blood/tissue sampling and acquisition of OCT images during PCIs were performed by the interventional cardiologist(s) for each case. A subset of subjects included for the analysis in the pre-analytic effect of plasma preparation was recruited from the Adiporedox Study by Dr Alexios Antonopoulos and Dr Marios Margaritis (Ethics Ref: 11/SC0140). Dr Charalambos Antoniades provided advice on many key aspects of the study related to candidate marker measurement and analysis. In the Kessler Lab: Dr Philip Charles provided advice on statistics, and performed off line analysis using *R* or Perl scripts for several sections in this study; Dr Katalin Di Gleria offered generous assistance to familiarise me with the MALDI-TOF-MS workflow, and performed the pilot experiments (not included in this thesis); Dr Alessandro Valli assisted me in the development of organic extraction protocol for plaque debris, performed the pilot experiments (not included in this thesis), and provided guidance on the LC-MS metabolomics workflow throughout; Dr Joanna McGouran performed the initial pilot experiments on plaque proteomics (not included in this thesis); Dr Roman Fischer at the Kessler Lab provided generous teaching on proteomics throughout this research, and assisted with the sample preparation, data acquisition and initial data analysis for proteomics.

8.4 Research Publications arising from work in this thesis

- **Lee R**, Antonopoulos AS, Alexopoulou Z, Margaritis M, Kharbanda RK, Choudhury RP, Antoniades C, Channon KM. Artifactual elevation of plasma sCD40l by residual platelets in patients with coronary artery disease. International Journal of Cardiology. 2013 Sep 30; 168(2):1648-50

- **Lee R**, Adlam D, Antoniades C, Digby JE, Kharbanda RK, Choudhury RP, Channon KM. Heparin administration leads to rapid decrease in plasma matrix metalloproteinase-9. International Journal of Cardiology. 2013;163:212-213

8.5 Other publications during DPhil study

- Kaudewitz D*, **Lee R*,** Willeit P, McGregor R, Markus HS, Kiechl S, Zampetaki A, Storey RF, Channon KM, Mayr M. Impact of intravenous heparin on quantification of circulating microRNAs in patients with coronary artery disease. Thrombosis and Haemostasis. 2013;110:609-615 (* Joint First Author)

- Margaritis M, Antonopoulos AS, Digby J, **Lee R**, Reilly S, Coutinho P, Shirodaria C, Sayeed R, Petrou M, De Silva R, Jalilzadeh S, Demosthenous M, Bakogiannis C, Tousoulis D, Stefanadis C, Choudhury RP, Casadei B, Channon KM, Antoniades C. Interactions between vascular wall and perivascular adipose tissue reveal novel roles for adiponectin in the regulation of endothelial nitric oxide synthase function in human vessels. Circulation. 2013;127:2209-2221

- Cunnington C, Van Assche T, Shirodaria C, Kylintireas I, Lindsay AC, Lee JM, Antoniades C, Margaritis M, **Lee R**, Cerrato R, Crabtree MJ, Francis JM, Sayeed R, Ratnatunga C, Pillai R, Choudhury RP, Neubauer S, Channon KM. Systemic and vascular oxidation limits the efficacy of oral tetrahydrobiopterin treatment in patients with coronary artery disease. Circulation. 2012;125:1356-1366

- Adlam D, Antoniades C, **Lee R**, Diesch J, Shirodaria C, Taggart D, Leeson P, Channon KM. Oct characteristics of saphenous vein graft atherosclerosis. JACC Cardiovasc Imaging. 2011;4:807-809

- **Lee R**, Margaritis M, Channon KM, Antoniades C. Evaluating oxidative stress in human cardiovascular disease: Methodological aspects and considerations. Curr Med Chem. 2012;19:2504-2520

- **Lee R,** Channon KM, Antoniades C. Therapeutic strategies targeting endothelial function in humans: Clinical implications. Curr Vasc Pharmacol. 2012;10:77-93

- Psarros C, **Lee R,** Margaritis M, Antoniades C. Nanomedicine for the prevention, treatment and imaging of atherosclerosis. Nanomedicine: nanotechnology, biology, and medicine. 2012;8 Suppl 1:S59-68

- Antonopoulos AS, Margaritis M, **Lee R,** Channon K, Antoniades C. Statins as anti-inflammatory agents in atherogenesis: Molecular mechanisms and lessons from the recent clinical trials. Curr Pharm Des. 2012;18:1519-1530

- Antonopoulos AS, **Lee R**, Margaritis M, Antoniades C. Adiponectin as a regulator of vascular redox state: Therapeutic implications. Recent Patents on Cardiovascular Drug Discovery. 2011;6:78-88

- **Lee R**, Antoniades C, Adlam D, Channon KM. Treatment of recurrent vein graft "stent-in-stent" re-stenosis guided by optical coherence tomography. International Journal of Cardiology. 2012;156:e20-21

- **Lee R,** Adlam D, Clelland CA, Channon KM. Lines of Zahn in coronary artery thrombus. European Heart Journal. 2012;33:1039

- Mayr M, **Lee R**, Kaudewitz D, Zampetaki A, Channon KM. Letter to the Editor: Effects of Heparin on Temporal MicroRNA Profiles. Journal of American College of Cardiology. 2013 Nov 25. doi:pii: S0735-1097(13)06231-1. 10.1016/j.jacc.2013.07.118. [Epub ahead of print]

- **Lee R**. Preanalytic considerations for using plasma myeloperoxidase as a biomarker in acute coronary syndrome. American heart journal. 2012;163:e39-40; author reply e41

- **Lee R**. Matrix metalloproteinase-9 in patients with acute coronary syndrome. Chin Med J (Engl). 2012;125:720

- **Lee R**. Methodological considerations for utilizing plasma matrix metalloproteinase-9 as a biomarker in acute vascular syndromes. Circ J. 2012;76:1044; author reply 1045

- **Lee R,** Antoniades C. Thiobarbituric acid reactive substances as a biomarker for coronary heart disease. Journal of atherosclerosis and thrombosis. 2011;18:1127-1128

- **Lee R**. Letter by Lee regarding article, "cc chemokine receptor-1 activates intimal smooth muscle-like cells in graft arterial disease". Circulation. 2010;121:e437; author reply e438

8.6 Abstracts presented at scientific conferences

- **Lee R,** Adlam D, Fischer R, Di Gleria K, Valli A, Charles, P, McGouran J, Ruparelia N, Dawkins S, Kharbanda KK, Choudhury RP, Antoniades C, Kessler BM, Channon KM. Integrated plaque and plasma proteo-lipidomics reveal novel signatures of coronary atherosclerotic plaque disruption AHA Dallas 2013 (oral presentation – Council of Clinical Cardiology International Mentor Program Travel Award)

- **Lee R**, Antonopoulos AS, Alexopoulou Z, Margaritis M, Kharbanda RKK, Choudhury RP, Antoniades C, Channon KM. Artifactual elevation of plasma sCD40L by residual platelets in cardiovascular disease. European Atherosclerosis Society Congress Lyon 2013 (poster presentation– Trinity College Briton Travel Grant)

- **Lee R**, Channon KM. Pre-analytic pitfalls leading to artifactual biomarker changes in clinical cardiovascular research. University of Oxford Medical Sciences Division DPhil Open day 2013 (Award for Best Oral Presentation)

- **Lee R**, Channon KM. Pre-analytic pitfalls leading to artifactual biomarker changes in clinical cardiovascular research. ANZSVS Congress 2013, Hobart, Australia (oral presentation)

- **Lee R,** Adlam D, Antoniades C, Kharbanda RK, Choudhury RP, Channon KM. Plaque morphology on optical coherence tomography determines biomarker response after stent induced plaque rupture. *Eur Heart J* (2012):33 (Abstract supplement):1-18 (ESC Congress Munich 2012) (oral presentation - ESC BCVS council travel award)

- **Lee R,** Antoniades C, Adlam D, Choudhury RP, Kharbanda RK, Channon KM. Differential biomarker release after percutaneous coronary intervention reflects early vascular remodelling, myocardial injury and systemic inflammatory response. International Atherosclerosis Society Congress Sydney 2012 (poster presentation – Early Career Poster Award)

- **Lee R**, Antoniades C, Adlam D, Choudhury RP, Kharbanda RK, Channon KM. Matrix metalloproteinase 9 is involved in human coronary artery remodelling after plaque disruption by percutaneous coronary angioplasty. International Atherosclerosis Society Congress Sydney 2012 (poster presentation)

8.7 Figure legends not included in main text

Figure 1: Dynamic nature of plaque progression and potential biological signatures of plaque rupture

Plaque progression is a dynamic process, whereby plaque rupture can trigger significant arterial thrombosis and clinical complications, or remain clinically silent and results in plaque remodelling and contributes to stepwise progression of the lesion. Such divergent pathological cascades can be the results of differential biological pathway(s) activation after the plaque rupture event. For example, plaque rupture may lead to the acute release of protein molecules that activate an enzymatic pathway, and corresponding changes of the substrates involved in the process. Alternatively, the acutely released substance(s) can mediate biological signals, resulting in activation of other cell types and secondary uptake or release of molecules and further downstream signalling as a para-phenomenon (Figure 1). Such complex interactions form the spectrum of biomarkers the plaque rupture event, but are

challenging to characterise using conventional candidate marker based research techniques. Such Plaque rupture

Figure 2: Summary of study procedures and blood sampling time points

(A): In this research, percutaneous coronary intervention (PCI) with stenting of the lesion was used as the model to induce plaque disruption *in vivo* to mimic plaque rupture. Patients aged 30-90 who were referred for non-emergency coronary angiography with the view to proceed to stenting were invited to participate in the study. Coronary angiography procedure was performed by the interventional cardiologist(s) in accordance to routine clinical practice. Optical coherence tomography of the diseased coronary artery segment was performed prior to the deployment of stent in a subset of patients, as deemed anatomically suitable by the interventional cardiologist. Where clinically indicated, a distal protection device was used to prevent downstream embolisation and for the retrieval of cellular debris liberated by the stent placement. Blood samples were collected from targeted anatomical sites, at specific time points in reference to stent placement. This included coronary aspiration catheter for sampling of arterial blood downstream of the lesion, and/or coronary sinus sampling in a subset of subjects. Platelet poor plasma were prepared from each blood sample, and stored in -80°C for subsequent analysis.

(B): This table presents the full schedule of blood sampling planed for each patient. At the early time points (at baseline, and at 5 minutes / 15 minutes after plaque disruption), paired samples were collected from coronary artery, peripheral vein, and coronary sinus at baseline. Peripheral venous blood sampling continued at subsequent time points (at 30 minutes, 1 hour, 2 hours, 6 hours, and 18 hours after plaque disruption). The same time points were applied to diagnostic angiography patient where there was no plaque disruption. Therefore, the beginning of the procedure (baseline) was used as the reference for subsequent time points.

***** Where anatomically feasible, coronary arterial blood sample downstream of the disrupted plaque were collected using an *aspiration catheter* at 5 minutes and 15 minute. Otherwise proximal coronary blood was collected using a *guide catheter*.

Figure 5: Flowchart for the centrifugation protocol to obtain plasma with differential residual platelet counts, and the experimental design to test the effect of residual platelet count on the level of plasma candidate markers

Protocol A was designed to obtain plasma enriched with platelets. [Platelet rich plasma (PRP)]. In this protocol, whole blood (WB) was centrifuged at 200g for 12 minutes. The resultant supernatant (PRP1) was transferred to a tube without additive. A fraction of this PRP1 was stored at -80°C. The residual fraction was subjected to an additional centrifugation at 200g for 15 minutes to obtain PRP2 and stored at -80°C.

Protocol B was designed to obtain routine plasma, and subsequently platelet poor plasma (PPP) from the same patient. WB was centrifuged at 1300g for 12 minutes. The supernatant layer, containing "routine" plasma, was transferred to a tube without additive. A fraction of the plasma was stored at -80°C. The residual fraction was centrifuged at 2500g for 15 minutes to obtain PPP and stored at -80°C.

Experiment I was designed to investigate the effect of residual plasma platelet on subsequent candidate marker measurement in plasma. All steps in experiment I were performed in room temperature.

Experiment II was designed to investigate the effect of temperature (during transit and centrifugation) on residual platelets and candidate marker measurement in the resultant plasma matrix. In this experiment, paired samples were prepared either under room temperature (RT) or refrigerated conditions (transferred on ice, centrifuged at 4°C).

Figure 6: Significant correlations between residual plasma platelets and soluble CD40 ligand in both healthy volunteers and CAD patients

Plasma samples with differential residual platelet counts were collected from healthy volunteers (HV, n=15) or subjects with coronary artery disease (CAD, n=15), using the staged centrifugation protocols described in section 2.6.1 of this thesis. Platelet counts were measured by Sysmex XE2100 analyser immediately after sample preparation. Quantification of sCD40L was performed using an enzyme-immunoassay. Data are presented by median and the range between 10-90 percentile. Wilcoxon matched-pairs signed rank tests were used for comparisons between the sample types within each cohort. P values of less than 0.05 were considered statistically significant.

Plasma prepared using different protocols resulted in gradients of residual platelet counts in both the HV and CAD samples. After the first centrifugation step at 1300g for 12 minutes, a proportion of the samples (Plasma) did not fulfil the criteria for platelet poor plasma (PPP, as defined by platelet count<$10x10^3/\mu l$). After the second centrifugation at 2500g for 15 minutes, all fulfilled the PPP criteria (Panel A, B).

In both HVs and CAD patients, the centrifugation protocol resulted in significant reduction of residual platelets between PRP1/PRP2, and between plasma/PPP (Panel A, B). Progressive removal of platelets also resulted in significant reduction of sCD40L between PRP1/PRP2, and between plasma/PPP (C, D; P<0.001 for all). Samples which contained more than $10x10^3/\mu l$ platelets (non-PPPs) and sCD40L level above the LLOQ were included to assess their association using Spearman's Rank correlation. In both HVs and CAD patients, there was a highly significant correlation between the residual platelet and sCD40L in the sample (Panel E, F; P<0.0001 for both).

(*Lee, R., et al. Int J Cardiol, 2013. Sep 30;168(2):1648-50*[81] *This figure is reproduced with permission from Elsevier*)

Figure 8: Comparison between protein profiles in paired plasma samples prepared using EDTA or lithium heparin as anticoagulant

Panel A: Paired EDTA (ethylene-diamine-tetra-acetic acid) and lithium heparin (LH) platelet poor plasma (PPP) sample (n=2) were prepared using the staged centrifugation protocol specified in Section 2.7 of this thesis. Plasma proteomic screen was performed according to methods described in Chapter 5. The samples were analysed in technical duplicates. Principal component analysis (PCA) scores plot of the proteomic profiles showed distinct separations between the paired plasma prepared using different anticoagulant

Panel B: While the majority of proteins showed no differences in abundance between the two plasma types, the levels for 41 proteins differed significantly between the paired PPP samples. LH samples contained significantly lower abundance of 33 proteins, while EDTA sample had lower abundance in 8 proteins (X axis: technical replicates for each subject; Y axis: normalised abundance of each protein; each line represents a protein feature).

Panel C: Amongst the significantly different proteins, matrix metalloproteinase 9 (MMP9) was one of the proteins found to be lower in abundance in LH samples (X axis: type of plasma; Y axis: normalised abundance; data are presented as mean ± SD; *:$P<0.05$).

Panel D: A separate experiment was performed using paired EDTA and LH PPP samples collected from patients with coronary artery disease (CAD, n=6). The levels of MMP9 in were measured using enzyme immunoassay (EIA). Levels of MMP9 were significantly lower in LH plasma compared to EDTA plasma. (bars represent median, *:$P<0.05$ by Wilcoxson matched pair signed rank Test.)

Figure 9: Comparison between metabolite and lipid profiles in paired plasma samples prepared using EDTA or lithium heparin as anticoagulant

Paired EDTA (ethylene-diamine-tetra-acetic acid) and lithium heparin (LH) platelet poor plasma (PPP) sample (n=2) were prepared using the staged centrifugation protocol described in Section 2.7 of this thesis. Plasma small molecules screen was performed according to methods described in Chapter 4. Principal component analysis (PCA) scores plot of the metabolomics profile (Panel A) and lipidomics profile (Panel B) showed distinct separations between the paired plasma prepared using different anticoagulants.

Figure 12: Representative features of coronary artery obtained by intravascular optical coherence tomography imaging

Intravascular optical coherence tomography (OCT) imaging of coronary arteries was performed according to methods described in section 3.5.2 of this thesis. In a normal coronary artery, the vessel wall appears as a tri-laminar structure (Panel A). The circular rings in the lumen are due to image artifacts from the imaging wire (Panel A, white arrow). The presence of a lipid rich core can be readily differentiated from other lesions which contain mainly a calcific or fibrotic core. Necrotic lipid cores typically have a poorly delineated and diffuse distal border surrounding signal poor regions (lipid pool, Panel B, white arrow). The overlying signal rich band corresponds to the fibrous cap (Panel B, yellow arrow). The presence of a thin fibrous cap overlying a lipid pool in Panel B is consistent with the morphology of a thin cap fibro-atheroma. In contrast, calcific contents within the plaque typically appear as well-delineated regions with relatively low reflectivity and low attenuation to light (Panel C, white arrow), while fibrous plaques appear as well-delineated, homogenous regions with high back scattering (Panel D, white arrow).

Figure 15: Baseline comparison of candidate marker levels between CAD patients who presented with acute coronary syndrome or stable angina

EDTA plasma was collected from subjects with coronary artery disease at the baseline of the percutaneous coronary intervention procedure according to methods described in section 2.3 and 2.4 of this thesis. Levels of candidate markers (MMP2, MMP3, MMP8, MMP9, TIMP1, TIMP2 and TIMP4) were measured using Luminex® assays. Subjects were grouped according to clinical status at presentation [acute coronary syndrome (ACS) n= 21; stable angina pectoris (SAP), n= 37] for comparison. Comparisons between groups were made using Mann-Whitney tests. P values less than 0.05 were considered to be statistically significant. Significantly higher levels were observed in MMP8, MMP9, TIMP1 and TIMP4 were observed in subjects who presented with ACS than SAP. (Data are presented as median with interquartile range).

Figure 17: Evidence of myocardial injury and systemic inflammation after plaque disruption

Peripheral venous blood was collected from subjects with coronary artery disease undergoing either percutaneous coronary intervention (PCI) or diagnostic (Dx) angiography according to methods described in Section 2.3 and 2.4 of this thesis. Plasma levels of Creatin Kinase–MB (CKMB), cardiac troponin I (TnI) and c-reactive protein (CRP) at baseline (0hr), at 6 hours (6hr) and 8 hours (8hr) were measured (by the biochemistry laboratory at John Radcliffe Hospital). Comparison within group was performed Wilcoxon matched pair signed rank test. P values less than 0.05 were considered statistically significant. Values below the lower limit of quantification (LLOQ) for CKMB and TnI were assigned an arbitrary value at ½ the value of LLOQ to allow for comparison. (Data are presented as median with interquartile range.)

Baseline levels of CKMB, TnI and CRP were significantly higher in the subject who presented with acute coronary syndrome (ACS) as compared to those who presented with stable angina (SAP) (Panel B, D). Amongst the subjects who received PCIs, plasma level of CKMB and TnI were significantly increased by 18 hours after the procedure (Panel A, C). These changes were particularly pronounced in the SAP group after PCI (Panel B, D). Similar patterns of change were also observed for CRP (Panel E, F). No significant changes in CKMB and TnI were observed in the control subjects without plaque disruption, although significant increase in CRP was also observed in the control group at 18 hours after the diagnostic (Dx) angiography (Panel E). Amongst subjects who underwent PCI, the area under curve (AUC) for CKMB and TnI correlated significantly with the AUC of CRP (Panel G, H).

Figure 18: Plasma levels of MMP8 and MMP9 after plaque disruption

Peripheral venous blood was collected from subjects with coronary artery disease undergoing either percutaneous coronary intervention (PCI) or diagnostic (Dx) angiography according to methods described in Section 2.3 and 2.4 of this thesis. Levels of MMP8 and MMP9 were measured using Luminex® assays. Subjects were further grouped according to clinical status at presentation [acute coronary syndrome (ACS) or stable angina (SAP)]. Comparisons within groups, between subsequent time points and baseline (0min), were made using Wilcoxson matched pair sign rank tests. P-values less than 0.01 were considered to be statistically significant, to correct for multiple testing. (Data are presented as median with interquartile range.)

Significant increases in plasma levels of MMP8 and MMP9 were observed at various time points. For MMP9, significant elevation was observed as soon as 30 minutes after plaque disruption (Panel A); for MMP8, the significant elevation was observed by 2 hours after plaque disruption (Panel B). When examined in subgroups according to clinical status, there was differential trend of MMP8 and MMP9 between patients who presented with ACS or SAP (Panel C, D, E, F). For both MMP8 and MMP9, significant elevations after plaque disruption were observed earlier in ACS patients. The peak levels of MMP8 and MMP9 in SAP patients were observed at 6 hours after plaque disruption, and reached similar levels observed at baseline in ACS patients. Trends observed within the diagnostic angiography group did not reach statistical significance (Panel G, H).

Figure 19: Plasma levels (fold change) of MMP2, MMP3, MMP8, MMP9, TIMP1, TIMP2, and TIMP4 after plaque disruption

Peripheral venous blood was collected from subjects with coronary artery disease undergoing either percutaneous coronary intervention (PCI) or diagnostic (Dx) angiography according to methods described in Section 2.3 and 2.4 of this thesis. Levels of these candidate markers were measured using Luminex® assays. Subjects were further grouped according to clinical status at presentation to ascertain trends within the subgroup. The level of each candidate marker at subsequent time points were normalised against baseline (fold change). Area under curve (AUC) for each subject over the entire time course was calculated for each candidate marker. Comparisons were made between groups by ANOVA. P values less than 0.05 were considered to be statistically significant. (Data at each time point are presented as mean±SEM).

AUC of MMP9 ($MMP9_{AUC}$) was significantly higher in the ACS subjects after plaque disruption compared to control subjects who received Dx angiography, but was not different between the SAP and control subjects (Panel-D). Amongst the other candidate markers, significant difference between the ACS and Dx subjects was observed only in $MMP3_{AUC}$ (Panel B). There was no statistically significant difference in the AUC between SAP and ACS subjects, or the AUC between SAP and Dx subjects, in the remaining candidate markers.

Figure 20: Comparison of MMP9 and TIMP1 after plaque disruption according to clinical status and plaque morphology

Subjects undergoing PCI (n=58: ACS n=21, SAP n=37) were recruited for serial blood sampling according to methods described in section 3.5. OCT images were obtained in a subset of these subjects (n=36). Plaque morphology was classified as either lipid rich (n=23) or non-lipid (n=13) based on the scoring system outlined in Section 3.3. Plasma levels of MMP9 and TIMP1 were measured using Luminex® assays.

Panel A: Significance of fold change at each time point was tested using one-sample t-test (against a theoretical value of 1). Comparison between subgroups at each time point was performed by unpaired t-test. P value less than 0.05 was considered significant. The trend for MMP9 and TIMP1 amongst subjects with lipid plaques closely mimicked the trend for patients presenting with ACS. Vice versa between subjects presenting with SAP and those found to have non-lipid target lesions on OCT. The early elevation of MMP9 in subjects with lipid rich plaques was subsequently followed by a significant increase in plasma TIMP1 at 18 hours after plaque disruption. This pattern was not observed in subjects with non-lipid plaques. Higher fold changes at 6 and 18 hours after plaque disruption were observed in lipid rich plaques. (Data at each time point after plaque disruption are expressed as fold change against baseline and as mean±SEM.

Panel B: Comparisons were made between groups using AUC for MMP9 over the 18 hours after plaque disruption. $MMP9_{AUC}$ was significantly higher for patients with lipid rich plaques compared to non-lipid plaques; whereas no significant difference was observed in $MMP9_{AUC}$ between subjects who presented with ACS or SAP. (Data are presented as median with interquartile range)

Panel C: Logistic regression analysis was performed by SPSS, using the two independent variables (clinical status and plaque morphology) in a backward elimination approach to assess their effect on MMP9 release after plaque disruption (as reflected by $MMP9_{AUC}$). Plaque morphology, not clinical status, was the only significant predictor of MMP9 release after plaque disruption, having accounted for the clinical status of each individual subject ($P<0.05$).

Figure 21: Candidate marker response after plaque disruption, stratified by area under curve over the entire time course

Subjects undergoing PCI (n=58) or Dx angiography (n=16) were recruited for serial blood sampling according to methods described in section 3.5. Venous plasma levels of candidate markers were measured using Luminex® assays. The level of each candidate marker at subsequent time points after plaque disruption were normalised against baseline (to obtain fold change). Area under curve (AUC) for a subject over the entire time course was calculated for each candidate marker. For each candidate marker, PCI subjects were stratified into tertiles according to the AUC, while Dx angiography subjects were stratified in halves ($Dx^{upper1/2}$ – above median AUC, $Dx_{lower1/2}$ – below median AUC). PCI subjects within the highest tertile ($PCI^{upper1/3}$) were compared against the Dx angiography subgroups using ANOVA. P-values less than 0.05 were considered to be statistically significant. (Data at each time point are presented as mean±SEM)

In each candidate marker analysed, significant differences in time course were observed between the AUC for $PCI^{upper1/3}$ and the control subjects within the lower half of AUC ($Dx_{lower1/2}$). Significant difference between the $PCI^{upper1/3}$ and the Dx angiography subjects within the upper AUC half ($Dx^{upper1/2}$) was only observed in MMP9 and MMP8.

Figure 22: Correlations between MMPs, TIMPS to CRP, CKMB and cTnI

Subjects undergoing PCI (n=58) were recruited for serial blood sampling according to methods described in section 3.5. Plasma levels of MMPs and TIMPs were measured using Luminex® assays. Plasma level of CRP, CKMB and cTnI were measured by the hospital laboratory. Area under curve (AUC) for a subject over the entire time course was calculated for each candidate marker. Correlations between the AUC of candidate markers were assessed using the Spearman correlation with permutation testing, and Bonferroni correction for multiple testing, as described in section 3.5.7. A Bonferroni-corrected p-value of <0.01, and Spearman rho-value within the 99% confidence interval of the null hypothesis (-0.344021 to 0.345041) were considered significant.

Panel A: correlation matrix containing the Spearman rho-value and Bonferroni corrected p-values. Statistically significant values are highlighted in yellow. MMP2, MMP3, MMP8, TIMP1, TIMP2 and TIMP4 were significantly correlated with at least one of CRP, CKMB, or cTnI. MMP2, MMP3 and TIMP1 were only significantly correlated with CKMB and cTnI, and MMP8 was only significantly correlated with cTnI. MMP9 was the only candidate marker that did not show statistically significant correlation to CRP, CKMB or cTnI.

Correlation to $cTnI_{AUC}$ to each of the MMPs and TIMPs is further illustrated in the rest of the figure.

Figure 23: Changes in arterial MMP9 at early time points after plaque disruption

Blood samples were collected from subjects with coronary artery disease undergoing either PCI or Dx angiography according to methods described in Section 2.3 and 2.4 of this thesis. In patients with suitable anatomical features, optical coherence tomography, and/or blood sampling of coronary arterial blood downstream of the disrupted plaque at 5 and 15 minutes downstream of the disrupted plaque (by aspiration catheter) were performed. Otherwise proximal coronary arterial blood samplings (by guide catheter) were performed at 5 and 15 minutes using a routine guide catheter. Plaque morphology on OCT was defined using the method described in section 3.5.2. Plasma levels of MMP9 were measured using Luminex® assays. Data for each candidate marker measurement were log transformed. Comparisons within groups, between subsequent time points and baseline (0min), were made using paired t-tests. P values less than 0.05 were considered to be statistically significant. (Data are presented in median with interquartile range).

Panel A: Amongst all PCI (n=58) subjects, no significant change in plasma MMP9 was observed in arterial blood (collected by either a coronary artery guide catheter or an aspiration catheter) at 5 or 15 minutes after stenting. [#Control in this graph refers the Dx angiography subjects (n=16, light grey).] **Panel B**: amongst the subgroup of patients (n=30, dark grey) in whom coronary blood sampling at these time points were performed by an aspiration catheter advanced downstream of the stented lesion, no changes in MMP9 was observed at 5 or 15 minutes after plaque disruption. [#Control in this graph refers to the subjects in who proximal coronary arterial blood were collected using a guide catheter at 5 and 15 minutes (n=28, light grey)]. **Panel C**: Subjects who had proximal arterial blood collection by guide catheter were grouped according to clinical status (ACS: n=11, SAP: n=17. There were no significant changes in *arterial* MMP9 at 5 or 15 minutes in either group. **Panel D**: Subjects who had arterial blood downstream of the disrupted plaque (by an aspiration catheter) were grouped according to clinical status (ACS: n=10, SAP: n=20). Significant elevations of MMP9 in distal coronary artery blood were observed in the SAP subjects at 15 minutes after plaque disruption, but not in the ACS group. **Panel E and F**: When subjects were grouped according to plaque morphology [Panel E: lipid rich (n=23), non-lipid (n=13); Panel F: lipid rich (n=15), non-lipid (n=11)], no changes in arterial MMP9 at 5 or 15 minutes in either proximal coronary arterial blood collected by guide catheter, or downstream arterial blood collection by aspiration catheter. **Panel G and H**: Subjects were stratified into tertiles according to their *venous* $MMP9_{AUC}$ after plaque disruption. Amongst those within highest *venous* $MMP9_{AUC}$ tertile ($PCI^{upper1/3}$), but only had proximal coronary arterial blood collected at 5 and 15 minutes (n=10), no significant change was observed for *arterial* MMP9 at 5 or 15 minutes (G). In comparison, amongst those $PCI^{upper1/3}$, but had downstream coronary arterial blood collected at 5 and 15 minutes (n=10), significant elevations in *arterial* MMP9 were observed by 5 minutes after plaque disruption (H).

Figure 24: Plasma levels of NGAL and GDF15 in the discovery subject subset after plaque disruption

The discovery subject subset consisted of 3 groups of subjects (PCI: n=20, Dx angiography: $CONTROL_{Dx,}$ n=10), selected according to considerations outlined in Chapter 3. The PCI group further comprise two sub groups, as determined by venous $MMP9_{AUC}$ after plaque disruption ($PCI_{MMP9High}$ and $PCI_{MMP9Low,}$ n=10 each). The levels of plasma NGAL and GDF15 were measured using Luminex® assays in blood samples collected at baseline (0hr), 30 minutes (30m) and 6 hours (6hr) after plaque disruption. Comparison within groups against baseline was performed using Wilcoxon matched pair signed rank test. (In the box plots data is presented by median±10 to 90 percentile range.) Data at 30m and 6hr was further normalised against the individual's baseline to obtain fold changes, and area under curve for this time course was calculated accordingly. Comparison between the AUC of each group was performed using one way ANOVA. Two-way ANOVA for repeated measures with Bonferroni correction for multiple testing was also performed to further examine the differences between groups at different time points. (In the line graph, data are presented by mean±SEM). P-value less than 0.05 was considered to be significant.

Panel A: Significant elevation of NGAL was observed in the PCI subjects at 6 hours after plaque disruption, this was not observed in the $CONTROL_{Dx}$ group. $NGAL_{AUC}$ was significantly higher in the $PCI_{MMP9High}$ groups compared to the others (ANOVA $P<0.05$). When the trends for individual group were compared according to fold changes of NGAL at subsequent time points, the levels observed in the $PCI_{MMP9High}$ group was significantly higher at 30 minutes as compared to $PCI_{MMP9Low}$ and $CONTROL_{Dx}$ ($P<0.01$ and $P<0.001$ on two-way ANOVA, respectively).

Panel B: Significant elevation of GDF15 was observed in both the PCI and Dx angiography subjects at 6 hours after plaque disruption. However, $GDF15_{AUC}$ was significantly higher in $PCI_{MMP9High}$ group compared to the others. When the trends for individual groups were compared according to fold changes of GDF15 at subsequent time points, the levels observed in the $PCI_{MMP9High}$ group was significantly higher at 6

hours as compared as compared to $PCI_{MMP9Low}$ and $CONTROL_{Dx}$ ($P<0.05$ and $P<0.001$ on two-way ANOVA, respectively).

Figure 29: Sample size consideration for discovery -omics research

Sample size consideration in comparative -omics research, whereby samples are compared according to a disease condition (such as before and after plaque rupture) to screen for up or down regulation of "novel/unknown" molecular signatures, is different from the traditional power calculation approach for "known" candidate markers. The traditional approach of sample size calculation, which requires prior knowledge of the variance observed in a particular measurement, is not feasible in discovery –omics workflow. Instead, the biological variance (differences observed between patients) and technical variance (differences observed between replicates) can be used to calculate sample size. This calculation can be performed using *R* script. Assuming the combined biological and technical variance of 100% between samples, the sample size of 10 in each arm of the study will be sufficient to detect a 2.25 fold change (up or down regulation) in a given protein/metabolite with 80% power and α of 0.05 (Panel A). The ability to detect lower fold change with a given number of samples can be improved if the technical variance can be minimised. When the combined variation is reduced to 40%, the sample size of 6 in each arm will be sufficient to detect a 2 fold change with 80% power and α of 0.05 (Panel B). The sample size can be theoretically reduced further while achieving the same statistical power when the combined variation is only 20% (Panel C).

(Levin, Y *et al. The role of statistical power analysis in quantitative proteomics.* Proteomics, 2011. **11**(12): p. 2565-7.[132] *These figures are reproduced with permission from Elsevier*.)

Figure 30: Conceptual illustration of how a PCA is performed

Principal component analysis is a useful tool to project complex datasets observed within the samples and allow the visual assessment of similarity, or differences, between the samples, based on spatial distribution of samples in dimension(s) defined by variances observed within the dataset. This figure is a conceptual illustration of how a PCA can be used to project a population of subjects with different features.

Panel A: Imagine a group of subjects with a mix of skin colour, height, body mass index (BMI), hair style, and hair colour.

Panel B: Skin colour is the prevailing difference between these subjects. Using skin colour as a variable [principal component 1-(PC1)], these subjects can be separated into distinct clusters on a single dimension space defined by PC1.

Panel C: Having separated them based on skin colour, BMI is the next prevailing difference between the individuals. A second dimension can be defined by an axis (PC 2) orthogonal to PC 1, using BMI as the variable. These subjects can be further separated into distinct clusters one a two-dimensional space defined by PC1 and PC2.

Panel D: Within the residual body features, height is the next prevailing difference between the individuals. A third dimension can therefore be defined by an axis (PC 3) orthogonal to PC 1 and PC 3, using height as the variable. The addition the third dimension results in further separation of distinct clusters. Subjects with most similar body features are clustered closer in this this 3 dimensional space.

Figure 31: Sample analysed during the discovery phase of this thesis

Panel A: Plaque debris for analysis. Collection of coronary plaque debris was performed using methods described in Section 2.4.2. To assess if blood components in circulation (other than coronary plaque debris) would adhere to the filterwire during the PCI procedure, therefore giving rise to artifactual protein signals unrelated to coronary plaque debris, a paired filterwire device was prepared as matched control. After the diagnostic angiography confirmed suitability for stenting with filterwire distal protection, an additional 10 ml of arterial blood was aspirated from the coronary guide catheter and transferred into a 15 ml falcon tube. A filterwire was then positioned downstream of the coronary lesion, followed by the PCI procedure. Concurrently, an unused filterwire was placed in the falcon tube containing the individual's blood. This was immediately transferred to a water bath and incubated at 37.5°C for the duration of the stenting procedure. At the end of the PCI procedure, both filterwires (one containing plaque debris, and one from *ex vivo* incubation) were retrieved and immediately frozen on dry ice and stored at -80°C for subsequent analysis.

Panel B: Plasma samples for analysis. Plasma samples analysed during the Discovery Phase included the 30 subjects selected from the *Screening Phase*, as detailed in Section 3.6.15. This consisted of 10 subjects in each of the $PCI_{MMP9High}$, $PCI_{MMP9Low}$, and $CONTROL_{Dx}$ group. To capture the earliest changes in the plasma proteins, plasma collected from the coronary artery at *5 minutes* after plaque disruption were used for comparison against the baseline sample collected from the coronary artery prior to stent (0 min). Plasma samples from 10 healthy volunteers without any prior medical history were also included.

Figure 32: Summary of the organic extraction protocol used for the extraction of lipid and metabolite from plaque debris and plasma samples

Extraction of lipid and metabolite from plaque debris: The filterwire device containing plaque debris was first transferred to a 2ml eppendorf tube and immersed in 500µl of H_2O. The sample was subjected to sonication in a water bath for 2 minutes to achieve cell lysis. The tissue lysate was retrieved for the staged extraction of each of the protein, metabolite and lipid fraction using an organic extraction protocol with sequential concentration gradients of methanol, chloroform and H_2O. This protocol utilised the variable miscibility of lipids according to the concentration of methanol in the organic solvent. Using this protocol, the metabolite portion was extracted in the aqueous phase, followed by separation of the lipid and protein fractions after an additional step of methanol extraction.

After the first stage of methanol and chloroform extraction, the aqueous phase supernatant (containing the polar metabolites) were ultra-filtered using a molecular weight cut off spin column (Corning® Spin-X UF 6mL concentrator). The filtrate was diluted 1 in 10 with 0.2% trifluroacetic acid, followed by followed by sequential washes of Buffer A (consisting of 0.1% TFA) and Buffer B (consisting of 0.1% trifluroacetic acid with 65% acetonitrile) to remove inorganic salt. The final eluent was aliquoted and vacuumed dried, then stored at -80°C for subsequent analysis. After extraction of the aqueous phase, a further 1125µL of methanol was added to the residual organic phase, vortexed, and centrifuged at 16000g for 2 minutes to pellet out the protein. The supernatant contained the lipid fraction. Each of the final fractions was vacuum dried and stored at -80°C for subsequent analysis. Biological controls samples (FW INC, described in Section 4.3.1 and Figure 31) and negative control (NC, described in section 4.3.3) were processed in the same way.

Extraction of lipid and metabolite from plasma: Plasma was diluted 1:50, then processed through the same organic extraction protocol as plaque debris samples.

Figure 33: MALDI-TOF-MS spectra showing unique features in biological samples analysed during the *discovery phase*

MALDI-TOF-MS lipidomics spectra were acquired from samples included in the discovery phase, according to methods described in Section 4.3. Visual inspection of the spectra using Flexanalysis^{TM} software revealed several peaks which are consistently observed in biological samples, but absent in the matrix and negative controls. One of the mass peaks present in all biological samples was m/z 369.00, which was consistent with cholesterol (-H_2O) (**Panel I**). There were mass peaks unique to plaque debris collected from the native coronary artery (**Panel II**) or plasma (**Panel III**). One of the mass feature (m/z 919.37) was absent in the plaque debris and baseline plasma samples, but appeared in plasma after plaque disruption in both PCI groups (**Panel IV**). [X axis – mass to charge ratio (m/z), Y axis – intensity (arbitrary units)].

Figure 34: Lipidomic profiles differ between types of samples, and in plasma samples before and after plaque disruption

MALDI-TOF-MS lipidomics spectra were acquired from samples included in the discovery phase, and analysed according to methods described in Section 4.3 and Section 4.4.1.1.

Panel A: PCA scores plot of all lipid features from filter wire and controls showed tight clustering of the HV sample technical replicates, while clear separation was observed between the different sample types.

Panel B: PCA scores plot of all lipid features from plasma also show distinct patterns between plasma samples before and after plaque disruption. Greater separation was observed between the plasma samples before and after plaque disruption in the $PCI_{MMP9High}$ group, while less separation was observed in the $PCI_{MMP9Low}$ group. This was in contrast to the $CONTROL_{Dx}$ group, in which minimal separation was observed between the plasma samples taken at baseline and 5 minutes after.

$PCI_{MMP9High}$	discovery subject subset which was selected from PCI subjects in the upper tertile of venous $MMP9_{AUC}$ after plaque disruption
$PCI_{MMP9Low}$	discovery subject subset which was selected from PCI subjects in the lower tertile of venous $MMP9_{AUC}$ after plaque disruption
$CONTROL_{Dx}$	discovery subject subset which was selected from the Dx angiography subjects in the lower ½ of venous $MMP9_{AUC}$

Figure 35: Correlation matrix of the 15 most significantly changed mass features selected by the Medicwave Spectrolyzer™ software in each of the discovery subject subset

MALDI-TOF-MS lipidomics spectra were acquired from *individual patient* samples included in the discovery phase, and analysed by Medical Wave Spectrolyzer™ software according to methods described in Section 4.3 and Section 4.4.1.2. Using the Spectrolyser™ Multiple Biomarker Detection algorithm, 15 most significantly changed plasma mass peaks at 5 minutes after baseline for each group were selected. The correlation coefficients between these 15 features in each group are displayed in a correlation matrix. (Colour scale reflects the magnitude of correlation; green - positive correlation; red – negative correlation). (Note: multiple testing correction algorithm is not an available feature in the Spectrolyzer™ software).

$PCI_{MMP9High}$	discovery subject subset which was selected from PCI subjects in the upper tertile of venous $MMP9_{AUC}$ after plaque disruption
$PCI_{MMP9Low}$	discovery subject subset which was selected from PCI subjects in the lower tertile of venous $MMP9_{AUC}$ after plaque disruption
$CONTROL_{Dx}$	discovery subject subset which was selected from the Dx angiography subjects in the lower ½ of venous $MMP9_{AUC}$

Figure 36: Metabolomic profiles differ between types of samples, and in plasma samples before and after plaque disruption

LC-MS metabolomics spectra were acquired from samples included in the *discovery phase*, and analysed according to methods described in Section 4.3 and Section 4.4.2.1

Panel A: PCA scores plot of all metabolite features demonstrated tight clustering of the technical replicates for QC samples, while clear separation was observed between the different sample types [plasma, plaque debris (FW), and matched control for plaque debris (FW INC)].

Panel B: PCA scores plot of all metabolite features also demonstrated distinct patterns between plasma samples before and after plaque disruption. Greater separation was observed between the plasma samples before and after plaque disruption in the $PCI_{MMP9Low}$ group, compared to the separation observed in the $PCI_{MMP9High}$ group. Separation in the plasma samples in the $CONTROL_{Dx}$ was also evident, although less than that observed in the PCI groups. (Each data point represents the average of technical triplicates.)

$PCI_{MMP9High}$	discovery subject subset which was selected from PCI subjects in the upper tertile of venous $MMP9_{AUC}$ after plaque disruption
$PCI_{MMP9Low}$	discovery subject subset which was selected from PCI subjects in the lower tertile of venous $MMP9_{AUC}$ after plaque disruption
$CONTROL_{Dx}$	discovery subject subset which was selected from the Dx angiography subjects in the lower ½ of venous $MMP9_{AUC}$

Figure 37: Metabolite features which were differentially detected in plaque debris and in plasma after plaque disruption

LC-MS metabolomics spectra were acquired from samples included in the *discovery phase*, and analysed according to methods described in Section 4.3 and Section 4.5.2.1. These heatmaps display the metabolite features which fulfil the following criteria: (i) present in at least 70% of the quality control (QC) sample replicates; (ii) absent in the negative control (NC) sample replicates; (iii) significantly different between subgroups of samples. The X-axis describes the mass and retention time of each feature. Clustering of the metabolites was performed, and were summarised by the dendrogram on the Y-axis of each heatmap.

To generate each heatmap, the average level of a metabolite feature observed in the QC replicates was set as the reference value (This is a default function by the MassHunter Mass Profiler Professional software). The colour scale represents the fold difference of each metabolite feature in a particular sample, *as compared to the average level of the metabolite measured in the QC replicates.* The range of colour scale is further normalised to fit the upper and lower limit bounds of 1 and -1.

Panel A: This heatmap displays metabolite features which are significantly different between the FW and FW INC samples (n=44). Amongst these, significantly higher levels of 17 features are observed in FW samples compared to the FW INC samples.

Panel B: This heatmap displays metabolite features which are significantly changed between the plasma samples of $PCI_{MMP9High}$ group, taken at baseline and 5 minutes after plaque disruption (n=17). Amongst them, the level of 5 metabolites increased significantly after plaque disruption, while the level of 12 metabolites significantly decreased at the same time.

Panel C: This heatmap displays metabolite features which are significantly changed between the plasma samples of $PCI_{MMP9Low}$ group, taken at baseline and 5 minutes after plaque disruption (n=82). Amongst them, the level of 19 metabolite features increased significantly after plaque disruption, while the level of 63 metabolite features significantly decreased at the same time.

$PCI_{MMP9High}$	discovery subject subset which was selected from PCI subjects in the upper tertile of venous $MMP9_{AUC}$ after plaque disruption
$PCI_{MMP9Low}$	discovery subject subset which was selected from PCI subjects in the lower tertile of venous $MMP9_{AUC}$ after plaque disruption
$CONTROL_{Dx}$	discovery subject subset which was selected from the Dx angiography subjects in the lower ½ of venous $MMP9_{AUC}$

Figure 38: Mass features which demonstrate distinct patterns in plasma samples analysed during the *discovery phase*

LC-MS metabolomics spectra were acquired from samples included in the discovery phase, and targeted search of metabolite features were performed according to methods described in Section 4.3 and Section 4.5.2.2. The figures presents examples of metabolite features that fulfil the criteria of: (i) not detected in the negative control sample, (ii) acutely appeared or disappeared within the 5 minutes of sampling, or absent in at least one group. [The intensity of each metabolite is presented as mean±SEM, in arbitrary units (a.u.)]

Panel A: Each of the named metabolite features from this panel was selected for the targeted search its involvement(s) in lipid metabolism pathways. Mass spectra acquired from this experiment were matched these named metabolites according to analysis described in Section 4.4.4.2.

Panel B: These mass features were examples highlighted by results from semi-quantitative analysis (described in section 4.5.2.1), which showed significant change at 5 minutes after plaque disruption in the $PCI_{MMP9Low}$ group. The mass spectra of these features matched empirically to the molecular formula listed. However, the identity of these molecular features could not be assigned.

$PCI_{MMP9High}$	discovery subject subset which was selected from PCI subjects in the upper tertile of venous $MMP9_{AUC}$ after plaque disruption
$PCI_{MMP9Low}$	discovery subject subset which was selected from PCI subjects in the lower tertile of venous $MMP9_{AUC}$ after plaque disruption
$CONTROL_{Dx}$	discovery subject subset which was selected from the Dx angiography subjects in the lower ½ of venous $MMP9_{AUC}$

Figure 39: Overview of untargeted "shotgun" proteomics workflow

Proteins are first extracted from the samples and digested by a protease (such as trypsin) to form peptide sequences. The resultant peptides are subjected to liquid chromatography to space out the peptides according to elution profile prior to the mass spectrometer steps. An energy source is applied to the peptides to form charged molecules (or precursor ions). These charged ions are analysed by a mass spectrometer, which determines the mass to charge ratio (m/z) ratio of the ions and the abundance (intensity) of each precursor ions. In order to ascertain identification of the individual peptides (and infer the identity of the protein from which the tryptic peptides are derived from), select peptides from the precursor ion scan are further fragmented by an energy source and subjected to an additional MS scan (hence the term “tandem MS”, or “MS/MS”). Using the pattern of fragment ions generated, it is feasible to computationally determine the individual peptide sequences. Certain peptide sequences are unique to the parent protein, and allow the identification of its parent protein through computational algorithms.

In shotgun proteomics workflows, internal standards are not applied to the samples. Therefore it is not feasible to provide absolute quantification of individual proteins in a given sample. Characterisation of the protein profile for individual samples is only qualitative. However, the relative abundance between proteins within one sample can be inferred by mathematical algorithms, such as the emPAI (exponentially modified protein abundance index) score. Semi-quantitative comparison of protein abundance between samples can be achieved in shotgun proteomics through post processing of data, using algorithms to perform data normalisation between samples.

Figure 40: The wide dynamic range of human plasma proteome, and under sampling of low abundance protein peptides by shotgun proteomics

Panel A: The wide dynamic range of human plasma proteome is highlighted in this diagram, which plots out some of the commonly measured proteins on the log scale in terms of abundance (Left Y-axis) and the corresponding concentration (Right Y-axis). In addition to classical soluble proteins, plasma also contains tissue "leakage" proteins such as troponin and prostate specific antigen. The dynamic range of plasma proteome in term of protein concentration can span more than 10 orders of magnitude, ranging from the most abundant proteins such as albumin, which exhibits concentration in the mg/ml range, to low abundant proteins such as interleukins and cytokines that have concentrations in the pg/ml range.

Panel B: The wide dynamic range of human plasma proteome presents particular challenges for shotgun proteomic analysis, as the more abundant proteins will result in higher abundance of tryptic peptides. The most abundant ions will attract the proportionally more charges during electrospray ionization, making it less likely for low level peptides to get ionised. At the precursor ion scan stage, these peptide in higher abundance are likely to be preferentially selected for subsequent tandem MS leading to under-sampling of the low abundance peptide sequences. Please refer to Figure 39 for further description on the overall shot gun proteomics workflow.

Figure 41: Two strategies utilised in this thesis for improving protein peptide coverage for shotgun proteomics analysis

Several strategies were utilised for improving resolution for the shot gun proteomics experiment in this thesis. Two of them are illustrated by this figure.

Panel A: At the liquid chromatography step, a long separation gradient of 2 hours was performed. This meant fewer peptides were eluted at a given point in time, therefore the resultant eluent contained relatively fewer peptides to be analysed as compared to a shorter separation gradient.

Panel B: The samples were analysed in duplicates, with separate mass range included for subsequent tandem MS analysis in each duplicate, which were then combined. This improved the chances of lower abundant peptides being selected for subsequent tandem MS, and partially addressed issue of under sampling.

Figure 42: The concept of inferential pathway analysis

Data from the proteomics analysis can be utilised to focus interrogations of the small molecular screen. Using the proteins as a guide, it may be feasible to infer implication of a set of metabolites by way of their association in a known biological pathway implicated by the protein data. This approach of inferring identity of the unknown small molecules, using knowledge of known biological pathway involvements in the same samples, is referred to "inferential pathway analysis".

Figure 43: The Progenesis LC-MS™ workflow

Acquisition of protein mass spectra has been described in Section 5.3.7. The routine workflow by Progenesis LC-MS™ (Non-linear Dynamics, New Castle, UK, Version 3.1) is illustrated in this figure and consists of the following steps: (i) individual raw data files are first uploaded, and one sample is chosen as the reference run; (ii) data files between samples are aligned against each other, prior to automated extraction of mass peaks from each sample; (iii) normalisation of peak intensity is performed to allow comparison of intensity between samples; (iv) peptides from each sample are characterised. At this stage, peptide information gained from any sample within the experiment is used to help characterisation of peptides across the sample collection, even if the peptide is of low abundance in the other samples (This improves under sampling). Peptide information are used to search against the online database to obtain protein identification. Following this, semi-quantitative analysis for protein features can be performed (PCAs, clustering, or ANOVA).

Figure 44: Qualitative proteomics profile of samples analysed during the *discovery phase*

Peptide spectra were acquired from individual samples included in the discovery phase, and protein identifications assigned by search against the online Mascot database as described in Section 5.3. The grey bars for each sample consist of a list of individual proteins by accession number. Over 1,000 proteins were identified for each of the plaque debris samples (plaque 1, n=1016; FW 2, n=1175). However, a number of proteins were also detected in the paired incubated control (FW INC) samples (FW INC 1, n=509; FW INC 2, n=410). Plaque debris consistently contained more proteins compared to plasma samples, and an average of 362 proteins detected in each plasma sample. Alpha- and Beta-actin were examples of two ubiquitous cellular protein (accession number P68133 and P60709) detected in all FW and FW INC samples (black and red bars), but were not detected in any of the plasma. Calponin (accession number P99439, Figure 44 - blue bars), an actin binding protein and a marker of smooth muscle cells, was detected in both FW samples, but also present in one of the FW controls (FW INC 1).

Despite the plasma albumin and IgG depletion step described in section, albumin (orange bars) was detected in all samples, while CRP (accession number P02741, green bars) was one of the proteins detected in only patients who received PCI induced plaque disruption, but not in the plasma of HVs or patients who underwent Dx angiography only. According to the Mascot search, MMP9 (accession number P14780, purple bars) was detected in the FW and FW INC samples, but not in the plasma samples.

$PCI_{MMP9High}$	discovery subject subset which was selected from PCI subjects in the upper tertile of venous $MMP9_{AUC}$ after plaque disruption
$PCI_{MMP9Low}$	discovery subject subset which was selected from PCI subjects in the lower tertile of venous $MMP9_{AUC}$ after plaque disruption
$CONTROL_{Dx}$	discovery subject subset which was selected from the Dx angiography subjects in the lower ½ of venous $MMP9_{AUC}$

Figure 45: emPAI scores for individual samples highlight one limitation of qualitative analysis in a shotgun proteomics design

Peptide spectra were acquired from individual samples included in the discovery phase, and protein identification assigned by search against the online Mascot database as described in Section 5.3 (for detailed explanation of the samples prepared for analysis, refer to Section 4.3.1).

According to the Mascot database search, β-actin was present in each of these samples: negative control (NC), plaque debris collected by filterwires (FW 1 and 2), FW INC 1 and 2, and incubated control of filterwires (FW INC 1 and 2). In each of these samples, β-actin was associated with a good Mascot probability based score for identification (red boxes). A high score represents a low probability of random identification of a protein, which is calculated by Score=-10*Log_{10}(p-value). For example, a mascot score of 20 denotes a p-value of 0.01.

However, the emPAI (exponentially modified protein abundance) scores for β-actin were different between samples. (emPAI score is an index of the relative abundance of the particular protein within the sample.) Higher emPAI scores were observed for β–actin in the FW samples compared to the matched FW INCs. In the NC sample, a very low emPAI score for β–actin was observed. Furthermore, there were more peptide matches in the FW samples as compared to the FW INCs and NC (green highlights). These information indicate very different nature of enrichment in β–actin amongst these samples, but β–actin would be considered to be present in all of these samples in a qualitative analysis of this dataset.

FW	plaque debris samples collected by the filterwire device during PCI
FW INC	filterwire incubated in whole blood at 37°C (*ex vivo*) for the duration of PCI

Figure 46: Proteomic profiles differ between plaque debris and plasma

Proteomic data were acquired from samples included in the discovery phase, and analysed according to methods described in Section 5.3. The pooled HV sample was analysed as technical replicates, both at the beginning and at the end of the mass spectrometry acquisition work flow, as quality control in additional to the lock mass (Poly-dimethylcyclosiloxane) analysed for real time calibration. PCA scores plot of the proteins detected in the experimental group containing quadruplicate HV samples, duplicate FW samples and duplicate FW INC samples showed close clustering of the technical replicates, indicating technical reproducibility between mass spectra acquisitions. There were also clear separations between the plasma and non-plasma samples, and between FW and FW INC samples.

FW	plaque debris samples collected by the filterwire device during PCI
FW INC	filterwire incubated in whole blood at 37°C (*ex vivo*) for the duration of PCI

Figure 47: Rapid changes in the global proteomic profile are observed after plaque disruption

Proteomic data were acquired from plasma samples included in the discovery phase and analysed according to methods described in Section 5.3. PCA of the proteins in plasma samples was performed using the averaged value between technical replicates. This demonstrated separation of the samples between baseline (0min) and 5min in both the plaque disruption ($PCI_{MMP9High}$, $PCI_{MMP9Low}$) and $CONTROL_{Dx}$ group. However, the separation within the plaque disruption group, particularly the $PCI_{MMP9Low}$ group, was wider than the control group.

$PCI_{MMP9High}$	discovery subject subset which was selected from PCI subjects in the upper tertile of venous $MMP9_{AUC}$ after plaque disruption
$PCI_{MMP9Low}$	discovery subject subset which was selected from PCI subjects in the lower tertile of venous $MMP9_{AUC}$ after plaque disruption
$CONTROL_{Dx}$	discovery subject subset which was selected from the Dx angiography subjects in the lower ½ of venous $MMP9_{AUC}$

Table 6: List of plasma proteins significantly changed after plaque disruption in the $PCI_{MMP9High}$ group

Proteomic data were acquired from plasma samples included in the discovery phase, and analysed according to methods described in Section 5.3. Thirteen proteins showed significant changes at 5 minutes after plaque disruption in the $PCI_{MMP9High}$group. Six of these were acutely increased in plasma at 5 minutes. Amongst the proteins which were acutely elevated in this group, lipopolysaccharide binding protein (LBP), cytochrome B5 reductase 3 (CYB5R3) were also significantly enriched in the plaque debris samples (FW) as compared to the incubated controls (FW INC) (Column: "Protein present in FW?")

Each of the significantly changed proteins observed in this group was manually searched against the Ingenuity Pathway Analysis (IPA) Knowledge Base to ascertain its involvement in curated canonical pathways. In addition, the overall dataset for plasma proteins in the $PCI_{MMP9High}$ was analysed using the standard IPA workflow.

Canonical pathways which were flagged up by both of these analyses were subjected to further examination. To further minimise the likelihood of random observation, the additional criteria of $P<0.0001$ [i.e. $-Log(P\ value) \geq 4$] and percentage representation greater than 20% of the canonical pathway were applied. Based on this approach, two pathways were highlighted as mostly likely to be implicated in the dataset, with high proportion of protein coverage: LXR/RXR activation and acute phase response signalling pathway. LBP has a role in both of these pathways, which is highlighted in yellow.

$PCI_{MMP9High}$	discovery subject subset which was selected from PCI subjects in the upper tertile of venous $MMP9_{AUC}$ after plaque disruption
$PCI_{MMP9Low}$	discovery subject subset which was selected from PCI subjects in the lower tertile of venous $MMP9_{AUC}$ after plaque disruption
$CONTROL_{Dx}$	discovery subject subset which was selected from the Dx angiography subjects in the lower ½ of venous $MMP9_{AUC}$

Table 7: List of plasma proteins significantly changed after plaque disruption in the $PCI_{MMP9Low}$ group (over two pages)

Proteomic data were acquired from plasma samples included in the discovery phase, and analysed according to methods described in Section 5.3. Eleven proteins showed significant changes at 5 minutes after plaque disruption in the $PCI_{MMP9Low}$ group. Five of these were acutely increased in plasma at 5 minutes.

Each of the significantly changed proteins observed in this group was manually searched against the Ingenuity Pathway Analysis (IPA) Knowledge Base to ascertain its involvement in curated canonical pathways. In addition, the overall dataset for plasma proteins in the $PCI_{MMP9Low}$ group was analysed using the standard IPA workflow.

Canonical pathways which were flagged up by both of these analyses were subjected to further examination. To further minimise the likelihood of random observation, the additional criteria of $P<0.0001$ [i.e. $-Log(P\ value) \geq 4$] and percentage representation greater than 20% of the canonical pathway were applied. LXR/RXR activation and acute phase response signalling pathways are also the most implicated pathways in this dataset, while two proteins implicated in these pathways were also significantly changed in plasma at 5 minutes after plaque disruption in the $PCI_{MMP9Low}$ group: hemopexin and alpha-1B-glycoprotein. These are highlighted in yellow.

$PCI_{MMP9High}$	discovery subject subset which was selected from PCI subjects in the upper tertile of venous $MMP9_{AUC}$ after plaque disruption
$PCI_{MMP9Low}$	discovery subject subset which was selected from PCI subjects in the lower tertile of venous $MMP9_{AUC}$ after plaque disruption
$CONTROL_{Dx}$	discovery subject subset which was selected from the Dx angiography subjects in the lower ½ of venous $MMP9_{AUC}$

Figure 48: Rapid changes of LXR/RXR pathway and acute phase response signalling pathway are observed after plaque disruption

Proteomic data were acquired from plasma samples included in the *discovery phase*, and analysed according to methods described in Section 5.3. LXR/RXR activation and the acute phase response pathways were the two most highly implicated pathways after plaque disruption (refer to Section 5.4.2). PCAs of proteins specific to these two pathways were performed for the dataset. In both, greater separation between the $PCI_{MMP9Low}$ plasma at baseline and 5 minutes after plaque disruption were observed. However, similar degrees of separation were observed between the $PCI_{MMP9High}$ and $CONTROL_{Dx}$ groups in both cases. In the case of LXR/RXR activation pathway, disparate directions of separation were observed between $PCI_{MMP9High}$ and $PCI_{MMP9Low}$ groups.

$PCI_{MMP9High}$	discovery subject subset which was selected from PCI subjects in the upper tertile of venous $MMP9_{AUC}$ after plaque disruption
$PCI_{MMP9Low}$	discovery subject subset which was selected from PCI subjects in the lower tertile of venous $MMP9_{AUC}$ after plaque disruption
$CONTROL_{Dx}$	discovery subject subset which was selected from the Dx angiography subjects in the lower ½ of venous $MMP9_{AUC}$

Figure 49, 50, 51: LXR/RXR activation pathway superimposed with the protein fold change level of detected components at 5 minutes for the $CONTROL_{Dx}$, $PCI_{MMP9High}$, and $PCI_{MMP9Low}$ group

Proteomics and metabolomics data were acquired from plasma samples included in the discovery phase and analysed according to methods described in Section 5.3 and Section 4.3. LXR/RXR pathway was the most highly implicated canonical pathway in the plasma dataset based analysis described in Section 5.4.2.1. For each protein detected in this pathway, fold change values at 5 minutes (against the baseline value) were superimposed on the protein component in the canonical pathway. All proteins detected in the dataset with more than two tryptic peptides and false discovery rate less than 1% were included in the figure. The colour scale represents the direction and magnitude of fold change, with red being an upward change and green being down. Proteins which were significantly changed at 5 minutes according to the Progenesis LC-MS™ analysis ($P<0.05$) are represented with dark red (LBP, significantly increased in the $PCI_{MMP9High}$ group – Figure 51) and dark green (HPX and A1BG, significantly decreased in the $PCI_{MMP9Low}$ group – Figure 52). Note that the overall pattern of change in the $CONTROL_{Dx}$ group (mostly upwards - Figure 50) is distinct from the pattern observed in the $PCI_{MMP9High}$ group (an even mix of up- and downward changes – Figure 51). (*Figures 50, 51, and 52 are reproduced with permission from Ingenuity systems®, Redwood, USA.*)

$PCI_{MMP9High}$	discovery subject subset which was selected from PCI subjects in the upper tertile of venous $MMP9_{AUC}$ after plaque disruption
$PCI_{MMP9Low}$	discovery subject subset which was selected from PCI subjects in the lower tertile of venous $MMP9_{AUC}$ after plaque disruption
$CONTROL_{Dx}$	discovery subject subset which was selected from the Dx angiography subjects in the lower ½ of venous $MMP9_{AUC}$

Figure 52: γ-Linoleate biosynthesis pathway may be implicated after coronary atherosclerotic plaque rupture

Proteomic data were acquired from plasma samples included for the discovery phase, and analysed according to methods described in Section 5.3.

Panel A: Cytochrome B5 reductase 3 (CYB5R3) is a member to the family of linoleoyl-CoA desaturase (E.C. 1.13.19.3), and has a central role for the conversion between linoleoyl-CoA and γ-linoleoyl-CoA). It was present in the plaque debris and significantly elevated at 5 minutes in plasma after plaque disruption in the $PCI_{MMP9High}$ group (dark red icon, $P<0.05$ against baseline). Amongst the other elements of the pathway, mass features which matched to the upstream subtrates (linoleate and coenzyme-A, orange icons) of this pathway were found in the plasma dataset using targeted search for molecular features in the metabolomics dataset, as described in Section 4.4.4.1. However, mass peaks matching the same molecular formula / mass to linoleyl-CoA or γ–linoleoyl-CoA were not detected in the MALDI-TOF-MS or LC-MS experiments presented in Chapter 4. Of note, the acquisition of data was set to the mass range of 50 – 1000 m/z in the experiment described in Section 4.3.6. This range was short of the mass for linoleoyl-CoA (1029.96Da). (*Panel A is reproduced with permission from Ingenuity Systems®, Redwood, USA*)

Panel B: The intensities (arbitrary units) for metabolite features matching to that of linoleate and coenzyme A in each plasma sample group. (Data are presented in mean±SEM).

Figure 53: Non-performance of the commercially available ELISA kits for CYB5R3, HADH and CD84

The performance of commercially available ELISA kits for these analytes was assessed in terms of linearity of dilution range and recovery for spiked in protein standards. The assay procedures were otherwise performed according to manufactures' protocols.

Panel A: In this experiment, the highest and lowest dilutions for standard were measured (Standard 7 and Standard 1) for each analyte, using the standard stocks supplied in the kits. Serial dilutions of plasma samples were created with phosphate buffered solution (PBS). None of the measured optical densities (O.D.) were within the range of quantification (between standard 1 to standard 7), even though the manufacturer recommended to measure non-diluted plasma samples (1:1) for these kits. In all three kits, progressive increases in O.D. were observed with further dilution.

Panel B, C, D: In a separate experiment, serial dilutions of the standard stock solution was performed in order to generate a standard curve (1:1, 1:10, 1:100, 1:200, 1:300). Serial dilution of plasma sample from one representative CAD patient was created using PBS (1:1, 1:2, 1:20, 1:50, 1:100, 1:500, 1:1000, 1:5000, 1:10000, 1:500000, 1:10000000). Further, plasma from a healthy volunteer was spiked with the standard stock solution and serial dilution performed using neat plasma from the same HV (1:20, 1:50, 1:100, 1:500, 1:1000). Although each of the standard curves demonstrated a linear range (Figure 53-B), serial dilutions of standard stock using HV plasma did not show linear recovery (Figure 53-C).Further, the levels of each protein were below or bordering the LLOD for each assay regardless of the dilution factor (Figure 53-D).

Figure 56: Potential mechanisms of biological pathway activations due to acute release of LBP and CYB5R3 after plaque disruption

This figure presents two potential biological signatures of plaque disruption proposed by this thesis. Plaque disruption can result in acute release of lipopolysaccharide binding protein (LBP), leading to activation of circulating monocytes or neutrophils via toll like receptor 4 (TLR4) mediated signalling. This results to subsequent release of MMP9, likely via the NFκB signal transduction pathway (Panel A). Alternatively, plaque disruption can result in acute liberation of cytochrome B5 reductase 3 (CYB5R3). CYB5R3 is a key enzyme in the linoleoyl-CoA biosynthesis pathway and catalyses the acute conversion of linoleoyl-CoA to γ-linoleoyl-CoA in circulation (Panel B).

Figure 57: Glutaryl–CoA degradation pathway may be involved after coronary atherosclerotic plaque rupture

Proteomics and metabolomics data were acquired from plasma samples included for the discovery phase, and analysed according to methods described in Section 5.3 and Section 4.3. Several metabolite components of this pathway were observed in the metabolomics datasets (orange icons), including acetyl-CoA, coenzyme A, acetoacetyl-CoA, NADH, 3-hydroxybutanoyl-CoA, and crotonyl CoA. (For the intensities observed in individual samples, refer to Figure 38).

Hydroxyacyl-CoA dehydrogenase (E.C. 1.1.1.35) is a family of enzymes central to this pathway. Members of this family includes hydroxysteroid dehydrogenases (HSD14B10 and HSD14B4), and hydroxyl-CoA dehydrogenase (HADH). These proteins were detected in plasma samples of the discovery subject subset and are highlighted as colour icons in the inset box. Colours of these icons reflect the direction of change at 5 minutes after plaque disruption (Red: increased, Green: decreased). Although the changes in these proteins did not reach statistical significance at 5 minutes, the patterns of directional change between these three groups were distinct. (*This figure is reproduced with permission from Ingenuity systems®, Redwood, USA.)*

Figure 58: Tryptophan metabolism pathway may be involved after coronary atherosclerotic plaque rupture

Proteomics and metabolomics data were acquired from plasma samples included for the discovery phase and analysed according to methods described in Section 5.3 and Section 4.3. Several components of this pathway were observed in the metabolomics and proteomics analysis (orange and pink icons, respectively). Many components of this pathway were observed in the discovery subject subset. This is another example that demonstrates the utility of "inferential pathway analysis" for directing the focus of future investigations. (*This figure is reproduced with permission from Ingenuity systems®, Redwood, USA.)*

Appendix Table 1

Proteomic data were acquired from coronary plaque debris samples (FWs) and paired controls (FW INCs), and analysed according to methods described in Section 5.3. Proteins with more than two tryptic peptides and false discovery rate less than 1% were included for analysis. Comparison between FWs and FW INCs were made by ANOVA, using the Progenesis LC-MS™ workflow detailed in section 5.3.8.2. ANOVA P-value less 0.05 was considered to be significant. A protein with AVNOA p-value less than 0.05 in this analysis was considered to be specifically present in plaque debris. Proteins are presented in this table according to fold change differences observed between FW and FW INC samples.

8.8 Acknowledgements

Few experiences in life define a person like that of completing a DPhil at Oxford University. Everyone who has done it knows the importance of a support network from colleagues, friends and family throughout this period, many of whom would have witnessed my gradual development of a budding scientist and the triumphant displays after each achievements. My closer companions will no doubt have noticed the more subtle transformations during this journey.

My foremost gratitude goes to Prof Keith Channon. This DPhil journey would not have started without his support from the outset. The rigor of scientific training provided by Prof Channon, and other members of the Channon Lab, have set strong foundations for my DPhil research, and will prepare me for future challenges in a likely academic career. The opportunities to learn from Prof Channon spanned far beyond the realms of science. In him is a model I aspire to, but doubt will successfully replicate even a fraction.

The later part of this research would not have been possible without the support from my secondary supervisor, Dr Benedikt Kessler. I had the fortune to witness the expansion of his group, and the help and support from many members. I particularly want to thank Dr Roman Fischer in the Kessler Lab for his enthusiasm on my project, and his willingness to impart knowledge. I am glad our interactions has transcended above that of a routine collaboration.

Most of the colleagues and mentors who have helped me throughout this period have been individually acknowledged throughout this Thesis. In addition, I want to thank Dr Janet Digby at the Choudhury lab and members of the Greave's lab for showing me the ropes to many basic research skills during the initial period. At the Channon group, Dr Eileen McNeil has always shown extra interest in my development and offered many valuable advices, including the arduous task of proof reading my pending New York Times Best Seller. Dr Charalambos Antoniades has been a particular sources of guidance and inspiration during this period, and another role model for me.

Of the surgical mentors, Dr Alan Scott has been my strongest advocate in the surgical community back in Australia, and the catalyst for several of the critical processes required for this research to continue; Prof John Fletcher has supported my work since my master of surgery, and provided ongoing encouragement. I particularly thank Prof Ashok Handa for planting the first seed of success for my career in academic surgery.

I could not have completed this endurance race without the constant infusion of encouragement and moral support from those closest to me. My parents, Willman and Gin, have endured the angst of having their only son living abroad for the past five years. Although having received little science training themselves, they have given me some of the most important advice during this journey. I would like to dedicate this Thesis to them, and hope to have made them very proud parents.

Finally, a big heart felt Thank You to my love, Claire, for cheering me on and healing my wounds throughout this race. I have been blessed to meet you from the very beginning, and to have benefited from your scientific training as a fellow DPhil. At our first date, I spoke of my aspiration to pursue a DPhil at Oxford. Four years later, on the eve of our marriage and the arrival of our first child, I am so proud to announce: "We have done it!"

REFERENCES

1. Falk E, Nakano M, Bentzon JF, Finn AV, Virmani R. Update on acute coronary syndromes: the pathologists' view. European heart journal. 2013;34(10):719-28.
2. Falk E. Plaque rupture with severe pre-existing stenosis precipitating coronary thrombosis. Characteristics of coronary atherosclerotic plaques underlying fatal occlusive thrombi. Br Heart J. 1983;50(2):127-34.
3. Falk E. Unstable angina with fatal outcome: dynamic coronary thrombosis leading to infarction and/or sudden death. Autopsy evidence of recurrent mural thrombosis with peripheral embolization culminating in total vascular occlusion. Circulation. 1985;71(4):699-708.
4. Libby P. Mechanisms of acute coronary syndromes and their implications for therapy. The New England journal of medicine. 2013;368(21):2004-13.
5. Hackett D, Davies G, Maseri A. Pre-existing coronary stenoses in patients with first myocardial infarction are not necessarily severe. European heart journal. 1988;9(12):1317-23.
6. Arbab-Zadeh A, Nakano M, Virmani R, Fuster V. Acute coronary events. Circulation. 2012;125(9):1147-56.
7. Little WC, Constantinescu M, Applegate RJ, Kutcher MA, Burrows MT, Kahl FR, et al. Can coronary angiography predict the site of a subsequent myocardial infarction in patients with mild-to-moderate coronary artery disease? Circulation. 1988;78(5 Pt 1):1157-66.
8. Schoenhagen P, Stone GW, Nissen SE, Grines CL, Griffin J, Clemson BS, et al. Coronary plaque morphology and frequency of ulceration distant from culprit lesions in patients with unstable and stable presentation. Arteriosclerosis, thrombosis, and vascular biology. 2003;23(10):1895-900.
9. Prati F, Uemura S, Souteyrand G, Virmani R, Motreff P, Di Vito L, et al. OCT-based diagnosis and management of STEMI associated with intact fibrous cap. JACC Cardiovasc Imaging. 2013;6(3):283-7.
10. Kubo T, Imanishi T, Takarada S, Kuroi A, Ueno S, Yamano T, et al. Assessment of culprit lesion morphology in acute myocardial infarction: ability of optical coherence tomography compared with intravascular ultrasound and coronary angioscopy. Journal of the American College of Cardiology. 2007;50(10):933-9.
11. O'Connor RE, Brady W, Brooks SC, Diercks D, Egan J, Ghaemmaghami C, et al. Part 10: acute coronary syndromes: 2010 American Heart Association Guidelines for Cardiopulmonary Resuscitation and Emergency Cardiovascular Care. Circulation. 2010;122(18 Suppl 3):S787-817.
12. Yamagishi M, Miyatake K, Tamai J, Nakatani S, Koyama J, Nissen SE. Intravascular ultrasound detection of atherosclerosis at the site of focal vasospasm in angiographically normal or minimally narrowed coronary segments. Journal of the American College of Cardiology. 1994;23(2):352-7.
13. Buffon A, Biasucci LM, Liuzzo G, D'Onofrio G, Crea F, Maseri A. Widespread coronary inflammation in unstable angina. The New England journal of medicine. 2002;347(1):5-12.

14. van der Wal AC, Becker AE, van der Loos CM, Das PK. Site of intimal rupture or erosion of thrombosed coronary atherosclerotic plaques is characterized by an inflammatory process irrespective of the dominant plaque morphology. Circulation. 1994;89(1):36-44.
15. Newby AC. Dual role of matrix metalloproteinases (matrixins) in intimal thickening and atherosclerotic plaque rupture. Physiol Rev. 2005;85(1):1-31.
16. Sugiyama S, Kugiyama K, Aikawa M, Nakamura S, Ogawa H, Libby P. Hypochlorous acid, a macrophage product, induces endothelial apoptosis and tissue factor expression: involvement of myeloperoxidase-mediated oxidant in plaque erosion and thrombogenesis. Arteriosclerosis, thrombosis, and vascular biology. 2004;24(7):1309-14.
17. Rajavashisth TB, Liao JK, Galis ZS, Tripathi S, Laufs U, Tripathi J, et al. Inflammatory cytokines and oxidized low density lipoproteins increase endothelial cell expression of membrane type 1-matrix metalloproteinase. The Journal of biological chemistry. 1999;274(17):11924-9.
18. Burke AP, Farb A, Malcom GT, Liang YH, Smialek J, Virmani R. Coronary risk factors and plaque morphology in men with coronary disease who died suddenly. The New England journal of medicine. 1997;336(18):1276-82.
19. Ohayon J, Finet G, Gharib AM, Herzka DA, Tracqui P, Heroux J, et al. Necrotic core thickness and positive arterial remodeling index: emergent biomechanical factors for evaluating the risk of plaque rupture. Am J Physiol Heart Circ Physiol. 2008;295(2):H717-27.
20. Hansson GK. Inflammation, atherosclerosis, and coronary artery disease. The New England journal of medicine. 2005;352(16):1685-95.
21. Cristell N, Cianflone D, Durante A, Ammirati E, Vanuzzo D, Banfi M, et al. High-sensitivity C-reactive protein is within normal levels at the very onset of first ST-segment elevation acute myocardial infarction in 41% of cases: a multiethnic case-control study. Journal of the American College of Cardiology. 2011;58(25):2654-61.
22. Mittleman MA, Mostofsky E. Physical, psychological and chemical triggers of acute cardiovascular events: preventive strategies. Circulation. 2011;124(3):346-54.
23. Newby DE. Triggering of acute myocardial infarction: beyond the vulnerable plaque. Heart (British Cardiac Society). 2010;96(15):1247-51.
24. Wentzel JJ, Chatzizisis YS, Gijsen FJ, Giannoglou GD, Feldman CL, Stone PH. Endothelial shear stress in the evolution of coronary atherosclerotic plaque and vascular remodelling: current understanding and remaining questions. Cardiovascular research. 2012;96(2):234-43.
25. Nesto RW, Waxman S, Mittleman MA, Sassower MA, Fitzpatrick PJ, Lewis SM, et al. Angioscopy of culprit coronary lesions in unstable angina pectoris and correlation of clinical presentation with plaque morphology. The American journal of cardiology. 1998;81(2):225-8.
26. Takano M, Inami S, Ishibashi F, Okamatsu K, Seimiya K, Ohba T, et al. Angioscopic follow-up study of coronary ruptured plaques in nonculprit lesions. J Am Coll Cardiol. 2005;45(5):652-8.

27. Davies MJ, Bland JM, Hangartner JR, Angelini A, Thomas AC. Factors influencing the presence or absence of acute coronary artery thrombi in sudden ischaemic death. European heart journal. 1989;10(3):203-8.
28. Frink RJ. Chronic ulcerated plaques: new insights into the pathogenesis of acute coronary disease. The Journal of invasive cardiology. 1994;6(5):173-85.
29. Kotani J-i, Mintz GS, Castagna MT, Pinnow E, Berzingi CO, Bui AB, et al. Intravascular Ultrasound Analysis of Infarct-Related and Non–Infarct-Related Arteries in Patients Who Presented With an Acute Myocardial Infarction. Circulation. 2003.
30. Mann J, Davies MJ. Mechanisms of progression in native coronary artery disease: role of healed plaque disruption. Heart (British Cardiac Society). 1999;82(3):265-8.
31. Burke AP, Kolodgie FD, Farb A, Weber DK, Malcom GT, Smialek J, et al. Healed plaque ruptures and sudden coronary death: evidence that subclinical rupture has a role in plaque progression. Circulation. 2001;103(7):934-40.
32. Davies MJ, Thomas A. Thrombosis and acute coronary-artery lesions in sudden cardiac ischemic death. The New England journal of medicine. 1984;310(18):1137-40.
33. Davies MJ. The contribution of thrombosis to the clinical expression of coronary atherosclerosis. Thromb Res. 1996;82(1):1-32.
34. Cheruvu PK, Finn AV, Gardner C, Caplan J, Goldstein J, Stone GW, et al. Frequency and distribution of thin-cap fibroatheroma and ruptured plaques in human coronary arteries: a pathologic study. Journal of the American College of Cardiology. 2007;50(10):940-9.
35. Stone GW, Maehara A, Lansky AJ, de Bruyne B, Cristea E, Mintz GS, et al. A prospective natural-history study of coronary atherosclerosis. The New England journal of medicine. 2011;364(3):226-35.
36. Calvert PA, Obaid DR, O'Sullivan M, Shapiro LM, McNab D, Densem CG, et al. Association between IVUS findings and adverse outcomes in patients with coronary artery disease: the VIVA (VH-IVUS in Vulnerable Atherosclerosis) Study. JACC Cardiovasc Imaging. 2011;4(8):894-901.
37. Kubo T, Maehara A, Mintz GS, Doi H, Tsujita K, Choi SY, et al. The dynamic nature of coronary artery lesion morphology assessed by serial virtual histology intravascular ultrasound tissue characterization. Journal of the American College of Cardiology. 2010;55(15):1590-7.
38. Rioufol G, Gilard M, Finet G, Ginon I, Boschat J, Andre-Fouet X. Evolution of spontaneous atherosclerotic plaque rupture with medical therapy: long-term follow-up with intravascular ultrasound. Circulation. 2004;110(18):2875-80.
39. Berry C, Noble S, Ibrahim R, Gregoire J, Levesque S, L'Allier P L, et al. Remodeling is a more important determinant of lumen size than atheroma burden in left main coronary artery disease. American heart journal. 2010;160(1):188-94 e1.
40. Lindahl B. Are there really biomarkers of vulnerable plaque? Clinical chemistry. 2012;58(1):151-3.

41. Hamm CW, Ravkilde J, Gerhardt W, Jorgensen P, Peheim E, Ljungdahl L, et al. The prognostic value of serum troponin T in unstable angina. The New England journal of medicine. 1992;327(3):146-50.
42. Alpert JS, Thygesen K, Antman E, Bassand JP. Myocardial infarction redefined--a consensus document of The Joint European Society of Cardiology/American College of Cardiology Committee for the redefinition of myocardial infarction. Journal of the American College of Cardiology. 2000;36(3):959-69.
43. Thygesen K, Alpert JS, White HD, Jaffe AS, Apple FS, Galvani M, et al. Universal definition of myocardial infarction. Circulation. 2007;116(22):2634-53.
44. Keller T, Zeller T, Ojeda F, Tzikas S, Lillpopp L, Sinning C, et al. Serial changes in highly sensitive troponin I assay and early diagnosis of myocardial infarction. Jama. 2011;306(24):2684-93.
45. Naylor AR. Time to rethink management strategies in asymptomatic carotid artery disease. Nat Rev Cardiol. 2012;9(2):116-24.
46. Griffin JL, Atherton H, Shockcor J, Atzori L. Metabolomics as a tool for cardiac research. Nat Rev Cardiol. 2011;8(11):630-43.
47. Tunon J, Martin-Ventura JL, Blanco-Colio LM, Lorenzo O, Lopez JA, Egido J. Proteomic strategies in the search of new biomarkers in atherothrombosis. Journal of the American College of Cardiology. 2010;55(19):2009-16.
48. Ekroos K, Janis M, Tarasov K, Hurme R, Laaksonen R. Lipidomics: a tool for studies of atherosclerosis. Current atherosclerosis reports. 2010;12(4):273-81.
49. Bagnato C, Thumar J, Mayya V, Hwang SI, Zebroski H, Claffey KP, et al. Proteomics analysis of human coronary atherosclerotic plaque: a feasibility study of direct tissue proteomics by liquid chromatography and tandem mass spectrometry. Mol Cell Proteomics. 2007;6(6):1088-102.
50. de la Cuesta F, Barderas MG, Calvo E, Zubiri I, Maroto AS, Darde VM, et al. Secretome analysis of atherosclerotic and non-atherosclerotic arteries reveals dynamic extracellular remodeling during pathogenesis. Journal of proteomics. 2012;75(10):2960-71.
51. Kopetz VA, Penno MA, Hoffmann P, Wilson DP, Beltrame JF. Potential mechanisms of the acute coronary syndrome presentation in patients with the coronary slow flow phenomenon - insight from a plasma proteomic approach. International journal of cardiology. 2012;156(1):84-91.
52. Distelmaier K, Adlbrecht C, Jakowitsch J, Wagner O, Gerner C, Lang IM, et al. Proteomic profiling of acute coronary thrombosis reveals a local decrease in pigment epithelium-derived factor in acute myocardial infarction. Clin Sci (Lond). 2012;123(2):111-9.
53. Sabatine MS, Liu E, Morrow DA, Heller E, McCarroll R, Wiegand R, et al. Metabolomic identification of novel biomarkers of myocardial ischemia. Circulation. 2005;112(25):3868-75.
54. Lewis GD, Wei R, Liu E, Yang E, Shi X, Martinovic M, et al. Metabolite profiling of blood from individuals undergoing planned myocardial infarction reveals early markers of myocardial injury. The Journal of clinical investigation. 2008;118(10):3503-12.

55. Dunn WB, Bailey NJ, Johnson HE. Measuring the metabolome: current analytical technologies. Analyst. 2005;130(5):606-25.
56. Fuchs B, Suss R, Schiller J. An update of MALDI-TOF mass spectrometry in lipid research. Prog Lipid Res. 2011;50(1):132.
57. Guerrera IC, Astarita G, Jais JP, Sands D, Nowakowska A, Colas J, et al. A novel lipidomic strategy reveals plasma phospholipid signatures associated with respiratory disease severity in cystic fibrosis patients. PLoS One. 2009;4(11):e7735.
58. Singhal R, Carrigan JB, Wei W, Taniere P, Hejmadi RK, Forde C, et al. MALDI profiles of proteins and lipids for the rapid characterisation of upper GI-tract cancers. Journal of proteomics. 2013;80C:207-15.
59. Stubiger G, Aldover-Macasaet E, Bicker W, Sobal G, Willfort-Ehringer A, Pock K, et al. Targeted profiling of atherogenic phospholipids in human plasma and lipoproteins of hyperlipidemic patients using MALDI-QIT-TOF-MS/MS. Atherosclerosis. 2012;224(1):177-86.
60. Langley SR, Dwyer J, Drozdov I, Yin X, Mayr M. Proteomics: from single molecules to biological pathways. Cardiovascular research. 2013;97(4):612-22.
61. Sana TR, Gordon DB, Fischer SM, Tichy SE, Kitagawa N, Lai C, et al. Global mass spectrometry based metabolomics profiling of erythrocytes infected with Plasmodium falciparum. PLoS One. 2013;8(4):e60840.
62. Mayr M, Chung YL, Mayr U, Yin X, Ly L, Troy H, et al. Proteomic and metabolomic analyses of atherosclerotic vessels from apolipoprotein E-deficient mice reveal alterations in inflammation, oxidative stress, and energy metabolism. Arteriosclerosis, thrombosis, and vascular biology. 2005;25(10):2135-42.
63. Mayr M, Zampetaki A, Sidibe A, Mayr U, Yin X, De Souza AI, et al. Proteomic and metabolomic analysis of smooth muscle cells derived from the arterial media and adventitial progenitors of apolipoprotein E-deficient mice. Circulation research. 2008;102(9):1046-56.
64. Mayr M, Grainger D, Mayr U, Leroyer AS, Leseche G, Sidibe A, et al. Proteomics, metabolomics, and immunomics on microparticles derived from human atherosclerotic plaques. Circ Cardiovasc Genet. 2009;2(4):379-88.
65. Mayr M, Yusuf S, Weir G, Chung YL, Mayr U, Yin X, et al. Combined metabolomic and proteomic analysis of human atrial fibrillation. Journal of the American College of Cardiology. 2008;51(5):585-94.
66. De Souza AI, Cardin S, Wait R, Chung YL, Vijayakumar M, Maguy A, et al. Proteomic and metabolomic analysis of atrial profibrillatory remodelling in congestive heart failure. J Mol Cell Cardiol. 2010;49(5):851-63.
67. Mayr M, Liem D, Zhang J, Li X, Avliyakulov NK, Yang JI, et al. Proteomic and metabolomic analysis of cardioprotection: Interplay between protein kinase C epsilon and delta in regulating glucose metabolism of murine hearts. J Mol Cell Cardiol. 2009;46(2):268-77.
68. Jove M, Ayala V, Ramirez-Nunez O, Serrano JC, Cassanye A, Arola L, et al. Lipidomic and metabolomic analyses reveal potential plasma biomarkers of early atheromatous plaque formation in hamsters. Cardiovascular research. 2013;97(4):642-52.

69. Taking Blood Samples from Colleagues or Students for Research and Teaching [updated 01 Sep 2011]. OHS Policy Document 1/03]. Available from: http://www.admin.ox.ac.uk/uohs/policies-guidance/blood/
70. Aguilar-Mahecha A, Kuzyk MA, Domanski D, Borchers CH, Basik M. The effect of pre-analytical variability on the measurement of MRM-MS-based mid- to high-abundance plasma protein biomarkers and a panel of cytokines. PLoS One. 2012;7(6):e38290.
71. Mannello F. Serum or plasma samples? The "Cinderella" role of blood collection procedures: preanalytical methodological issues influence the release and activity of circulating matrix metalloproteinases and their tissue inhibitors, hampering diagnostic trueness and leading to misinterpretation. Arteriosclerosis, thrombosis, and vascular biology. 2008;28(4):611-4.
72. Meng Z, Veenstra TD. Proteomic analysis of serum, plasma, and lymph for the identification of biomarkers. Proteomics Clinical applications. 2007;1(8):747-57.
73. Weber C. Platelets and chemokines in atherosclerosis: partners in crime. Circ Res. 2005;96(6):612-6.
74. Gawaz M, Langer H, May AE. Platelets in inflammation and atherogenesis. J Clin Invest. 2005;115(12):3378-84.
75. Aukrust P, Muller F, Ueland T, Berget T, Aaser E, Brunsvig A, et al. Enhanced levels of soluble and membrane-bound CD40 ligand in patients with unstable angina. Possible reflection of T lymphocyte and platelet involvement in the pathogenesis of acute coronary syndromes. Circulation. 1999;100(6):614-20.
76. de Lemos JA, Zirlik A, Schonbeck U, Varo N, Murphy SA, Khera A, et al. Associations between soluble CD40 ligand, atherosclerosis risk factors, and subclinical atherosclerosis: results from the Dallas Heart Study. Arteriosclerosis, thrombosis, and vascular biology. 2005;25(10):2192-6.
77. Viallard JF, Solanilla A, Gauthier B, Contin C, Dechanet J, Grosset C, et al. Increased soluble and platelet-associated CD40 ligand in essential thrombocythemia and reactive thrombocytosis. Blood. 2002;99(7):2612-4.
78. Tammen H, Schulte I, Hess R, Menzel C, Kellmann M, Mohring T, et al. Peptidomic analysis of human blood specimens: comparison between plasma specimens and serum by differential peptide display. Proteomics. 2005;5(13):3414-22.
79. Antoniades C, Bakogiannis C, Tousoulis D, Antonopoulos AS, Stefanadis C. The CD40/CD40 ligand system: linking inflammation with atherothrombosis. Journal of the American College of Cardiology. 2009;54(8):669-77.
80. Heeschen C, Dimmeler S, Hamm CW, van den Brand MJ, Boersma E, Zeiher AM, et al. Soluble CD40 ligand in acute coronary syndromes. The New England journal of medicine. 2003;348(12):1104-11.
81. Schonbeck U, Varo N, Libby P, Buring J, Ridker PM. Soluble CD40L and cardiovascular risk in women. Circulation. 2001;104(19):2266-8.
82. Verma S, Wang CH, Li SH, Lonn E, Charbonneau F, Title LM, et al. The relationship between soluble CD40 ligand levels and Framingham coronary heart disease risk score in healthy volunteers. Atherosclerosis. 2005;182(2):361-5.

83. Victor RG, Haley RW, Willett DL, Peshock RM, Vaeth PC, Leonard D, et al. The Dallas Heart Study: a population-based probability sample for the multidisciplinary study of ethnic differences in cardiovascular health. The American journal of cardiology. 2004;93(12):1473-80.
84. Slichter SJ, Bolgiano D, Corson J, Jones MK, Christoffel T. Extended storage of platelet-rich plasma-prepared platelet concentrates in plasma or Plasmalyte. Transfusion. 2010;50(10):2199-209.
85. Lee R, Antonopoulos AS, Alexopoulou Z, Margaritis M, Kharbanda RK, Choudhury RP, et al. Artifactual elevation of plasma sCD40L by residual platelets in patients with coronary artery disease. International journal of cardiology. 2013.
86. Varo N, Nuzzo R, Natal C, Libby P, Schonbeck U. Influence of pre-analytical and analytical factors on soluble CD40L measurements. Clin Sci (Lond). 2006;111(5):341-7.
87. Amos PJ, Cagavi Bozkulak E, Qyang Y. Methods of cell purification: a critical juncture for laboratory research and translational science. Cells, tissues, organs. 2012;195(1-2):26-40.
88. Hinghofer-Szalkay H. Volume and density changes of biological fluids with temperature. J Appl Physiol. 1985;59(6):1686-9.
89. Banfi G, Salvagno GL, Lippi G. The role of ethylenediamine tetraacetic acid (EDTA) as in vitro anticoagulant for diagnostic purposes. Clin Chem Lab Med. 2007;45(5):565-76.
90. Capila I, Linhardt RJ. Heparin-protein interactions. Angew Chem Int Ed Engl. 2002;41(3):391-412.
91. Perrotta G, Roberts L, Glazier J, Schumacher HR. Use of sodium citrate anticoagulant for routine hematology analysis on the CELL-DYN 4000: An opportunity to enhance efficiency in the clinical laboratory. Laboratory Hematology. 1998;4:156-62.
92. Lee R, Adlam D, Antoniades C, Digby JE, Kharbanda RK, Choudhury RP, et al. Heparin administration leads to rapid decrease in plasma matrix metalloproteinase-9. International journal of cardiology. 2013;163(2):212-3.
93. Campbell Lee S, Shaz B, Arena R, Sloan S, Fung M, Ramsey G. Red blood cell products: consideration of the discrepant temperature ranges permitted for storage versus transport. Transfusion. 2012;52(1):195-200.
94. Sparrow RL, Greening DW, Simpson RJ. A protocol for the preparation of cryoprecipitate and cryodepleted plasma. Methods Mol Biol. 2011;728:259-65.
95. Kaudewitz D, Lee R, Willeit P, McGregor R, Markus HS, Kiechl S, et al. Impact of intravenous heparin on quantification of circulating microRNAs in patients with coronary artery disease. Thrombosis and haemostasis. 2013;110(3).
96. Lindahl B. Are There Really Biomarkers of Vulnerable Plaque? Clinical chemistry. 2011.
97. Klebanoff SJ, Waltersdorph AM, Rosen H. Antimicrobial activity of myeloperoxidase. Methods in enzymology. 1984;105:399-403.

98. Zhang R, Brennan ML, Fu X, Aviles RJ, Pearce GL, Penn MS, et al. Association between myeloperoxidase levels and risk of coronary artery disease. Jama. 2001;286(17):2136-42.
99. Galis ZS, Sukhova GK, Lark MW, Libby P. Increased expression of matrix metalloproteinases and matrix degrading activity in vulnerable regions of human atherosclerotic plaques. The Journal of clinical investigation. 1994;94(6):2493-503.
100. Park JP, Lee BK, Shim JM, Kim SH, Lee CW, Kang DH, et al. Relationship between multiple plasma biomarkers and vulnerable plaque determined by virtual histology intravascular ultrasound. Circ J. 2010;74(2):332-6.
101. Kai H, Ikeda H, Yasukawa H, Kai M, Seki Y, Kuwahara F, et al. Peripheral blood levels of matrix metalloproteases-2 and -9 are elevated in patients with acute coronary syndromes. Journal of the American College of Cardiology. 1998;32(2):368-72.
102. Kobayashi N, Hata N, Kume N, Yokoyama S, Shinada T, Tomita K, et al. Matrix metalloproteinase-9 for the earliest stage acute coronary syndrome. Circ J. 2011;75(12):2853-61.
103. Vanhoutte D, Schellings M, Pinto Y, Heymans S. Relevance of matrix metalloproteinases and their inhibitors after myocardial infarction: a temporal and spatial window. Cardiovascular research. 2006;69(3):604-13.
104. Fabunmi RP, Sukhova GK, Sugiyama S, Libby P. Expression of tissue inhibitor of metalloproteinases-3 in human atheroma and regulation in lesion-associated cells: a potential protective mechanism in plaque stability. Circulation research. 1998;83(3):270-8.
105. Moreau M, Brocheriou I, Petit L, Ninio E, Chapman MJ, Rouis M. Interleukin-8 mediates downregulation of tissue inhibitor of metalloproteinase-1 expression in cholesterol-loaded human macrophages: relevance to stability of atherosclerotic plaque. Circulation. 1999;99(3):420-6.
106. Lubos E, Schnabel R, Rupprecht HJ, Bickel C, Messow CM, Prigge S, et al. Prognostic value of tissue inhibitor of metalloproteinase-1 for cardiovascular death among patients with cardiovascular disease: results from the AtheroGene study. European heart journal. 2006;27(2):150-6.
107. Nishi K, Itabe H, Uno M, Kitazato KT, Horiguchi H, Shinno K, et al. Oxidized LDL in carotid plaques and plasma associates with plaque instability. Arteriosclerosis, thrombosis, and vascular biology. 2002;22(10):1649-54.
108. Hakkinen T, Luoma JS, Hiltunen MO, Macphee CH, Milliner KJ, Patel L, et al. Lipoprotein-associated phospholipase A(2), platelet-activating factor acetylhydrolase, is expressed by macrophages in human and rabbit atherosclerotic lesions. Arteriosclerosis, thrombosis, and vascular biology. 1999;19(12):2909-17.
109. de Kleijn DP, Moll FL, Hellings WE, Ozsarlak-Sozer G, de Bruin P, Doevendans PA, et al. Local atherosclerotic plaques are a source of prognostic biomarkers for adverse cardiovascular events. Arteriosclerosis, thrombosis, and vascular biology. 2010;30(3):612-9.

110. te Boekhorst BC, Bovens SM, Hellings WE, van der Kraak PH, van de Kolk KW, Vink A, et al. Molecular MRI of murine atherosclerotic plaque targeting NGAL: a protein associated with unstable human plaque characteristics. Cardiovascular research. 2011;89(3):680-8.
111. Schaub N, Reichlin T, Twerenbold R, Reiter M, Steuer S, Bassetti S, et al. Growth differentiation factor-15 in the early diagnosis and risk stratification of patients with acute chest pain. Clinical chemistry. 2012;58(2):441-9.
112. Overgaard MT, Boldt HB, Laursen LS, Sottrup-Jensen L, Conover CA, Oxvig C. Pregnancy-associated plasma protein-A2 (PAPP-A2), a novel insulin-like growth factor-binding protein-5 proteinase. The Journal of biological chemistry. 2001;276(24):21849-53.
113. Prasad A, Tsimikas S. Candidate biomarkers for the detection of coronary plaque destabilization and rupture. Current atherosclerosis reports. 2008;10(4):309-17.
114. Narula J, Garg P, Achenbach S, Motoyama S, Virmani R, Strauss HW. Arithmetic of vulnerable plaques for noninvasive imaging. Nature clinical practice. 2008;5 Suppl 2:S2-10.
115. Prati F, Regar E, Mintz GS, Arbustini E, Di Mario C, Jang IK, et al. Expert review document on methodology, terminology, and clinical applications of optical coherence tomography: physical principles, methodology of image acquisition, and clinical application for assessment of coronary arteries and atherosclerosis. European heart journal. 2010;31(4):401-15.
116. Lanza IR, Zhang S, Ward LE, Karakelides H, Raftery D, Nair KS. Quantitative metabolomics by H-NMR and LC-MS/MS confirms altered metabolic pathways in diabetes. PLoS One. 2010;5(5):e10538.
117. Isabel Padrao A, Ferreira R, Vitorino R, Amado F. Proteome-base biomarkers in diabetes mellitus: progress on biofluids' protein profiling using mass spectrometry. Proteomics Clin Appl. 2012;6(9-10):447-66.
118. Zampetaki A, Kiechl S, Drozdov I, Willeit P, Mayr U, Prokopi M, et al. Plasma microRNA profiling reveals loss of endothelial miR-126 and other microRNAs in type 2 diabetes. Circulation research. 2010;107(6):810-7.
119. Brennan ML, Penn MS, Van Lente F, Nambi V, Shishehbor MH, Aviles RJ, et al. Prognostic value of myeloperoxidase in patients with chest pain. The New England journal of medicine. 2003;349(17):1595-604.
120. Schaub N, Reichlin T, Meune C, Twerenbold R, Haaf P, Hochholzer W, et al. Markers of plaque instability in the early diagnosis and risk stratification of acute myocardial infarction. Clinical chemistry. 2012;58(1):246-56.
121. Baldus S, Rudolph V, Roiss M, Ito WD, Rudolph TK, Eiserich JP, et al. Heparins increase endothelial nitric oxide bioavailability by liberating vessel-immobilized myeloperoxidase. Circulation. 2006;113(15):1871-8.
122. Rudolph TK, Rudolph V, Witte A, Klinke A, Szoecs K, Lau D, et al. Liberation of vessel adherent myeloperoxidase by enoxaparin improves endothelial function. International journal of cardiology. 2010;140(1):42-7.
123. Jefferis BJ, Whincup P, Welsh P, Wannamethee G, Rumley A, Lennon L, et al. Prospective study of matrix metalloproteinase-9 and risk of myocardial

infarction and stroke in older men and women. Atherosclerosis. 2010;208(2):557-63.
124. Tayebjee MH, Lip GY, Tan KT, MacFadyen RJ. Abnormal circulating neutrophil linked matrix metalloproteinase -9 in stable coronary artery disease. Thrombosis and haemostasis. 2006;95(1):202-4.
125. Jonsson S, Lundberg A, Kalvegren H, Bergstrom I, Szymanowski A, Jonasson L. Increased levels of leukocyte-derived MMP-9 in patients with stable angina pectoris. PLoS One. 2011;6(4):e19340.
126. Mannello F, Jung K, Tonti GA, Canestrari F. Heparin affects matrix metalloproteinases and tissue inhibitors of metalloproteinases circulating in peripheral blood. Clinical biochemistry. 2008;41(18):1466-73.
127. Fernandez-Patron C, Martinez-Cuesta MA, Salas E, Sawicki G, Wozniak M, Radomski MW, et al. Differential regulation of platelet aggregation by matrix metalloproteinases-9 and -2. Thrombosis and haemostasis. 1999;82(6):1730-5.
128. Higo S, Uematsu M, Yamagishi M, Ishibashi-Ueda H, Awata M, Morozumi T, et al. Elevation of plasma matrix metalloproteinase-9 in the culprit coronary artery in patients with acute myocardial infarction: clinical evidence from distal protection. Circ J. 2005;69(10):1180-5.
129. Brown AJ, Leong SL, Dean RT, Jessup W. 7-Hydroperoxycholesterol and its products in oxidized low density lipoprotein and human atherosclerotic plaque. Journal of lipid research. 1997;38(9):1730-45.
130. Tsimikas S, Lau HK, Han KR, Shortal B, Miller ER, Segev A, et al. Percutaneous coronary intervention results in acute increases in oxidized phospholipids and lipoprotein(a): short-term and long-term immunologic responses to oxidized low-density lipoprotein. Circulation. 2004;109(25):3164-70.
131. Tsimikas S, Bergmark C, Beyer RW, Patel R, Pattison J, Miller E, et al. Temporal increases in plasma markers of oxidized low-density lipoprotein strongly reflect the presence of acute coronary syndromes. Journal of the American College of Cardiology. 2003;41(3):360-70.
132. Itabe H, Ueda M. Measurement of plasma oxidized low-density lipoprotein and its clinical implications. Journal of atherosclerosis and thrombosis. 2007;14(1):1-11.
133. Want EJ, Masson P, Michopoulos F, Wilson ID, Theodoridis G, Plumb RS, et al. Global metabolic profiling of animal and human tissues via UPLC-MS. Nature protocols. 2013;8(1):17-32.
134. Fuchs B, Suss R, Schiller J. An update of MALDI-TOF mass spectrometry in lipid research. Prog Lipid Res. 2010;49(4):450-75.
135. Broadhurst DI, Kell DB. Statistical strategies for avoiding false discoveries in metabolomics and related experiments. Metabolomics. 2006;2(4):171-96.
136. Cairns DA, Barrett JH, Billingham LJ, Stanley AJ, Xinarianos G, Field JK, et al. Sample size determination in clinical proteomic profiling experiments using mass spectrometry for class comparison. Proteomics. 2009;9(1):74-86.
137. Levin Y. The role of statistical power analysis in quantitative proteomics. Proteomics. 2011;11(12):2565-7.

138. Kendziorski C, Irizarry RA, Chen KS, Haag JD, Gould MN. On the utility of pooling biological samples in microarray experiments. Proc Natl Acad Sci U S A. 2005;102(12):4252-7.
139. Diz AP, Truebano M, Skibinski DO. The consequences of sample pooling in proteomics: an empirical study. Electrophoresis. 2009;30(17):2967-75.
140. Trygg J, Holmes E, Lundstedt T. Chemometrics in metabonomics. Journal of proteome research. 2007;6(2):469-79.
141. Bligh EG, Dyer WJ. A rapid method of total lipid extraction and purification. Canadian journal of biochemistry and physiology. 1959;37(8):911-7.
142. Sana TR, Roark JC, Li X, Waddell K, Fischer SM. Molecular formula and METLIN Personal Metabolite Database matching applied to the identification of compounds generated by LC/TOF-MS. J Biomol Tech. 2008;19(4):258-66.
143. Zhu ZJ, Schultz AW, Wang J, Johnson CH, Yannone SM, Patti GJ, et al. Liquid chromatography quadrupole time-of-flight mass spectrometry characterization of metabolites guided by the METLIN database. Nature protocols. 2013;8(3):451-60.
144. Langley RJ, Tsalik EL, Velkinburgh JC, Glickman SW, Rice BJ, Wang C, et al. An integrated clinico-metabolomic model improves prediction of death in sepsis. Science translational medicine. 2013;5(195):195ra95.
145. Wilm M, Shevchenko A, Houthaeve T, Breit S, Schweigerer L, Fotsis T, et al. Femtomole sequencing of proteins from polyacrylamide gels by nano-electrospray mass spectrometry. Nature. 1996;379(6564):466-9.
146. Ishihama Y, Oda Y, Tabata T, Sato T, Nagasu T, Rappsilber J, et al. Exponentially modified protein abundance index (emPAI) for estimation of absolute protein amount in proteomics by the number of sequenced peptides per protein. Mol Cell Proteomics. 2005;4(9):1265-72.
147. Lundgren DH, Hwang SI, Wu L, Han DK. Role of spectral counting in quantitative proteomics. Expert review of proteomics. 2010;7(1):39-53.
148. Schiess R, Wollscheid B, Aebersold R. Targeted proteomic strategy for clinical biomarker discovery. Molecular oncology. 2009;3(1):33-44.
149. Fischer R, Trudgian DC, Wright C, Thomas G, Bradbury LA, Brown MA, et al. Discovery of candidate serum proteomic and metabolomic biomarkers in ankylosing spondylitis. Mol Cell Proteomics. 2012;11(2):M111 013904.
150. Trudgian DC, Thomas B, McGowan SJ, Kessler BM, Salek M, Acuto O. CPFP: a central proteomics facilities pipeline. Bioinformatics. 2010;26(8):1131-2.
151. Tolosano E, Fagoonee S, Morello N, Vinchi F, Fiorito V. Heme scavenging and the other facets of hemopexin. Antioxid Redox Signal. 2010;12(2):305-20.
152. Michel JB, Virmani R, Arbustini E, Pasterkamp G. Intraplaque haemorrhages as the trigger of plaque vulnerability. European heart journal. 2011;32(16):1977-85, 85a, 85b, 85c.
153. Cheng S, Rhee EP, Larson MG, Lewis GD, McCabe EL, Shen D, et al. Metabolite profiling identifies pathways associated with metabolic risk in humans. Circulation. 2012;125(18):2222-31.

154. Wang Y, Liu H, McKenzie G, Witting PK, Stasch JP, Hahn M, et al. Kynurenine is an endothelium-derived relaxing factor produced during inflammation. Nature medicine. 2010;16(3):279-85.
155. Method of the Year 2012. Nature methods. 2013;10(1):1.
156. Gillet LC, Navarro P, Tate S, Rost H, Selevsek N, Reiter L, et al. Targeted data extraction of the MS/MS spectra generated by data-independent acquisition: a new concept for consistent and accurate proteome analysis. Mol Cell Proteomics. 2012;11(6):O111 016717.
157. Porto I, Selvanayagam JB, Van Gaal WJ, Prati F, Cheng A, Channon K, et al. Plaque volume and occurrence and location of periprocedural myocardial necrosis after percutaneous coronary intervention: insights from delayed-enhancement magnetic resonance imaging, thrombolysis in myocardial infarction myocardial perfusion grade analysis, and intravascular ultrasound. Circulation. 2006;114(7):662-9.
158. Okura H, Asawa K, Kubo T, Taguchi H, Toda I, Yoshiyama M, et al. Incidence and predictors of plaque rupture in the peripheral arteries. Circ Cardiovasc Interv. 2010;3(1):63-70.
159. Wald DS, Morris JK, Wald NJ, Chase AJ, Edwards RJ, Hughes LO, et al. Randomized trial of preventive angioplasty in myocardial infarction. The New England journal of medicine. 2013;369(12):1115-23.
160. Ulmert D, Becker C, Nilsson JA, Piironen T, Bjork T, Hugosson J, et al. Reproducibility and accuracy of measurements of free and total prostate-specific antigen in serum vs plasma after long-term storage at -20 degrees C. Clinical chemistry. 2006;52(2):235-9.
161. Libby P, Ridker PM, Hansson GK. Progress and challenges in translating the biology of atherosclerosis. Nature. 2011;473(7347):317-25.
162. Phinikaridou A, Hallock KJ, Qiao Y, Hamilton JA. A robust rabbit model of human atherosclerosis and atherothrombosis. Journal of lipid research. 2009;50(5):787-97.
163. Granada JF, Kaluza GL, Wilensky RL, Biedermann BC, Schwartz RS, Falk E. Porcine models of coronary atherosclerosis and vulnerable plaque for imaging and interventional research. EuroIntervention. 2009;5(1):140-8.